Design and validation of bioorthogonal probes for cellular disease models

Thèse N° 9709

Pier Luca D'ALESSANDRO

2019

ÉCOLE POLYTECHNIQUE
FÉDÉRALE DE LAUSANNE

Acknowledgements

Abstract

Well-validated chemical probes enable testing of biological hypotheses, investigation of target tractability and translatability to the clinical phase. Consequently, these important tool compounds play a key role in the drug discovery process. Moreover, their use for target validation may ultimately help to decrease the attrition rate encountered by new molecular entities in clinical trials.

Despite the number of publications describing well-validated chemical probes, for several reasons, it remains a difficult challenge to identify and select the appropriate high quality molecule enabling the desired biological and pharmacological studies in the relevant disease model. Various reports describe sets of principles to be fulfilled by high quality chemical probes, which mainly rely on verifying that chemical probes are potent, engage their intended targets in the relevant cellular model, have sufficient exposure at the desired site of action and express functional pharmacological activities by a selective modulation of their targets.

Classical chemical probes include low molecular weight ligands, which inform on the functional consequences of interacting with a particular biological target in a model system. To get information on other parameters (such as sub-cellular distribution of target or compound) different tools may need to be used, often requiring specific chemical functionalization in order to observe the molecule using the currently available technologies.

Compared to classical chemical probes, bioorthogonal probes can also be small molecules that elicit a functional response but with the additional advantage of being able to undergo reaction with a variety of chemical reporters (e.g. fluorophores) in situ, in biological model systems such as cells and animals. Therefore, this increases their versatility; for example, their visualization using imaging technologies (bioluminescence and fluorescence imaging) can provide important insights on compound permeability, intracellular distribution, and potentially co-localization with its protein target in relevant cellular disease models. Hence, the use of a bespoke bioorthogonal probe may answer key biological questions, which are usually only addressed by using multiple classical probes.

Herein, we describe the design and the synthesis of bioorthogonal probes to study the inhibition of the p53-Mdm2 protein-protein interaction. Furthermore, we report the development of a set of assays based on fluorescence and bioluminescence techniques enabling the validation of these molecules in a cellular osteosarcoma model.

Our approach for chemical probe design and validation in cellular disease models may be applied in principle to a wide range of novel drug discovery projects to provide early mechanistic understanding.

Keywords

Bioluminescence imaging

Bioorthogonal Chemistry

Chemical probe

Fluorescence imaging

Mdm2

p53

Protein-protein interaction

Tesi Abstract

L'utilizzo di "Chemical probes" ampiamente confermati sperimentalmente permette di testare ipotesi biologiche, investigare la trattabilita' di proteine bersaglio e la trasferibilita' dei dati sperimentali di laboratorio alle seguenti fasi cliniche. Inoltre, il loro uso nello studio di proteine bersaglio puo' aiutare a diminuire gli atriti riscontrati da nuovi potenziali farmaci negli studi clinici.

Per svariate ragioni ed a dispetto del crescente numero di pubblicazioni riguardanti i "Chemical probes" e' ancora difficile identificare e selezionare le molecole piu' appropriate per lo studio biologico e farmacologico di modelli sperimentali di patologie. Sebbene un gran numero di ariticoli scientifici descrivano un elenco di caratteriche che un "chemical probe" debba soddisfare per essere considerato valido, sostanzialmente tutte queste pubblicazioni fanno riferimento alla potenza di queste molecole, alla loro capacita' di colpire le proteine bersaglio in modelli sperimentali di patologie, alla loro concentrazione al sito d'azione ed infine alla loro capacita' di attivare un risposta farmacologica grazie alla modulazione dei loro bersagli biologici.

I classici "chemical probes" forniscono informazioni sugli effetti scatenati delle loro interazioni con le proteine bersaglio in modelli sperimentali. Comunque, per ottenere informazioni, per esempio sulla loro distribuzione nei vari compartimenti cellulari, e' richiesto l'utilizzo di varie tecniche avanzate d'indagine o e' necessario modificare i "chemical probes" redendoli visibili con le attuali tecnologie di microscopia investigativa.

A differenza dei classici "chemical probes", i "bioorthogonal probes" permettono anche loro di scatenare un effetto farmacologico, ma allo stesso tempo hanno il vantaggio di poter essere modificati attraverso reazioni chimiche con agenti fluorescenti o bioluminescenti in situ, all'interno del modello sperimentale cellulare od animale. Queste molecole dimostrano una superiore versatilita', consentendo di ottenere informazioni sulla loro permeabilita' cellulare, sulla loro distribuzione nei compartimenti cellulari e sulla loro colocalizazzione con le proteine bersaglio. Quindi l'utilizzo di uno specifico "chemical probe" puo' aiutare a capire processi biologici chiave che sono di solito studiati con l'uso di diverse molecole e varie tecnologie analitiche.

Qui descriviamo il disegno e la sintesi dei "bioorthogonal probes" per studiare l'inibizione dell'interazione fra p53 e Mdm2, inoltre, descriviamo lo sviluppo di saggi basati su tecniche di fluorescenza e bioluminescenza che permettano lo studio e la validazione dei nostri "bioorthogonal probes" in un modello cellulare di osteosarcoma.

Questo studio, infine, ci ha portati a ritenere che il nostro approccio per il disegno e la validazione di "chemical probes" possa essere applicato ad un ampio numero di progetti di ricerca di nuovi farmaci per fornire nelle prime fasi sperimentali importanti informazioni sui meccanismi biologici sotto investigazione.

Parole chiave

Chemical probe

Chimica bioortogonale

Interazioni proteiche

Mdm2

p53

Spettroscopia di bioluminescenza

Spettroscopia di fluorescenza

Contents

x

List of Figures

List of Tables

Chapter 1. Introduction

1.1   The use of Chemical probes in drug discovery

The validation of the biological target in a relevant cellular disease model is one of the major challenges encountered at the inception of a drug discovery program. This is particularly true when our validation approach is enabled by the use of chemical probes and when our cellular disease model provides a phenotypic read-out.[1] Despite the key role played by chemical probes at this stage, their use might not be exempt from biased interpretations and incorrect conclusions due to unknown off-target effects.[2]

As defined by Arrowsmith et al. in 2015, a chemical probe is "a reagent, a selective small molecule modulator of a protein's function that allows the user to ask mechanistic and phenotypic questions about its molecular target in biochemical, cell-based or animal studies".[2]

Since the 1990s, the great development in genomics technologies (e.g. DNA sequencing, interference RNA, short hairpin RNA, CRISPR-Cas9 genome-editing technology) has led to the identification of new biological targets, which apparently have a clear link to the pathogenesis and progression of pathologies.[3-5] Hence, the drug discovery community has focused its efforts toward target-based approaches supported by the idea that a known Mode of Action (MoA), the possibility to access more high throughput screen assays, in silico tools for drug design and potentially the structural knowledge of the target would deliver drug candidates faster and with better translatability in clinical phases.[3] However, in the last few years the number of small molecule drugs discovered via phenotypic screening was superior to that identified through target-based approaches, with reduced cost and time.[3,6,7] Furthermore, many of these new drugs have been discovered applying phenotypic screening approaches through intentional targeting of a specific phenotype or serendipity.[3,6] Finally, a phenotypic screening campaign often requires a subsequent target identification and validation where chemical probes have crucial impact.
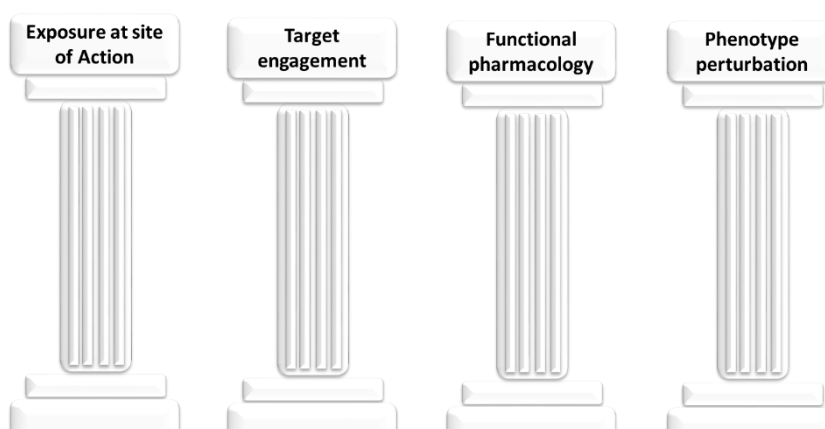
Figure 1.1-1 The four pillars for cellular disease model validation using chemical probes (adapted from *M.E. Bunnage, L.H. Jones et al. Nature Chemical Biology, 2013*)

As reported by Bunnage and Jones, one of the major causes of failure of drug discovery programs in clinical trials (analysis of 44 programs in Phase 2 clinical trials at Pfizer) is a lack of efficacy of the drug substance in human.[1] Some of the possible explanations for this are a poor understanding of the biological role of the target in the human disease, a low compound exposure in the relevant target tissue, a target validation on a phenotype not specific for a particular disease or in a disease model with poor translatability to human and so on.

Chemical probes can be used for investigating the biological relevance of a target and the chemical tractability of a phenotype in order to improve the understanding of the target potential in the early drug discovery phase. It is also important to mention that these molecules can be used for answering translatability questions by, for instance, helping the identification of biomarkers. Consequently, the important knowledge built by employing well validated chemical probes in preclinical phase studies enables a reduction of the attrition rate in clinical trials due to a lack of efficacy.[8] The two previously cited authors nicely defined a new drug discovery concept, the "three pillars of survival", as a framework to be satisfied by validated chemical probes to improve the chances of success of a drug discovery project. These three pillars are exposure at the site of action, target engagement and expression of functional pharmacological activity. Moreover, the two authors proposed to add a fourth pillar to their initial analysis, the proof of phenotype perturbation. Finally, the fourth pillar aims to strengthen the link between target perturbation and disease-relevant pharmacological modulation (**Figure 1.1-1**).[1]

In addition to the suitable pharmacokinetic characteristics and pharmacodynamic properties that a high quality probe has to satisfy, it is important to remember that crucial prerequisites for these chemical compounds are chemical and metabolic stability, purity, solubility, potency, selectivity (in particular against target subfamilies, orthologs and paralogs), selectivity against targets interfering with the pharmacodynamic readout, cellular permeability (for an intracellular target) and a known mode of action (**Figure 1.2-4**).[2,9]

Highly valuable chemical probes have enabled pioneering of new areas and pathways in biology and discovery of new first in class medicines. On the contrary, misuse of poorly validated probes or molecules for which data concerning liabilities (e.g. target promiscuity) have not been properly reported in databases might lead to observed biological effects not linked to the functional pharmacology under investigation.

Several remarkable examples of chemical probes used for understanding fundamental biology are shown in **Figure 1.1-2**. The study of proteasome function in the cytosol and nucleus was enabled by the probe MG132.[10] L-731,988 provided important insights into the mechanism for incorporating viral DNA in the host genome.[11] GW683965 was an important tool compound to investigate the role of nuclear liver X receptors (LXRα and LXRβ) in regulating the intracellular level of cholesterol.[12] Finally, ubiquitination of the IKAROS family transcription factors by CRBN-CUL4 E3 ubiquitin ligase complex was elucidated using Thalidomide.[13,14] **It** is worth mentioning in more detail three additional molecules which contributed to increase awareness of the important role of chemical probes in drug discovery, Rapamycin, (+)-JQ1 and CCT251545 **(Figure 1.1-2)**.[15-17]

Rapamycin (Sirolimus) is a natural product, isolated in the 1970s and clinically approved as an immunosuppressive agent. This molecule binds to immunophilin FKBP12 forming a ternary complex with the FRB domain of a serine-threonine kinase, the mammalian target of Rapamycin (mTOR).[18] The formation of the ternary complex prevents the kinase activity of mTOR toward its substrates. Rapamycin has been successfully used for understanding mTOR signaling,

a key component of the PI3K–AKT–mTOR pathway.[19] This intracellular signaling pathway modulates the translation of mRNA sub-populations important for cell survival and proliferation and its dysfunction has implications in several pathologies from metabolic to cardiovascular and cancer diseases.[19,20] The O-hydroxyethyl derivative of Rapamycin, an optimized analogue, RAD-001 (Everolimus) **(Figure 1.1-2)** is a marketed medication for prevention of organ rejection after transplantation. Since 2009, the FDA also approved the use of Everolimus (marketed as Afinitor®) as an anticancer drug for several forms of solid tumors (e.g. renal cell cancer in 2009, subependymal giant cell astrocytoma in 2010 and some forms of advanced neuroendocrine tumors in 2011).
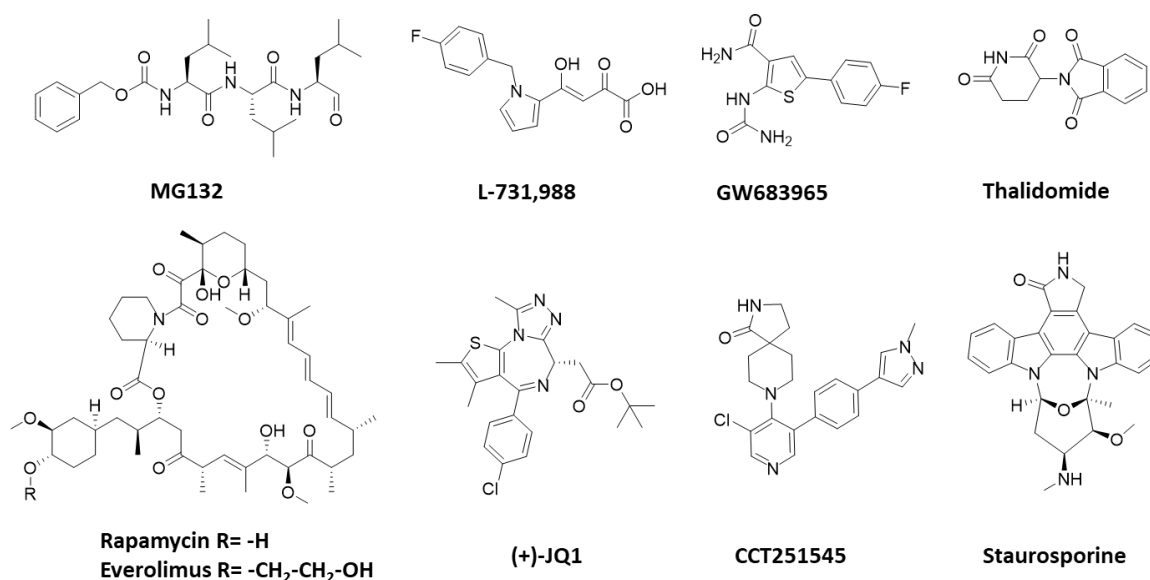
Figure 1.1-2 Examples of well-validated chemical probes (MG132, L-731,988, GW683965, Thalidomide, Rapamycin, (+)-JQ1 and CCT251545) and a promiscuous kinase inhibitor several times misemployed as a chemical probe (Staurosporine). Everolimus, a clinically approved immunosuppressive and anticancer agent, is also depicted.

The discovery of BET Bromodomain inhibitors is one of the most well-known and recent successful examples of the use of chemical probes for investigating and linking target modulation to therapeutic effect. The disclosure by Mitsubishi Pharmaceuticals of the thienotriazolediazepine as a chemical class of compounds inhibiting binding of acetylated histones with bromodomain containing proteins set up an interesting chemical starting point for further investigation of the modulation of epigenetic targets by small molecules.[21] SAR analysis and computer-aided drug design methods (CADD) in addition to the development of a screening platform for bromodomain isoforms led to the identification of (+)-JQ1 **(Figure 1.1-2)** as a prototype ligand for the BET bromodomain family.[16] X-Ray studies on co-crystal structures and molecular dynamics investigation aided by the availability of an inactive enantiomer as a negative control compound, (-)-JQ1, enabled the discovery of the ligand binding mode and understanding of the key features of the ε-N-acetylated lysine pocket (Kac pocket) where (+)-JQ1 binds.[16] In addition, (+)-JQ1 was applied to a disease relevant phenotype of human osteosarcoma cell (U2OS) transfected with fluorescently labelled BRD4 (GFP-BRD4) for proving in cell BRD4 target engagement using fluorescent recovery after photo bleaching techniques (FRAP). This experiment clearly showed that the chemical probe binds with BRD4 in competition with chromatin. Furthermore, the compound was used to validate the inhibition of BET protein as a mechanism for inducing cell differentiation and growth arrest in nuclear protein in testis midline carcinoma cells derived from patients (NMC 797 cells).[16]

CCT251545 **(Figure 1.1-2)** is another example of a chemical probe which had a major impact in drug discovery for investigating the Mediator complex involved in several human pathologies.[17,22] This molecule was developed by optimization of the 3,4,5-trisubstituted pyridine chemical series identified through phenotype-based screening for modulators of the Wnt signaling pathway.[23] A nice target identification effort using Stable Isotope Labeling by Amino acids in Cell culture associated to Mass Spectroscopy (SILAC-MS), kinase selectivity data, *in vitro* and in cell biophysical approaches and correlation between biochemical and cellular data led to the discovery that CCT251545 is a potent and selective cellular inhibitor of cyclin-dependent kinase 8 and 19 (CDK8 and CDK19). Using X-Ray crystallography its binding mode was revealed. CCT251545 is a Type I binder which brings peculiarly the C-terminus of CDK8 inside the molecule binding site thanks to a pi-cation interaction between the compound phenyl ring and Arg356 of the C-terminus. This particular binding mode provides an exquisite cellular activity and selectivity not previously observed using Type II inhibitors of CDK8 and CDK19. This molecule is, therefore, a potent and selective chemical probe for the human Mediator complex associated to CDK8 and CDK19. Additionally, CCT251545 enabled the identification of phospho-STAT1[SER727]as a biomarker for CDK8 inhibition *in vitro* and *in vivo*. As a final point, CCT251545 acts by downregulating the expression of Wnt pathway-regulated genes showing efficacy in Wnt-driven colorectal and breast cancer models.[17] The discovery of CCT251545 and the understanding of its on-target effects clearly increased the interest of targeting CDK8 in the drug discovery community. CCT251545 and a structurally different highly selective dual CDK8/19 modulator, MSC2530818, are now under preclinical evaluation for efficacy, tolerability and safety.[24]

Contrary to the previously mentioned successful stories about the use of chemical probes in drug discovery, there is still a significant use of "poor quality" chemical tools with potential to mislead. This phenomenon is observed despite several commentaries and reviews advising the users to choose carefully and wisely their chemical probe utilizing guidelines such as "Fitness Factors", ''Dos and Don'ts'', databases (e.g. https://probeminer.icr.ac.uk/#/) and knowledge built by chemical biology organizations (e.g. Structural Genomics Consortium) or pre-competitive collaboration projects between academia and industry (e.g. Donated Chemical Probes project; http://www.sgc-ffm.uni-frankfurt.de).[25-27]

Staurosporine (ST) **(Figure 1.1-2)** is a classic example reported in several commentary articles of a molecule misused as a chemical probe.[2,9,28] Frey defines ST as the "archetype of the probe gone bad".[9] This compound, a microbial alkaloid, was originally identified as a potent Protein Kinase C (PKC) inhibitor with interesting antiproliferative and antifungal effects.[29] However, further biological profiling of ST against a kinase panel of 290 proteins clearly highlighted its extremely high kinase inhibition promiscuity with a selectivity score equal to 0.87 (the selectivity score was calculated dividing the number of protein kinases to which a certain compound was binding with K_d<3 µM by the total number of kinases tested).[30] The poor selectivity of ST should clearly discourage its use as a chemical probe to investigate mechanistic and phenotypic questions; instead, more highly selective compounds should be chosen. Nevertheless, ST was still used as a chemical probe after being discovered to be a pan-Kinase inhibitor.[2]

The use of chemical probes for target validation is clearly complementary to some genetic approaches to interrogate biological pathways such as RNAi and CRISPR-Cas9[31,32] while offering certain advantages. A great advantage of chemical probes compared to genetic approaches is the possibility to induce reversibly a biological effect in a time dependent manner.[2] Likewise, the possibility to use structurally distinct probes (orthogonal probes) at the same time to investigate the link between different pathways is another advantage. Furthermore, using a combination of genetic approaches

and chemical probes can be exceptionally advantageous for confirming on-target effects, excluding scaffolding effects and to rule-out false positives due to cross-talk between unknown off-target activities and pathways.[2]

1.2   Bespoke chemical probes

Certain small molecule chemical probes can be modified by introducing a "Click" reactive group (e.g. azide, alkynes etc.) to be further biotinylated or conjugated to resin or beads generating new probes useful for protein affinity purification (PAP) followed by subsequent mass spectrometry (MS) proteomics. Recent advanced methods combining quantitative proteomics (e.g. SILAC and Tandem Mass Tag) with affinity enrichment have been utilized for assessing target engagement and selectivity.[33] Tool compounds can also be modified by an orthogonal addition of a photoactivatable group such as alkyl diazirine for photo affinity labelling (PAL) followed by visualization of the crossed-linked protein using a reporter group (e.g. fluorophore, radioactive label or biotin).[34] Finally, chemical modification of tool compounds with an electrophile (e.g. α-chloroacetyl, acrylamide) might allow generation of chemical probes for activity-based protein profiling (ABPP)[35]. Consequently, the chemical versatility of orthogonally reactive probes enables the user to apply diverse approaches for investigating the tool compound selectivity, validating the target and exploring its pharmacology.

A nice example of application of ABPP for reversible inhibitors was reported by Salisbury and Cravatt in 2007.[36] The authors used ABPP for identifying the targets and investigating the selectivity profile of the histone deacetylase (HDAC) inhibitor suberoylanilide hydroxamic acid (SAHA) (**Figure 1.2-1**). Their studies proved that SAHA binds only 4 histone deacetylases (HDACs) and not all the HDAC enzymes belonging to class I and II.[36] Histone acetyl transferases (HATs) and histone deacetylases (HDACs) are enzyme families regulating the acetylation of histone tails. The acetylation status of the histone tails modulates transcriptional activation and repression of genes.[36] Removal of acetyl groups from histones by HDACs induces a chromatin remodeling which communicates to the transcriptional machinery through "reader proteins" recognizing and binding specific chromatin sites.[37]
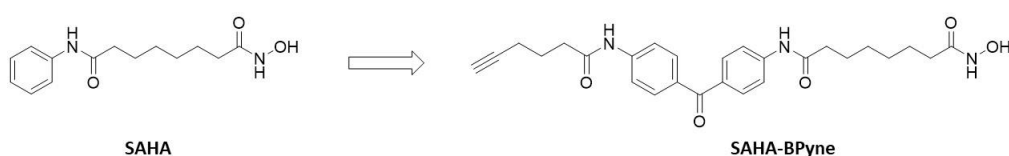
Figure 1.2-1 Suberoylanilide hydroxamic acid (SAHA) and the affinity based chemical proteomics chemical probe for HDAC (SAHA-Bpyne) developed by Salisbury and Cravatt for target identification and compound selectivity assessment.

Hence, this epigenetic event, if not tightly regulated, appears to be linked to the onset and progression of disease, such as cancer. HDACs are divided into three classes using yeast homology models. Class I and II are zinc-dependent metallohydrolases and Class III are NAD$^+$-dependent deacetylases.[36] Class I/II pan inhibitors induce growth arrest, differentiation and apoptosis of tumor in cell disease models.[38] In cells HDACs are part of big functional complexes required for the deacetylating activity while the isolated enzymes are inactive.[36] For that reason, biochemical studies using purified proteins and recombinant systems are difficult and poorly representative of the cellular machinery.[36]

Salisbury and Cravatt designed a covalent activity-based proteomic probe (SAHA-BPyne) starting from the reversible HDAC inhibitor, SAHA **(Figure 1.2-1).** Their chemical probe contained a benzophenone moiety capable of covalent

tagging proximal proteins upon UV irradiation (benzophenone produces a reactive triplet diradical upon UV irradiation)[39] and a "Click" chemistry handle (alkyne) for conjugation to a fluorophore reporter (Rhodamine based) or biotin containing group for target enrichment **(Figure 1.2-2).**
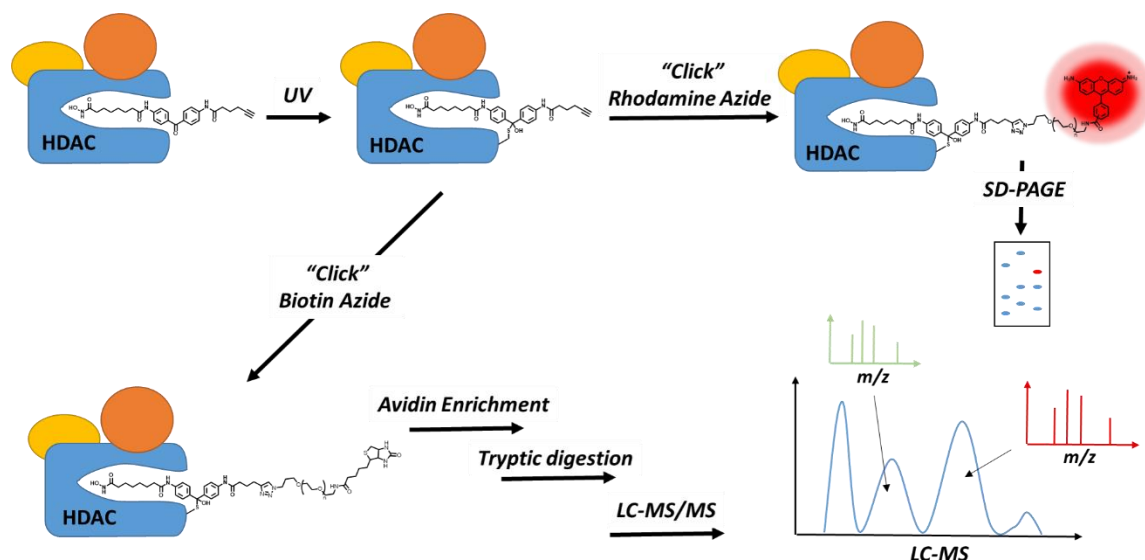
Figure 1.2-2 Schematic representation of the activity-based protein profiling approach applied by Salisbury and Cravatt to identify the targets of SAHA (picture adapted from *Nature Methods 4, 822-827 (2007)*).

They applied SAHA-BPyne to lysates obtained from aggressive and nonaggressive human melanoma cell lines (MUM2B and MUM2C respectively) in the presence or absence of SAHA as a competitor (control sample). Upon activation of the photo-affinity handle using UV light, they treated the samples with a fluorescent chemical reporter for a fast detection of the potential targets and a chemical reporter for affinity enrichment. The samples were reacted with azide reporters using copper-catalyzed azide-alkyne cycloaddition (CuAAC) "Click" chemistry conditions (**Figure 1.2-2**).[40] Therefore, the first sample was reacted with a rhodamine-azide and analyzed using sodium dodecyl sulfate polyacrylamide gel electrophoresis (SDS-PAGE) coupled with fluorescent visualization scanning (**Figure 1.2-2**). Target proteins with molecular mass in the range of HDAC proteins were identified. Subsequently, they were able to restrict the number of potential target hits following a similar protocol but using a biotin-azide as reporter and analyzing the sample with ABPP-multidimensional protein identification technology (ABPP-MudPIT)(**Figure 1.2-2**). As a result, they identified HDAC1, HDAC2 and HDAC6 as potential targets of SAHA and additional non-HDAC proteins as components of HDAC complexes (e.g. CoREST, MBD3, p66β etc.). Finally, their protein hits were confirmed in a separate experiment by western blotting. A similar approach was applied to live cells too. Cells were incubated with SAHA-BPyne alone and in the presence of an excess of SAHA. After UV irradiation and some washing steps, the cells were lysed. The obtained samples were then analyzed using SDS-PAGE. Besides confirming HDAC1, HDAC2 as SAHA targets, other HDACs were identified. To explain this finding, the authors suggested a possible interference between the homogenization processes and the HDAC complex stability.

This example clearly highlights the great potential of using chemical probes tagged with biologically silent groups, which can be subsequently activated or reacted with bioorthogonal reagents to identify targets, prove target engagement and assess selectivity of tool compounds.
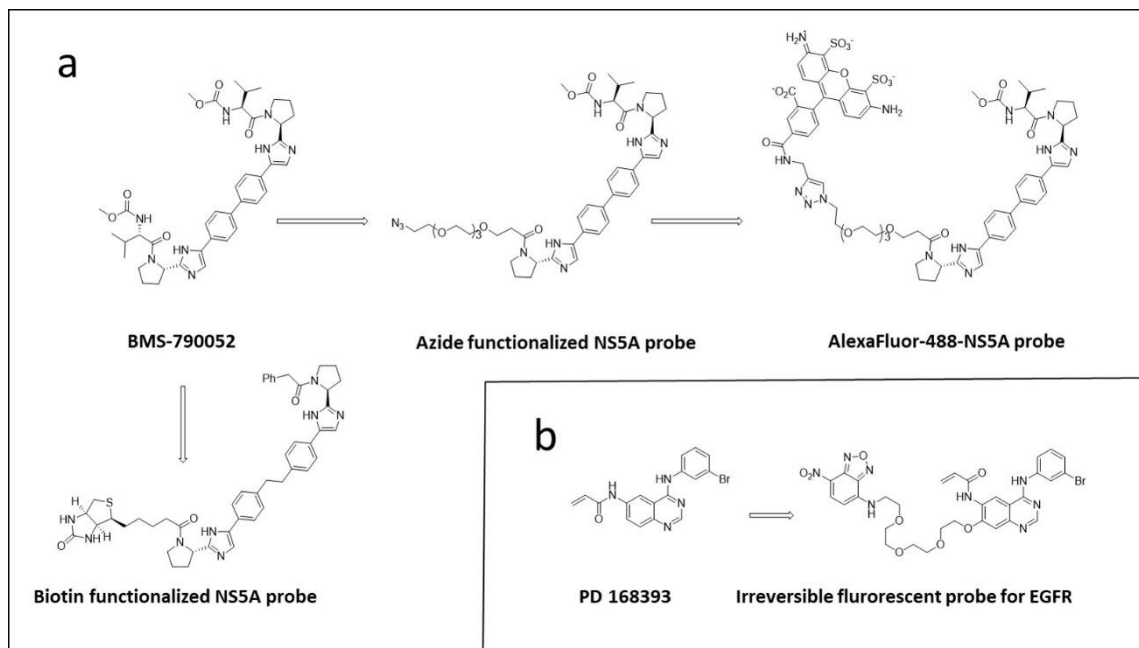
Figure 1.2-3 **a**) BMS-790052 (selective inhibitor of NS5A) and its respective azide and biotin derivatives used to investigate the compound MoA. Depicted in the picture the AlexaFluor488-BMS-790052 "Click" chemistry product used for investigating intracellular distribution and probe and target co-localization. **b**) The EGFR covalent inhibitor PD168393 and its fluorescent analogue used for receptor occupancy studies.

Other interesting literature examples report the use of the same chemical probe modified with a variety of moieties (e.g. biotin) and functional groups (e.g. azide) to confirm MoA by pull down experiment and fluorescent imaging methods for intracellular distribution and probe-target co-localization.

Daclatasvir (BMS-790052) is a highly selective inhibitor of HCV NS5A. Starting from this compound and knowing SAR around this chemotype, Jones et al. prepared a set of chemical probes to investigate its MoA **(Figure 1.2-3a)**.[41] Using a similar strategy, fluorescent imaging approaches have been used to determine tool compound receptor occupancy using pre-labeled probes (e.g. covalent EGFR inhibitors) **(Figure 1.2-3b)**.[42]

1.2.1. Chemical probe design

Despite the number of publications describing well-validated chemical probes, often and for several reasons, it is very difficult to identify and select the appropriate high quality molecule for validating a disease model.

This is particularly true for exploration of new biological targets. In the ideal scenario, the researcher would have access to compounds which are commercially available, potent, well characterized in terms of selectivity and chemically and metabolically stable etc.[2,9] Additionally, a close analogue of the selected chemical probe (e.g. inactive enantiomer) with no activity on the target of interest should be made available to be used as a negative control compound **(Figure 1.2-4)**.[1,2]

To address a lack of availability of the desired chemical probe, the researcher might engage in the validation of bespoke probes identified by phenotypic screening or known in the literature but not fully validated and characterized.[1] The chemical probe design should aim at compounds with high potency in biochemical and cellular assays, which are selective against target subfamilies and potentially known scaffold, related specific off-targets. Furthermore, they should be cellularly permeable, soluble, chemically stable and chemically readily accessible and easily modifiable (**Figure 1.2-4)**. Further, the chemical probe design may be strengthened by in silico tools, virtual screening and a scrupulous data mining.[43]
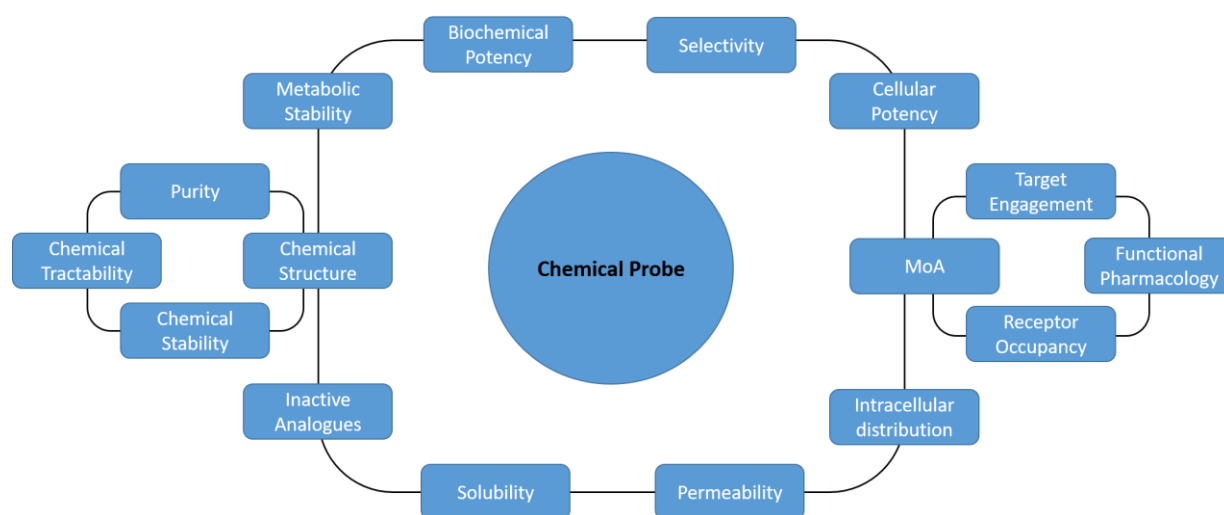
Figure 1.2-4 Criteria for chemical probe design and validation in cellular disease models.

A chemical probe should not be confused with a lead compound to be progressed in a drug optimization phase. Therefore, for its design and identification, the medicinal chemist should not apply the typical selection criteria employed during the analysis of a HTS campaign. Those criteria aim at the identification of compounds without innate chemical structure burdens (e.g. chemically intractable) and potential toxicity issues, which might be liabilities for a lead compound, however may not exclude their use as chemical probes. Furthermore, the selectivity criteria applied to the chemical probe design and its validation should be more stringent compared to the one applied to a lead compound for which a poly-pharmacology is, sometimes, desired.[1] However, if off-target activities are known and judged unrelated to the biology under investigation, a less selective chemical probe might be still employed.[2]

1.3   Chemical probe validation in cellular disease model

After the probe synthesis, a careful chemical characterization (e.g. purity and chemical stability) and an assessment of the physico-chemical properties (e.g. solubility) should be carried out before starting the set of validation studies in cells. These final investigations should aim to confirm the compound exposure, target engagement, functional pharmacology and phenotypic perturbation in the cellular disease model (**Figure 1.1-1**).

While the assessment of the chemical properties, the physico-chemical properties and the biochemical profile (biochemical activity and selectivity) of a chemical probe is becoming increasingly straightforward for a conventional chemical biology institution, the validation in the cellular disease model is more tedious.

Some aspects of the cellular chemical probe validation and in particular, the assessment of chemical probe permeability, intracellular concentration, target engagement, receptor occupancy, are still quite laborious tasks which often involve the use of diverse advanced technologies in parallel.

Assessing compound permeability using high-throughput methods is now routine in drug discovery. These methods use prevalently Caco-2 (human colon carcinoma) and MDCK (Madin Darby canine kidney) cell lines as model barrier systems.[44] The first model well represents passive permeation, while the second one can be additionally used to investigate compound efflux (e.g. P-glycoprotein) and active transport.[45] The molecule's permeability is expressed as a permeability coefficient P (measured in cm/s) and represents the capacity of the molecule to permeate the cell monolayers.[44] Despite the important role that these assays have in drug discovery for prediction of oral absorption during pharmacokinetic optimization, their use for predicting cellular permeability of a chemical probe in a disease model should be discouraged due to differences in membrane transporter expression between cell lines.

While it is possible to apply fairly simple and readily available technologies for estimating cellular up-take of chemical probes (e.g. LC-MS), the accurate assessment of the intracellular concentration requires more advanced approaches and equipment. Besides, the analytical method of MS-based technologies is usually run on samples obtained after lysis of the compound-treated cells. The obvious drawback of this process is the possibility to underestimate uptake by losing membrane-bound compound during the sample preparation. When the chemical probe is a peptide, the protocol for applying MS-based technologies becomes even more complicated and requires, for example, labelling of the chemical probe and use of internal standards for improving sensitivity.[46]

More advanced approaches are now under development with the intent to minimize the perturbation of the cell model by sampling intracellular content using technologies such as the micro capillary or the fluidic force microscopy associated to MS (e.g. fluidic force microscopy, followed by matrix assisted laser desorption/ionization time of flight mass spectrometry (FluidFM-MALDI-TOF-MS)).[47,48]

For peptidic molecules, imaging methods such as confocal microscopy and flow cytometry applied on fluorescently tagged compounds are the most used for cellular uptake studies,[49-51] however fluorescence technologies can also be used for more detailed mechanistic investigation (as described below).

In order to generate a biological response the chemical probe not only has to penetrate the cells but, as well, reach the intracellular location of its target at the concentration required to elicit the biological effect.[52] Many compounds, for which intracellular distribution studies have been reported, showed subcellular distribution into single organelles and compartments while only a minority of them showed distribution to multiple sites.[53] Additionally, intracellular distribution of molecules is governed by several factors such as transporters and specific compartmental pH which can be dissimilar in different cell lines.[52] In summary, the compound intracellular distribution can be heterogeneous between the subcellular compartments and cell specific; consequently, intracellular distribution studies in the specific cellular disease model becomes even more relevant for validating our chemical probes.

Fluorescent imaging technologies are the most used methods for studying compound intracellular distribution and, when the chemical probe is a peptide, are the most used for studying cellular uptake too. These approaches usually require the labelling of the chemical probe with a fluorophore which might greatly impact the intracellular distribution and uptake of the parent compound.[54] However, the use of "Click" mediated labelling can greatly improve the quality

and sensitivity of our study. In this approach, the compound can be labelled using a small alkyne moiety with less impact on the properties of the parent compound therefore acting as a better surrogate molecule.[41,55]

Target engagement is the ability of a compound to bind a target in a living system (cells or animals). The proof of target engagement enables correlation of the target modulation to the observed phenotypic effect. Target occupancy studies aim to quantify the binding of a compound to its target and to link this measurement with a pharmacodynamic (PD) effect measured with biomarkers. The quantification of the target engagement can be proved by measuring the interaction between the probe and the protein in the desired disease model or, if the target is an enzyme, by assessing modulation of enzymatic activity and its substrates (e.g. measuring downstream phosphorylated substrate using chemoproteomics methods).[56] Several approaches have been developed to investigate target engagement such as radioligand displacement,[57] Fluorescence Resonance Energy Transfer Fluorescence Lifetime Imaging Microscopy (FRET-FLIM)[58] and Bioluminescence Resonance Energy Transfer (BRET),[59] the previously mentioned ABCP using covalent binders,[36] Ligand-Directed Protein Labeling,[60] Cellular Thermal Shift Assay (CETSA)[61,62] and so on.[63] Most of these methods required the modification of the chemical probe, the target or both, with radiolabels, fluorophores or chemical tags (e.g. bioorthogonally reactive groups). The only label free approach, the CETSA, based on the modified thermal stability of the protein induced by the binding compound, suffers potential drawbacks related to the level of expression of the target, its size and a potential weak stabilization of the target induced by the probe.[63]

One of the common features of the previously mentioned approaches is the tagging of the chemical probe with a "clickable" moiety. This reactive chemical functionality can be used as a handle to react with an imaging reporter. This approach has been used to study cellular uptake (Alkyne functionalized geranylgeranyl-CPP, **Figure 1.3-1),**[55] intracellular distribution (Azide functionalized NS5A probe, **Figure 1.2-3a**),[41] target engagement and receptor occupancy (SAHA-BPyne, **Figure 1.2-1 and 1.2-2**)[36]
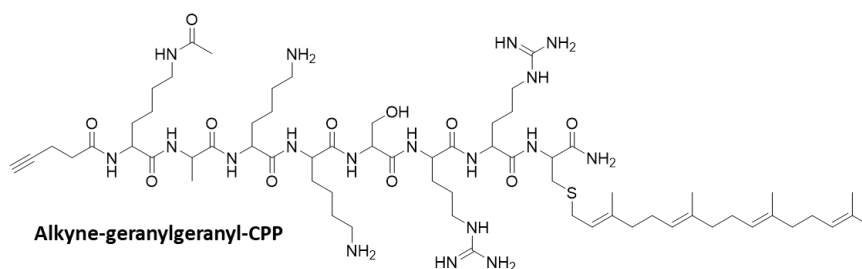
Figure 1.3-1 Alkyne functionalized geranylgeranyl-CPP used for cellular uptake studies

The reported examples generally require the lysis of cells treated with the chemical probe, although this drawback could be overcome, in most cases, by employing a bioorthogonal functionalization approach.

1.4   Bioorthogonal chemistry

The term "Bioorthogonal chemistry" was coined by Carolyn Bertozzi about 10 years ago to describe chemical reactions which can be performed in living organisms without interfering with their native biochemical processes. Most of the early work in this field related to tagging of biomolecules in cellular systems.

Being able to simply chemically functionalize the bioorthogonal probes in a living system allows us to run experiments to study mechanisms in a non-destructive way (e.g. study target engagement using fluorescent reporters rather than pulldown experiment in cell lysates) and to use wild-type cell lines rather than engineered lines. Thus, a bioorthogonal tagging approach overcomes certain disadvantages and is complementary to other chemical biology methods.

1.4.1. The bioorthogonal chemistry reaction toolbox

In the last two decades, the bioorthogonal chemistry reaction toolbox has significantly grown. A bioorthogonal reaction should be efficient, chemoselective and tolerate aqueous environments. In particular, the bioorthogonal groups should be stable in the presence of high concentrations of cellular nucleophiles.

1.4.2. Bioorthogonal chemistry associated to fluorescence and bioluminescence techniques

Nucleic acids, lipids, proteins and small molecules can be covalently tagged with fluorescent and bioluminescent reporters such as dyes, quantum dots and bioluminescent enzyme substrates to enable imaging in a cell system. Furthermore, great developments in the field of cell imaging technologies has made this a powerful technique to investigate chemical probes and provide insights on their mode of action and inform on complex dynamic cellular processes including transient responses.[64]

Although a pre-labelling approach of the molecule of interest is an important strategy for monitoring its intracellular localization and its dynamic activities, this has its drawbacks and limitations.

For example, the fusion of fluorescent proteins (e.g. GFP) to a protein of interest can raise concerns regarding the perturbation of its intracellular localization, its expression level and activity due to the relatively high increase in size brought by the fluorescent protein (e.g. ca. 27 kDa). On the contrary, a site-specific modification of the protein of interest with un-natural amino acids functionalized with bioorthogonal groups (e.g. trans-Cyclooctene, tetrazine etc.) is a relatively small modification. Subsequent chemical labelling of the protein in a cellular system might overall provide a better surrogate model for studying the protein of interest, such as its intracellular trafficking.[65]

Bioorthogonal chemistry applied to fluorescence and bioluminescence techniques has been used for imaging the behavior of small molecules such as Taxol[66,67] or proteins such as Aurora A[68] and Polo-like kinase 1[69] in cells, to study intracellular uptake of compounds such as fatty acids[70] and for several other biomedical research applications.[71-76] This technology can be an extremely powerful tool to validate and investigate the chemical and pharmacological properties of probes. Although, several papers described intracellular distribution studies for small molecules via bioorthogonal approaches, only a few of them describe intracellular quantification methods.[70,73,77,78] To date, bioorthogonal chemistry is one of the emerging technologies to study target engagement using activity-based protein profiling reagents[79,80], which can be used in living organisms.[81]

1.5   Conclusion

A lack of efficacy of the drug candidates and poor validation and translatability of their proposed mechanisms of action are key factors in the high attrition rate that many drug discovery programs are facing in clinical trials. A better

characterization of the new molecular entities (NME) (e.g. target engagement, exposure at the site of action, pharmacological activity) would improve pharmacokinetics-pharmacodynamics models (PK-PD) in the preclinical phase and increase the proof of concept (POC) rate in clinical trials.[82] Well-validated chemical probes enable testing of a biological hypothesis, investigation of target tractability and aid translatability in the clinical phase. Besides, these important tool compounds can contribute to identifying biomarkers and building pharmacodynamic models for testing drug candidates. While, several well validated chemical probes are now available to the drug discovery community, there is still a high need for bespoke probes to investigate new biological hypotheses. The validation of bespoke chemical probes in cell disease models requires the assessment of their cellular permeability, intracellular distribution, target engagement and occupancy. Despite several technologies to enable the investigation of chemical probe characteristics, specialized scientists, the use of different equipment and advance software are required for each study. Furthermore, a chemical functionalization of the molecule is often necessary. Bioorthogonal probes can be generated via modifying chemical probes such as low molecular weight compounds (LMW), peptides etc. with moieties that are inert in biological systems but very reactive towards other bioorthogonal functional groups. A small derivatization of the chemical probes is preferable in order to avoid an excessive modification of their biological and physico-chemical properties. Contrary to chemical probes, bioorthogonal probes can be modified in cells via biocompatible reactions with chemical reporters (e.g. fluorophores), allowing their direct visualization rather than measuring downstream effects. An assay platform may be established in order to validate bioorthogonal probes in relevant cell disease models. Their visualization using imaging techniques can provide information regarding their permeability and intracellular distribution while immunostaining of the target and fluorescent labeling of the chemical probe can confirm their co-localization [66,69] and enable the design of target engagement and occupancy assays.

Chapter 2. Mdm2-p53 interaction inhibition as a biological model for bioorthogonal probe validation

We selected the inhibition of the Mdm2-p53 protein-protein interaction as the biological model for generating a set of bioorthogonal probes. Subsequently, we made use of the synthesized molecules to develop a set of assays based on imaging techniques enabling the bioorthogonal probe validation in a cell model of osteosarcoma. Our biology model selection was based on the extensive and well-documented knowledge of the Mdm2-p53 pathway in combination with the availability of a large set of chemical structures with known mode of action.

2.1   Mdm2-p53 auto-regulatory feedback loop

The activity and protein level of the tumor suppressor p53 is regulated by murine double minute 2 protein (Mdm2, also called HDM2) through an auto-regulatory feedback-loop (**Figure 2.1-1**).[83]

Wild type p53 acts as a transcription factor targeting the Mdm2 gene for its activation and, as a consequence, regulating Mdm2 expression level (**Figure 2-1**).[84] p53 contains a transactivation domain to which Mdm2 can bind; this binding event leads to p53 inactivation by blocking its sequence-specific DNA-binding factor.[85]
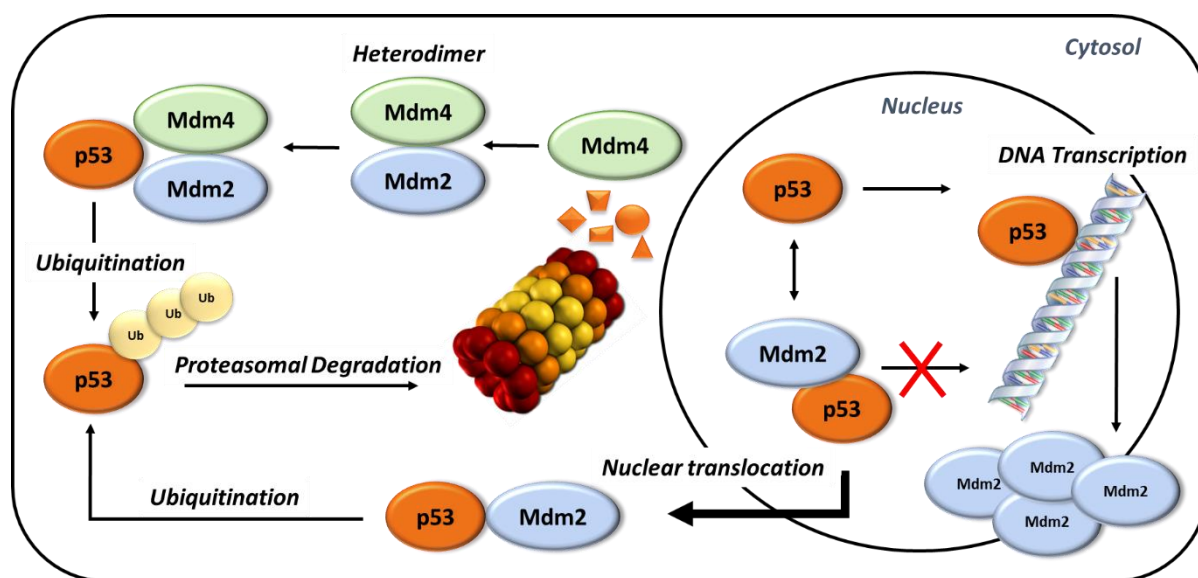
Figure 2.1-1 Role of Mdm2 and Mdm4 in regulating p53 activity and expression level

Mdm2 is a ubiquitously expressed protein with p53 dependent and independent functions. This protein travels between the cytoplasm and the nucleus thanks to an export signal sequence similar to the one of some protein viruses.[86] Mdm2 is an E3 ubiquitin protein-ligase (RING finger family) that represses transcriptional activity of p53, it transports p53 from the nucleus to the cytoplasm where, finally, it ubiquitinates p53 inducing its degradation through the proteasome (**Figure 2.1-1**).

In normal cells, p53 is constantly degraded by Mdm2 which maintains its cellular concentration at a low level. On the contrary, during genotoxic and cytotoxic stress, p53 phosphorylation precludes its degradation since the protein is incapable of binding to Mdm2.[87] In normal cells, Mdm2 sumoylation (another post-translational protein modification)[88] preserves the protein by auto-ubiquitination and, consequently, it prevents its own degradation increasing its ability to ubiquitinate p53. Finally, cell stress induced by extracellular events (e.g. DNA damage induced by UV and IR) and intracellular events (e.g. oncogenes, cell cycle transition) regulate Mdm2 levels via very diverse mechanisms and pathways.[89]

After the discovery of the Mdm2-p53 feedback loop, another protein of the Mdm family, Mdm4 (previously named MdmX) was identified.[90] This protein has high structural homology with Mdm2 and also binds to p53. Hence, in both Mdm proteins the C-terminals are RING-domains while the N-terminals are p53 binding domains.[91] Mdm4 regulates p53 activity by binding to its transactivation domain in analogy with the Mdm2 binding mode. Despite both Mdm2 and Mdm4 have a RING finger domain, Mdm4 does not have E3 ligase activity.[92] On the contrary, the heterodimers formed by the binding between Mdm4 and Mdm2 have ubiquitin ligase activity toward p53 in physiological states (**Figure 2.1-1**).[91] As a consequence, Mdm4 appears to act as a potentiator of the Mdm2 E3 ligase activity.[93]

2.2   Disrupting the Mdm2-p53 interaction: a promising approach for cancer therapy

The protein p53 is involved in regulating diverse cellular processes such as cell cycle, apoptosis, DNA repair, angiogenesis and senescence.[94] Deletion or mutations of the p53 gene, *TP53*, lead to protein loss or inactivation and were found in about 50% of human cancers.[95] Moreover, *in vivo* studies using p53 knockout mice (homozygous p53$^{-/-}$ lacking both p53 functional alleles) showed that the animals had a normal development while being more prone to developing tumors.[96] Finally, a major conversion from benign to malignant forms was observed in p53 knockout mice compared to wild-type animals.[97] While p53 is a tumor suppressor, an amplification of Mdm2 is oncogenic.[85]

The p53-Mdm2 autoregulatory feedback loop (**Figure 2.1-1**) highlights the role played by Mdm2 as a negative regulator of wild-type p53. Consequently, disruption of the p53-Mdm2 complex should prevent p53 translocation to the cytosol, stop degradation of p53 induced by Mdm2 mediated ubiquitination and, as a result, restore p53 activity as transcription factor.

The important role of p53 as a tumor suppressor became clear in the period between 1980 and the early 1990s, following evidence provided by cell biology experiments,[98,99] molecular genetics[100-104] and animal model studies[96,97,105].[94] However, it was only in 1992 that the protein-protein interaction (PPI) between p53 and Mdm2 was discovered.[106] Levine and Pavletich from the Memorial Sloan-Kettering Cancer Center, New York, reported for the first time in 1996 a high-resolution co-crystal structure of the amino-terminal domain of Mdm2 (109 residues) bound to a peptide part of the p53 transactivation domain (15 residues).[107] This peptide, in a α-helical conformation, binds to the Mdm2 cleft primarily by burying three hydrophobic amino acids, Phe19, Trp23, and Leu26 in a relatively deep hydrophobic pocket on the protein surface.[107]

Since then, it became very clear to the oncology research community that disrupting the p53-Mdm2 complex was not only a new attractive approach for targeted cancer therapy but this could be supported by rational drug design.[83,108,109]

Consequently, several research groups put significant effort into trying to disrupt this protein complex by developing initially large PPI inhibitor peptides [110-112].

At the time, the protein-protein interaction targets were considered almost "undruggable" with small molecules. In general, PPI interfaces are quite flat, large (about 1000-2000 A^2), and relatively shallow. For those reasons, it appeared to be reasonably difficult to identify a small molecule with enough affinity for one of the protein interfaces to disrupt the protein-protein interaction while retaining drug-like properties. Nevertheless, PPI small molecule inhibitors were considered very attractive for the potential interesting selectivity profile which such molecules could have reached in comparison to active site inhibitors (active sites are usually more conserved).[113]

In 2004, the Roche group reported the first small molecule inhibitors of the Mdm2-p53 PPI complex.[114] These compounds belong to the chemical series of the *cis*-imidazolines and they were named Nutlins. A co-crystallization of one of these analogues (Nutlin-2) (**Figure 2.2-1**) with Mdm2 highlighted that this compound occupies the same pocket previously identified by Levine and Pavletich using the 15 residue p53 peptide. Furthermore, this experiment showed that the imidazoline scaffold is a sort of replacement of the p53 peptide backbone and directs the two halo-phenyl groups into the Leu26 and
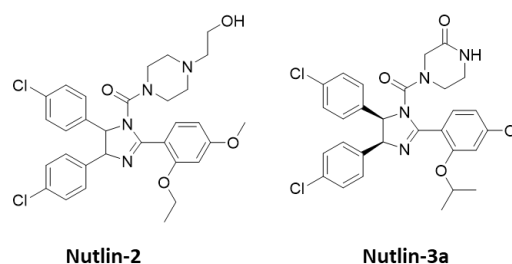
Nutlin-2   **Nutlin-3a**

Figure 2.2-1 The structure of Nutlin-2 and Nutlin-3a, two of the first reported molecules Mdm2-p53 PPI inhibitors

Trp23 pockets and the alkyl ether group into the Phe19 pocket. The Nutlins tested on wild-Type p53 human cell lines (HCT116 and RKO) showed the expected pharmacological profile leading to increased levels of p53, Mdm2 and p21 (a transcriptional target of p53). Furthermore, the compounds tested on p53 mutated cell lines did not show an increase of Mdm2 and p21 which confirmed the effect of Nutlins on the p53 pathway. Finally, a pure enantiomer and the most active compound (Nutlin-3a) (**Figure 2-2**) showed efficacy in a tumor xenograft animal model (human osteosarcoma cell line (SJSA-1) grafted on nude mice).

2.3   Mdm2-p53 protein-protein interaction inhibitors

Several pharmaceutical companies and research laboratories have invested in the discovery of Mdm2-p53 PPI inhibitors and seven of their small molecule compounds and one stapled peptide (ALRN-6924 from Aileron) have progressed to clinical trials and are now under evaluation, either alone or as part of a combination therapy for the treatment of diverse forms of oncology disease.[85,115] Hence, the structures of six of those clinical candidates, RG7112, RG7388, MI-77301 and AMG 232, NVP-CGM097 and S-3032b (**Figure 2.3-1**) have been disclosed.[85]

Furthermore, numerous additional Mdm2-p53 PPI chemotypes have been released into the public domain by the medicinal chemistry community (see **Figure 2.3-2** for some examples).

RG7112
Hoffmann-La Roche

RG7388
Hoffmann-La Roche

MI-77301
Univ.Michigan - Sanofi

AMG 232
Amgen

NVP-CGM097
Novartis

S-3032b
Daiichi-Sankyo
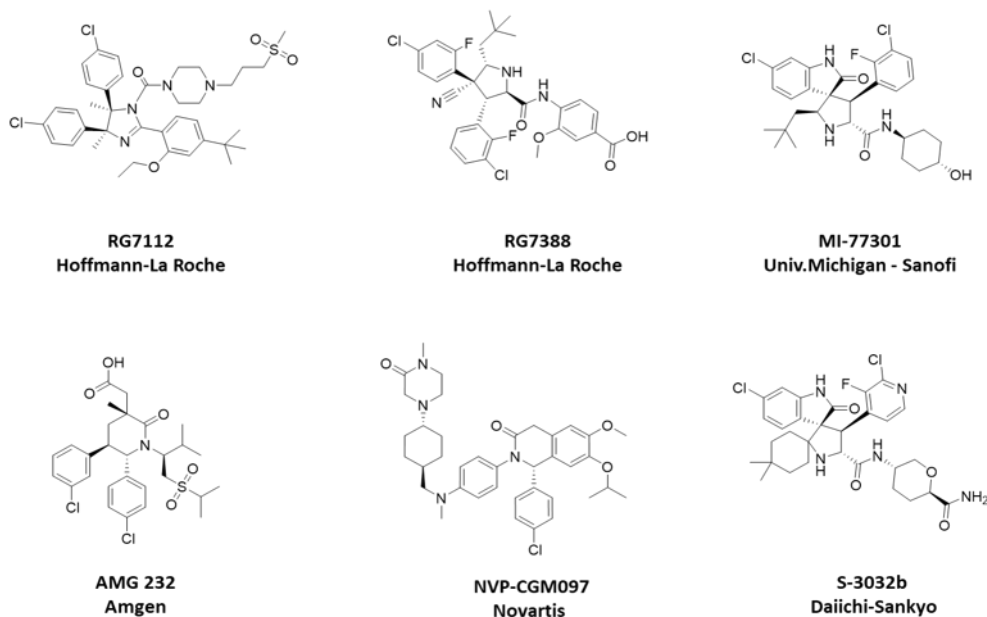
Figure 2.3-1 The six clinical candidates for which the structures have been disclosed (adapted from *R.P. Wurz; J. Med. Chem. 2019, 62, 445–447*)

Despite these molecules not reaching clinical investigation and their binding modes being very similar (with key substituent groups occupying Leu 26,Trp 23 and Phe 19 pockets) they are useful tool compounds for probing the effect of inhibiting the Mdm2-p53 PPI. Furthermore, the availability of chemical probes based on different chemical scaffolds (see **Figure 2.3-2**) enables the user to choose between very diverse chemical matter bearing a range of physico-chemical properties and biological activity profiles (e.g. on target potency and selectivity) (see **Figure 2-4** for reported biochemical IC_{50} and MW, CLogP and tPSA calculated using ChemBioOffice software).

1,4-benzodiazepine-2,5-dione
IC_{50}= 394 nM
MW= 654; CLogP=6.9; tPSA = 68

Isoindolinone
IC_{50}= 170 nM
MW= 478; CLogP=4.8; tPSA =101

3-imidazolyl-indole
IC_{50}= 30 nM
MW= 574; CLogP=5.9; tPSA=69

Morpholinone
IC_{50}= 0.4 nM
MW= 568; CLogP=5.5; tPSA=100

spiro[pyrrolidine-3,6'-thieno[3,2-b]pyrrol]-5'(4'H)-one
IC_{50}= 6 nM
MW= 619; CLogP=4.8; tPSA=122

Piperidine
IC_{50}= 169 nM
MW= 680; CLogP=5.7; tPSA = 83

Chromenotriazolopyrimidine
IC_{50}= 350 nM
MW= 636; CLogP=7.2; tPSA=77

2-oxospiro[indoline-3,2'-thiazolidine]
IC_{50}= > 5 µM
MW= 481; CLogP=5.5; tPSA=67

Figure 2.3-2 Example of Mdm2-p53 PPI inhibitors belonging to very diverse chemotypes. The structures and their reported biochemical IC_{50} are depicted in the figure. MW, CLogP and tPSA were calculated using ChemBioOffice. (Figure adapted from *Zhao,Y., et al. J Med Chem, 2015. 58(3): p. 1038-52*).

2.4 Selection of a chemical scaffold for building Mdm2-p53 protein-protein interaction inhibitor bioorthogonal probes

After the selection of the biological model, we engaged in the identification of a suitable chemical scaffold for developing bioorthogonal probes. The 3-imidazolyl-indole chemical series (**Figure 2.3-2**) [116,117] was an attractive candidate for several reasons. First of all, these compounds showed high biochemical and cellular potency as reported by Furet et al.[116] As an example, the authors reported a biochemical IC_{50}= 30nM for the analogue depicted in **Figure 2.3-2** when tested in a p53 derived peptide-Mdm2 TR-FRET assay and a cellular IC_{50}= 7.3 µM for the inhibition of proliferation of SJSA-1 cells (Mdm2 gene amplified cells).[116] Secondly, some members of this chemical series displayed good selectivity towards the off target p53-Mdm4 interaction in a TR-FRET biochemical assay. As an example, the compound depicted in **Figure 2.3-2** showed more than 600-fold selectivity over the inhibition of the p53-Mdm4 interaction.

The 3-imidazolyl-indole chemical series was developed around the central Valine concept.[116] This concept is based on the use of an aromatic 5-membered ring as a chemical scaffold able to bind to the Valine 93 of the Mdm2 pocket while enabling the juxtaposition of its functional groups into the Mdm2 sub-pockets (Leu 26,Trp 23 and Phe 19) (**Figure 2.4-1a**).

Furthermore, a co-crystallization experiment of the example depicted in **Figure 2.3-2** with Mdm2 highlighted how the chlorophenyl group of the molecule occupies the Leucine 26 sub-pocket making an aromatic stacking interaction with the Mdm2 residue Histidine 96 (**Figure 2.4-1b**). This interaction is not possible for the Mdm4 homolog protein where the Histidine 96 is replaced by a Proline residue. Thus, the difference in a single residue confers the interesting selectivity of these analogues with respect to Mdm4.

Consequently, the knowledge of the binding mode supported by biological data, a co-crystal structure and a selectivity rationale allowed the design of bioorthogonal probes based on the 3-imidazolyl-indole chemical series with good potential for retaining the desired properties of the starting tool compound.
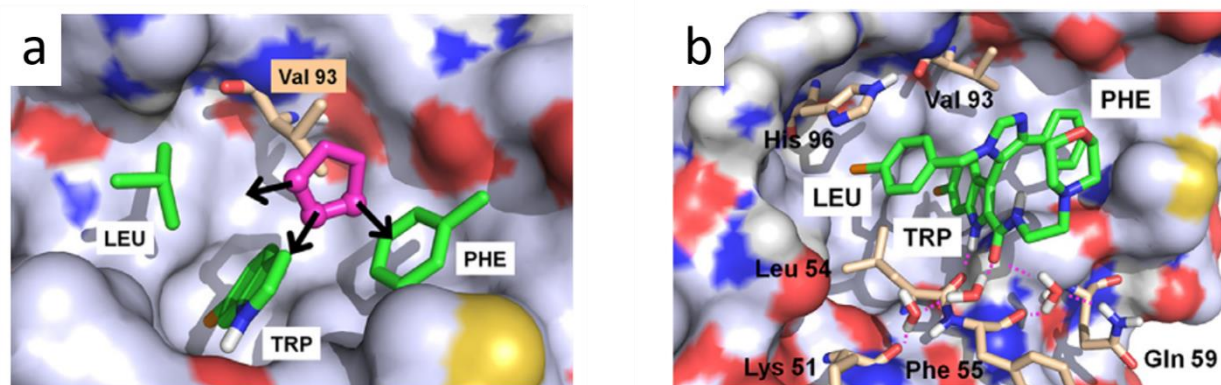
Figure 2.4-1 (a) A representation of the "central Valine concept"; (b) Crystal structure of a 3-imidazolyl-indole analogue in the Mdm2 pocket highlights the juxtaposition of the imidazole substituents in the Mdm2 sub-pockets. The co-crystal structure showed as well the close proximity between the chlorophenyl group and the His 96 important for the selectivity against Mdm4.

2.5   Design of Mdm2-p53 PPI inhibitor bioorthogonal probes

Using the SAR knowledge on the 3-imidazolyl-indole chemical series acquired inside our organization we selected compound **1** (**Figure 2.5-1a**) as an interesting chemical starting point for bioorthogonal probe design. Molecular docking of **1** and **2**, with the crystal structure of Mdm2 (**Figure 2.5-1b**) strongly suggested that the introduction of bioorthogonal tags on the carboxylic acid would expose the label towards the solvent without interfering with activity against the biological target (Mdm2). Therefore, this moiety was identified for chemical modification.
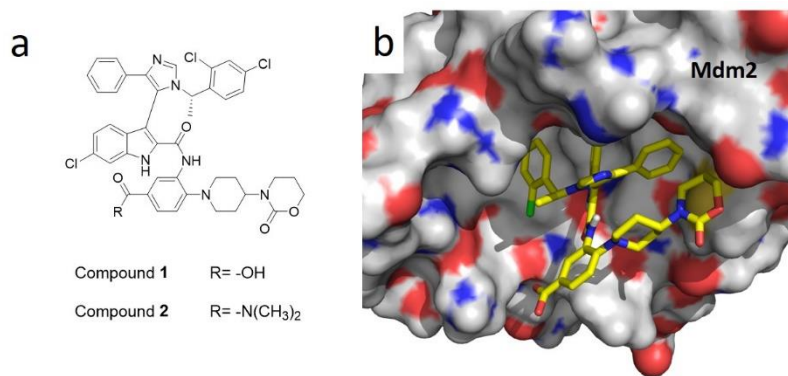
Figure 2.5-1 (**a**) structure of compound **1** and **2**; docking of **1** (b) in a crystal structure of Mdm2 (Adapted from *D'Alessandro, P.L., et al. Angew Chem Int Ed Engl, 2016*).

While the bioorthogonal chemical reaction toolbox is constantly growing, the task of finding the right reaction for each application remains challenging[118]. Despite there being over twenty published bioorthogonal reactions, cycloaddition and ligation reactions are still the main reactions applied. These reactions are employed in biological systems with different objectives and aims which vary from triggering fluorophore un-quenching for imaging studies[119] to pro-drug deprotection [120] and in situ synthesis of biologically active compounds[121].

During our attempt to identify the most suitable reactions for our application, we set some criteria to be fulfilled by both reactions and reactive groups before engaging in synthesis. Setting these criteria aimed at reducing potential misleading results such as false positives. The reactions should have fast kinetics, be irreversible and chemoselective. The bioorthogonal probe label should be reasonably stable and not excessively modify the physico-chemical properties of the probe.

In order to broaden the scope and demonstrate a certain adaptability of our approach toward different chemical classes of probes, we decided to apply this technology not only to study LMW compounds but also peptides. Consequently, the synthetic approach for labelling the molecules played an important role too. The bioorthogonal label should be easily introduced, ideally at the last synthetic step via an efficient and clean chemical reaction compatible with a great variety of chemical compound classes.

Two reactions fulfilled our criteria: the Inverse Electron Demand Diels-Alder (IED-DA) with strained dienophiles first described by Fox as a bioorthogonal reaction[122] and the strained promoted [3 + 2] azide-alkyne cycloaddition (SPAAC)[123] pioneered by Bertozzi[124-127] and by Boons[128].

The IED-DA is a biocompatible reaction between electron-rich dienophiles and electron-poor dienes. While the toolbox of electron-rich dienophiles offers an interesting range of strained olefins and alkynes (**Figure 2.5-2**), the electron-poor dienes for bioorthogonal reaction (non-PhotoClick) share a common tetrazine moiety.
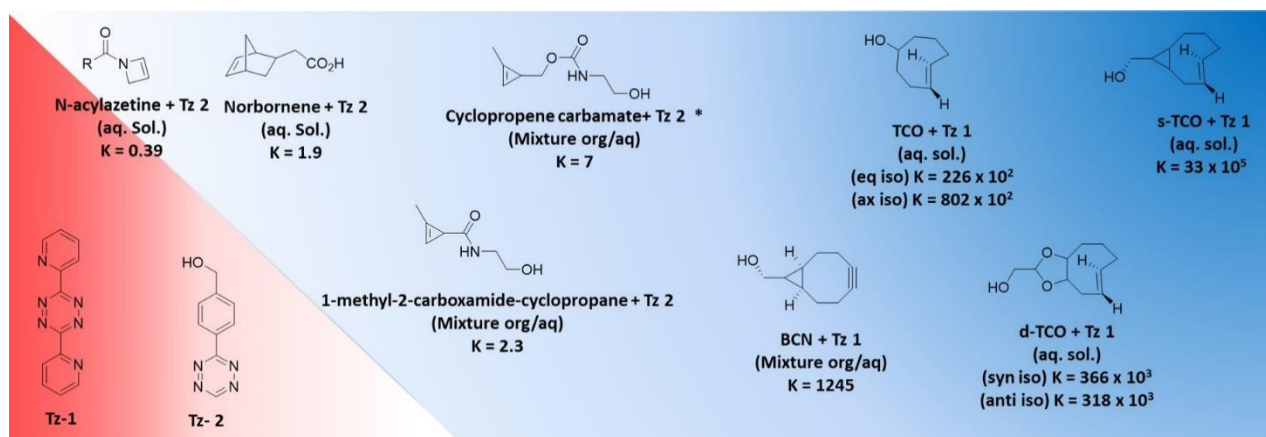
Figure 2.5-2 Electron-rich dienophiles used for bioorthogonal chemistry approaches (depicted in the blue area). K reported $M^{-1} \cdot s^{-1}$ represents the conversion rate when the dienophile reacts with a tetrazine (Tz-1 or Tz-2 in the red area). Increased reactivity of bioorthogonal groups represented by color intensity. K values obtained for compound* obtained from Ravasco, J.M., et al. Organic Chemistry Frontiers, 2017. 4(6): p. 1167-1198. All the remaining K values obtained from Oliveira, B.L., et al. Chemical Society Reviews, 2017. 46(16): p. 4895-4950.

We reasoned that the strained alkenes would be a better functionalization for LMW chemical probes rather than the tetrazines, since the introduction of at least two aromatic rings to a LMW molecule might consistently hamper its cellular permeability. Thus, aiming at performing Inverse Electron Demand Diels–Alder (IED-DA) and Copper Free "Click" chemistry reactions in cells, we decide to introduce strained alkenes (**Figure 2.5-3**). Specifically, we oriented our choice of bioorthogonal groups toward the trans-cyclooctene (TCO) and the cyclopropenes. These motifs showed reasonably fast kinetics in the EID-DA with tetrazine derivatives, while being easily accessible synthetically (cyclopropenes) or incorporated in commercially available building blocks (TCO).

Figure 2.5-3 Structure of LMW Mdm2-p53 PPI inhibitor chemical probes

To enable SPAAC reactions in a living system, we opted for the azide group instead of the strained alkynes for the functionalization of our chemical probes (**Figure 2.5-3**). This choice was justified by the well-documented stability of this chemical group in living systems and by its small size. The alkyne could then be incorporated in the reacting reporter.

Hence, compound **1** was synthesized following a previously well established and high yielding procedure reported in the synthetic scheme in **Figure 2.5-4.**[129]
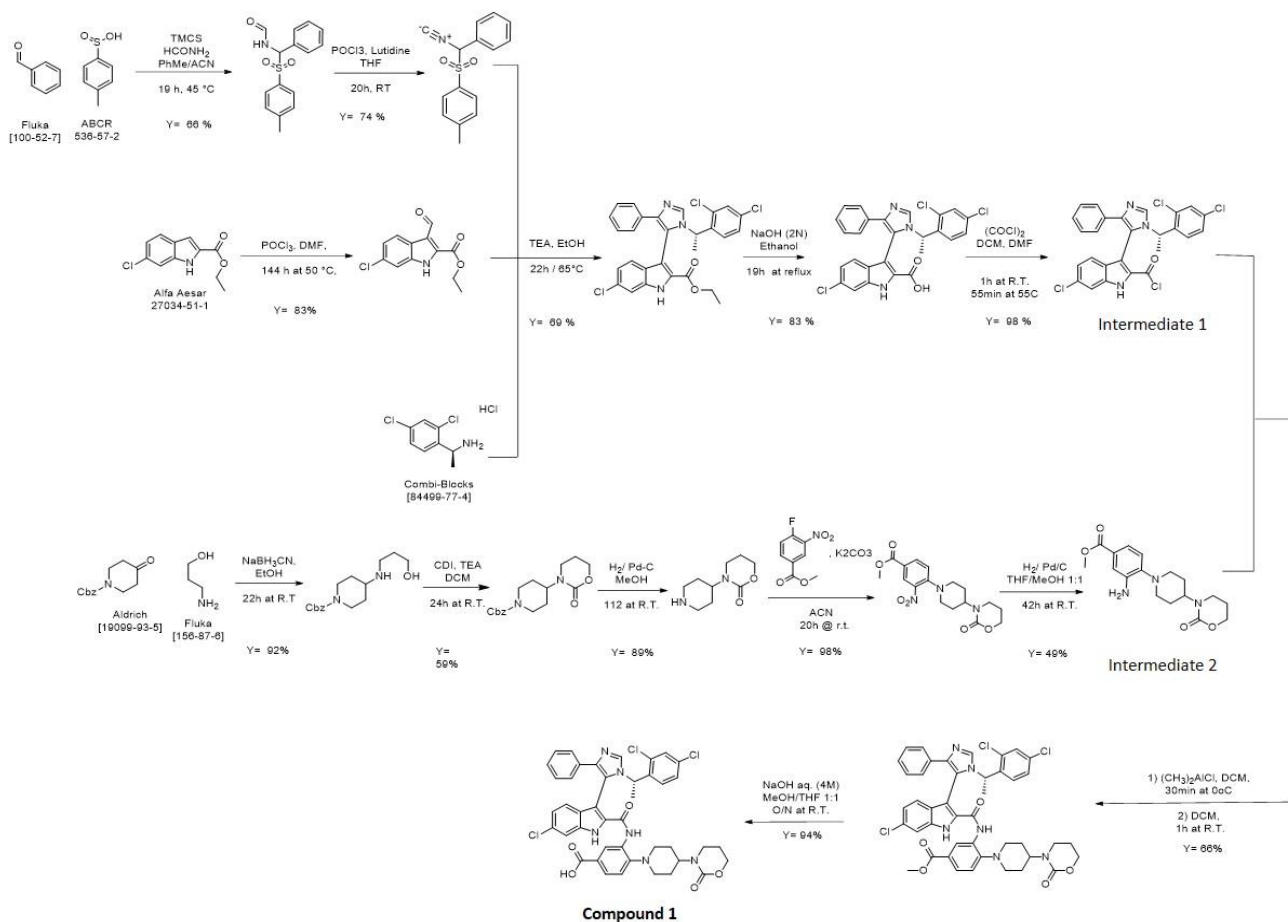
Figure 2.5-4 Synthetic route for the preparation of compound **1**

The chemistry approach for the preparation of **1** was based on a convergent synthesis starting from four commercially available compounds, benzaldehyde, ethyl 6-chloro-1H-indole-2-carboxylate, (S)-1-(2,4-dichlorophenyl)ethan-1-amine and N-Benzyloxycarbonyl-4-piperidone. Two key intermediates, intermediate 1 and 2 (depicted as in **Figure 2.5-4**), were prepared in six and five synthetic steps respectively.

The first intermediate was synthesized starting from benzaldehyde through a two step formation of a tosylmethyl isocyanide (TosMIC) via dehydration of the corresponding formamide precursor.[130] The TosMIC derivative was then engaged in a Van Leusen three-component type reaction run in one-pot with an aldehyde and a benzylamine to afford the 1,4,5-trisubstituted imidazolyl derivative.[131,132] The resulting compound was then subjected to ester hydrolysis followed by acyl chloride formation using oxalyl chloride to afford intermediate 1.

Intermediate 2 was prepared from N-benzyloxycarbonyl-4-piperidone through a linear synthetic sequence. This involved a reductive amination followed by a carbamate formation using 1,1'-Carbonyldiimidazole (CDI) to afford the benzyl 4-(2-oxo-1,3-oxazinan-3-yl)piperidine-1-carboxylate. This compound was subjected to hydrogenation for Cbz de-

protection and the resulting secondary amine was engaged in an aromatic nucleophilic substitution reaction to obtain the nitro-phenyl piperidine derivative, which was subsequently reduced to afford intermediate 2.

In conclusion, the two key intermediates were coupled via a trimethylaluminum mediated amide bond formation, which afford the methyl ester derivative of compound **1**. Finally, the ester was hydrolyzed to obtain compound **1**.

Next, compound **1** was modified to provide the desired tagged probes; i.e. with a *trans*-cyclooctene (TCO) introduced with a carbamate linker (**3**), a methyl cyclopropene introduced with a carbamate linker (**4**), a methylene linker (**5**), or an amide linker (**6**), and an azide (**7**) (**Figure 2.5-3).**

The target compounds were docked with Mdm2 in order to verify the availability of the bioorthogonal label to take part in a reaction once the compound was bound to the target (see **Figure 2.5-5a** and **2.5-5b** for docking of compound **3** and compound **6** to Mdm2).
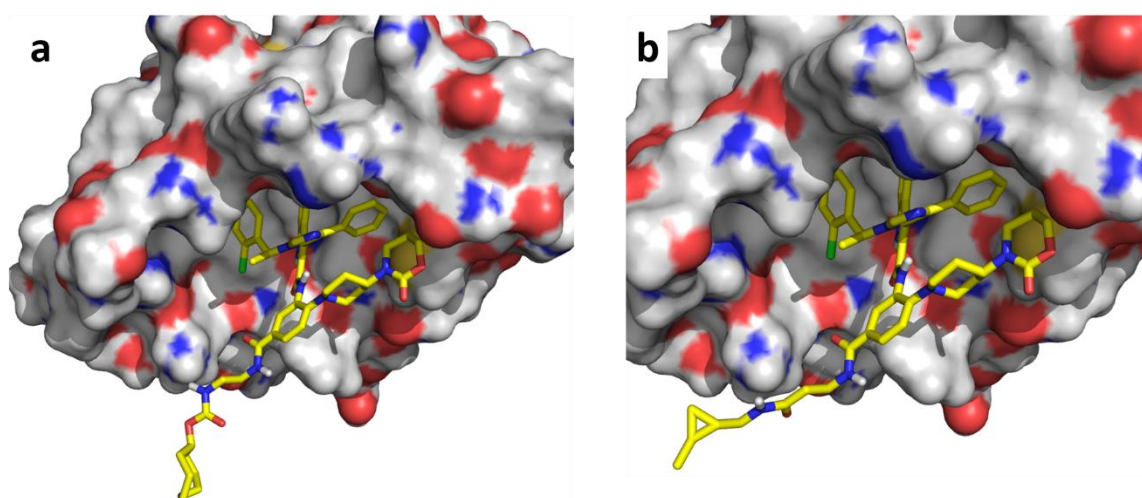
Figure 2.5-5 Docking of compound **3** (**a**) and compound **6** (**b**) on the crystal structure of Mdm2 (Adapted from *D'Alessandro, P.L., et al. Angew. Chem. Int. Ed. Engl, 2016*).

Furthermore, to confirm that this technology can be applied to peptide molecules two dual Mdm2/Mdm4 inhibitor stapled peptides (**8** and **9**) [131,133,134] were functionalized with bioorthogonal groups. The poor selectivity profile of these compounds versus Mdm4 (see **Table 2.6-1**) limits their use as chemical probes to study function, although they are suitable to study whether our bioorthogonal approach can be applied to the imaging of peptidic molecules; this might enable future studies with more selective compounds. A TCO moiety (replacing the acetyl group of both (**8**) and (**9**)) was attached at the N-terminus via a carbamate linker, yielding respectively two diastereoisomeric mixtures for each peptide functionalization; (**10**) and (**11**) as TCO labelled (**8**) and (**12**) and (**13**) as TCO labelled (**9**). Additionally, an azide containing peptide (**14**) was prepared by replacing the C-terminal alanine of compound (**9**) with an azido-lysine (**Figure 2.5-6**).
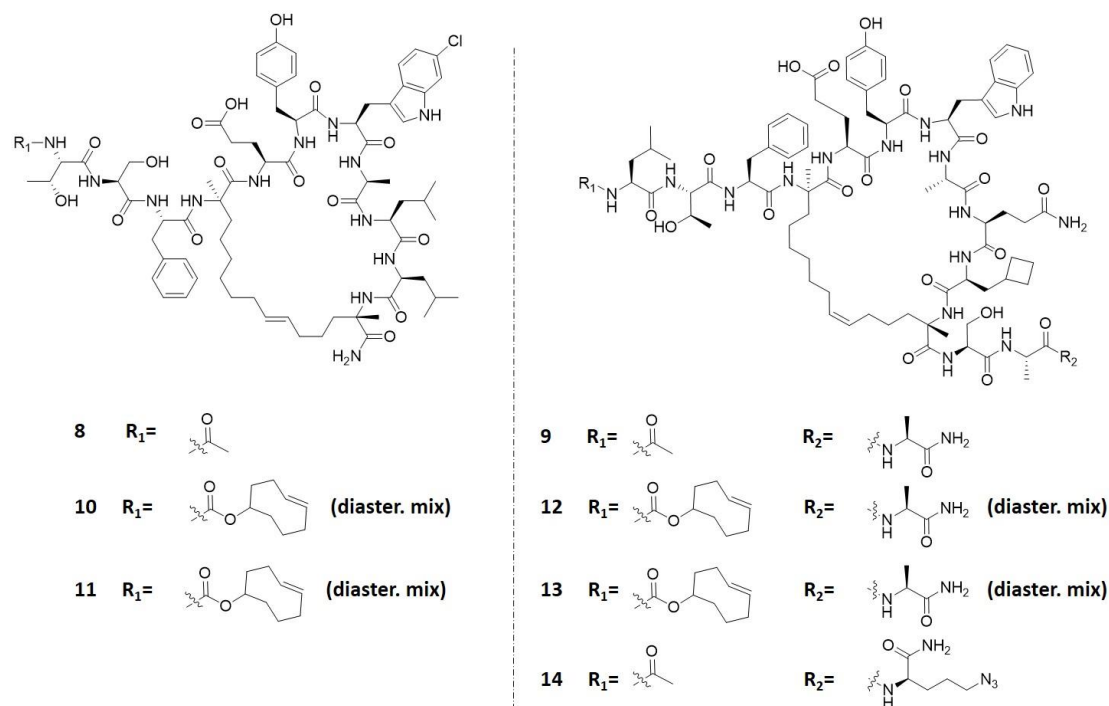
Figure 2.5-6 Structure of Mdm2/Mdm4 inhibitor stapled peptides (**8** and **9**) and their corresponding labelled analogues (**10-11** and **12-14**)

2.6   Measuring biochemical potency of the chemical probes

The potency of the probes towards Mdm2 and Mdm4 was assessed with a TR-FRET assay[135] (**Table 2.6-1**). The un-labelled chemical probes (**1** and **2**) exhibited PPI IC_{50} values in the double-digit and triple-digit picomolar range respectively; Nutlin 3a (Figure 2.2-1) appeared to be at least 10-fold less potent compared to **1** and **2** (hMdm2-p53 TR-FRET = 8.89 ± 0.01 nM). Furthermore **1** and **2** showed an exquisite selectivity against the off target p53-Mdm4 interaction (both compounds are more than 500-fold selective over the inhibition of the Mdm4-p53 PPI) as postulated by Furet[116]. The bioorthogonal probes (**3-7**, **10-14**) retained inhibitory activity on the Mdm2-p53 interaction. The replacement of the carboxylic acid group of compound (**1**) with a secondary or tertiary amide functionality (**2-7**) induced a marginal loss in activity (3 to 14 fold) although the precise nature of the linker and the bioorthogonal tag did not further influence the potency of the compounds; no great difference in potency was observed between the probes (**3-7**). Furthermore, a small loss in activity was observed for the peptides tagged with TCO at the N-terminus (comparing **8** and **9** with **10-11** and **12-13** respectively); the introduction of the azido-lysine on the C-terminus does not affect potency (see **Table 2.6-1**, **9** vs. **14**).

Table 2.6-1 Potency of PPI inhibitors tested towards Mdm2 and Mdm4 using a TR-FRET assay (value determined using at least three independent measurements) (Adapted from D'Alessandro, P.L., et al. *Angew Chem Int Ed Engl*, 2016).

Compound	hMdm2-p53 TR-FRET IC_{50} (nM)	hMdm2-p53 TR-FRET $C_{max}\%$	hMdm4-p53 TR-FRET IC_{50} (nM)	hMdm4-p53 TR-FRET $C_{max}\%$	hMdm4-p53 / hMdm2-p53 TR-FRET (IC_{50} ratio)
1	0.034 ± 0.002	99.7	17.00 ± 2.71	99.5	500
2	0.130 ± 0.009	99.3	130.00 ± 17.00	86.0	1000
3	0.48 ± 0.03	98.9	344.00 ± 46.20	70.0	716
4	0.23 ± 0.02	97	276.35 ± 66.05	71.3	1200
5	0.25 ± 0.02	95.7	201.05 ± 51.66	75.0	804
6	0.23 ± 0.02	97.0	211.00 ± 22.50	81.0	917
7	0.20 ± 0.02	99.8	390.28 ± 95.80	54.2	1951
8	0.15 ± 0.01	> 100	5.18 ± 0.65	98.5	34
9	0.17 ± 0.01	99.6	1.03 ± 0.09	> 100	6
10	0.51 ± 0.05	> 100	9.73 ± 3.37	94.5	19
11	0.49 ± 0.03	99.5	44.10 ± 2.78	94.5	90
12	2.50 ± 0.23	> 100	23.85 ± 4.74	92.0	9
13	0.62 ± 0.07	100	7.23 ± 1.03	97.0	2
14	0.19 ± 0.02	96.3	0.44 ± 0.05	100.0	2

Finally, the functionalization of both LMW and peptide molecules was not detrimental for selectivity over inhibition of the Mdm4-p53 interaction; overall similar selectivity ratios were seen for tagged probes and their closest untagged molecules (**Table 2.6-1**).

2.6.1. Biochemical kinetics of probe binding

Planning to react our bioorthogonal probes with chemical reporters for studying not only their intracellular distribution but also their target engagement and occupancy using imaging techniques, we envisaged to first investigate the compound-target binding kinetics in a biochemical assay. The dissociation half-life of the compound-target complex (defined as the average time required to liberate half of the initially occupied protein or receptor) can play a crucial role in achieving meaningful co-localization images. It appears intuitive that transient interactions between compounds and proteins will be hardly captured while complexes with a slow off-rate might be more easily imaged. Also, compounds with very slow on-rate might be misinterpreted if visualized when a steady state was not reached and the compounds are accordingly not bound to their targets. Therefore, we measured the kinetic values (K_D, K_{on}, K_{off} and $T_{1/2}$) using pseudo first-order conditions (concentration of inhibitor exceeding the MDM2 concentration) for some representative examples of our bioorthogonal probes (compound **3**-**5** and **7**) and for compound **1** (**Table 2.6-2**).

Table 2.6-2 Binding kinetics for representative example of probes

Compound	K_D (nM)	K_{on} $M^{-1} \cdot s^{-1}$ x 10^6	K_{off} s^{-1} x 10^{-3}	$T_{1/2}$ dissociation (min)
1	N.D.	N.D.	N.D.	N.D.
3	0.35 ± 0.12	0.8 ± 0.0	0.2 ± 0.05	58 ± 14
4	0.19 ± 0.03	3.0 ± 0.9	0.6 ± 0.08	20 ± 3
5	0.23 ± 0.08	2.4 ± 0.7	0.5 ± 0.04	22 ± 2
7	0.16 ± 0.06	4.5 ± 1.2	0.7 ± 0.10	17 ± 3

While we were not able to determine kinetic values for compound **1** using the method we applied (the affinity constant of compound **1** might be too close to the Mdm2 protein concentration (0.1nM) used in the assay), we were able to measure the kinetic values for the representative examples of our bioorthogonal probes. As expected, the bioorthogonal probes (**3-5** and **7**) exhibited K_D values in the 10^{-1} nM range which indicate relatively long binding times. As reference, it is worth remembering that enzyme-substrate complexes, which have very short binding times, show values in the micromolar to millimolar range.[136] Furthermore, all the compounds tested showed a fast on-rate with a Kon in the range of 10^6 $M^{-1} \cdot s^{-1}$ and a slow dissociation rate constant with a Koff in the range of 10^{-4} s^{-1}. Finally, the half-life values of the probe-Mdm2 complex (determined as $T_{1/2} = -\ln(0.5) / K_{Off}$)[137] were in the range from 17 minutes to 58 minutes which we thought would be sufficient for the different imaging experiments. Despite the kinetic values being measured under closed system conditions, which may poorly reflect a live cell system, the generated data gave us confidence it would be possible to image the chemical probes not only to study their intracellular distribution but to investigate their target engagement and occupancy.

2.6.2. Assessing compound solubility for small molecule bioorthogonal probes

Earlier we introduced some design criteria for chemical probes that we applied to our bioorthogonal probe design. The selected chemical series showed good potency and selectivity, which are pre-requisites for chemical probe development. In addition, we should take into careful consideration, the physico-chemical properties of our molecules (e.g. lipophilicity and solubility) and how they are impacted by the bioorthogonal tags. These properties will influence the probe exposure at the site of action, its target engagement and finally its ability to trigger a functional pharmacological effect and a phenotypic perturbation in the cell disease model.

A comprehensive understanding of the physico-chemical properties could enable a better biological experimental design while reducing the risk of creating false positive or misleading results due, for example, to compound aggregation.

While selecting our biological model we were aware of the potential challenges of developing PPI inhibitor chemical probes. Despite the great step forward made in targeting the disruption of protein-protein interactions using small molecules in the last 20 years, most of these compounds are still high in molecular weight, quite lipophilic and consequently poorly soluble.[138] All these unfavorable properties might lead to chemical probes with poor cellular permeability, exhibiting unspecific binding to intracellular organelles and membranes and finally showing cellular toxicity.

The chemical series we choose, the 3-imidazolyl-indole, is not exempt from such unfavorable physico-chemical properties. For example, compound **1** has a MW equal to 812 g/mol, a clogP equal to 8.09, a logD $_{oct/wat}$ measured at pH 7.4 equal to 7.7 and a solubility equal to 0.012 g/L at pH=6.8. Furthermore, the polar moieties of **1** give only small contributions to highly significant electrostatic protein–ligand interactions, as suggested by a low lipophilic ligand efficiency (LLE for compound **1** is equal to 2.3 where LLE is calculated as $pIC_{50} - logP$); LLE values for drug-like compounds are usually greater than 5.[138]

As shown earlier the bioorthogonal tag does not greatly affect the compound potency (**Table 2.6-1**). This is further confirmed by a modest decrease of the LLE of our probes (**Table 2.6-3**, compounds **3 – 5** and **7**) which seems to exclude an addition of unspecific hydrophobic interactions due to hydrophobic collapse of the ligand tag onto the protein.

Nevertheless, an increase in lipophilicity can clearly influence the solubility of our probes. For this reason, we decide to investigate the solubility of our small molecule bioorthogonal probes (**3 – 5** and **7**) by assessing their aggregation at four concentrations ranging from 0.5 μM to 10 μM in PBS and PBS containing 10% of fetal calf serum (FCS) using dynamic light scattering (DLS) (**Table 2.6-3**).

This assessment can help in guiding the design of the cellular biological experiment while more conventional solubility measurements using UV or MS as detection methods would not discriminate soluble aggregates from compound monomers.[139]

The bioorthogonal probes showed aggregation at concentration above 0.5 μM in PBS while they only start to aggregate at 15 μM in PBS containing 10% of FCS.

The formation of soluble aggregates might lead to misleading results during the staining of the bioorthogonal probes with the fluorescent reporters in the cellular system. Therefore, the aggregation data of the bioorthogonal probes were used to define with confidence the maximal concentration of probe to be applied to the subsequent cellular imaging experiments.

Table 2.6-3 MW, cLogP, LLE and Aggregation in PBS and PBS containing 10% FCS for LMW Mdm2-p53 PPI inhibitors

Compound	MW g/mol	cLogP	LLE (pIC_{50} – ClogP)	Aggregation (PBS)	Aggregation (PBS + 10% FCS)
1	812.1	8.3	2.3	-	-
2	839.2	7.2	2.6	-	-
3	1006.4	10.0	- 0.7	≥ 0.5 μM	≥ 15 μM
4	964.3	8.4	1.2	≥ 0.5 μM	≥ 15 μM
5	877.2	8.3	1.3	≥ 0.5 μM	≥ 15 μM
7	880.2	8.5	1.2	≥ 0.16 μM	≥ 15 μM

2.7 Testing the bioorthogonal probe activity in a cellular model of osteosarcoma

Subsequently to the biochemical profiling of the synthesized bioorthogonal probes (Mdm2-p53 TR-FRET and Mdm4-p53 TR-FRET; **Table 2.6-1**) we next studied their effects on the Mdm2-p53 PPI in a cellular model of osteosarcoma (SJSA-1). In addition, we investigated the metabolic stability of the bioorthogonal probes in the SJSA-1 cell line.

We assessed the potency of our probes by measuring the overproduction and localization of Mdm2 in SJSA-1 cells by high-content single cell fluorescence analysis upon immunostaining with a specific Mdm2 antibody. The disruption of the Mdm2-p53 PPI leads to p53 stabilization and consequent enhancement of p53 transcriptional activity targeting different genes (e.g. *Mdm2* gene) (**Figure 2.1-1**). Accordingly, the activation of the p53 pathway with PPI inhibitors induces a dose-dependent increase of p53 transcriptional targets such as Mdm2 and p21 in cells with wild-type p53 (**Figure 2.1-1**).[114] Finally, a prolonged treatment of p53 dependent cell lines with the Mdm2-p53 PPI inhibitors leads to cell cycle arrest (G_1 and G_2 phases) or apoptosis as previously described applying Nutlin-3a (**Figure 2.2-1**) respectively to U-2 OS or to SJSA-1 cell lines.[114,140]

The SJSA-1 cell line (formerly OsA-CL) is a human osteosarcoma cell line established in 1982 and obtained from a 19 year old patient diagnosed with primitive multi-potential sarcoma of the femur.[141] This cell line is a p53 dependent osteosarcoma cell model where Mdm2 is amplified.[142] It has been used as a standard model for assessing the cellular activity of Mdm2-p53 PPI inhibitors and their efficacy in an *in vivo* xenograft model.[114]

Thus, we incubated SJSA-1 cells overnight with the small molecule probes (**1-7**); after fixation of the cells, Mdm2 was immuno-stained and fluorescence intensity in the nuclei was measured on single cells. In addition, to investigate if the reactive strained alkyne groups could interfere with our cell assay, we included as a negative control, a TCO tagged
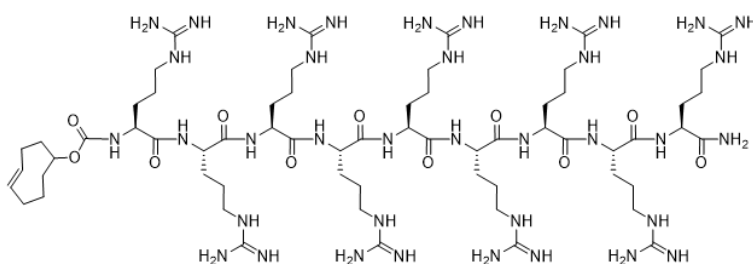
Figure 2.7-1 CPP Nona-Arginine peptide tagged with TCO (Compound **15**)

cell penetrating peptide (CPP) for which the intracellular target is unknown. Therefore, we labelled a nona-Arginine (R9)[143] by introducing a TCO at the peptide N-terminus with a carbamate linker (Compound **15**) (**Figure 2.7-1**). As cellular assay readout, we generated pharmacological dose-response curves by plotting the percentage of cells in which an increase of fluorescent signal in the nuclei was detected versus the compound concentration (**Figure 2.7-2**). While all Mdm2-p53 PPI inhibitor small molecules (compound **1-7)** induced the PD marker (Mdmd2 level) in a dose dependent manner reaching signal saturation at about 0.5 µM, the negative control (compound **15**) did not show any pharmacological effect. Furthermore, we extrapolated an EC_{50} for each compound tested (**Table 2.7-1**).
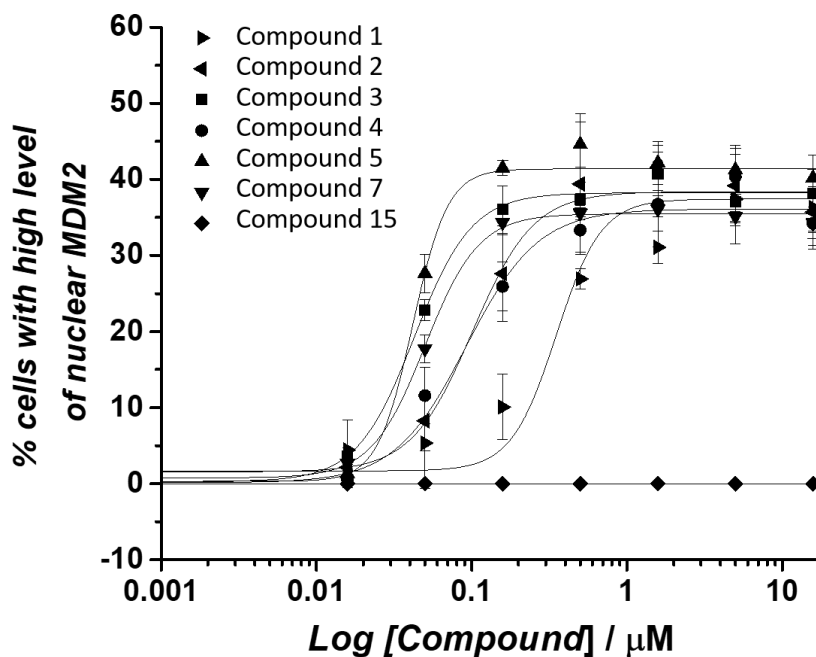
2.7-2 Cellular activity of chemical probes reported as percentage of SJSA-1 cells with high level of Mdm2 in nuclei (F.I. threshold Cy 5 Mean > 130) (adapted from *D'Alessandro, P.L., et al., Angew. Chem. Int. Ed. Engl, 2016. 55(52): p. 16026-16030*).

Compound	1	2	3	4	5	7	15
EC_{50} (nM)	291	100	43	92	42	50	-

Table 2.7-1 EC50 values for Mdm2-p53 PPI inhibitor probes in SJSA-1 cells (adapted from *D'Alessandro, P.L., et al., Angew Chem Int Ed Engl, 2016. 55(52): p. 16026-16030*).

All the chemical probes (**1-7**) induced Mdm2 expression level in the nuclei (**Figure 2.7-2**) with EC_{50} in the nanomolar range (**Table 2.7-1**). Compounds **2-7** showed EC_{50} values between 40 and 100 nanomolar, while **1** exhibited an EC_{50} equal to 291 nanomolar, despite being the most potent probe tested in the TR-FRET biochemical assay (**Figure 2.7-3**). We hypothesized that the observed drop in cellular potency of **1** might be due to the anionic nature of its carboxylic acid group at physiological pH that might impair its cellular permeability. Finally, the EC_{50} of **3**-**7** clearly highlighted that the bioorthogonal groups were not detrimental for the cellular potency of the compounds and instead they might improve their permeability.
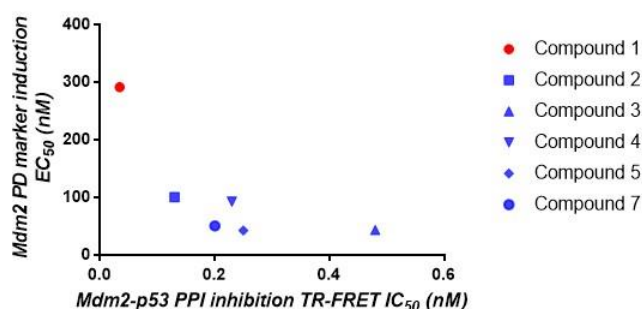
Figure 2.7-3 Mdm2 nuclear induction EC50 vs Mdm2-p53 PPI inhibition TR-FRET for chemical probe 1-7. Compound **1** (•) is the least potent probe tested in the cellular assay despite its remarkable biochemical activity.

2.7.1. Testing the cellular activities of the peptide molecules

As for the chemical probes, we tested the cellular activity of the synthesized Mdm2-p53 PPI inhibitor peptides tagged with the TCO bioorthogonal group (**8-14**) in the SJSA-1 model. However, expecting much higher EC_{50} values for peptide molecules, we decided to normalize their activities as percentage relative to Mdm2 nuclear induction triggered by 10 micromolar Nutlin-3a (**Figure 2.7-4**).

Figure 2.7-4 Cellular activity of Mdm2-p53 PPI inhibitors peptides tested on SJSA-1 cells. The peptide activities were reported as percentage of nuclear PD marker induction ((Intensity threshold Cy 5 Mean > 130) triggered by 10 µM of Nutlin-3a. In the experiments was added compound **15** as negative control. (**a**) Cellular activity profiling of peptides (**8**), (**9**) and Nutlin-3a. (**b**) (**11**) did not significantly induce the PD marker while compound **10** showed similar activity to its parent compound, (**8**). (**c**) Activity profile of (**12**) and (**13**) was very close to their un-labeled analogue (**9**).

Table 2.7-2 EC_{50} Mdm2-p53 PPI inhibitor peptides in SJSA-1 cells

Compound	Nutlin-3a	8	9	10	11	12	13
EC_{50} (µM)	2.7	> 20	12.3	> 20	-	9.1	8.2

The reported cellular activity profiles for compound **8** and **9** were confirmed in our cellular assay (**Figure 2.7-4a and Table 2.7-2**).[133,134] Compound **9** is the most active un-labelled peptide. Considering that **8** and **9** displayed a very similar biochemical profile in TR-FRET, compound **9** is consequently the more cellularly permeable peptide. Compound **8** showed a very weak activity (EC_{50} > 20 micromolar). Furthermore, its analogue (**10**) showed a very similar cellular activity profile while (**11**) is completely inactive (**Figure 2.7-4b**). Finally, both (**12**) and (**13**) showed a cellular activity profile very similar if not slightly superior to their parent peptide (**9**). In addition, at 10 micromolar dose they reached similar PD marker induction as elicited by Nutlin-3a at the same dosage (**Figure 2.7-4c**).

2.7.2. Investigating bioorthogonal probe cellular stability

The bioorthogonal probes are labelled with chemically reactive groups (strained alkenes and azide) that might impair their cellular stability. Therefore, we investigated the cellular stability of representative examples of bioorthogonal

probes, each of them labelled with the different bioorthogonal groups investigated (TCO, cyclopropene and azide groups).

Hence, a compound labelled with the TCO (**3**), a compound functionalized with the cyclopropene (**4**) and a compound functionalized with the azide group (**7**) were incubated at 1.5 and 5 µM concentrations in SJSA-1 cells for 1, 3, 5, 8 and 24 hours. The probe stability was measured within the selected time course by Mass spectrometry. Compound stability was assessed in either supernatant or cell lysates using Alprenolol as internal standard for detection.

Table 2.7-3 Stability of bioorthogonal probes in SJSA-1 cell (data generated using two independent measurements)

Compound	Concentration (µM)	$T_{1/2}$ in supernatant (h)	$T_{1/2}$ in cell lysate (h)
3	1.5	> 48	29.1 ± 2.2
3	5	> 48	> 48
4	1.5	> 48	38.2 ± 7.4
4	5	> 48	> 48
7	1.5	> 48	> 48
7	5	> 48	> 48

The bioorthogonal probes tested (**3**, **4** and **7**) showed overall excellent stability with a long half-life at both 1.5 and 5 µM incubations (**Table 2.7-3**). The TCO tagged compound (**3**), with a $T_{1/2}$= 29.1 ± 2.2 h when incubated at 1.5 µM, was the bioorthogonal probe with the shortest half-life. Interestingly, the azide labelled compound (**7**) was the one displaying the lowest intrinsic clearance (**Figure 2.7-5**). This might be due to a superior chemical stability of the azide group compared to the strained alkenes and not to a diverse metabolic fate of the compounds in cells.
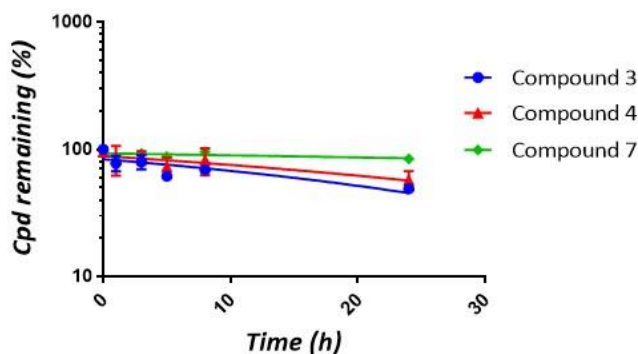
Figure 2.7-5 Clearance of bioorthogonal probes (**3,4** and **7**) assessed by plotting the percentage of probe remaining in lysate obtained by treating SJSA-1 cells with 1.5 µM of compound for 1, 3, 5, 8 and 24 hours. The % of compound remaining was calculated as $LN\{[(\frac{AREA\ (Prob)}{AREA\ (ISTD)})]\%\}$. Alprenolol was used as internal standard (ISTD)

2.8 Results and discussion

We identified an exit vector to functionalize the 3-imidazolyl-indole chemical series with bioorthogonal groups by docking compound **1** into the crystal structure of Mdm2. The docking of the designed bioorthogonal probes into Mdm2

was evaluated before compound synthesis in order to give confidence that the introduction of the bioorthogonal group would not adversely affect compound binding or selectivity toward the Mdm4 homolog protein.

The synthesized bioorthogonal probes exhibited remarkable activity in disrupting the Mdm2-p53 interaction in the sub-nanomolar range, when tested in a TR-FRET biochemical assay. Only a marginal loss of potency (between 1 - 10 fold) was observed when compared to their parent compounds. Also, the chemical probes retained a high selectivity toward Mdm4.

The introduction of the bioorthogonal groups did not appear to influence in either a positive or a negative way the binding affinity of the compounds to the target as shown by a decrease in lipophilic ligand efficiency. Furthermore, despite the increase in lipophilicity, the bioorthogonal probes displayed a relatively high critical association concentration (CAC= 15 µM) in cellular media (PBS containing 10% of fetal calf serum). The formation of soluble aggregates might have led to misleading results while carrying out the cellular studies for investigating the probes cellular activities or their intracellular distribution. Hence, the probe aggregation data were used as guidance for selecting the suitable compound concentration range to be applied in the cellular system.

The ligand-protein interaction kinetics, assessed by a biochemical method, highlighted a fast formation of the binding complex. Furthermore, the ligand-complex half-life appeared adequate for enabling further visualization experiments using imaging fluorescence techniques (e.g. co-localization of probes and target).

Additionally, the chemical probes were tested in a disease cellular model of osteosarcoma, SJSA-1 cell line. The compounds induced the PD marker (increased level of Mdm2 in nuclei) in a dose-dependent manner reaching a plateau at 0.5 µM. The extrapolated EC_{50} values of the bioorthogonal probes were between 0.5 and 1 fold that of the parent compound (**2**) suggesting that the introduction of the bioorthogonal functionality might have increased the compound permeability. Finally, we investigated the stability of some of the synthesized bioorthogonal probes in SJSA-1 cells. Despite, some differences in terms of clearance being observed between the compounds tagged with the strained alkenes and the azide, all of them showed a long half-life (e.g. Compound **3** $T_{1/2}$= 29.1 ± 2.2 h).

All together, these data build a solid foundation for the subsequent experiments aiming at validating the bioorthogonal probes in the cellular disease model.

Finally, we synthesized Mdm2-p53 PPI stapled peptide inhibitors functionalized with bioorthogonal probes. Despite, the selectivity profile of these molecules limiting their use as bioorthogonal probes for functional pharmacology investigations, their use in our studies might provide a better understanding of the applicability of our approach to peptidic molecule imaging; this might enable future studies with more selective peptides.

2.9　Experimental section

2.9.1.　Docking experiment

Modeling and docking were performed with a version of MacroModel enhanced for graphics by A. Dietrich. MacroModel.[144] The compounds were manually constructed and docked in the MDM2 derived from the previously published crystal structure of MDM2 in complex with a related 3-imidazolyl indole inhibitor (PDB entry code 4DU). The resulting ligand-protein complexes were energy-minimized using the AMBER*/H2O/GBSA force field.

2.9.2.　Biochemical assays

Time Resolved Fluorescence Energy Transfer (TR-FRET) Assay for IC50 determination
The inhibition of p53-MDM2 and p53-MDM4 interactions was measured by time resolved fluorescence energy transfer (TR-FRET). Fluorescence energy transfer (or Foerster resonance energy transfer) describes an energy transfer between donor and acceptor fluorescent molecules. For this assay, human MDM2 protein (amino acids 2-188) and human MDM4 protein (amino acids 2-185), tagged with a C-terminal biotin moiety, were used in combination with a Europium labeled streptavidin (Perkin Elmer, Inc., Waltham, MA, USA) serving as the donor fluorophore. The p53 derived, Cy5 labeled peptide Cy5-TFSDLWKLL (p53 aa18-26) was the energy acceptor. Upon excitation of the donor molecule at 340nm, binding interaction between MDM2 or MDM4 and the p53 peptide induces energy transfer and enhanced response at the acceptor emission wavelength at 665 nm. Disruption of the formation of the p53-MDM2 or p53-MDM4 complex due to an inhibitor molecule binding to the p53 binding site of MDM2 or MDM4 results in decreased donor emission at 665 nm. The ratiometric FRET assay readout was calculated from the raw data of the two distinct fluorescence signals measured in time resolved mode (fluorescence 665 nm/fluorescence 620 nm x 1000).

The test was performed in white 384-well plates (Greiner Bio-One, reference 781207) in a total volume of 60 µL by adding 1 µL of compounds tested at different concentrations diluted in 100% DMSO (1.7% final DMSO concentration) in reaction buffer (PBS, 125mM NaCl, 0.001% Novexin (consists of carbohydrate polymers), designed to increase the solubility and stability of proteins; Expedeon Ltd., Cambridgeshire, United Kingdom), 0.01% Gelatin, 0.01% 0.2%, Pluronic F-127 (block copolymer from ethylenoxide and propyleneoxide), 1 mM DTT). After addition of 0.05 nM MDM2-biotinylated or 0,1 nM MDM4-biotinylated (internal preparations), and 0.625 nM Europium labeled streptavidin (Perkin Elmer), the solution was pre-incubated for 30 minutes at room temperature, then 10 nM Cy5-p53 peptide (internal preparation) was added before an incubation at room temperature for 30 minutes prior to reading the plate. For measurement of samples, a TECAN F500 microplate reader was used with the following settings: Excitation 340 nm, Emission Donor 620 nm and Emission Acceptor 665 nm. IC$_{50}$ values are calculated by curve fitting using XLfit. If not specified, reagents were purchased from Sigma-Aldrich Chemie GmBH, Buchs, Switzerland.

2.9.3.　TR-FRET Assay for binding kinetics

The rapid mixing tool of Infinite F-500 reader (Tecan) was used to study fast binding kinetics (single well mode). Microplate containing the different concentrations of compound and 20 nM Cy5-p53 peptide in 50 µl assay buffer, were placed in the reader. After 10 min equilibration at 25°C, binding reactions were initiated by injecting 50 µl of buffer containing biotinylated 0.1 nM MDM2 and 0.2nM europium-streptavidin at 475 µl/s. Fluorescence was measured at a

single wavelength (665 nM) and at various time intervals until steady-state was achieved. All experiments were performed in pseudo first-order conditions (with the inhibitor exceeding the MDM2 concentration). KD, koff, kon were calculated by 2 methods: by using a global fit (more accurate method), and from plots kobs vs. inhibitor concentration (for confirmation). Data were validated when the KD obtained was similar to the IC_{50}.

2.9.4. Dynamic Light Scattering

DLS was performed diluting the probes in PBS, or PBS containing 10% of fetal calf serum (FCS). Each probe was measured at four concentrations ranging from 0.5 to 10 µM in a DLS 384-well plate (Corning Low Volume, Non-Treated, Black with Clear Bottom, #3540). After transfer, the final dilutions are centrifuged and covered with 10 µL of mineral oil (Sigma, #M1180) to prevent evaporation during the measurement. Before starting the measurement the dilutions were incubated for about 60 min. The DLS measurement is performed using WYATT DYNAPro Plate reader. The last two columns of the plate were filled with PBS as background control. To obtain the normalized signal to background value, the compound value was divided by the median of the PBS background controls.

2.9.5. Cell culture

SJSA-1 cells were maintained in RPMI1640 medium containing L-Glutamine (Invitrogen) supplemented with 10% FCS heat inactivated (Bioconcept) and 1% Pen/Strep (Invitrogen). Cells were split every two to three days. To split cells, these were washed with PBS and Trypsin-EDTA (0.5%) was added for 5 minutes at 37°C. Cells were collected in warm medium and centrifuged for three minutes at 2200 rpm (Multifuge 3s-R, Heraeus), the supernatant was discarded and cells re-suspended in medium and seeded at a density of 2-2.5 million cells in a T175 culturing flask. Cells were counted using a Cedex cell counter (Innovatis). For storage, cells were re-suspended in FCS containing 10% DMSO (vol/vol) and stored in liquid nitrogen. To determine the exact cell number and cell viability, 300 µL cell suspensions are measured with Cedex Cell Counter (Innovatis). From the obtained cell number the seeding cell number is calculated. For each new passage a cell number of $2 \cdot 10^6$ - $2.5 \cdot 10^6$ is seeded in a T175 cell culturing flask.

2.9.6. MDM2 cellular assay

To measure probe potency in cells MDM2 immunostaining was performed following overnight probe incubation and fixation as described above. Cells were washed with H/H buffer using Tecan power washer and incubated for 30 minutes at R.T. with 10 µL blocking solution (10% FCS, 0.1% TritonX100 in The primary MDM2 antibody (Abcam, #ab38618) was added at 1:100 in blocking solution. After 1 hour incubation at RT, cells were washed with H/H buffer and the secondary antibody (goat anti-rabbit Alexa Fluor 647 labeled) (1:500), and Hoechst (1:10000) (Invitrogen) were added with 1% fetal calf serum (FCS) in H/H buffer and incubated for 60 minutes protected from light. Cells underwent four washing cycles with H/H buffer and were stored in H/H buffer containing 1 % Pen/Strep at 4°C until imaging.

2.9.7. High content imaging and image analysis

Images were acquired with an InCell2000 high throughput microscope (GE Healthcare) using a 20x objective. DAPI was excited at 350 nm and emission was sampled at 470 nm. Alexa Fluor 647 was excited at 649 nm and emission was sampled at 666 nm. Image analysis was performed using Columbus software 2.3.2 (Perkin Elmer). First, nuclei was detected based on Hoechst staining. The intensity of the fluorophores signals were measured in the cytoplasm or nuclei

region, depending on the readout of the assay. The intensity of secondary antibody- Alexa Fluor 647 was measured in the nuclei region. For the MDM2 detection assay, an intensity threshold (Intensity Cy 5 Mean > 130) was set to calculate the number of cells overexpressing Mdm2. Data was exported as average of the well and for individual cells.

2.9.8. Data analysis

Dose response curves were performed with OriginPro software (OriginLab, Northampton, MA).

2.9.9. Protocol for compound stability in PBS

Compounds are prepared as 50 µM solutions from 10 mM stocks in PBS. Following 1.5 h incubation the measurements are performed by Ultra performance Liquid Chromatography by Acquity UPLC/SQD (Waters). The instrument contains an Acquity HSS T3 1.8 µm 2.1x50 mm column. The mobile phase A consists of water, 0.05% formic acid and 3.75mM ammonium acetate (pH 3.8), the mobile phase B of acetonitrile and 0.04% formic acid. Massspectrometric detection is perform using a Single Quadrupole Detector (SQD) Waters Acquity SQD and UV-detection is measured by a Photo Diode Array (PDA).

2.9.10. LC-MS-Analysis for assessing cellular stability

Analysis of samples was performed on a high performance liquid chromatography–tandem mass spectrometry system (LC-MS) consisting of a Dionex Ultimate 3000 LC-system and a TSQ Quantum Discovery Max mass spectrometer equipped with an electrospray ion source (Ion Max electrospray interface) controlled by QuickQuan 2.0 from Thermo Fisher Scientific Inc. (Waltham, MA, USA). Compound specific parameters (tube lens and precursor ion, collision energy and product ion for single reaction monitoring (SRM)) were obtained by automatic tuning using the QuickQuan software. These parameters were stored in a QuickQuan database to be used for selective quantitation of each test article. Samples were separated on a Phenomenex Synergi PolarRP, 2*50 mm, 2.5 µm (Brechbühler, Schlieren, Switzerland). The components were eluted with a gradient of 0.1 % formic acid (mobile phase A) versus 0.1 % formic acid in acetonitrile (mobile phase B) at a flow of 500 µL/min at 50°C using the following gradient: 0 min 5 % B; 0.1 min 5 % B; 0.6 min 95 %B; 1.6 min 95 % B; 1.7 min 5 % B; 2 min 5 % B. The injection volume was 5 µL. The first 0.1 minutes of eluent were diverted to waste to protect in ion source from salts and polar impurities from incubation. For the estimation of the stability, the percentage of test article remaining relative to time zero minute incubation was used to determine the elimination-rate constant ($k_{incubation}$) and half-life ($t_{1/2}$).

2.9.11. Chemical material and Methods

General considerations: all chemicals were purchased from Sigma Aldrich, unless noted, and were used as received. All solvents were of reagent grade or higher and were used without further purification.

Instruments for chemical synthesis and characterization of LMW compounds
Analytical LC/MS were performed on a Waters Acquity UPLC/SQD equipped with a UPLC PDA (Photo Diode Array with full scan 210 - 450 nm and one user selectable wavelength), a Waters Acquity SQD (Single Quadrupole Detector), and a Waters Acquity HSS T3 1.8 µm 2.1 x 50 mm column at a flow rate of 1.0 mL/min and 60°C column temperature. Analytical

runs were performed using two methods: (a) LC-MS 10 min run method and (b) LC-MS 2 min run method using eluent A water + 0.05% formic acid + 3.75mM ammonium acetate and Acetonitrile +0.04% formic Acid.

LC-MS 10 min run method (a)			LC-MS 2 min run method (b)		
Stop Time 10 min			Stop Time 2 min		
Mass range ESI +/-: 100 – 1600 m/z			Mass range ESI +/-: 100 – 1200 m/z		
Time (min)	Eluent A (%)	Eluent B (%)	Time (min)	Eluent A (%)	Eluent B (%)
0.00	95	5	0.00	95	5
9.40	2	98	1.40	2	98
9.80	2	98	1.80	2	98
9.90	95	5	1.90	95	5
10	95	5	2	95	5

MS-spectra were recorded on a Waters Xevo G2-XS QTof. Purification of low molecular weight compounds and fluorophores via preparative high performance liquid chromatography (HPLC) were performed on a Varian 210 instrument equipped with a 335 diode array detector and a Varian Pursuit XRs 10 C18 250 X 21.2 mm column using a flow rate of 21 mL/min. Buffer A consists of water with 0.1% TFA. Buffer B is acetonitrile containing 10% water and 0.1% TFA. Purification of compound 7 was performed using a Waters UV-Autopurification system using a Waters 2767 sample manager, Waters 2545 binary gradient module, a Waters solvent-fluid-organizer, a Waters 2489 UV/visible detector, and a Waters SunFire C18 column (5 µm 50 x 150mm) running a gradient from 0% Buffer A to 25% Buffer B at 100 mL/min. Buffer A consists of water with 0.1% TFA. Buffer B is acetonitrile. Flash chromatography was performed using a CombiFlash RF200 equipped with Silica RediSep Column of different size. ^1H and ^{13}C NMR experiments were recorded with a Bruker 600 MHz Avance III or a Bruker 400 MHz Avance III spectrometer equipped with a 5 mm [^1H, ^{13}C, ^{15}N] CryoProbe™ with a z-gradient system. ^1H and ^{13}C detected 1D and 2D NMR spectra of the sample were recorded at 300K. All spectra were referenced to the internal solvent signal (^1H: d6-DMSO = 2.50 ppm and ^{13}C: d6-DMSO = 39.5 ppm; ^1H: CDCl$_3$= 7.26 ppm and ^{13}C: CDCl$_3$= 77.16 ppm; ^1H: (CD$_3$)$_2$CO = 2.05 ppm and ^{13}C: (CD$_3$)$_2$CO= 29.84 ppm, ^1H: D$_2$O = 4.79 ppm).

Instruments for chemical synthesis and characterization of peptides

Analytical LC/MS were performed on a Waters Acquity UPLC/QTOF equipped with a UPLC TVU (Photo Diode Array with 214 nm wavelength), a Waters Acquity SQD (Single Quadrupole Detector), and a Waters Acquity UPLC BEH300 C18 1.7 µm 2.1 x 50 mm at a flow rate of 0.5 mL/min and 80°C column temperature. The eluents for the analytical runs were A (water + 0.05% TFA) and B (acetonitrile + 0.04% TFA). Chromatography runs were performed using a 10 minutes method with 5% to 98% B in 9.4 min. Mass spectra over a mass range from 300 m/z to 3000 m/z are acquired using positive-ion Electrospray Ionization (ESI). Both, MS and MSE – at low and high collision energy – were recorded. The analytical method for peptide analysis will be reported as Method C. The purification of the peptides were performed using a Waters UV-Autopurification system using a Waters 2767 sample manager, Waters 2545 binary gradient module, a

Waters solvent-fluid-organizer, a Waters 2489 UV/visible detector, and a Waters SunFire C18 column (5 μm 50 x 150mm) running a gradient from 0% Buffer A to 25% Buffer B at 100 mL/min. Buffer A consists of water with 0.1% TFA. Buffer B is acetonitrile.

Compound synthesis

Compound 1: 3-(6-chloro-3-(1-((S)-1-(2,4-dichlorophenyl)ethyl)-4-phenyl-1H-imidazol-5-yl)-1H-indole-2-carboxamido)-4-(4-(2-oxo-1,3-oxazinan-3-yl)piperidin-1-yl)benzoic acid
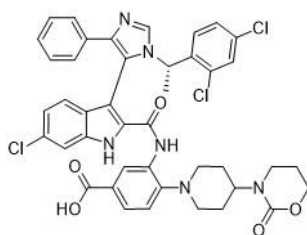
The compound was synthesized following the literature described procedure.[129]

^{1}H NMR (600 MHz, DMSO-d6) δ 12.77 (s, 1H), 9.71 – 9.07 (m, 2H), 8.40 (s, 1H), 7.76 (dd, J = 8.4, 1.8 Hz, 1H), 7.53 (s, 1H), 7.41 – 7.34 (m, 2H), 7.31 (d, J = 8.5 Hz, 1H), 7.26 (d, J = 5.7 Hz, 3H), 7.18 (dd, J = 8.5, 1.9 Hz, 1H), 7.10 – 7.01 (m, 2H), 6.75 (dd, J = 8.6, 1.3 Hz, 1H), 6.49 (d, J = 8.6 Hz, 1H), 5.78 (q, J = 6.5 Hz, 1H), 4.14 – 4.06 (m, 2H), 3.99 (td, J = 14.0, 12.2, 3.6 Hz, 1H), 3.22 (d, J = 10.5 Hz, 1H), 3.01 (t, J = 11.6 Hz, 2H), 2.91 (s, 1H), 2.81 (t, J = 11.4 Hz, 1H), 2.71 (d, J = 11.1 Hz, 1H), 1.91 – 1.67 (m, 7H), 1.51 (dd, J = 23.8, 10.9 Hz, 2H).

^{13}C NMR (151 MHz, DMSO) δ 167.35, 158.98, 158.73, 158.50, 158.27, 152.66, 149.02, 137.01, 136.67, 136.61, 133.35, 131.89, 131.81, 130.69, 129.94, 129.24, 129.00, 128.67, 128.50, 127.41, 126.78, 125.75, 125.26, 124.89, 121.88, 121.59, 121.26, 120.53, 117.53, 115.58, 112.45, 105.20, 91.96, 66.05, 53.87, 53.63, 51.49, 50.94, 28.66, 28.39, 22.42, 20.09.

LC-MS [M+H]$^+$ m/z calcd. for [C$_{42}$H$_{38}$Cl$_3$N$_6$O$_5$]$^+$ 813.1 found 813.5 at 1.15 min. (UV Detector: TIC) (LC-MS method b).

Compound 2: (S)-6-chloro-3-(1-(1-(2,4-dichlorophenyl)ethyl)-4-phenyl-1H-imidazol-5-yl)-N-(5-(dimethylcarbamoyl)-2-(4-(2-oxo-1,3-oxazinan-3-yl)piperidin-1-yl)phenyl)-1H-indole-2-carboxamide
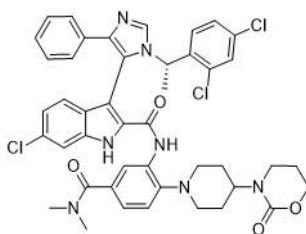
The compound was synthesized following the literature described procedure.[129]

^{1}H NMR (600 MHz, Chloroform-d) δ 9.45 (s, 1H), 8.88 (s, 1H), 8.52 (s, 1H), 8.11 (s, 1H), 7.57 (d, J = 7.5 Hz, 2H), 7.34 (s, 1H), 7.26 (q, J = 8.3 Hz, 2H), 7.22 – 7.13 (m, 3H), 6.87 (d, J = 8.6 Hz, 1H), 6.82 (d, J = 1.8 Hz, 1H), 6.67 (d, J = 8.7 Hz, 1H), 6.48 (d, J = 8.4 Hz, 1H), 6.36 (d, J = 8.6 Hz, 1H), 5.67 (q, J = 6.9 Hz, 1H), 4.19 – 3.97 (m, 3H), 3.15 (d, J = 29.2 Hz, 6H), 3.01

(s, 1H), 2.94 (d, J = 11.7 Hz, 1H), 2.85 – 2.71 (m, 2H), 2.41 (t, J = 11.9 Hz, 1H), 2.21 – 2.10 (m, 1H), 1.87 – 1.75 (m, 1H), 1.74 – 1.66 (m, 2H), 1.65 – 1.53 (m, 4H), 1.42 – 1.33 (m, 1H), 1.31 – 1.21 (m, 1H).

^{13}C NMR (151 MHz, CDCl3) δ = 170.98, 159.07, 153.24, 143.53, 137.22, 136.88, 135.80, 133.90, 133.70, 133.24, 132.00, 131.87, 131.63, 128.69, 128.43, 127.75, 127.27, 126.83, 126.67, 124.84, 124.04, 121.95, 121.91, 120.87, 119.22, 111.33, 106.37, 65.96, 54.38, 53.43, 52.62, 51.08, 39.70, 38.89, 35.53, 29.03, 28.55, 22.36, 20.16, 14.22.

LC-MS [M+H]+ m/z calcd. for [C44H43Cl3N7O4]+ 838.2, found 838.3 at 1.19 min. (UV Detector: TIC) (LC-MS method b).

Compound 3: (E)-cyclooct-4-en-1-yl(2-(3-(6-chloro-3-(1-((S)-1-(2,4-dichlorophenyl)ethyl)-4-phenyl-1H-imidazol-5-yl)-1H-indole-2-carboxamido)-4-(4-(2-oxo-1,3-oxazinan-3-yl)piperidin-1-yl)benzamido)ethyl)carbamate (racemic mixture).
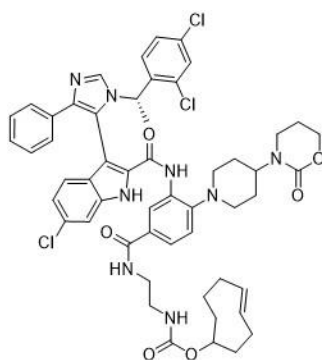
TEA (0.020 mL, 0.140 mmol) was added to a mixture of Intermediate 2 (40 mg, 0.047 mmol) and Intermediate 6 (17.73 mg, 0.061 mmol) in DMF (0.6 mL). The reaction was stirred at R.T. overnight, then evaporated under vacuum to obtain a yellow crude product. After purification via preparative HPLC (ACN/water mobile phase, TFA modifier), the fractions containing the desired product were combined and lyophilised to obtain a white solid. The solid was dissolved in DCM and NaHCO3 aq. sat solution was added. The organic phase was separated, washed with brine and evaporated to dryness to obtain compound 3 as a white solid.

^{1}H NMR (600 MHz, DMSO-d6) δ 12.65 (s, 1H), 9.22 (s, 1H), 8.43 (s, 2H), 7.63 (d, J = 8.5 Hz, 1H), 7.49 (s, 1H), 7.38 (d, J = 6.6 Hz, 2H), 7.30 (d, J = 8.4 Hz, 1H), 7.22 (d, J = 7.6 Hz, 3H), 7.17 (d, J = 10.4 Hz, 1H), 7.06 (s, 2H), 7.00 (s, 1H), 6.71 (d, J = 8.7 Hz, 1H), 6.40 (d, J = 6.4 Hz, 1H), 5.71 (s, 1H), 5.60 – 5.48 (m, 1H), 5.47 – 5.35 (m, 1H), 4.27 – 4.15 (m, 1H), 4.15 – 4.01 (m, 2H), 4.01 – 3.86 (m, 1H), 3.27 (q, J = 5.7 Hz, 4H), 3.11 (q, J = 5.9 Hz, 3H), 2.97 – 2.76 (m, 4H), 2.32 – 2.17 (m, 3H), 1.97 – 1.84 (m, 3H), 1.85 – 1.75 (m, 3H), 1.74 – 1.64 (m, 4H), 1.65 – 1.53 (m, 3H), 1.53 – 1.35 (m, 3H).

^{13}C NMR (151 MHz, DMSO) δ 166.26, 158.97, 158.59, 158.37, 156.40, 152.68, 147.03, 137.43, 136.99, 136.77, 135.41, 133.27, 133.01, 131.88, 131.61, 131.29, 130.31, 130.12, 130.00, 129.86, 129.13, 128.92, 128.67, 128.51, 126.72, 125.32, 124.41, 121.50, 121.42, 120.41, 112.42, 105.53, 79.60, 74.98, 66.07, 53.64, 53.41, 51.18, 41.17, 40.54, 40.42, 40.28, 40.14, 40.00, 39.86, 39.72, 39.58, 38.70, 34.25, 32.66, 31.08, 28.82, 28.50, 25.64, 25.06, 22.47, 20.15.

LC-MS [M+H]+ m/z calcd. for [C53H56Cl3N8O6]+ 1005.3, found 1005.4 at 1.32 min. (UV Detector: TIC) (LC-MS method b).

Compound 4: (2-methylcycloprop-2-en-1-yl)methyl(2-(3-(6-chloro-3-(1-((S)-1-(2,4-dichlorophenyl)ethyl)-4-phenyl-1H-imidazol-5-yl)-1H-indole-2-carboxamido)-4-(4-(2-oxo-1,3-oxazinan-3-yl)piperidin-1   yl)benzamido)ethyl)carbamate (diastereoisomers mixture)
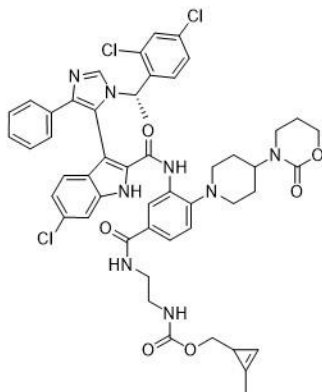
A solution of Intermediate 4 (58.4 mg, 0.234 mmol) in DMF (100 µl) was added dropwise to a solution of Intermediate 2 (50 mg, 0.059 mmol) and TEA (24.47 µl, 0.176 mmol) in DMF (500 µl) at R.T. under argon and the reaction was stirred at R.T. overnight. The reaction was poured in EA and the organic solution was washed with NaHCO$_3$ aqueous saturated solution and brine. The organic phase was dried with MgSO$_4$ and evaporated to dryness to obtain the crude material, then purified via prep-HPLC to afford Compound 4 (16 mg, 0.014 mmol, 24 % yield) as a TFA salt.

^{1}H NMR (600 MHz, DMSO-d6) δ 12.72 (s, 1H), 9.31 (s, 1H), 8.44 (s, 1H), 8.34 (s, 1H), 7.63 (d, J = 8.2 Hz, 1H), 7.50 (s, 1H), 7.35 (d, J = 6.4 Hz, 2H), 7.28 (d, J = 8.3 Hz, 1H), 7.22 (d, J = 6.6 Hz, 3H), 7.16 (d, J = 8.4 Hz, 2H), 7.04 (s, 1H), 7.02 (d, J = 8.3 Hz, 1H), 6.83 (s, 1H), 6.71 (d, J = 8.6 Hz, 1H), 6.44 (d, J = 8.4 Hz, 1H), 5.74 (s, 2H), 4.16 − 4.01 (m, 1H), 3.95 (s, 1H), 3.77 (ddd, J = 31.5, 11.1, 5.0 Hz, 1H), 3.35 − 3.22 (m, 1H), 3.15 (s, 3H), 3.15 − 3.06 (m, 3H), 2.99 − 2.87 (m, 2H), 2.87 − 2.75 (m, 2H), 2.62 (d, J = 22.9 Hz, 1H), 2.06 (d, J = 4.8 Hz, 3H), 1.86 − 1.58 (m, 7H), 1.48 (s, 3H).

^{13}C NMR (151 MHz, DMSO) δ 165.75, 158.42, 158.21, 157.98, 156.57, 152.19, 148.81, 146.82, 136.68, 136.22, 132.82, 131.39, 131.26, 130.59, 129.60, 129.39, 128.69, 128.46, 128.17, 127.99, 127.89, 126.24, 124.80, 124.05, 122.50, 121.04, 120.80, 120.30, 119.84, 111.93, 104.78, 102.24, 70.98, 65.55, 54.89, 53.13, 51.45, 50.69, 48.56, 28.25, 27.96, 21.91, 19.61, 16.72, 11.39. (3 carbon chemical shifts not reported hidden under the solvent peak were observed using HBMC).

LC-MS [M+H]+ m/z calcd. for [C50H50Cl3N8O6]+ 962.2, found 963.3 at 1.26 min. (UV Detector: TIC) (LC-MS method b).

Compound 5: 6-chloro-3-(1-((S)-1-(2,4-dichlorophenyl)ethyl)-4-phenyl-1H-imidazol-5-yl)-N-(5-(((2-methylcycloprop-2-en-1-yl)methyl)carbamoyl)-2-(4-(2-oxo-1,3-oxazinan-3-yl)piperidin-1-yl)phenyl)-1H-indole-2-carboxamide (diastereoisomeric mixture)
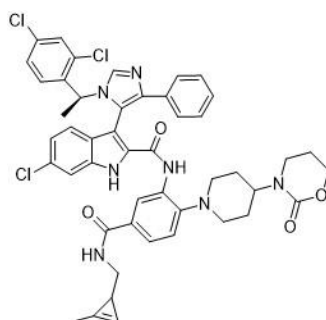
A mixture of Compound 1 (60 mg, 0.074 mmol), HBTU (56.0 mg, 0.148 mmol) and TEA (0.051 mL, 0.369 mmol) in DMF (1 mL) was stirred at R.T. for 15min. A solution of Intermediate 5 (34.4 mg, 0.222 mmol) in THF (0.1 mL) was added and the reaction was stirred at R.T. for 5h. EA (70 mL) and NaHCO$_3$ aq. sat. sol. (40 mL) were added. The organic phase was separated, washed with NaHCO$_3$ aq. sat. sol. (40 mL x 2), brine (40 mL), dried with MgSO$_4$ and evaporated to dryness to obtain the trimethylsilyl derivative of the desired product. This compound was dissolved in THF (3 mL), TBAF in THF (1M) (0.370 mL, 0.370 mmol) was added to the solution and the reaction was stirred at R.T. for 24h. The reaction was evaporated under vacuum to obtain a yellow residue which was purified via flash chromatography (silica column 4g, MeOH/DCM mobile phase). The fractions containing the desired product were combined and evaporated to dryness to obtain Compound 5 (33 mg, 0.037 mmol, 50 % yield) as a white solid.

^{1}H NMR (600 MHz, Chloroform-d) δ 9.64 (s, 1H), 8.74 (s, 1H), 8.67 (s, 1H), 8.00 (s, 1H), 7.55 (ddd, J = 8.0, 4.1, 1.9 Hz, 1H), 7.48 (d, J = 7.3 Hz, 2H), 7.28 (s, 1H), 7.21 – 7.14 (m, 1H), 7.12 – 7.03 (m, 3H), 6.79 (dd, J = 8.4, 1.9 Hz, 1H), 6.74 (s, 1H), 6.58 (s, 2H), 6.39 (d, J = 8.4 Hz, 1H), 6.28 (d, J = 8.6 Hz, 1H), 6.12 (d, J = 4.5 Hz, 1H), 5.57 (q, J = 6.9 Hz, 1H), 4.01 (ddd, J = 17.9, 9.0, 5.4 Hz, 2H), 3.96 – 3.89 (m, 1H), 3.41 (ddt, J = 13.5, 9.7, 4.9 Hz, 1H), 3.32 (tt, J = 13.7, 5.1 Hz, 1H), 2.97 – 2.88 (m, 1H), 2.84 (d, J = 18.4 Hz, 1H), 2.73 – 2.65 (m, 2H), 2.28 (t, J = 11.2 Hz, 1H), 2.11 (d, J = 5.0 Hz, 3H), 2.01 (d, J = 4.1 Hz, 1H), 1.67 – 1.58 (m, 2H), 1.52 – 1.44 (m, 4H), 1.37 (d, J = 2.1 Hz, 1H), 1.27 (d, J = 10.9 Hz, 1H), 1.20 – 1.12 (m, 2H).

^{13}C-NMR (151 MHz, CDCl3) δ 165.97, 165.92, 158.20, 152.22, 144.05, 142.17, 136.06, 135.93, 134.90, 132.77, 132.70, 131.06, 130.93, 130.61, 128.32, 128.11, 127.67, 127.40, 126.71, 126.24, 125.80, 125.63, 123.74, 123.24, 120.95, 120.85, 120.49, 120.45, 119.64, 117.56, 116.96, 116.93, 110.39, 105.41, 101.81, 101.78, 76.20, 75.99, 75.78, 64.91, 53.16, 52.32, 51.54, 49.81, 44.59, 44.55, 37.78, 27.95, 27.40, 21.28, 19.02, 16.95, 16.92, 10.68

LC-MS [M+H]$^+$ m/z calcd. for [C47H45Cl3N7O4]$^+$ 878.2, found 878.2 at 5.63 min. (UV Detector: TIC) (LC-MS method a).

Compound 6: 6-chloro-3-(1-((S)-1-(2,4-dichlorophenyl)ethyl)-4-phenyl-1H-imidazol-5-yl)-N-(5-((3-(((2-methylcycloprop-2-en-1-yl)methyl)amino)-3-oxopropyl)carbamoyl)-2-(4-(2-oxo-1,3-oxazinan-3-yl)piperidin-1-yl)phenyl)-1H-indole-2-carboxamide (diastereoisomeric mixture).
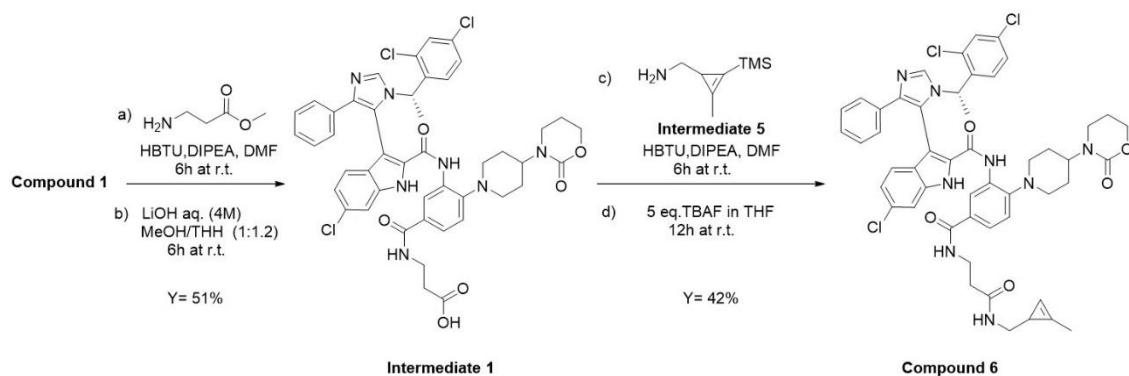
Scheme: Synthesis of **Compound 6**

A reaction mixture of Compound 1 (300 mg, 0.369 mmol), HBTU (280 mg, 0.739 mmol) and DIPEA (0.387 mL, 2.216 mmol) in DMF (3.8 mL) was stirred at R.T. for 20 min. Methyl 3-aminopropanoate (155 mg, 1.108 mmol) was added and the reaction was stirred at R.T. for 6h. The reaction mixture was then poured into EA, washed with NaHCO3 aq. sat. solution and brine. The organic solution was dried with MgSO$_4$ and evaporated to dryness to obtain a yellow solid. The

crude material was purified by flash chromatography (silica column 4g, MeOH/DCM mobile phase) to obtain the methyl ester derivative of Intermediate 1 (246 mg, 0.274 mmol, 74 % yield) as a yellow solid. LC-MS [M+H]$^+$ m/z calcd. for [C$_{50}$H$_{50}$Cl3N8O5]$^+$ 947.2, found 947.4 at 1.17 min. (UV Detector: TIC) (LC-MS method b).

LiOH aq. (4M) (0.343 mL, 1.371 mmol) was added to a solution of the methyl ester (246 mg, 0.274 mmol) in methanol (0.8 mL) and THF (1 mL) at 0°C. The reaction was allowed to reach R.T. and stirred for a further 6h. The reaction was concentrated under reduced pressure to obtain an oil. The oil was dissolved in DCM (120 mL) and aqueous HCl (0.5M; 100 mL) was added. The organic phase was separated, dried with MgSO$_4$ and evaporated to dryness to obtain Intermediate 1 (167 mg, 0.189 mmol, 69.0 % yield) as a yellow solid. LC-MS [M+H]$^+$ m/z calcd. for [C$_{45}$H$_{43}$Cl3N7O6]$^+$ 882.2, found 882.3.4 at 1.09 min. (UV Detector: TIC) (LC-MS method b).

A mixture of Intermediate 1 (102 mg, 0.115 mmol), HBTU (109 mg, 0.289 mmol) and TEA (0.080 mL, 0.577 mmol) in DMF (1 mL) was stirred at R.T. for 20 min. Intermediate 5 ((2-methyl-3-(trimethylsilyl)cycloprop-2-en-1-yl)methanamine) (53.8 mg, 0.346 mmol) was then added and the reaction was stirred at R.T. for 8h. The reaction was poured into EA (100 mL) and the solution was washed with NaHCO$_3$ aq. saturated solution (2 x 80 mL), brine (80 mL), dried with MgSO$_4$ and evaporated to dryness to obtain a yellow oil. TBAF in THF (1M) (0.575 mL, 0.575 mmol) was added to a solution of the oil in THF (2 mL) at R.T. and the reaction was stirred at R.T. for 12h. The reaction was evaporated to obtain a crude product which was purified via flash chromatography (silica column 12g, MeOH/DCM mobile phase) to obtain the desired product, Compound 6 (46 mg, 0.048 mmol, 41% yield) as a white solid.

^{1}H NMR (400 MHz, DMSO-d6) δ 12.34 (s, 1H), 8.79 (s, 1H), 8.70 (d, J = 2.0 Hz, 1H), 8.48 – 8.36 (m, 2H), 7.76 (t, J = 5.9 Hz, 1H), 7.57 (dd, J = 8.4, 2.0 Hz, 1H), 7.45 (d, J = 7.2 Hz, 2H), 7.39 (d, J = 1.6 Hz, 1H), 7.34 (d, J = 8.5 Hz, 1H), 7.18 – 7.10 (m, 3H), 7.08 (d, J = 7.3 Hz, 1H), 7.04 (d, J = 2.2 Hz, 1H), 6.80 – 6.71 (m, 2H), 6.62 (dd, J = 8.6, 1.9 Hz, 1H), 6.29 (d, J = 8.6 Hz, 1H), 5.54 (q, J = 7.0 Hz, 1H), 4.02 (dd, J = 8.3, 6.0 Hz, 1H), 3.98 – 3.90 (m, 1H), 3.84 (s, 1H), 3.43 (q, J = 6.9 Hz, 2H), 3.02 (d, J = 13.4 Hz, 1H), 2.90 (d, J = 7.6 Hz, 3H), 2.76 – 2.62 (m, 2H), 2.40 – 2.25 (m, 4H), 2.03 (d, J = 1.0 Hz, 3H), 1.79 – 1.42 (m, 7H), 1.36 (td, J = 4.4, 1.6 Hz, 1H), 1.26 – 1.20 (m, 2H).

^{13}C NMR (151 MHz, CDCl3) δ 171.53, 167.08, 159.09, 153.27, 145.36, 143.64, 143.13, 137.11, 136.91, 135.98, 133.72, 132.15, 131.55, 131.45, 129.30, 128.75, 128.45, 127.69, 127.29, 126.88, 126.67, 124.82, 123.85, 121.92, 121.81, 121.45, 120.56, 118.81, 111.53, 106.22, 102.86, 65.96, 54.14, 53.41, 52.64, 50.89, 45.36, 38.87, 36.32, 35.54, 28.97, 28.45, 22.33, 20.04, 17.77, 11.64.

LC-MS [M+H]$^+$ m/z calcd. for [C$_{50}$H$_{50}$Cl3N8O5]$^+$ 947.3, found 947.4 at 5.24 min. (UV Detector: TIC) (LC-MS method a).

Compound 7: (S)-N-(5-((2-azidoethyl)carbamoyl)-2-(4-(2-oxo-1,3-oxazinan-3-yl)piperidin-1-yl)phenyl)-6-chloro-3-(1-(1-(2,4-dichlorophenyl)ethyl)-4-phenyl-1H-imidazol-5-yl)-1H-indole-2-carboxamide
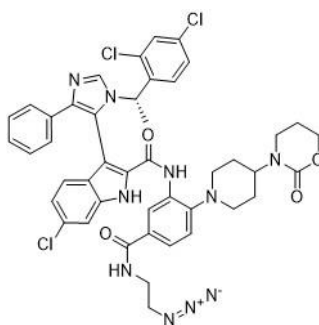
A mixture of Intermediate 2 (70 mg, 0.082 mmol), 1H-imidazole-1-sulfonyl azide (commercially available from SynAffix (20.61 mg, 0.098 mmol)), CuSO$_4$.5H$_2$O (1 mg, 4.01 μmol) and K2CO3 (16.99 mg, 0.123 mmol) in MeOH (1 mL) was stirred at R.T. for 4 h. The reaction was evaporated under reduced pressure to obtain a crude solid. The crude material was partitioned between DCM (100 mL) and water (50 mL). The organic phase was separated, dried with MgSO$_4$ and evaporated to dryness to obtain a residue. The residue was purified via flash chromatography (silica column 12g, MeOH/DCM mobile phase) to afford Compound **7** (43 mg, 0.048 mmol, 58.4 % yield) as a white solid.

^{1}H NMR (400 MHz, Chloroform-d) δ 9.49 (s, 1H), 8.80 (d, J = 1.8 Hz, 2H), 8.10 (s, 1H), 7.67 (dd, J = 8.3, 2.0 Hz, 1H), 7.60 – 7.54 (m, 2H), 7.37 (d, J = 1.4 Hz, 1H), 7.27 (s, 1H), 7.24 – 7.13 (m, 3H), 6.89 (dd, J = 8.4, 2.0 Hz, 1H), 6.83 (d, J = 2.0 Hz, 1H), 6.69 (dd, J = 8.6, 1.7 Hz, 1H), 6.57 (t, J = 5.5 Hz, 1H), 6.49 (d, J = 8.4 Hz, 1H), 6.38 (d, J = 8.6 Hz, 1H), 5.65 (q, J = 7.0 Hz, 1H), 4.17 – 4.07 (m, 2H), 4.07 – 3.97 (m, 1H), 3.65 (ddd, J = 25.1, 10.8, 5.1 Hz, 4H), 3.09 – 2.92 (m, 2H), 2.80 (dt, J = 12.2, 5.7 Hz, 2H), 2.39 (td, J = 11.9, 2.2 Hz, 1H), 2.14 (dt, J = 12.1, 6.1 Hz, 1H), 1.80 (s, 1H), 1.74 – 1.68 (m, 1H), 1.58 (d, J = 7.1 Hz, 4H), 1.41 – 1.33 (m, 1H), 1.32 – 1.23 (m, 2H).

^{13}C NMR (151 MHz, CDCl3) δ 167.29, 159.23, 153.30, 145.67, 143.01, 136.94, 136.06, 133.83, 132.07, 131.97, 131.67, 130.86, 129.17, 128.76, 128.49, 127.78, 127.42, 126.88, 126.65, 124.76, 124.43, 122.05, 121.79, 120.70, 118.42, 111.60, 106.45, 77.24, 65.99, 54.01, 53.47, 52.73, 50.83, 39.68, 39.56, 38.98, 29.72, 28.90, 28.39, 22.71, 22.32, 20.03, 14.16.LC-MS [M+H]$^+$ m/z calcd. for [C$_{44}$H$_{42}$Cl$_3$N$_{10}$O$_4$]$^+$ 879.2, found 879.3 at 1.22 min. (UV Detector: TIC) (LC-MS method b).

Compound 8 Ac-1TSFX$_r$EY(l-6-Cl)WALLX$_s$[11]-NH2
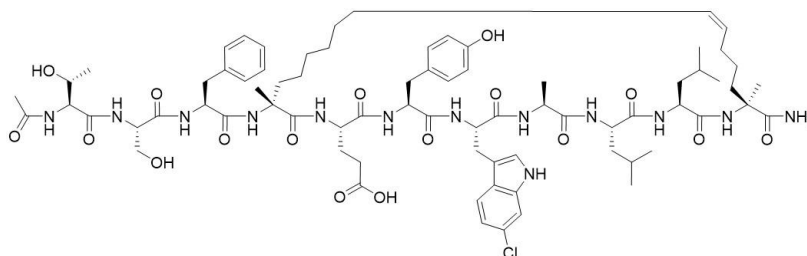
Intermediate 8 (261 mg, 0.075 mmol) was treated with 20% 4-Methyl-Piperidine in NMP (2 mL) and heated in a microwave for 30 seconds at 50 °C followed by 3 minutes at 75°C. The resin was washed with NMP (4 x 2 mL). Next, the acetylation of the N-terminus was performed adding on the swollen resin a solution of Ac$_2$O : Pyridine : DMA (1:1:8) (1 mL). The mixture was heated in a microwave for 30 second at 45° followed by additional 30 seconds at 50°C. The resin was washed with NMP (4 x 2 mL). The NMP-swollen Resin (Acetyl) was washed DCM (4 x 10 mL) and DCE (4 x 10 mL). Grubbs' first generation catalyst (0.025 mmol, 0.2 eq.) in DCE (2.5 mL) was added to the swollen resin and shake under N$_2$ bubbling. After 2.5 h the solution was removed and Grubbs' first generation catalyst (0.025 mmol, 0.2 eq.) in DCE (2.5 mL) was added. The reaction was run over night under N2 bubbling. Next, the resin was washed with DCM (3 x 20 mL) and NMP (4 x 15 mL), 5% Sodium diethyldithiocarbamate trihydrate in DMF (20 mL), NMP (3 x 20 mL), DCM (4 x 20 mL) and, finally the resin was dried. Next the resin was swollen again with DCM (dry) and a cleavage mixture (95% TFA, 5% H2O, 2.5% TIS and 2.5% DDT) was applied for 2.5h at R.T. After the cleavage solution was precipitated by adding cold diethyl ether (20 mL). The suspension was filtered over a Glass-frit (G4) and dried to obtain the crude material. The crude was dissolved in 95% TFA (2 mL) and purified via prep. HPLC. Two main peaks were separated. The fractions

containing the faster running compound were combined and lyophilized to obtain the desired product, compound **8** (2.62mg, 1.020 µM, 1.6% yield).

MS [M+H]$^+$ m/z calcd. for [C$_{75}$H$_{107}$ClN$_{13}$O$_{17}$]$^+$ 1496.7, found 1496.8 at 6.28 min. (UV Detector: TIC), [M+Na]$^+$ m/z calcd. For [C$_{75}$H$_{106}$ClN$_{13}$NaO$_{17}$]$^+$ 1518.7, found 1518.8 at 6.28 (LC-MS method c).

NMR analysis of compound 8 showed that the double bond on the stapling was in *Cys* conformation.

Compound 9
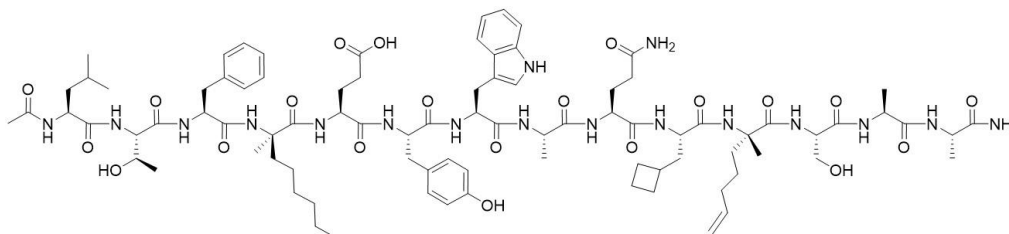
Intermediate 9 (47 mg, 0.024 mmol) was dissolved at R.T. In a solution containing DIEA (42.6 µl, 0.244 mmol), ACN (1.5 mL) and water (0.5 mL). N-Acetoxy Succinimide (46mg, 0.029mmol, 1.2 eq) in a solution of AcN (1.5 mL and water (0.5 mL) was added. After 7 minutes at R.T. the reaction was warmup to 45°C and heated for 30 minutes. A second addition of N-Acetoxy Succinimide 10% in AcN (46 mg, 0.029 mmo, 1.2 eq.) was done and the reaction was heated at 58° for 1h. The crude material was purified via prep. HPLC to afford after lyophilization compound **9** (29.8mg, 0.017mmol, 69% yield) as a white solid.

MS [M+H]$^+$ m/z calcd. for [C$_{87}$H$_{126}$N$_{17}$O$_{21}$]$^+$ 1745.1, found 1745.0 at 6.83 min. (UV Detector: TIC), [M+Na]$^+$ m/z calcd. For [C$_{87}$H$_{125}$N$_{17}$NaO$_{21}$]$^+$ 1567.0, found 1767.5 at 6.83 (LC-MS method c).

Compound 10 and 11
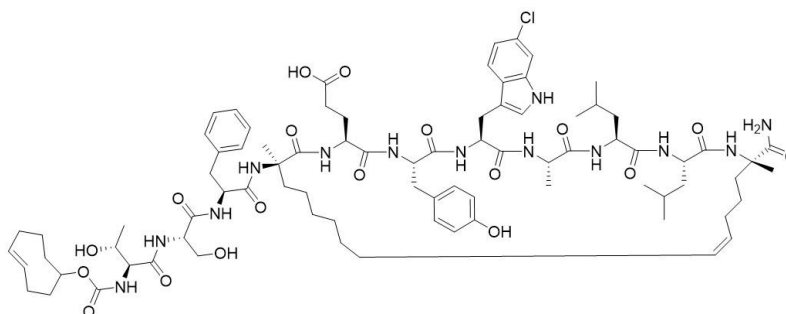
Intermediate 9 (21mg, 0.012 mmol) was dissolved in DMF (0.4 mL) containing DIPEA (10.53 µL, 0.060 mmol). Intermediate 6 (5.0mg, 0.017 mmol) dissolved in DMF (80 µL) was added and the solution was stirred at 50°C for 24h. The reaction was allowed to reach R.T. and was purified via prep. HPLC. Two peaks were separated and after lyophilization were obtained compound **10** (fast running diastereoisomers mixture) (4.52 mg, 2.81 µmol, 23% yield) as a while solid and compound (slow running diastereoisomers mixture) (4.75mg, 2.96 µmol, 24% yield).

Compound 10: MS [M+H]$^+$ m/z calcd. for [C$_{82}$H$_{117}$ClN$_{13}$O$_{18}$]$^+$ 1607.8, found 1607.8 at 7.11 min. (UV Detector: TIC) (LC-MS method c).

Compound 11: MS [M+H]$^+$ m/z calcd. for [C$_{82}$H$_{117}$ClN$_{13}$O$_{18}$]$^+$ 1607.8, found 1607.8 at 7.50 min. (UV Detector: TIC) and [M+Na]$^+$ m/z calcd. for [C$_{82}$H$_{116}$ClN$_{13}$NaO$_{18}$]$^+$ 1628.8, found 1628.8 at 7.50min (LC-MS method c).

Compound 12 and 13

Intermediate 10 was dissolved in a solution of DIPEA (37.5 µL, 0.215 mmol) and DMF (0.65 mL). Intermediate 6 (8.2mg,, 0.027 mmol) was added. The reaction was heated at 50 °C overnight. The reaction was allowed to reach R.T. and was purified via pre. HPLC. Two main peaks were isolated and lyophilized to obtain compound 12 (fast running diastereoisomers mixture) (10.8mg, 5.63 µmol, 30% yield) and compound 13 (slow running diastereoisomers mixture) (13mg, 6.81 µmol, 36% yield); both compound as white solids.

Compound 12: MS [M+H]$^+$ m/z calcd. for [$C_{94}H_{136}N_{17}O_{22}$]$^+$ 1856.0, found 1856.1 at 7.13 min. (UV Detector: TIC)(LC-MS method c).

Compound 13: MS [M+H]$^+$ m/z calcd. for [$C_{94}H_{136}N_{17}O_{22}$]$^+$ 1856.0, found 1856.1 at 7.24 min. (UV Detector: TIC)(LC-MS method c).

Compound 14

Intermediate 11 (56.2 mg, 0.030 mmol) was dissolved with DMA (440 µL) and DCE (6 mL). Grubbs catalyst first generation (3.7 mg, 4.54 µmol) in DCE (380 µL) was added. The mixture was shaken at 50°C under Argon for 30min. DMA (2 mL) was added. The DCE mixture was evaporated to obtain the solution of the crude material in DMA. The crude was purifed via prep. HPLC to afford, after lyophilization of the major isolated peak, compound **14** (20 mg, 9.94 µmol, 33 % yield) as a white solid.

MS [M+H]$^+$ m/z calcd. for [$C_{90}H_{131}N_{20}O_{21}$]$^+$ 1828.0, found 1828.0 at 3.46 min. (UV Detector: TIC)(LC-MS method c).

Compound 15: (E)-cyclooct-4-en-1-yl ((6S,9S,12S,15S,18S,21S,24S,27S,30S)-1,35-diamino-6-carbamoyl-9,12,15,18,21,24,27-heptakis(3-guanidinopropyl)-1,35-diimino-8,11,14,17,20,23,26,29-octaoxo-2,7,10,13,16,19,22,25,28,34-decaazapentatriacontan-30-yl)carbamate (**TCO-R₉-NH2**)
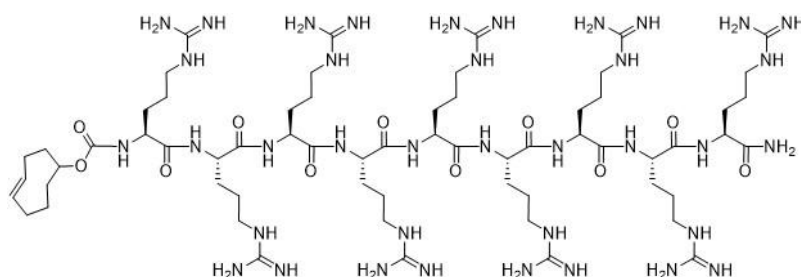
The peptide H-(Arg)₉-NH2 was obtained from American Peptide Company (Sunnyvale, CA, US) as a custom synthesis. 11.1 mg of this peptide (7.80 µmol) were dissolved in DMA (0.19 mL). DIPEA (0.117 mmol, 15eq) was added followed by Intermediate 6 (0.012 mmol, 1.5 eq) to achieve a peptide-concentration of about 5%. P-nitrophenol generation indicated the reaction was proceeding; this was complete after 17h. DMF (2 mL) was added to the reaction-mixture and the reaction mixture was evaporated to dryness in high vacuum. The resulting oil was dissolved in water (1.5 mL) and purified by preparative HPLC to give 2.6 mg of the product as a mixture of isomers. MS characterization shows the expected multi-charged peaks, e.g. MS calcd. for $[(M+7TFA+2)/2]^+=1187.0$ and $[(M+4TFA+3)/3]^+=715.7$ ($C_{63}H_{123}N_{37}O_{11}$ and MW 1574.9).

Intermediate 2: N-(5-((2-aminoethyl)carbamoyl)-2-(4-(2-oxo-1,3-oxazinan-3-yl)piperidin-1-yl)phenyl)-6-chloro-3-(1-((S)-1-(2,4-dichlorophenyl)ethyl)-4-phenyl-1H-imidazol-5-yl)-1H-indole-2-carboxamide
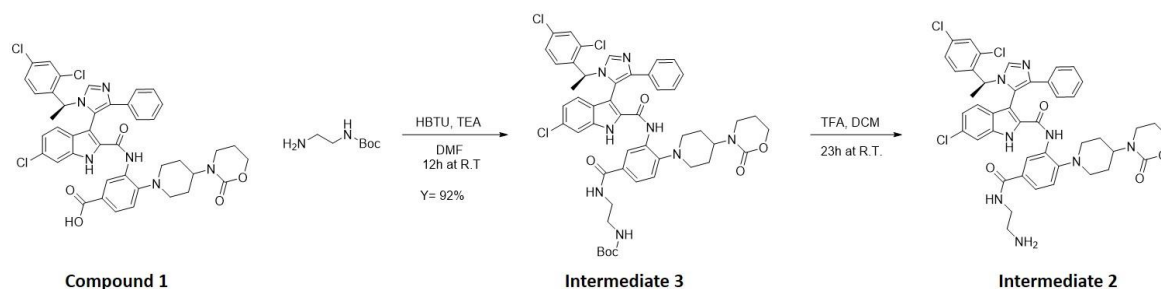
Scheme: Synthesis of Intermediate 2

A mixture of Compound **1** (643 mg, 0.792 mmol), HBTU (601 mg, 1.583 mmol) and TEA (0.552 mL, 3.96 mmol) in DMF (5 mL) was stirred in a flask under N2 for 20 min. N-Boc-Ethylenediamine [57260-73-8] Aldrich (0.314 mL, 1.583 mmol) was added and the reaction was stirred at R.T. overnight. The reaction was diluted with DCM, washed with NaHCO3 aq. sat. sol. and brine, dried with MgSO₄ and evaporated under vacuum to obtain a yellow solid. The crude product was purified via flash chromatography (silica column 40g, MeOH/DCM mobile phase). The fractions containing the desired product were combined and evaporated to dryness to obtain **Intermediate 3** (698 mg, 0.731 mmol, 92 % yield) as a white solid. LC-MS $[M+H]^+$ m/z calcd. for $[C49H52Cl3N8O6]^+$ 953.3, found 953.5 at 1.28 min. (UV Detector: TIC) (LC-MS method b).

TFA (1.0 mL, 13.0 mmol) was added to a solution of **Intermediate 2** (623 mg, 0.653 mmol) in DCM (7 mL) and the reaction was stirred at R.T. for 23h. The reaction was then diluted with DCM, washed with NaHCO3 aq. sat. solution and brine,

dried with MgSO₄ and evaporated to dryness to obtain Intermediate 3 (554 mg, 0.636 mmol, 97 % yield). LC-MS [M+H]⁺ m/z calcd. for $[C_{44}H_{44}Cl_3N_8O_4]^+$ 853.2, found 853.4 at 1.02 min. (UV Detector: TIC) (LC-MS method b).

Intermediate 4 (2-methylcycloprop-2-en-1-yl)methyl (4-nitrophenyl) carbonate (racemic mixture)
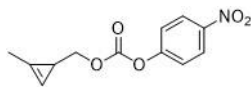
The title compound was prepared starting from Intermediate 7 following a literature procedure.[145]

¹H NMR (400 MHz, Chloroform-d) δ 8.32 – 8.22 (m, 2H), 7.38 (dt, J = 7.6, 2.6 Hz, 2H), 6.60 (s, 1H), 4.27 – 4.06 (m, 2H), 2.17 (d, J = 1.0 Hz, 3H), 1.77 (td, J = 5.3, 1.5 Hz, 1H).

Intermediate 5 (2-methyl-3-(trimethylsilyl)cycloprop-2-en-1-yl)methanamine (racemic mixture)

The title compound was prepared starting from Intermediate 7 following a literature procedure.[146]

¹H NMR (400 MHz, Chloroform-d) δ 2.60 (d, J = 4.5 Hz, 2H), 2.22 (s, 3H), 1.47 (t, J = 4.5 Hz, 1H), 0.17 (s, 9H).

Intermediate 6 (E)-cyclooct-4-en-1-yl (4-nitrophenyl) carbonate (racemic mixture)
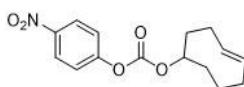
The title compound was prepared following a literature procedure.[147]

¹H NMR (400 MHz, Chloroform-d) δ 8.29 (d, J = 9.2 Hz, 2H), 7.39 (d, J = 9.2 Hz, 2H), 5.76 – 5.44 (m, 2H), 4.48 (dd, J = 10.5, 3.2 Hz, 1H), 2.51 – 2.34 (m, 3H), 2.27 – 2.10 (m, 2H), 2.08 – 1.86 (m, 3H), 1.77 (td, J = 14.2, 13.3, 4.3 Hz, 2H).

Intermediate 7 (2-methyl-3-(trimethylsilyl)cycloprop-2-en-1-yl)methanol (racemix mixture)

The title compound was prepared from 2-ethoxy-2-oxoethanediazonium and trimethyl(prop-1-yn-1-yl)silane following a literature procedure.[148]

¹H NMR (600 MHz, Chloroform-d) δ 3.31 (t, J = 5.4 Hz, 2H), 2.04 (s, 3H), 0.82 (s, 1H), 0.00 (s, 9H).

Intermediate 8:
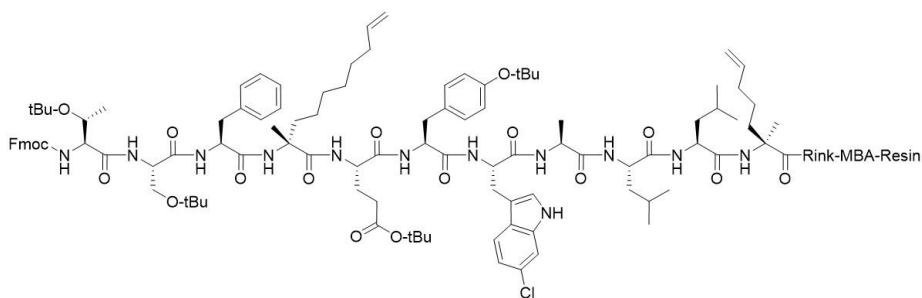
Fmoc-Rink-MBA-Resin (1.1 g, 0.473 mmol) was transferred in a reaction vessel and swollen with DCM for 20 min at R.T. The reaction vessel was transferred to a microwave peptide synthesizer (ALSTRA Biotage) already charged with stock

solutions of mixture of Fmoc aminoacids and Ethyl cyano(hydroxyimino)acetate (1:1) in NMP (0.2M). Stock solutions of Fmoc-(S)-2-(4-pentenyl)Ala-OH (Fmoc-S5-OH) , Fmoc-(R)-2-(7-octenyl)Ala-OH (Fmoc-R8-OH) and Fmoc-6-chloro-L-Tryptophan were also prepared by mixing the amino acids with Ethyl cyano(hydroxyimino)acetate (1:1) in NMP to obtain a 2M solution. The coupling was performed by adding a solution of DIPEA in DMA (2M) (1.5 mL), the coupling reagent and the amino acid. For all the couplings, except the reaction with Fmoc-S5-OH, Fmoc-R8-OH, Val in 7, Trp in 6 and Arg in 4, the coupling was performed with HCTU (0.946 mmol, 2.0 eq.). While the introduction of Fmoc-S5-OH, Fmoc-R8-OH, Val in 7, Trp in 6 and Arg in 4 was performed by double coupling using in the first coupling reaction PyOAP and in the second HATU, both (0.496 mmol, 1.05 eq). The reactions were performed heating in the microwave irradiation for 30 second to reach 60°C and for 7 minutes at 70°C. After synthesis, the resin was dried with high vacuum in a desiccator for 30min at R.T. to obtain 2.147g of loaded linear peptide resin, **Intermediate 8**.

Intermediate 9
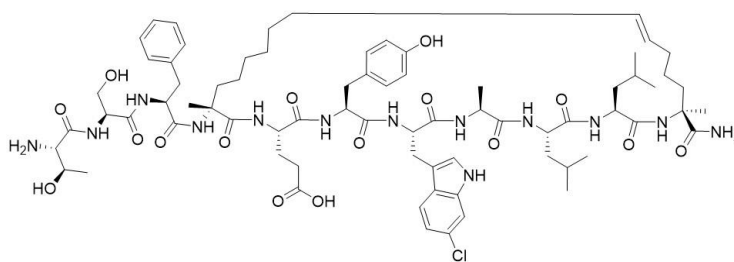
The loaded linear peptide resin, Intermediate 8, (1.677g, 0.255 mmol) was washed 3 x with DCM and swollen for 15 minutes in DCM at 50°C, under Argon-bubbling. Fresh prepared cleavage-solution (95%TFA : TIS (95:5)) (15 mL) was added to the resin. After 19 minutes at 50°C the mixture was cooled at R.T. and precipitated in DIP: PE = 1:1 (200 mL) under stirring at 0°C. The resin was washed 3 x with 95% TFA (4 mL) and precipitated. After 15 minutes at 0°C a white suspension was filtered over a glass-frit (G3). The filter-cake was washed 2 x with 50% Diisopropyl ether / Petrol ether (8 mL) and dry for 10 minutes at R.T. with high vacuum in a desiccator to obtain 310.8mg of linear peptide. The linear peptide (88 mg, 0.057 mmol) was dissolved in a solvent mixture of DMA (1.6 mL) and DCE (14 mL) (dry and degassed with Argon) at 50°C. During gentle bubbling with Argon, a deep purple solution of Grubbs I (9.4 mg, 0.11 mmol) in DCM (2 mL) was added with a syringe-pump (1.2 mL/h). After 1.5h the reaction was evaporated to about 2 mL. Next, 20% 4-Methyl-Piperidine in NMP (2 mL) was added to the solution and the resulting mixture was heated in a microwave for 30 seconds at 50 °C followed by 3 minutes at 75°C. After, solvent evaporation, the crude material was purified via HPLC. Two main peaks were separated. The faster eluting peak was lyophilized over night to afford **Intermediate 9** (31.8mg, 0.021mmol, 8% yields) as a white powder.

MS [M+H]$^+$ m/z calcd. for $[C_{73}H_{106}ClN_{13}O_{16}]^+$ 1454.7, found 1454.7 at 1.82 min. (UV Detector: TIC)(LC-MS method c).

Intermediate 10
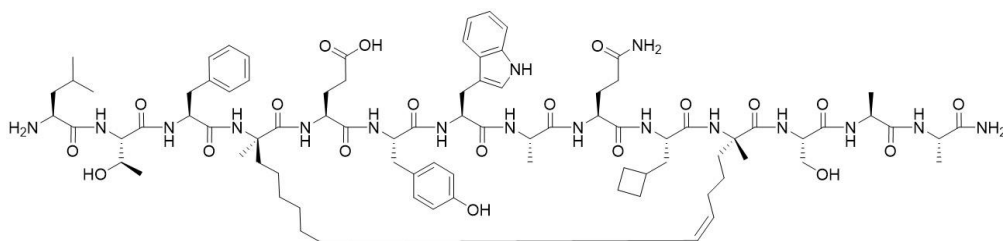
The title compound was outsourced from Aurigene Discovery Technologies Ltd.

Intermediate 11
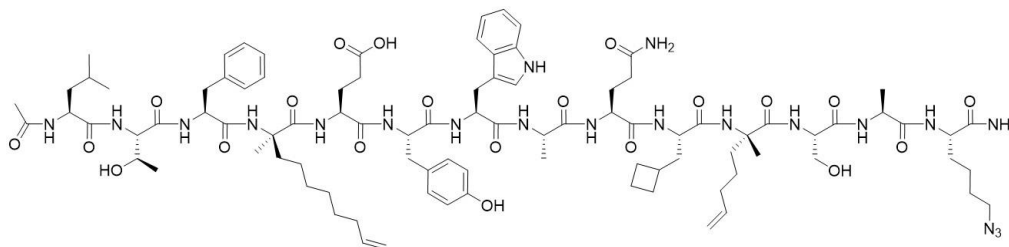
To intermediate 12 (1.37g, 0.44mmol, 0.32 mmol/g) swollen in DCM (4 mL) was applied twice a cleavage solution of 5% TIS in TFA (12 mL) for 10 min at R.T under shaking. The two cleavage solutions were combined and 50% Diisopropyl ether / Petrol ether (400 mL) was added under stirring. The resulted suspension was filtered over a glass-frit (G3) and washed with 50% Diisopropyl ether / Petrol ether (3 x 50 mL). The solid was dried under high vacuum overnight for 2h. Next, the solid was dissolved in ACN (8 mL) and heated at 45 °C overnight to afford a yellow solution which was evaporated to ca. 3 mL . The solution containing the desired product was purified via prep. HPLC to afford after lyophilization of the fractions containing the desired product, intermediate 11 (56mg, 0.029 mmol, 7% yield).

Intermediate 12
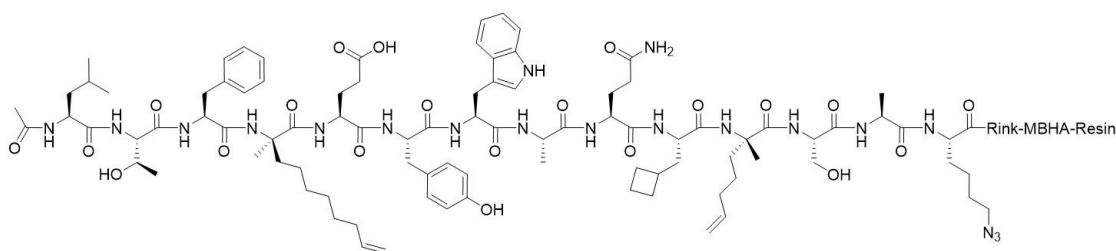
Fmoc-Rink-MBA-Resin (1.319 g, 0.660 mmol, 0.5 mmol/g) was transfred in a reaction vessel and swollen with DCM for 20min at R.T. The reaction vessel was transferred to a microwave peptide synthesizer (ALSTRA Biotage) already charged with stock solutions of mixture of Fmoc aminoacids and Ethyl cyano(hydroxyimino)acetate (1:1) in NMP (0.2M). Stock solutions of Fmoc-(S)-2-(4-pentenyl)Ala-OH (Fmoc-S5-OH) , Fmoc-(R)-2-(7-octenyl)Ala-OH (Fmoc-R8-OH) and Fmoc-lysine azide (Anspec Ltd.) were also prepared by mixing the amino acids with Ethyl cyano(hydroxyimino)acetate (1:1) in NMP to obtain a 2M solution. The coupling was performed by adding a solution of DIPEA in DMA (2M) (1.5 mL), the coupling reagent and the amino acid. For all the couplings, except the reaction with Fmoc-S5-OH, Fmoc-R8-OH and Fmoc-lysine azide, the coupling was performed with HCTU (0.946 mmol, 2.0 eq.) and AA (1.1 eq.). While the introduction of Fmoc-S5-OH, Fmoc-R8-OH and Fmoc-lysine azide was performed by using AA (2.0 rq.) and double coupling, where in the first coupling reaction was used HCTU and in the second HATU, both (0.496 mmol, 1.05 eq). The reaction were performed heating in the microwave irradiation for 30 second to reach 60°C and for 7 minutes at 70°C. After synthesis

the resin was dried with high vacuum in a desiccator for 30min at R.T. to obtain 2.046g of loaded linear peptide resin. The linear peptide resin was then subjected to Fmoc de-protection and N-terminus acetylation. To the shrink resin 20% 4-Methyl-Piperidine in NMP (20 mL) was added and the mixture was shaken for 10min. The procedure was repeated and the resin was washed with DCM, IPA and 0.3% DIEA in DCM. The DCM-swollen resin was acetylated with DMA : Ac2O : Pyridine (8:1:1) (10 mL) and shaked well for 10min at R.T. the resin was washed again with DCM, IPA and 0.3% DIEA in DCM and dried in high vacuum to obtain the linear peptide loaded on the resin (1.37g).

Chapter 3. The bioorthogonal probe intracellular distribution, target engagement and occupancy

The bioorthogonal probes synthesized were employed for developing a "two step" bioorthogonal imaging approach enabling studies of intracellular distribution and subsequently compound target engagement and target occupancy.

3.1   Two step imaging approach

Bioorthogonal chemistry associated to fluorescent imaging has been previously used for studying intracellular and extracellular distribution of wild type and metabolically or genetically modified endogenous molecules such as proteins[68,149], glycans[150] and fatty acids[151]. Additionally, this approach has been applied to enable investigations of intracellular distribution of xenobiotics such as small molecules[66,67] and peptides[41].

The latter studies are usually conducted following the so-called "two step" approach. In the first step, the test molecule labelled with a bioorthogonal group is applied to a cell culture. After cellular uptake, the molecule distributes to intracellular compartments and organelles or it binds to its targets. In the second step, a fluorescent reporter labelled with a second bioorthogonal group, able to react orthogonally and irreversibly with the molecule of interest, is applied to the cells. Upon its internalization and distribution, the fluorescent reporter will label the molecule of interest . Therefore, the irreversible formation of the bioorthogonal product (the product of the reaction between the tagged molecule and the fluorophore) will enable the visualization of the intracellular distribution of the molecule of interest.

The "two step" approach can be applied on live or fixed cells using reactions such as SPAAC, IED-DA and Staudinger–Bertozzi ligation.[152] Additionally, some literature examples reported the use of copper "Click" chemistry to visualize compounds either inside the cell[153] or metabolically incorporated on the cell surface.[154]

Figure 3.1-1 depicts how we envisaged applying the two-step approach to our MDM2-p53 inhibitor bioorthogonal probes using our chosen bioorthogonal reactions. The IED-DA approach (**Fig 3.1-1a**) utilizes a quenched fluorophore which is turned on as a result of the bioorthogonal coupling. The SPAAC approach (**Fig. 3.1-1b**) utilizes an un-quenched 'always on' fluorophore throughout. We chose not to use the Copper Catalyzed Azide-Alkyne Cycloaddition (CuAAC), first developed by Sharpless[40], which does offer some favourable features in terms of fast reaction kinetics, small size

of the reactive groups and their chemical stability. Nevertheless, to be used in a bioorthogonal setting the cytotoxicity of the active catalyst, Copper(I), and of sodium ascorbate (reducing agent used in excess to form Cu(I)) has to be circumvented using some stratagems. Indeed, Cu(I) generates reactive oxygen species (ROS) known for leading to breaks of double-stranded DNA,[155] and other diverse oxidative processes (e.g. protein oxidation[156] and bio-macromolecular damage[157]). Additionally, ascorbate and its oxidation product, dehydroascorbate, have been shown to induce
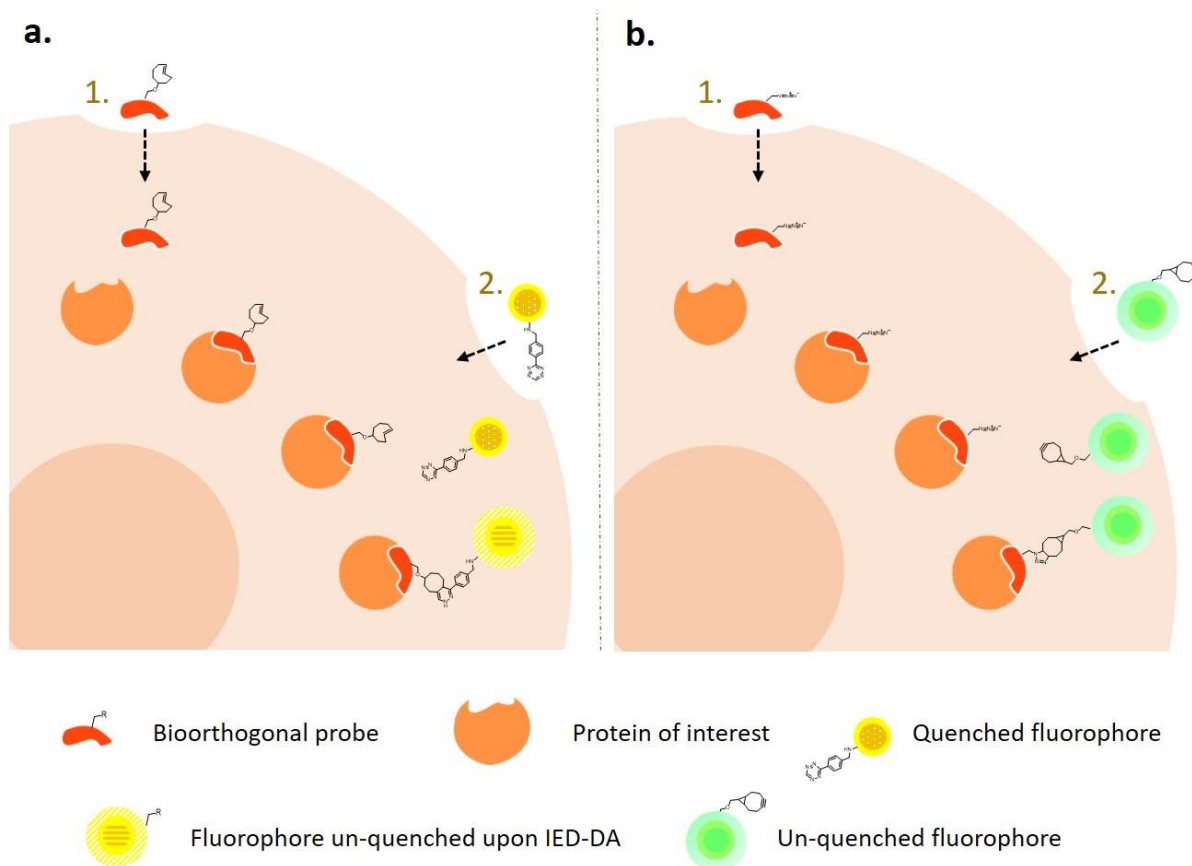
Figure 3.1-1 Depiction of two representations of the "two steps" imaging approach using in (**a**) a quenched fluorophore and in (**b**) an un-quenched fluorophore. Step 1. A functionalized small molecule permeates the cell and distributes inside the cell compartments. Step 2. Cells are incubated with a fluorophore which reacts bioorthogonally with the small molecule.

crosslinking with proteins[158]. Consequently, these induced cytotoxic effects may modify the target of the chemical probe (e.g. protein conformational changes due to oxidation) and, for that reason, affect the real intracellular distribution of the molecule of interest.

Several approaches have been developed to employ CuAAC for imaging studies of molecules in live systems by either circumventing the copper cytotoxicity and reducing the required level of sodium ascorbate (e.g. by using soluble ligands for stabilizing the copper ion and increasing the reaction speed[159]) or by simply performing the fluorescent staining step on fixed cells[55,153]. However, the SPAAC and IED-DA reactions appear to be still superior in terms of kinetics and they require a simpler protocol (no additional reagents have to be added to the cell culture).

Contrary to CuAAC, the use of SPAAC and IED-DA does not encounter any evident toxicity issues. Additionally, both reactions have fast kinetics with rate constants of the second-order (e.g. SPAAC between DIFO derivative and benzyl azide has K = 7.6×10^{-2} $M^{-1} \cdot s^{-1}$ and IEA-DA between a TCO derivative and 3,6-di(pyridin-2-yl)-1,2,4,5-tetrazine has K = 2×10^{3} $M^{-1} \cdot s^{-1}$)[122,160]. Ideally, the reaction employed in the imaging approach should have fast kinetics and proceed

efficiently with low concentrations of reactants in order to capture intracellular processes with sufficient sensitivity (e.g. intracellular distribution of the molecule of interest affected by the translocation of its protein target to different cell compartments).

As for IED-DA (**Figure 2.5-2**, page 39), the toolbox of bioorthogonally reactive groups for strain-promoted alkyne-azide [3 + 2] cycloaddition has grown considerably in the last 15 years (**Figure 3.1-2**). The pioneering work of Bertozzi on the use of cyclooctyne in SPAAC in living systems[161] (OCT, depicted in **figure 3.1-2**) raised the interest of different research groups in identifying new cyclooctynes with improved chemical and metabolic stability and faster kinetics. The toolbox allows the choice of the most appropriate bioorthogonal group for SPAAC accordingly to the study aim. While tagging a LMW with a DIBAC group (**Figure 3.1-2**) might significantly affect its physico-chemical properties, the tagging of a macromolecule (e.g. a protein) with this bioorthogonal tag may be acceptable in some circumstances.
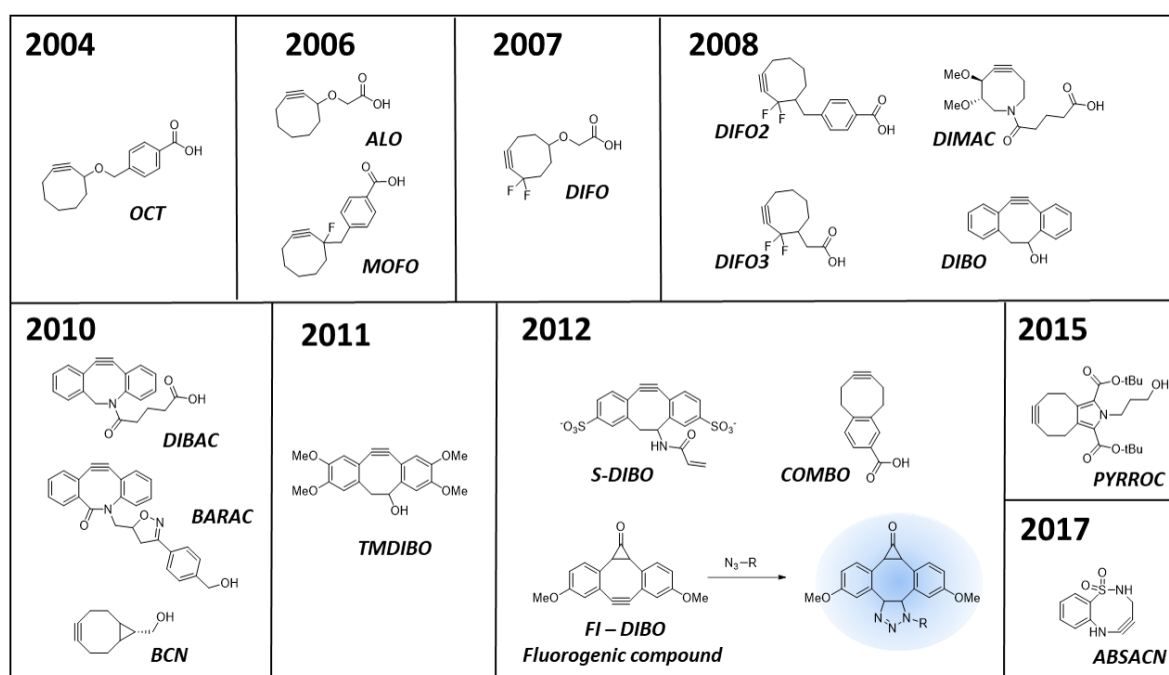
Figure 3.1-2 Strained Alkynes developed for SPAAC between 2004 and 2017 (adapted from Dommerholt, J., et all; *Topics in Current Chemistry*, 2016. 374(2): p. 16).

3.2   Fluorophore selection

The ideal tagged fluorophore for cell imaging using a bioorthogonal approach should combine classical fluorophore characteristics (such as maximum excitation and emission wavelength, extinction coefficient, quantum yield, Stokes shift, thermal and photochemical stability) with physico-chemical properties enabling its cellular permeability (suitable molecular weight, polarity, solubility, 3D shape, number of rotatable bonds and polar surface area (PSA).

Thus, for intracellular applications such molecules must show: 1) excellent membrane permeability accomplished via passive diffusion to accumulate inside the cell in high concentration; 2) have an even intracellular distribution and 3) good intracellular diffusivity[162].

The study of a set of structurally diverse fluorescent probes for potential imaging applications using intracellular chemistry published by Cunningham et al. highlighted the great advantages of BODIPY (Boron-dipyrromethene or 4,4-difluoro-4-bora-3a,4a-diaza-s-indacene) and TAMRA (*N,N,N',N'*-tetramethylaminorhodamine) based fluorophores (**Figure 3.2-1**).[162] Their work on BODIPY and TAMRA azide reporters showed that such BODIPY fluorophores have good cellular

BODIPY   **TAMRA**

Figure 3.2-1 BODIPY and TAMRA fluorophore cores

accumulation, whereas TAMRA-based probes have not only a good cellular uptake but the most uniform intracellular distribution and best cytosolic diffusivity (assessed using fluorescence recovery after photo-bleaching method, FRAP) as well. Other fluorophores included in their study such as Alexa Fluor 430, Oregon green, or Cascade Yellow unveiled inappropriate intracellular accumulation, low cytosolic diffusivity or localization in cell organelles and compartments.

The BODIPYs are extremely interesting fluorophores being relatively apolar, electrically neutral and lipophilic. Thanks to these physico-chemical properties, they usually have good membrane permeability. Furthermore, they are rather insensitive to pH and polarity of the environment and they exhibit high fluorescence quantum yield and narrow excitation and emission bandwidths enabling studies in combination with other fluorophores (e.g. multicolor microscopy on a single sample for imaging of multiple subcellular entities and co-localization studies).

Finally, by appropriately decorating the core structure, 4,4-difluoro-4-bora-3a,4a-diaza-s-indacene, their emission wavelengths can be tuned to cover the visible spectrum from green (e.g. BODIPY-FL with $\lambda_{max\ Abs}$= 503 nm and $\lambda_{max\ Em}$= 511)[163] to the far red zone (BODIPY-TR with $\lambda_{max\ Abs}$= 598 nm and $\lambda_{max\ Em}$= 625) (**Figure 3.2-2**).

3.2-2 Fluorescence excitation and emission spectra for BODIPY-FL, BODIPY-TMR and BODIPY-TR (from Fluorescence Spectra Viewer - https://www.thermofisher.com)

Devaraj et al. reported for the first time that tetrazine functionalization can be used to quench the BODIPY fluorescence and at the same time serve as a handle for IED-DA.[164] Tetrazines are electron-deficient heterocyclic aza dienes which react with high energy dienophiles such as *trans*-cyclooctenes via a retro [4 + 2] cycloaddition[165] (**Figure 3.2-3**). Upon cycloaddition, N_2 is released and the loss of the tetrazine functionality leads to fluorophore un-quenching.

As a result, a 10-20 fold increase in fluorescent signal upon reaction was reported for Tz-BODIPY FL and Tz-BODIPY TMR (**Figure 3.3-1**),[66] while a 1600 fold increase was achieved with some second generation tetrazine-BODIPYs; so-called "Superbright Bioorthogonal Turn-on Probes" (e.g. **dye 3** in **Figure 3.3-1**)[166].

Figure 3.2-3 IED Diels-Alder between tetrazine and *Trans*-cyclooctene (figure adapted *from J. Am. Chem. Soc., 2008. 130(41): p. 13518-9*).

The quenching mechanism is still under debate, although it was suggested a Förster resonance energy transfer (FRET) is operating for the first generation of Tz-BODIPY (Tz-BODIPY FL and Tz-BODIPY TMR)[66], while a FRET and through-bond energy transfer (TBET) mixed mechanism was hypothesized for the second generation of tetrazine-BODIPY, called simply Tz-BODIPY[166] (**Figure 3.3-1**). Thanks to this fluorescent induction upon reaction, a higher signal to background ratio was observed making the Tetrazine-BODIPYs excellent fluorophores for live cell imaging.

3.3 Building a fluorophore toolbox

Based on this data and the previously reported use of tetrazine functionalized BODIPY as "turn-on fluorophores" by the Weissleder's group we synthesized **dyes 1-2** (**Figure 3.3-3**) following the literature described procedures.[66,166,167]

Tz-BODIPY-FL
Dye 1

Tz-BODIPY-TMR
Dye 2

Second generation BODIPYs
Dye 3

Third generation BODIPYs
Dye 4

Silicon-Rhodamine-Tz
Dye 5
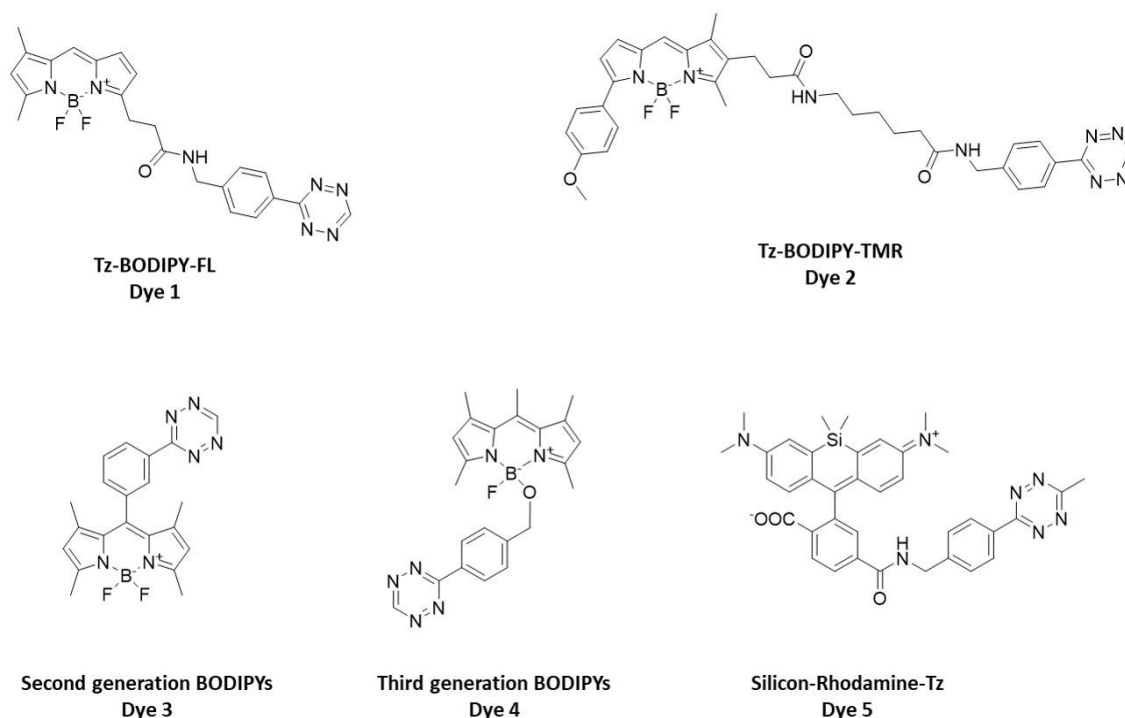
Figure 3.3-1 The tetrazine fluorophore toolbox, **Dye 1-5**

The synthesis of **dye 3** following the reported procedure[166] failed (**Figure 3.3-2**) therefore a new synthetic route for the preparation of this dye was established.

The reported synthetic route for the preparation of this dye and analogues was based on a two step synthesis where a BODIPY scaffold functionalized with the cyanophenyl group was a key intermediate. Next, this compound was engaged in the tetrazine formation using a zinc triflate (Zn(OTf)$_2$ catalyzed one-pot synthesis in the presence of hydrazine and
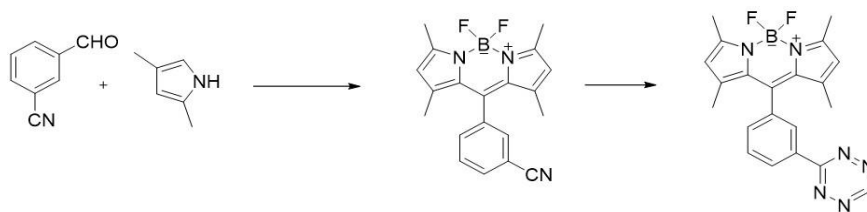
Figure 3.3-2 Literature synthetic approach for the synthesis of **dye 3**

acetonitrile and subsequent addition of sodium nitrite and HCl for the oxidation of the 1,2-dihydrotetrazines to the desired product (**Figure 3.3-2**).

Despite successfully synthesizing the cyanophenyl functionalized BODIPY scaffold, every attempt to form the tetrazine ring led to degradation products without formation of the desired dye.

Therefore, we decided to investigate if building up the BODIPY scaffold in the final synthetic step was feasible. Thus, we prepared the (3-(1,2,4,5-tetrazin-3-yl)phenyl)methanol using the previously reported metal catalyzed one-pot synthesis.[168] Next, we oxidized its benzyl alcohol group using Dess-Martin periodinane to afford the 3-(1,2,4,5-tetrazin-3-yl)benzaldehyde in good yield. Finally, we formed the BODIPY core using the previously describe procedure (**Figure 3.3-3**).
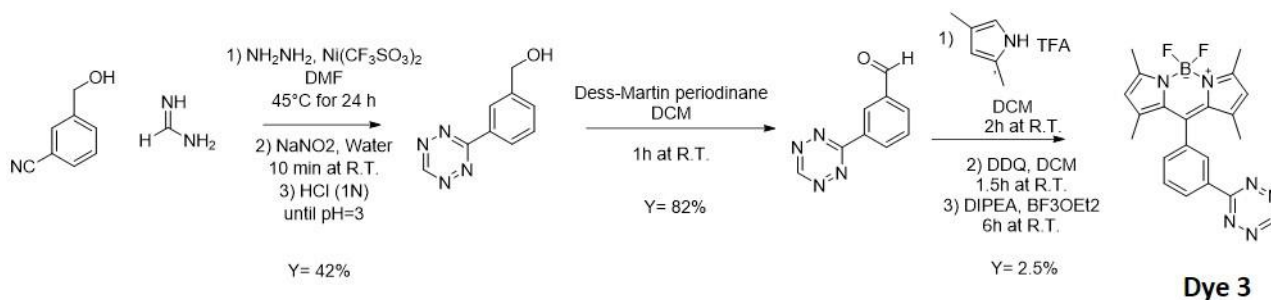
Figure 3.3-3 Synthetic scheme for preparation of **dye 3**.

Even though, the final synthetic step of the newly developed synthetic route was very low yielding, the same synthetic approach was applied for the synthesis of a di-substituted tetrazine analogue of dye 3 (not reported here) with improved yields. For this reason, we think that this synthetic approach may be a good alternative to the one previously published.

During the syntheses, we observed poor solubility for some of the tetrazine BODIPY analogues such as **dye 3**. Mazitschek's Group reported the development of a new class of BODIPY dyes, based on an alkoxy-fluoro-boron-dipyrromethene core, defined by us as the third generation BODIPYs, (**Figure 3.3-3**), which possess higher solubility.[169]

Accordingly, the alkoxy BODIPY, **dye 4**, was synthesized and added to our tetrazine fluorophore toolbox (**Figure 3-8**).For further improving our chances of success in developing a "two step" imaging strategy, we decided to include a near-infrared radiation (NIR) fluorophore in our library with potential to extend our imaging approach to super resolution microscopy. Hence, we chose to synthesize **dye 5** (**Figure 3.3-1**), a Silicon-Rhodamine core functionalized by a tetrazine.[170]

Quenched fluorophores that can be unquenched upon bioorthogonal reaction have the great advantage of improving the signal to background noise ratio and they may enable live cell real time imaging without the need for dye wash-out steps after staining. To date, most of the fluorophores presenting this peculiar characteristic possess a tetrazine moiety while only a small number of reported fluorophores are quenched with an azide group (e.g. 3-Azidocoumarins)[171] or with alkynes (e.g. Fl-DIBO depicted in **Figure 3.1-2**)[172]. Additionally, the published tetrazine quenched fluorophores cover a broader emission spectrum than reported 3-azidocoumarins. The latter have emission spectra in the range $\lambda_{Max\ Em}$ = 388-521 nm[171] which may limit their use in multicolor microscopy experiments, so we chose not to apply azide fluorophores in our work.

Nevertheless, we did want to evaluate azide functionalization of our chemical probes as this small and convenient tag offers a complementary approach (to our TCO method) by enabling a different bioorthogonal chemistry (SPAAC). This implies the use of an un-quenched fluorophore-alkyne reaction partner, which may necessitate developing a strategy to overcome issues due to high background noise. Thus, we included fluorophores functionalized with the bicyclo[6.1.0]non-4-yne group (BCN) in our tool box of fluorescent reporters.

The bicyclononynes were discovered by van Delft's group and used for labeling surface glycans on living human melanoma MV3 cells.[173] Van Delft highlighted the clear advantages of the BCN compared to earlier poorly soluble cyclooctynes. Maintaining a high reactivity, this bioorthogonal group is smaller and less lipophilic compared to derivatives such as 4-dibenzocyclooctynol and dibenzoazacyclooctyne (DIBO and DIBAC respectively) (see structures in **Figure 3.1-2**). Additionally, this label is easy to synthesize and is symmetrical, so its bioorthogonal cycloaddition product is a single regioisomer.[173] Thus, a BCN Rhodamine based fluorophore (**dye 6**) and a BCN-BODIPY (**dye 7**) were synthesized (**Figure 3.3-4**).

Finally, we included a fluorogenic fluorophore based on the dibenzocyclooctyne scaffold previously reported by Friscourt et al., Fl-DIBO[172] (**dye 8**) (**Figure 3.1-2** and **3.4-4**).

TAMRA-BCN
Dye 6

BODIPY FL-BCN
Dye 7

Fl-DIBO
Dye 8
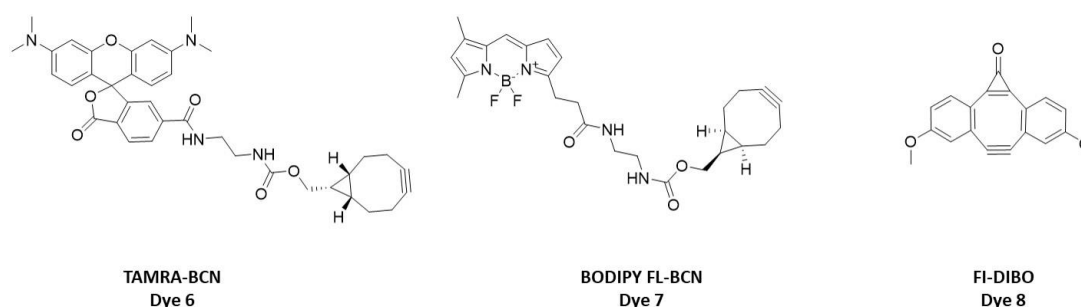
Figure 3.3-4 Strained alkyne fluorophores

3.3.1. Testing the reaction between bioorthogonal probes and dyes in vitro

Before engaging in the cellular experiments, we tested the bioorthogonal reactions between probes and dyes in PBS in a cell free system (see **Figure 3.3-5** for representative examples).
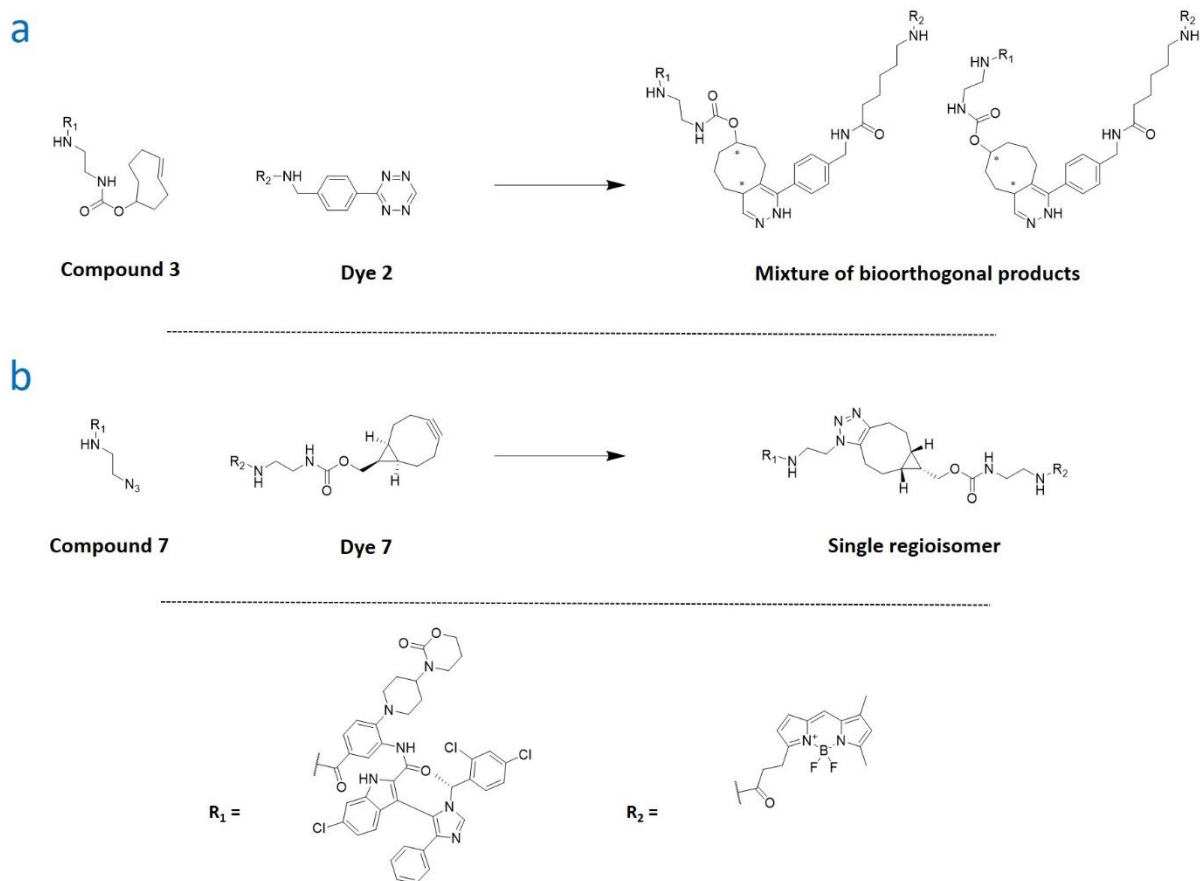
Figure 3.3-5 Depicted in the picture an IED-DA and a SPAAC reaction. In (**a**) the IED-DA between **3** and **dye 2** generates a mixture of bioorthogonal products. While in (**b**), upon SPAAC between **7** and **dye 7** a single regioisomer is produced.

The reactants were dissolved in DMSO to obtain 10 millimolar stock solutions, which were sequentially added to PBS in a 1 to 4 ratio, bioorthogonal probe to fluorophore, to obtain a final concentration of probe equal to 0.42 micromolar. The reactions were analyzed with LC-MS at time equal 0 (just after the addition of the last reagent) and after 4 hours. Furthermore, reagent control samples at equal concentrations to the one of the reaction were analyzed at time 0 and after 4 hours (see **Figure 3.3-6** and **3.3-7** for representative examples).

The reaction between the bioorthogonal strained alkenes (**3**-**6**) and the tetrazine-BODIPYs (**dyes 1**-**4**) reached completion after 4 hours with formation of the expected bioorthogonal products.
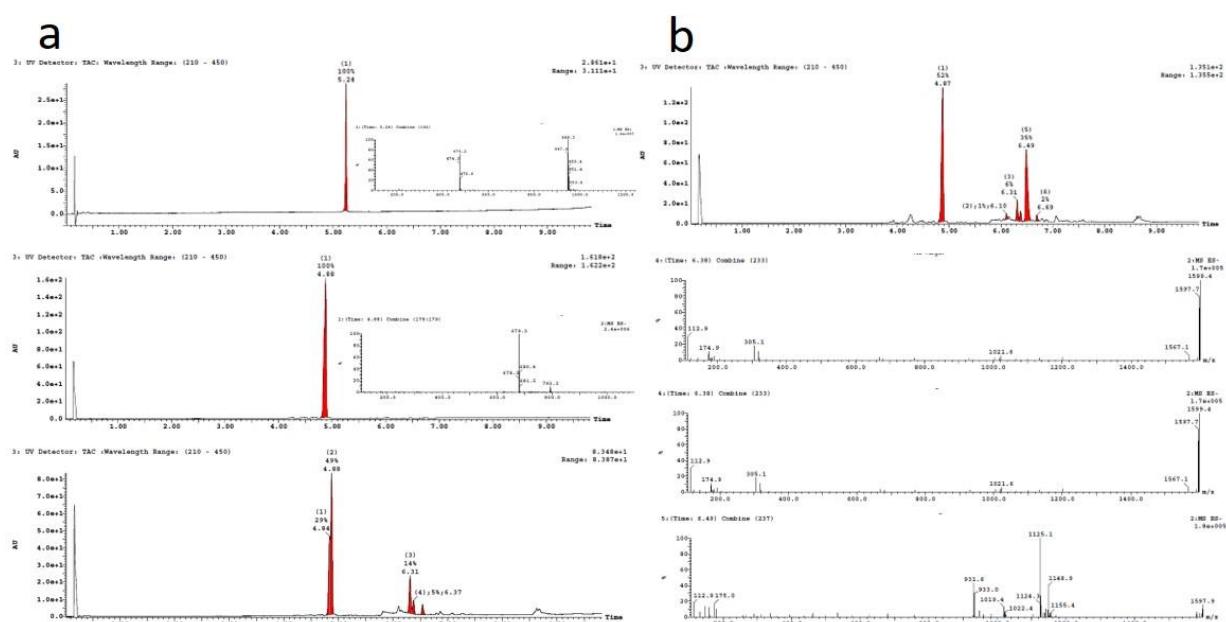
Figure 3.3-6 LCMS analyses of reaction between **6** and **dye 2** (1 : 4 cmpd to dye) at final concentration of probe equal to 0.42 mM. Depicted in the picture (**a**) LCMS analyses at t= 0 (just after the addition of the second reagent) and (**b**) at t= 4h. In (**a**) from top to down **6**, **dye 2** and reaction mixture. In (**b**) LCMS showed mixture of bioorthogonal product regioisomers; confirmed by MS of major peaks (Adapted from *D'Alessandro, P.L., et al. Angew. Chem. Int. Ed. Engl., 2016*).

The IED-DA between an unsymmetrical tetrazine and the chiral strained alkenes (TCO or cyclopropene) produced several regio-isomeric bioorthogonal products (see **Figure 3.3-6** for reaction between **6** and **dye 2**). Similar kinetics were observed for the reactions between the azide bioorthogonal probe (**7**) and the two BCN-fluorophores (**dye 6** and **7**).
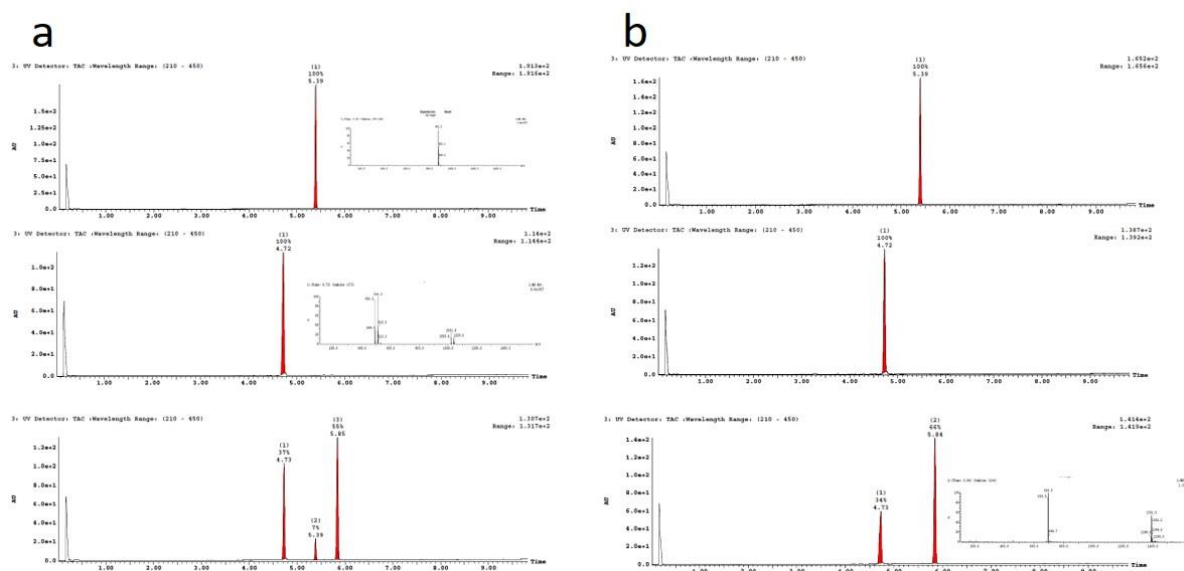
Figure 3.3-7 LCMS analyses of reaction between **7** and **dye 7** (1 : 4 cmpd to dye) at final concentration of probe equal to 0.42 mM. Depicted in the picture (**a**) LCMS analyses at t= 0 (just after the addition of the second reagent) and (**b**) at t= 4h. In both (**a** and **b**) from top to down **7**, **dye 7** and reaction mixture. Reaction went to completion when analyzed at 4h with formation of bioorthogonal product. (Adapted from *D'Alessandro, P.L., et al. Angew. Chem. Int. Ed. Engl., 2016*).

In these cases, the reaction affords a single regioisomer, due to the BCN being symmetric. Hence, a single product peak was observed by LC-MS (see **figure 3.3-7** for reaction between **7** and **dye 7**).

On the contrary, analyzing the reaction between a cyclopropene probe (**4**) and the tetrazine Silicon-Rhodamine (**dye 5**) and between the azide chemical probe (**7**) and the Fl-DIBO (**dye 8**), we did not observe full reaction conversion after 4 hours. Due to the slow reactivity of **dye 8**, its extremely poor solubility (observed preparing the compound stock solutions) and finally its low emission wavelength we decided not to progress this fluorophore to a cellular experiment.

We were very surprised by the poor reactivity of **dye 5.** This fluorophore contains a tetrazine functionalized with a methyl and a phenyl group, which should exhibit superior reactivity compared to its des-methyl analogue used for the functionalization of **dye 1-4**. To exclude that intermolecular interactions between **dye 5** and the bioorthogonal probe (**4)** might have hampered the reaction**,** we tested the reactivity of this dye with a 10 fold excess of a more reactive bioorthogonal group, the un-functionalized (E)-cyclooct-4-en-1-ol. In this case, we were even not able to detect traces of the desired bioorthogonal product. Therefore, **dye 5** was not progressed to the cellular studies.

3.3.2.   Evaluation of the intracellular distribution of the fluorophores

The intracellular permeability and distribution of the dyes play a very important role in the development of a "two step" bioorthogonal imaging approach for the validation of chemical probes. As shown by Cunningham et al, TAMRA and BODIPY based fluorophores exhibit properties favorable for cellular imaging studies.[162] Furthermore, some of the fluorophores we have synthesized such as **dyes 1 – 4** have been previously engaged in cellular imaging studies showing promising results.[66,166,169]

Despite, these studies being run in different cell lines, no data on the cellular permeability and intracellular distribution of these fluorophores in the SJSA-1 cell line (the selected cellular disease model) have been reported. In addition, **dyes 6** and **7** are new molecular entities and therefore their intracellular distribution has never been investigated.

Hence, planning to develop the "two step" approach, we investigated the intracellular distribution of the **dyes 1**-**4** and **6**-**7** in SJSA-1 cells using two different protocols, on fixed and live cells.

Therefore, **dyes 1**-**4** and **6**-**7** were applied to either fixed or live cells at 1 micromolar concentration. The cells were incubated with the fluorophores for two hours at R.T. for the fixed cells protocol or at 37 °C and 5% CO₂, for the live cells protocol. Additionally, BODIPY-FL methyl ester **dye 9** (**Figure 3.3-8**)[174] not labelled with a bioorthogonal probe was included in the live cell experiment as a negative control, after we established it was cellularly impermeable.

Figure 3.3-8 Dye **9**

The results obtained from fluorescence imaging of the tetrazine fluorophores (**dye 1**-**4**) and strained alkynes (**dye 6** and **7**) are depicted in **figure 3.3-9** and **figure 3.3-10** for the fixed and the live cell protocols respectively.

All the dyes distributed to every cell compartment, although we observed an uneven distribution in the cell organelles and the fluorescent signal appeared to be weaker toward the cell periphery. All the dyes, except **dye 6** (TAMRA-BCN), exhibited a tendency to accumulate around the nucleus in the Golgi apparatus / endoplasmic reticulum (ER) region

(stronger fluorescent signal detected). This staining distribution is typical of lipophilic dyes, which tend to reach cellular lipophilic compartments and therefore to accumulate in membranes and organelles.[175-177]

However, **dyes 1**, **2** and **7** (**Figure 3.3-9a**, **b** and **f** and **Figure 3.3-10a**, **b** and **e**) had the most comparable distribution when tested either on fixed or live cells. Furthermore, they all spread broadly within the cells without aggregate formations. Their fluorescent signal is lower in the nucleus and at the cell periphery while it is stronger in the Golgi region.

Dye 3 and **4** showed a similar distribution pattern (**Figure 3.3-9c** and **3.3-9d** respectively). However, both of them formed fluorescent aggregates around the nuclei in the Golgi regions.

Dye 6 seemed to be better distributed around the nuclear region, also its fluorescent signal appeared to be more homogeneous between cytoplasm and nucleus, making it almost difficult to differentiate its distribution between the two cellular compartments (**Figure 3.3-9e** and **3.3-10d**). Also, its fluorescent signal was weaker when tested in the live cell protocol. Therefore, this dye seems to be less permeable to live cells.
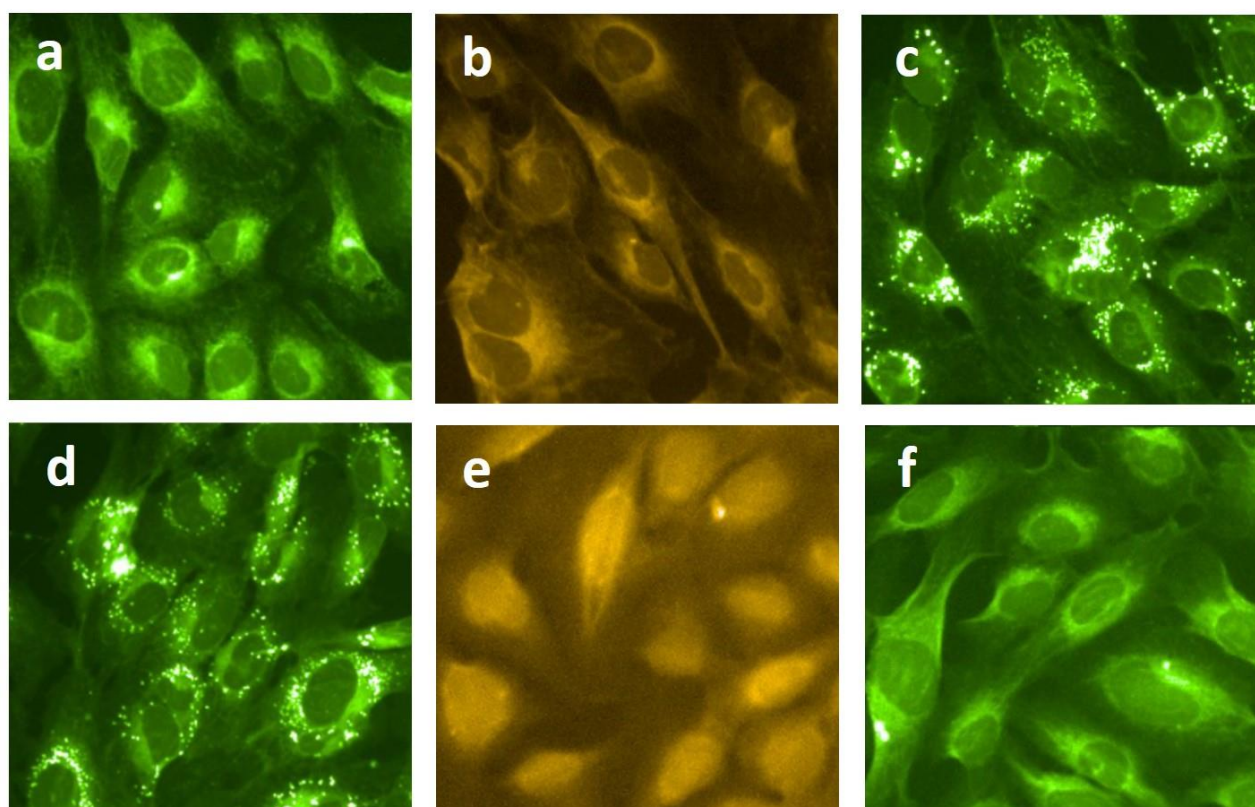
Figure 3.3-9 Intracellular distribution of fluorophores incubated at 1 µM for 2 hours on fixed SJSA-1 cells. The image sections show the distribution of dye **1**-**4** (picture (**a**) to (**d**) respectively) and of dye **6** and **7** (pictures (**e**) and (**f**) respectively). Images were recorded by IN Cell Analyzer 2000 using the 20 x objective and the FITC channel (green) for dye **1**, **3**, **4**, **and 7** or TexasRed channel (orange) for dye **2** and **6**. Image sections are illustrated using a 1:2 zoom factor.
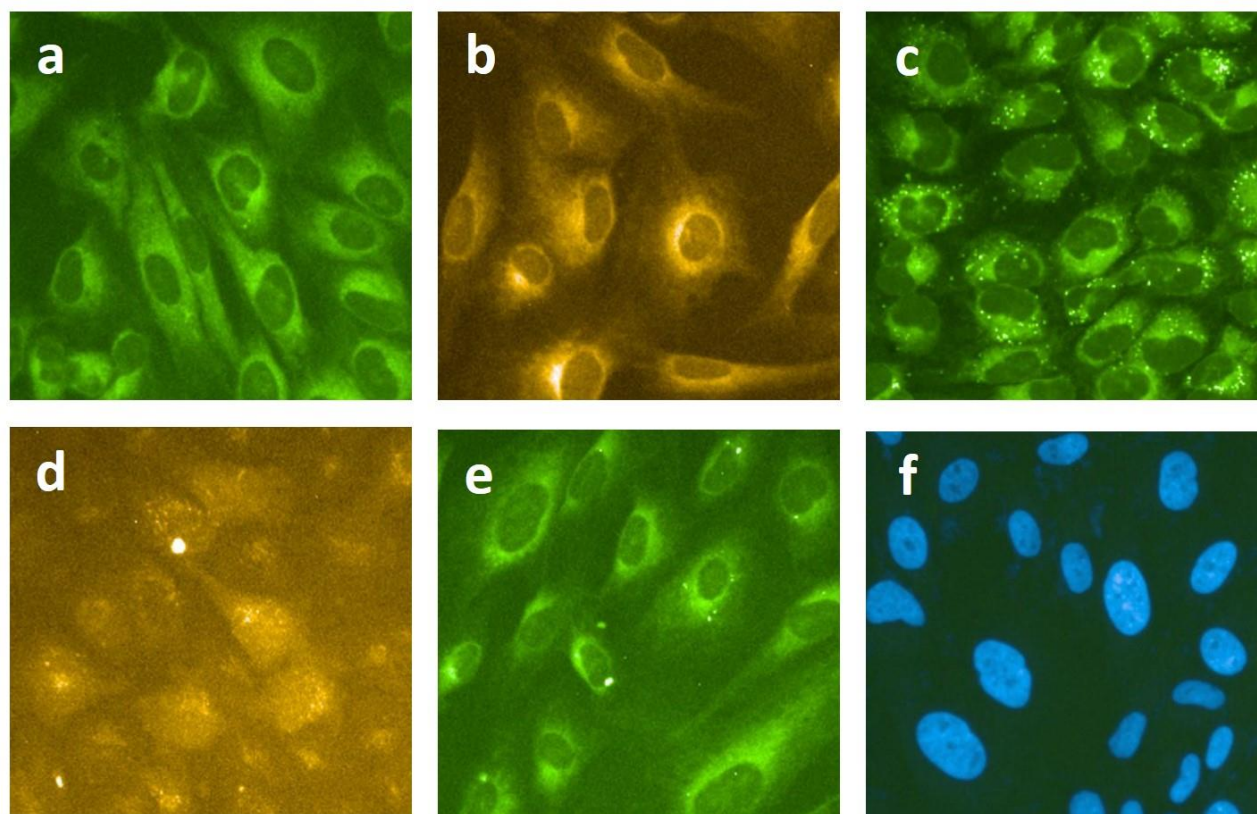
Figure 3.3-10 Intracellular distribution of fluorophores incubated at 1 μM for 2 hours on live SJSA-1 cells. The images sections show the distribution of dye **1**, **2** and **4** (pictures (**a**) to (**c**) respectively) and dye **6** and **7** (pictures (**d**) and (**e**) respectively). Picture (**e**) shows that negative control, **dye 9**, is not cellular penetrant as only the Hoechst nuclear staining is visible. Images were recorded by IN Cell Analyzer 2000 using the 20 x objective and the FITC channel (green) for dye **1**, **4**, **7** and **9** or TexasRed channel (orange) for dye **2** and **6**. Image sections are illustrated using a 1:2 zoom factor.

All the dyes were shown to be cell permeable while the negative control **dye 9** did not permeate the cell; only Hoechst dye nuclear staining (blue staining) was detected (**Figure 3.3-10f**).

In summary, the studies of cellular permeability and intracellular distribution of the dyes functionalized with a bioorthogonal probe using fixed and live cells protocols gave comparable results for **dyes 1**, **2** and **7**. These dyes, functionalized with either tetrazine or BCN, are cellularly permeable and distribute to the different cell compartments. **Dyes 3** and **4** exhibited a more heterogeneous distribution, however they formed aggregates. We decided to stop activities on **dye 3** but continue to investigate **dye 4**, still intrigued by its excellent physico-chemical properties (e.g. solubility) and cellular *in vitro* dataset previously reported for this class of mono-alkoxy-BODIPYs.[169]

Dye 6 displayed an apparent reduced permeability on live cells, although we reasoned that **dye 6** could be applied to a fixed cell approach therefore, its poor permeability in live cells was considered less significant.

In conclusion, all dyes except **dyes 3** and **5** were further studied in the development of the bioorthogonal two step approach.

3.4   Testing bioorthogonal reactions in fixed cells

The toolbox of probes and fluorophores were used for enabling the development of protocols for labelling the bioorthogonal probes in the cellular disease model. Initially, we opted to test the IED-DA and the SPAAC reactions between probes and fluorophores using a fixed cell protocol. Thus, SJSA-1 cells were treated with the Mdm2-p53 bioorthogonal probes functionalized with the strained alkenes (TCO and cyclopropene) or the azide at three concentration ranging from 0.16 micromolar to 16 micromolar. After 1 hour incubation, the cells were washed using H/H buffer and fixed using 4% paraformaldehyde (PFA) in H/H buffer. After a washing step, the dyes functionalized with the tetrazine and the strained alkyne groups were applied to the cells at 1 micromolar concentration and the bioorthogonal reactions were run for 2 hours at R.T. Finally, the excess of dye was removed by washing with H/H buffer. Before imaging, a nuclear staining for cell identification was carried out by treatment with Hoechst dye in H/H buffer for 10 minutes.

Hence, compound **3**, **4** and **5** functionalized with strained alkenes were reacted with **dye 1**, **2** and **4** (**Figure 3.4-1, 3.4-2** and **3.4-3** respectively). While, the azide functionalized probe, compound **7,** was engaged in the reaction with **dye 6** and **7** (**Figure 3.4-4a** and **b** respectively).
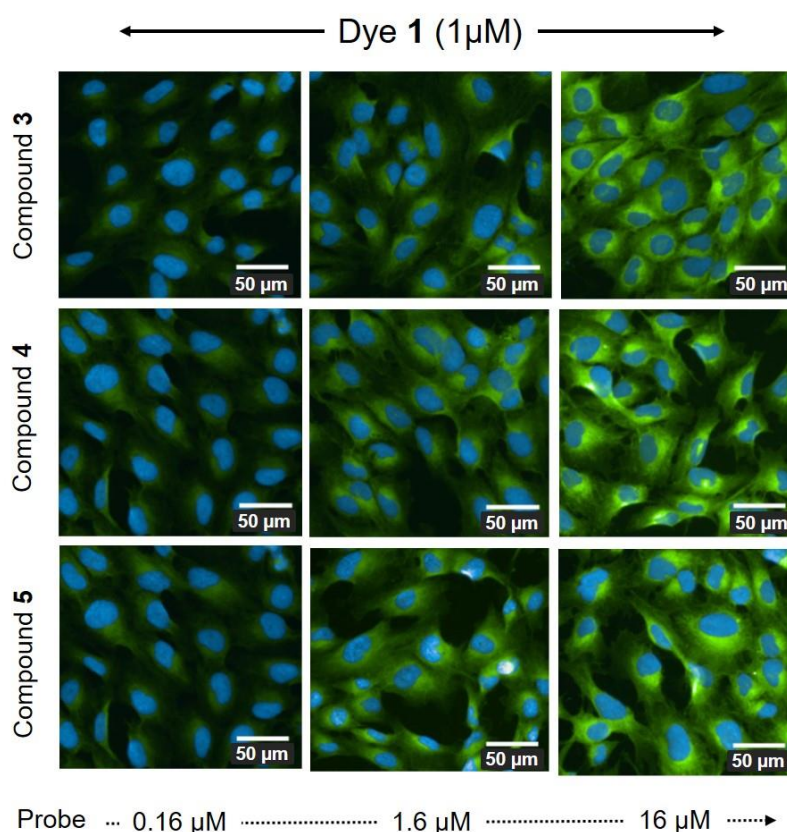
Figure 3.4-1 Bioorthogonal reaction between compounds **3**, **4** and **5** (from top down on fixed cells) and dye 1. The cells were treated with the bioorthogonal probes at three concentration 0,16, 1.6 and 16 µM for 1h at 37°C and 5% CO_2. After fixing the cells with 4% PFA the cell were treated with **dye 1** (1 µM) (green staining) for 1h. Following some washing steps, the nuclei were stained with Hoechst dye (blue staining) before imaging. The picture clearly showed a dose-dependent increase in fluorescence upon reaction.
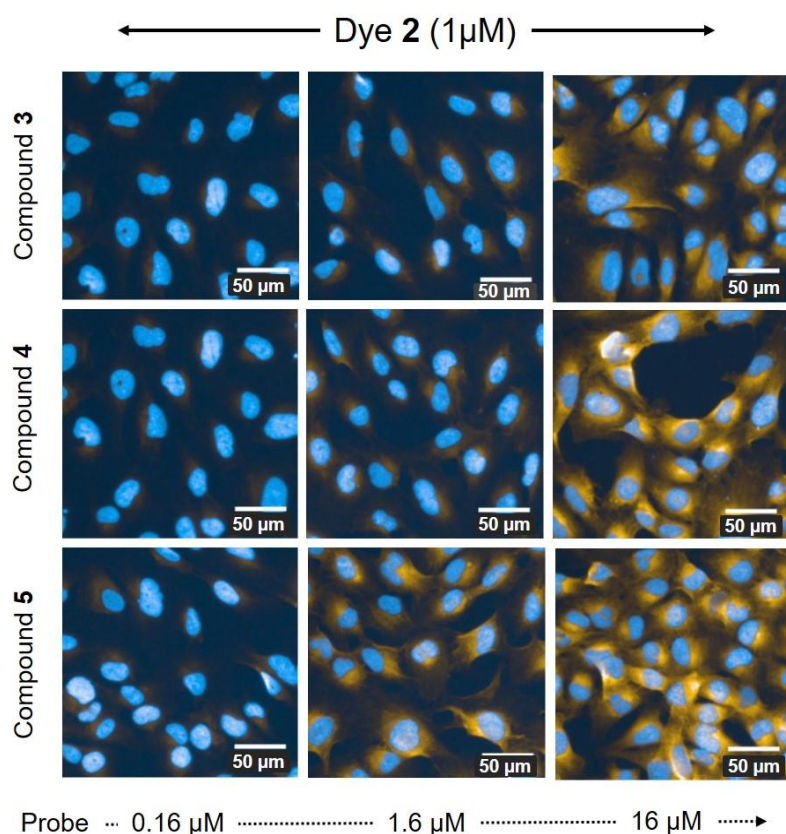
Figure 3.4-2 Bioorthogonal reaction between compound **3**, **4** and **5** (from top down on fixed cells) and dye **2**. The cells were treated with the bioorthogonal probes at three concentration 0,16, 1.6 and 16 μM for 1h at 37°C and 5% CO_2. After cells fixation the **dye 2** was incubated (1 μM) (red staining) for 1h. Straight after nuclear staining with Hoechst (blue staining), the imaging was performed. A dose-dependent increase in fluorescence upon reaction was observe
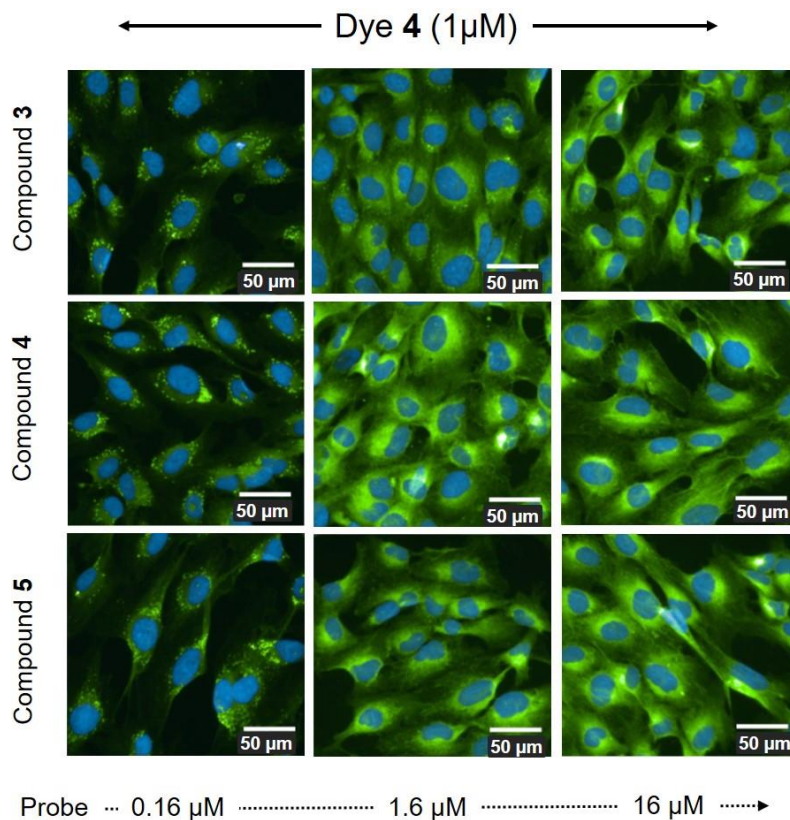
Figure 3.4-3 Bioorthogonal reaction between compounds **3**, **4** and **5** (from top down on fixed cells) and dye **4**. The cells were treated with the bioorthogonal probes at three concentration 0,16, 1.6 and 16 μM for 1h at 37°C and 5% CO_2. After cells fixation the **dye 4** was incubated (1 μM) for 1h (green staining). Straight after nuclear staining with Hoechst (blue staining), the imaging was performed. A dose-dependent increase in fluorescence upon reaction was observed.

While analyzing the IED-DA, we observed an evident dose-dependent increase in fluorescence in all the nine reactions between compounds **3**, **4** and **5** and **dyes 1**, **2** and **4**. As depicted in the pictures (**Figure 3.4-1**, **3.4-2** and **3.4-3**), the fluorescence signal was visible even at the lowest concentration tested (0.16 micromolar). The fluorescence was quite homogeneously distributed but more pronounced in the cytosol. Only at higher concentration did the signal appear to be stronger around the nuclei, within the GOLGI or ER region. In the samples undergoing the cycloaddition between the strained alkene probes and **dye 4** aggregates were clearly visible. This was not that surprising considering the previous intracellular study distribution of this dye on fixed cells, although it was unexpected to observe a higher level of aggregation at the lower concentrations. It is possible that this is only an optical effect and the stronger fluorescent signal at higher concentration might have concealed the aggregates.

Finally, it appeared that compounds **4** and **5** (cyclopropene derivatives) triggered a stronger signal compared to compound **3** (TCO derivative).
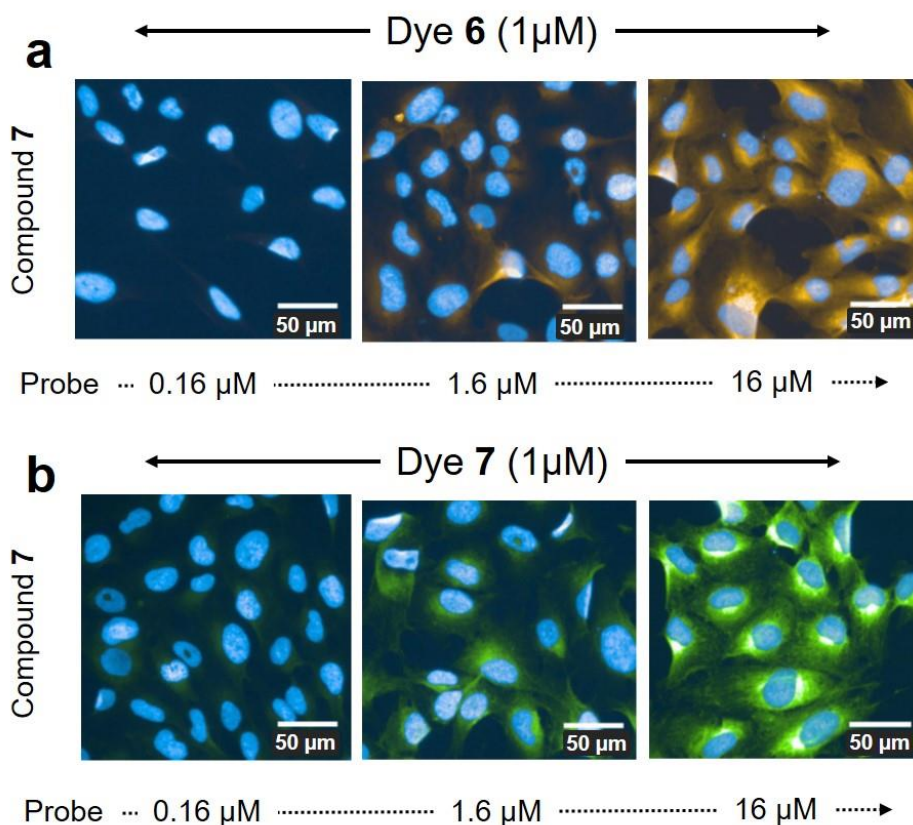
Figure 3.4-4 Bioorthogonal reaction between compound **7** and **dye 6** (**a**) (red fluorophore) or **dye 7** (**b**) (green fluorophore). The cells were treated with the bioorthogonal probes at three concentration 0,16, 1.6 and 16 µM for 1h at 37°C and 5% CO_2. After cells fixation, a treatment with the dyes (1 µM) for 1h was performed. Straight after nuclear staining with Hoechst (blue staining), the imaging was performed. A dose-dependent increase in fluorescence upon reaction was observed.

The SPAAC reaction between compound **7** and **dyes 6** and **7** also showed a dose-dependent increase in fluorescence. A homogeneous distribution of the fluorescent signal was visible for **dye 7** and, as for the tetrazine functionalized

BODIPYs, the signal appeared more localized around the nuclei, in the ER / Golgi regions only at higher probe concentration.

Contrary to what we observed with the BODIPY reactions, for the reaction between compound **7** and dye **6** (TAMRA-BCN), we were not able to record such sharp images. Thus, we rationalized that this might have been the result of a stronger extracellular background noise due to dye in the extracellular medium.

In conclusion, the preliminary investigation for the development of the "two step" bioorthogonal approach showed that upon cell incubation with increasing concentration of bioorthogonal probes and subsequent staining with a fixed concentration of fluorophores, a dose-dependent increase in fluorescence was observed. Additionally, these experiments reinforced what was previously observed while studying the intracellular distribution of fluorophores alone. **Dye 1**, **2** and **7** showed the characteristics required by the fluorescent reporter to enabling the bioorthogonal imaging approach. On the contrary, **dye 4** and **6** showed respectively formation of aggregates and unspecific staining or high background noise. While **dye 4** was not considered suitable for developing the "two step" bioorthogonal imaging approach, we further investigated **dye 6**, planning to quench the extracellular background noise using a novel imaging approach.

Dye 1, **2, 6** and **7** were further progressed to a more detailed validation and comparison of the bioorthogonal reactions in both fixed and live cells.

3.5   Fluorophores solubility assessment

Planning to use **dye 1**, **2, 6** and **7** for enabling the development of the bioorthogonal reactions in fixed and live cells, we investigated their solubility in PBS and PBS containing 10% of fetal calf serum (FCS) using DLS. Hence, we ran dynamic light scattering measurement on fluorophore samples at four concentrations ranging from 0.5 micromolar to 10 micromolar. All the tested fluorophores showed aggregation at concentrations superior or equal to 5 micromolar in both PBS and PBS containing 10 % of FCS (**Table 3.5-1** and **Figure 3.5-1**) .

The aggregation data generated for the fluorophore (**dyes 1**, **2, 6** and **7**) and for the bioorthogonal probes (**table 2.6-3**) were used for the design of the bioorthogonal reaction in the cellular system. Therefore, we performed the fluorescent reporter staining using 1 micromolar of fluorophore and a maximal concentration of probe of 16 micromolar.

Dye	Aggregation (PBS)	Aggregation (PBS + 10% FCS)
1	≥ 5 µM	> 5 µM
2	≥ 5 µM	≥ 10 µM
6	> 10 µM	≥ 10 µM
7	≥ 5 µM	> 10 µM

Table 3.5-1 Aggregation on dyes measured with DLS in four concentraction ranging from 0.5 µM to 10 µM in PBS and PBS containing 10% FCS.
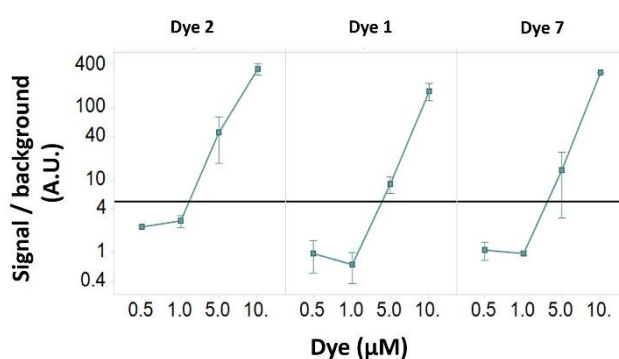
Figure 3.5-1 Depicted in the picture the Dynamic Light Scattering on dyes. Dyes were tested at four concentrations ranging from 0.5 µM up to 10 µM in PBS. Signal was normalized to background. The black line indicates the threshold for aggregation.

3.6 Developing the bioorthogonal reaction in cells

To further develop the bioorthogonal reactions in fixed and live cells we built dose-response curves of the fluorescent read-out (fluorescence increase) upon reactions between bioorthogonal probes and dyes in both fixed and live cells.

The different bioorthogonal probes, **3-5** and **7** were incubated at seven concentrations ranging from 0.0158 micromolar to 15.8 micromolar with SJSA-1 cells at 37 °C and 5% CO_2 for 1 hour. **Dye 1**, **2**, **6** or **7** were added upon cell fixation with PFA and the bioorthogonal reaction was run for 2 hours at R.T (**Figure 3.6-1**). Nuclei were stained with a Hoechst dye treatment for 10 minutes before imaging. As negative controls for the IED-DAs, we additionally performed the staining of compound **3** with **dye 9** (**Figure 3.6-1a** and **3.6-1b**), while we added the staining of compound **7** with **dye 1** as negative control for SPAAC (**Figure 3.6-1c**).
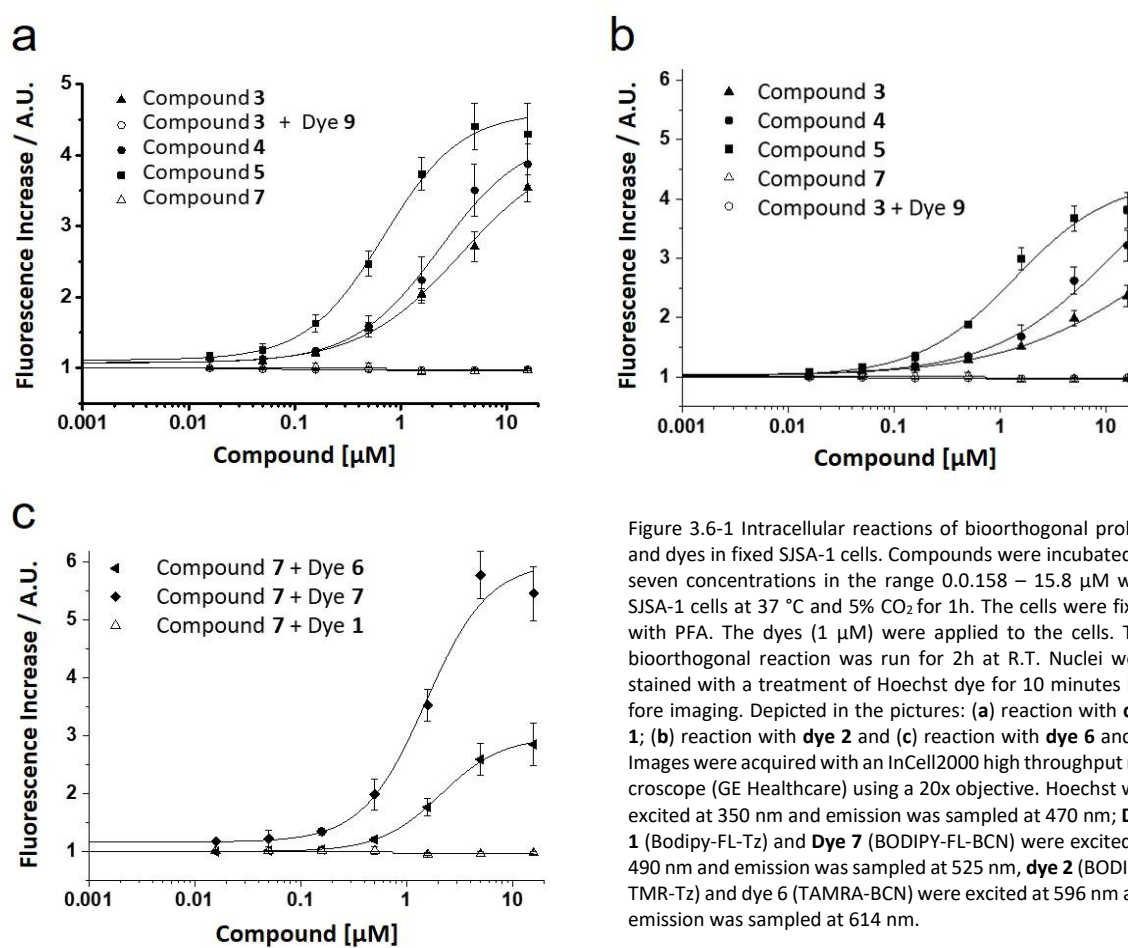
Figure 3.6-1 Intracellular reactions of bioorthogonal probes and dyes in fixed SJSA-1 cells. Compounds were incubated at seven concentrations in the range 0.0158 – 15.8 µM with SJSA-1 cells at 37 °C and 5% CO_2 for 1h. The cells were fixed with PFA. The dyes (1 µM) were applied to the cells. The bioorthogonal reaction was run for 2h at R.T. Nuclei were stained with a treatment of Hoechst dye for 10 minutes before imaging. Depicted in the pictures: (**a**) reaction with **dye 1**; (**b**) reaction with **dye 2** and (**c**) reaction with **dye 6** and **7**. Images were acquired with an InCell2000 high throughput microscope (GE Healthcare) using a 20x objective. Hoechst was excited at 350 nm and emission was sampled at 470 nm; **Dye 1** (Bodipy-FL-Tz) and **Dye 7** (BODIPY-FL-BCN) were excited at 490 nm and emission was sampled at 525 nm, **dye 2** (BODIPY-TMR-Tz) and dye 6 (TAMRA-BCN) were excited at 596 nm and emission was sampled at 614 nm.

Applying the live cell protocol, compound **3-5** and **7** were incubated at concentrations ranging from 0.158 micromolar to 15.8 micromolar with SJSA-1 cells at 37 °C and 5% CO_2 for 1 hour. **Dye 1** or **2** was added and the bioorthogonal reaction was run for 2 hours at 37 °C and 5% CO_2. After the reactions, the cells were fixed using PFA and treated with

the Hoechst dye for 10 minutes before imaging (**Figure 3.6-2**). As a negative control, compound **3** was stained with **dye 9** as previously done in the fixed cells protocol.
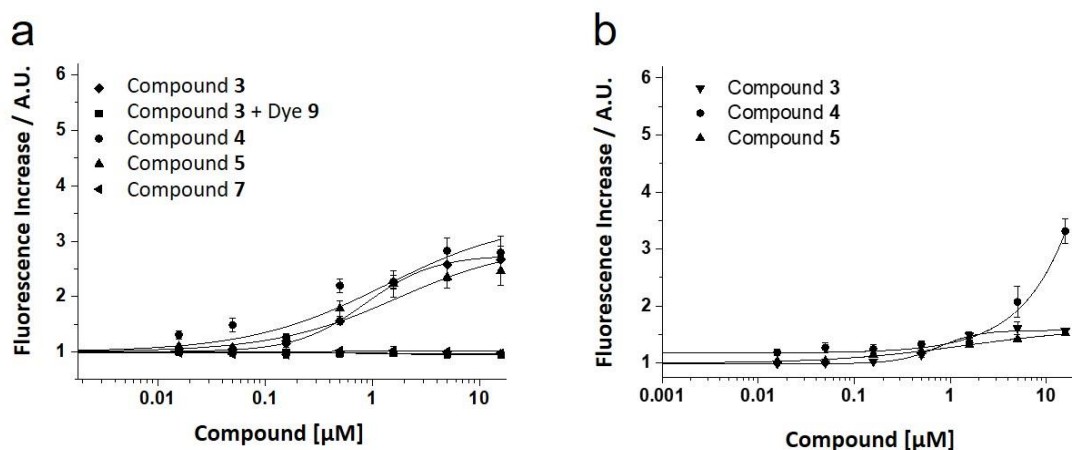
Figure 3.6-2 Intracellular reactions of bioorthogonal probes and dyes in SJSA-1 live cells. Compounds were incubated at seven concentrations in the range 0.0158 – 15.8 µM with SJSA-1 cells at 37 °C and 5% CO_2 for 1h. The dyes (1 µM) were applied to the cells. The bioorthgonal reaction was run for 2h at 37 °C and 5% CO_2 for 1h. The cells were fixed with PFA. Nuclei were stained with a treatment of Hoechst dye for 10 minutes before imaging. Depicted in the pictures: (**a**) reaction with **dye 1** and (**b**) reaction with **dye 2**. Images were acquired with an InCell2000 high throughput microscope (GE Healthcare) using a 20x objective. Hoechst was excited at 350 nm and emission was sampled at 470 nm; **Dye 1** (BODIPY-FL-Tz) was excited at 490 nm and emission was sampled at 525 nm, **dye 2** (BODIPY-TMR-Tz) was excited at 596 nm and emission was sampled at 614 nm.

We could observed a dose-dependent increase in the fluorescent signal in all the reactions run using both the fixed and the live cells protocols. We observed a general higher fluorescence increase when running the reactions using the fixed cell protocol. For instance, a maximum fluorescence increase equal to 3.5 fold was observed upon reaction between compound **5** and **dye 1** (**Figure 3.6-1a**) and a 4.5 fold increase between compound **7** and **dye 6** (**Figure 3.6-1c**). While, upon reaction between compound **3** and **dye 1** under fixed cell condition, only 1.8 fold fluorescence increase was observed (**Figure 3.6-1a**).

Dye 1 was the more efficient fluorescent reporter upon IED-DA under both fixed and live cells condition. **Dye 7** was superior to **dye 6** upon SPAAC in fixed cells. All the probes were highly taken up by the cell and we were able to detect probe uptake at the lowest concentration of 50 nanomolar.

In addition, the negative controls included in our experiment did not show a significant increase in fluorescence (**Figure 3.6-1a**, **3.6-1a**, **3.6-2a** and **3.6-2b**).

Finally, we compared the reaction between either **DMSO** or compound **3** at 1.6 micromolar incubation with **dye 1** on fixed cells using imaging (**Figure 3.6-3**).

As depicted in the pictures, no significant fluorescence was visible on the DMSO control sample (**Figure 3.6-3a** only blue nuclear staining was visible) while a clear BODIPY fluorescent signal was visible in the sample treated with the fluorescent reporter (**Figure 3.6-3b**).
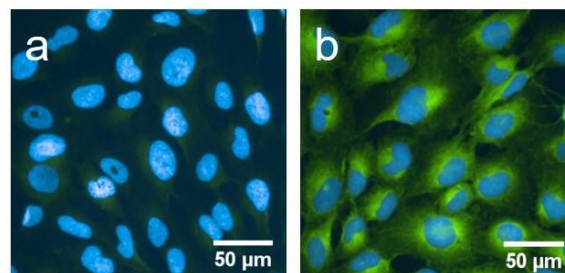
Figure 3.6-3 SJSA-1 cells treated DMSO control (**a**) and compound **3** at 1.6 µM (**b**) stained using with **Dye 1** (green fluorescence) and Hoechst dye (blue fluorescence). The control sample did not show significant staining of the fluorescent reported dye **1**.

In conclusion, the developed "two step" bioorthogonal approach allowed the assessment of the bioorthogonal probes cellular up-take in a dose-dependent manner with a good level of sensitivity (lower limit of detection equal to 50 nanomolar). The different reactions tested worked similarly well allowing flexibility in the choice of the fluorescent reporter. However, **dye 1** seems to be slightly superior in both fixed and live cell protocols.

3.7 A comparison between the pre-labelling and the two steps imaging approach

Results of prior studies have shown that conjugation of small molecules to conventional fluorescent dyes such as Alexa dyes (MW ranging between 700 and 1000 Da) significantly impact the distribution and biological activity of the small molecules.[178] Therefore, we thought to compare our "two step" bioorthogonal imaging approach to a pre-labelling approach.

Hence, compound **1** was labelled with BODIPY-FL through a 1,2-diaminoethane linker introduced via amide bonds to afford compound **16** (**Figure 3.7-1a**). We confirmed its biochemical activity with Mdm2 and its selectivity against Mdm4 using the TR-FRET biochemical assays(hMdm2-p53 TR-FRET IC50= 0.63 ± 0.08 nM, hMdm-p53 TR-FRET IC50= 139.72 ± 41.05 nM).
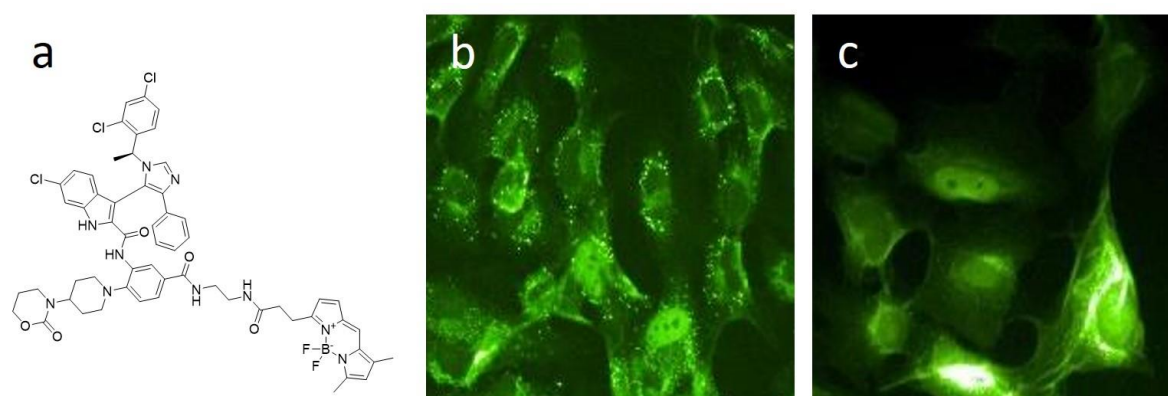
Figure 3.7-1 Depicted in the picture: (**a**) the chemical structure of compound **16**; (**b**) intracellular distribution of compound **16** incubated at 500 nM concentration with SJSA-1 cells at 37 °C and 5% CO_2 for 1 hour; (**c**) intracellular distribution of compound **3** incubated at 500nM concentration with SJSA-1 cells at 37 °C and 5% CO2 for 1 hour, followed by cells fixation and bioorthogonal staining with **dye 1** at 1μM concentration.

Compound **3** and compound **16** at 500 nanomolar concentration were separately incubated with SJSA-1 cells at 37 °C and 5% CO_2 for 1 hour. After fixation, we added **dye 1** at 1 micromolar concentration to the cells treated with compound **3** and DMSO to the cells treated with compound **16**. Subsequently, the cells were imaged. Both pre-labeled and TCO-functionalized probes were up-taken by the cells. However, as shown in **figure 3.7-1b**, the pre-labeled compound (**16**) formed several aggregates while compound **3** subjected to bioorthogonal staining showed a more homogeneous distribution without aggregate formation (**Figure 3.7-1c**).

As a result, the "two step" bioorthogonal approach displayed a clear difference compared to the fluorescence pre-labelling approach since it enabled the visualization of the probe uptake without formation of aggregates. We reckoned that the more minor chemical modification to the Mdm2 ligand in **3** gave a compound that more closely represented the expected behavior of the parent molecule than the pre-labelled compound **16**. However, this finding was demonstrated from a single prelabelled analogue and our conclusion could be re-inforced by testing a wider set of pre-labelled molecules.

3.8 Target engagement studies

After proving that the "two step" approach enabled the intracellular imaging of the bioorthogonal probes and allowed the assessment of their cellular uptake with a reasonable sensitivity, we investigated whether this approach might enable the study of the target engagement of our bioorthogonal probes.

As discussed, the disruption of the Mdm2-p53 protein-protein interaction stabilizes p53 and consequently activates its pathway leading to overproduction of Mdm2 (**Figure 2.1-1**, page 33). Accordingly, when SJSA-1 cells were treated overnight with the bioorthogonal probes **1-7**, a dose-dependent over expression of Mdm2 was observed in the nuclei with signal saturation at a probe concentration of ca. 0.5 micromolar (**Figure 2.7-2**, page 47). If the bioorthogonal probes were able to engage the target, they should consequently have co-localized with the target in the nuclei.

Hence, we incubated SJSA-1 cells with the compound **1-5** and **7** at 160 nanomolar concentration overnight to induce Mdm2 in the nuclei. Then we bioorthogonally labelled the probes with the diverse fluorescent reporters (**dye 1**, **2** and **7**) accordingly to their mutual reactivity via either IED-DA or SPAAC using the fixed and the live cells protocols. Finally, we immunostained the PD marker (Mdm2) and stained the nuclei (**Figure 3.8-1** for fixed cells protocols; **Figure 3.8-2** for live cells protocol).
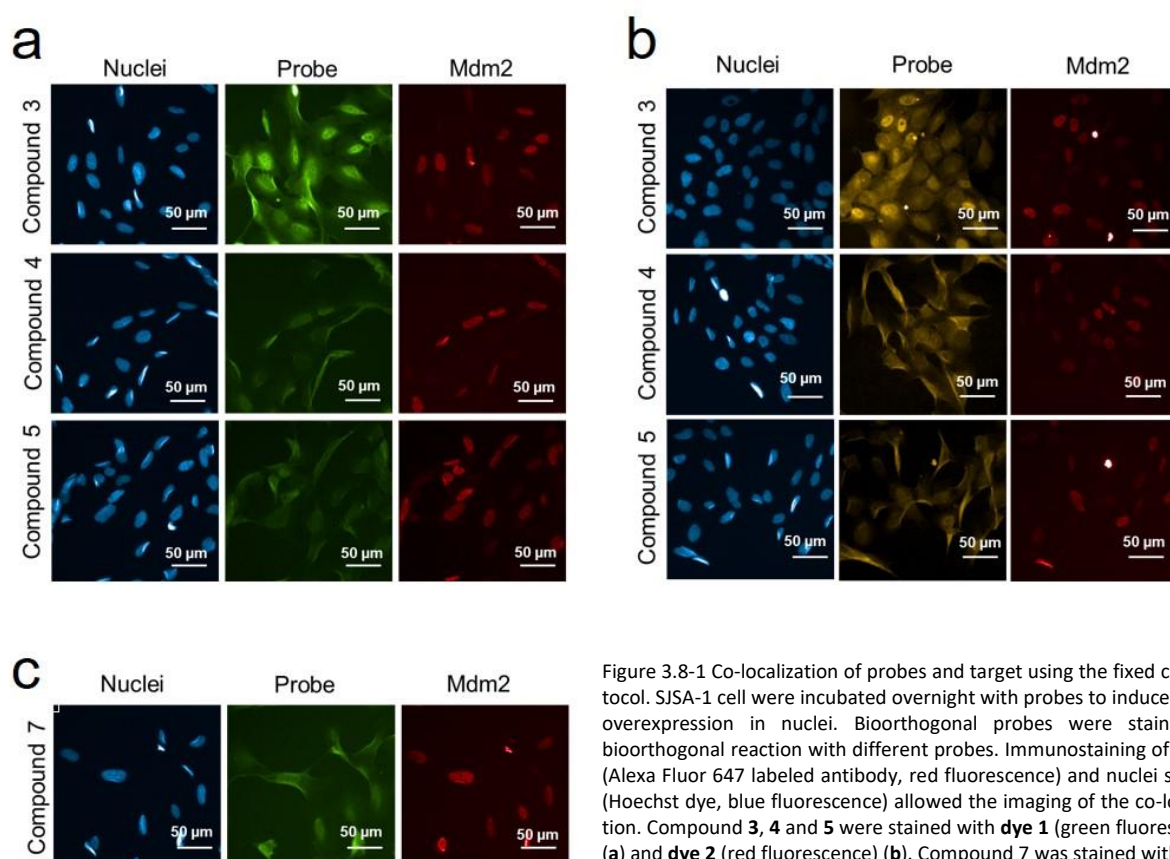
Figure 3.8-1 Co-localization of probes and target using the fixed cell protocol. SJSA-1 cell were incubated overnight with probes to induce Mdm2 overexpression in nuclei. Bioorthogonal probes were stained via bioorthogonal reaction with different probes. Immunostaining of Mdm2 (Alexa Fluor 647 labeled antibody, red fluorescence) and nuclei staining (Hoechst dye, blue fluorescence) allowed the imaging of the co-localization. Compound **3**, **4** and **5** were stained with **dye 1** (green fluorescence) (**a**) and **dye 2** (red fluorescence) (**b**). Compound 7 was stained with **dye 7** (green fluorescence) (**c**).
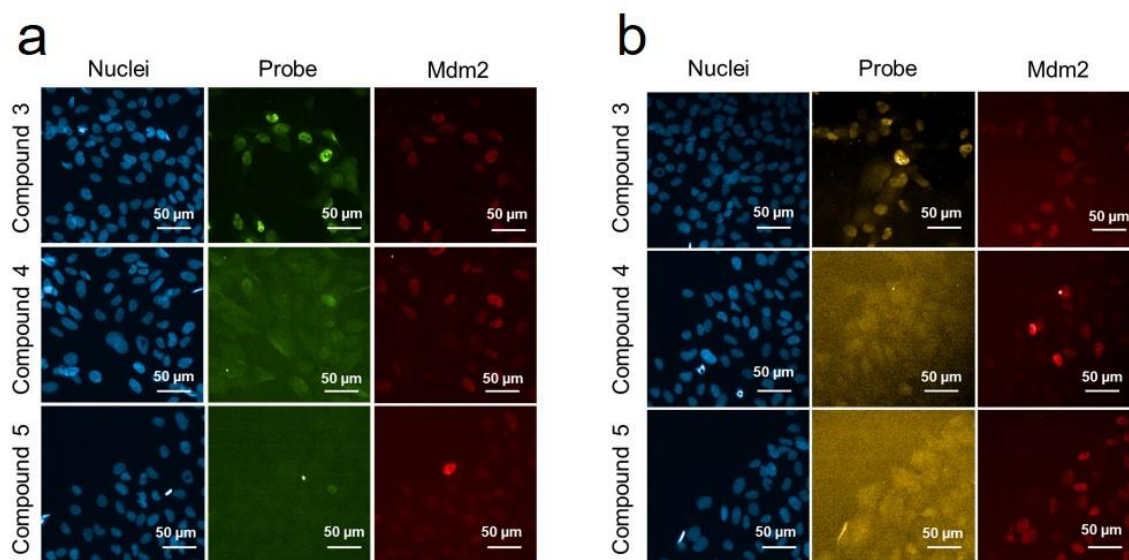
Figure 3.8-2 Co-localization of probes and target using the live cell protocol. SJSA-1 cell were incubated overnight with probes to induce Mdm2 overexpression in nuclei. Bioorthogonal probes were stained via bioorthogonal reaction with different probes. Immunostaining of Mdm2 (Alexa Fluor 647 labeled antibody, red fluorescence) and nuclei staining (Hoechst dye, blue fluorescence) allowed the imaging of the co-localization. Compound **3**, **4** and **5** were stained with **dye 1** (green fluorescence) (**a**) and **dye 2** (red fluorescence) (**b**).

While both fixed and live cells methods allowed co-localization of probes and target on cells with high content of Mdm2 to be visualized, the first method enabled more clear images to be captured (**Figure 3.8-1**).

Among the bioorthogonal probes tested, some clearly exhibited a better co-localization with the target. This might be due to different reasons. For instance, despite assessing a generally long half-life of the probe-target complex using the biochemical assay (**Table 2.6-2**), this is only suggestive of what could happen in the more complex cellular system. Additionally, we did not have information on the different half-lives of target-bioorthogonal product complexes, which clearly plays an important role for enabling co-localization images. Finally, it is reasonable to think that when the probes are bound to Mdm2, their bioorthogonal groups, introduced via different linkers, might be accessible to different degrees to the reactive dyes to enable the "Click" reactions. To summarize, we reasoned that both the reaction and the compound binding kinetics had clearly influenced the ability to image the co-localization of the bioorthogonally labelled probes with the target.

The analysis of these data, in addition to the *in vitro* and in live cell profiling of the bioorthogonal probes and the dyes (e.g. probe activity and selectivity, intracellular distribution and permeability of the dye) suggested that compound **3** and dye **1** are the most appropriate pair for "the two step approach" in our disease model (**Figure 3.8-3**). To further confirm our observation and finally prove compound target engagement, we ran additional experiments using compound **3** and **dye 1**.

Compound 3

Dye 1
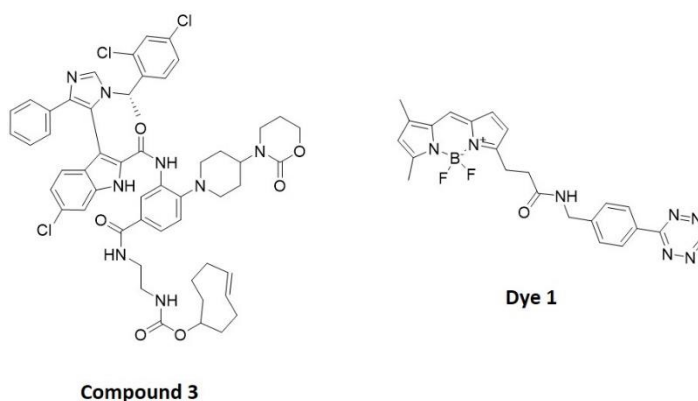
3.8-3 Preferred Bioorthogonal probe and dye pair

For instance , we performed comparative co-localization studies of compound **3** in two different cell lines, SJSA-1 and HT29 (**Figure 3.8-4a** and **3.8-4b** respectively). The latter expresses a p53 mutant which is unable to bind to DNA and therefore it is lacking transcriptional activity and tumor suppressor function.[179]. Additionally, we ran a negative control in SJSA-1 cells replacing compound **3** with compound **13** (Nona-Arginine TCO derivative) (**Figure 3.8-4c**).

Thus, the co-localization between compound **3** and Mdm2 in the nuclei was confirmed. As expected, compound **3** did not induce Mdm2 in the nuclei of HT-29, also the level of the protein target was too low to be detected by the immunostaining (**Figure 3.8-4b**). Additionally, we were able to visualize the bioorthogonal probe in this cell line and its localization was not almost exclusively nuclear, as in SJSA-1 cells, but was also present in the cytosol (**Figure 3.8-4b –** probe staining). Altogether, the experiment in HT-29 supported the mode of action of the bioorthogonal probe, the activation of the p53 pathway by disrupting the Mdm2-p53 protein-protein interaction. Finally, the negative control, compound **15,** did not induced Mdm2 in the nuclei of SJSA-1 while the compound staining confirmed its permeability (**Figure 3.8-4c**).
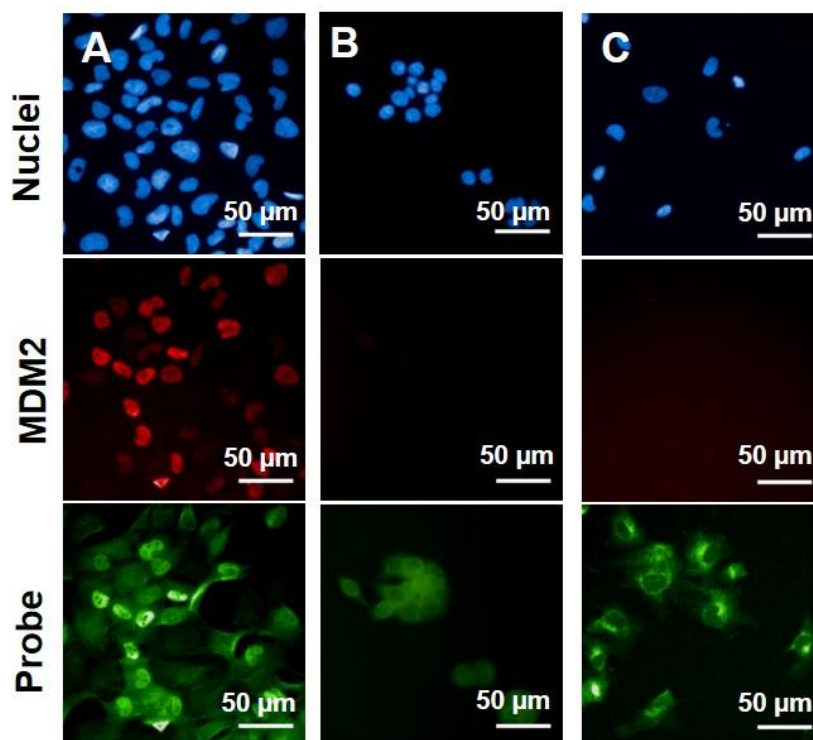
Figure 3.8-4 Comparative study of bioorthogonal probe-Mdm2 co-localization. SJSA-1 (**a**) and HT-29 (**b**) cells were treated with compound **3**. After staining with **dye 1** (green fluorescence), Mdm2 was immunostained (red fluorescence). Finally, cells were treated with Hoechst nuclear staining (Blue fluorescence). Following the same procedure, SJSA1 cells were treated with compound **15** as negative control (**c**) (Adapted from *D'Alessandro, P.L., et al. Angew. Chem. Int. Ed. Engl., 2016*).

Additionally, we ran a single-cell data analysis to correlate bioorthogonal labelling and Mdm2 nuclear level (**Figure 3.8-5**).
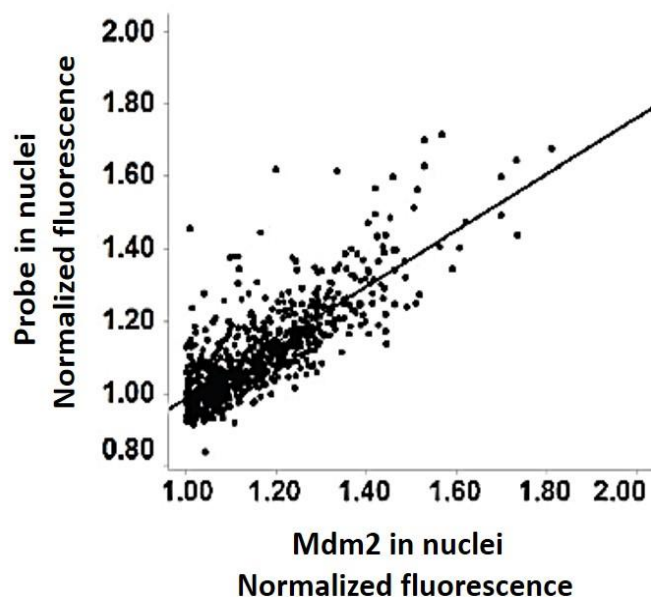
Figure 3.8-5 The graph obtained from single-cell data analysis of normalized fluorescent signal of labelled probe (**3**) versus immunostained Mdm2 reveals the correlation between probe in the nuclei and nuclear Mdm2 level (Adapted from *D'Alessandro, P.L., et al. Angew. Chem. Int. Ed. Engl., 2016*).

We observed a very good correlation between target protein level and bioorthogonal probe (**1**) which suggested that the bioorthogonal probes may be used not only to visualize the target but to measure its expression level too. Finally, the bioorthogonal probe was detected only in cells with a high Mdm2 content.

In conclusion, we proved target engagement of compound **3** by confirming its mode of action and correlating its target modulation to the observed phenotypic effect (increased Mdm2 protein level in nuclei).

3.9 Target occupancy

After the investigation of the target engagement of our bioorthogonal probe, compound **3**, we decided to explore if the "two step" bioorthogonal approach might also enable the assessment of the target occupancy of different chemical classes of Mdm2-p53 PPI inhibitor chemical probes.

Previously, we showed that compound **3** could be used for assessing the Mdm2 protein level and that this compound induced the maximal level of Mdm2 in the nuclei (signal saturation) when incubated with SJSA-1 cells overnight at 500 nanomolar concentration (**Figure 2.7-2**, page 47). Moreover, the compound treatment resulted in the complete translocation of the target to the nuclei. Therefore, we assumed full target occupancy dosing compound **3** at that concentration. We reasoned that an un-labelled inhibitor could be used to compete with the intracellular binding between the bioorthogonal probe and its target and, consequently, by assessing the reduction of the bioorthogonal probe signal, we could extrapolate the target occupancy of the un-labelled compound.

Hence, we incubated SJSA-1 cells with compound **3** at 500 nanomolar concentration overnight while maintaining the culture at 37 °C and 5% CO_2. Then, we treated the live cells with compound **1** (see structure on **Figure 2.5-1**, page 38) at 15 micromolar concentration for 2 hours. After cell fixation, we stained bioorthogonally compound **3** with dye **1** and we performed the immunostaining of Mdm2.

As represented in **figure 3.9-1a**, in the absence of the competitor compound **1** a full co-localization between the bioorthogonally stained compound **3** and the immunostained Mdm2 could be observed in the cells with high level of the protein target. When the competitor compound **1** was applied, a reduction of the fluorescent signal of compound **3** was evident, although the Mdm2 immunostaining was still visible (**Figure 3.9-1b**).
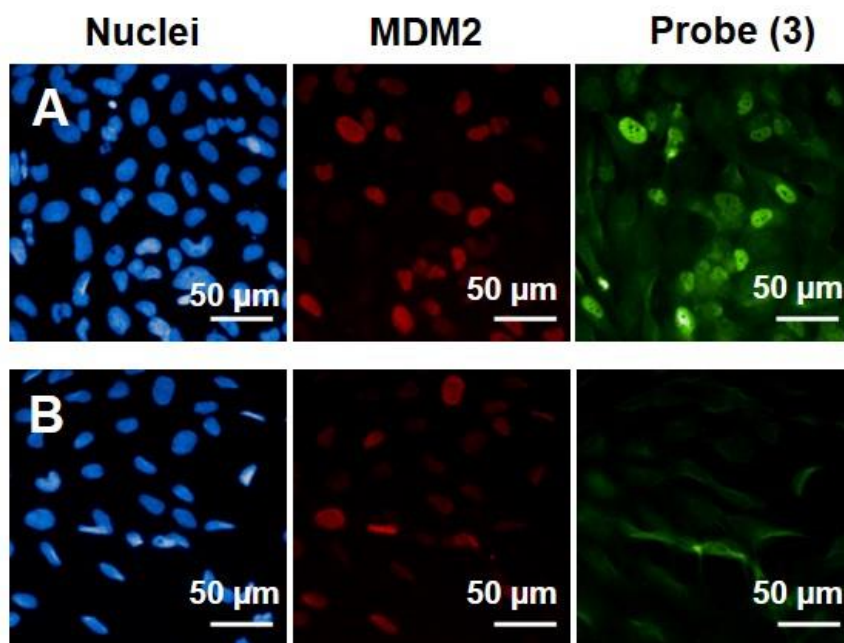
Figure 3.9-1 Competition experiment for studying target occupancy of compound **1**. SASJ-1 cells are treated with compound **3** (0.5 µM) overnight at 37 °C and 5% CO_2. (**A**) in absence of competitor (**1**) co-localization between compound **3** (green signal) and Mdm2 (red signal) can be observed. (**B**) by treating the live cells with compound **1** (15 µM), a reduction in the bioorthogonal probe signal is observed.

Based on this result, we decided to investigate if we could quantify the target occupancy. Therefore, we selected a set of five structurally different Mdm2-p53 PPI inhibitors, four LMW compounds, compound **1**, **17**,[180,181] **18**[182,183], **19**[184] and a stapled peptide, compound **9**[185] (**Figure 3.9-2**). The activities of these compounds were confirmed using the TR-FRET and the cellular PD induction assay (see **Table 3.9-1**). As in the previous experiment, we induced the PD marker by treating the cells overnight with compound **3** at 500 nanomolar concentration. Next, the competitors were applied for 2 hours at 37°C and 5% CO2 at different doses ranging from 0.0158 micromolar to 15.8 micromolar.
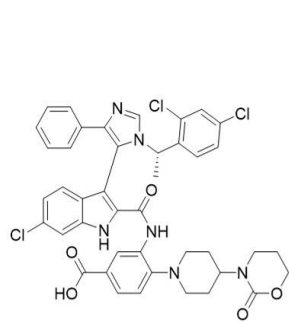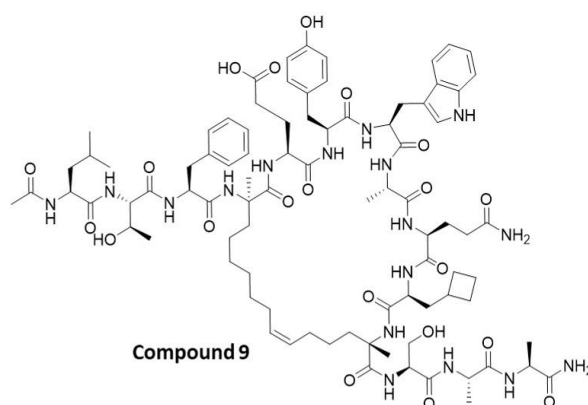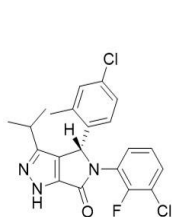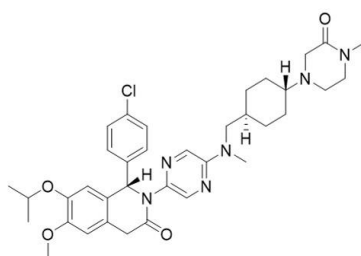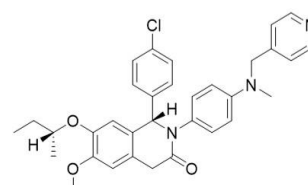
3.9-2 Structures of the LMW compounds **1**, **9**, **17, 18** and **19** and the stapled peptide **9**.

Cpds	hMdm2-p53 TR-FRET IC_{50} (nM)	Cellular Assay EC_{50} (µM)
1	0.034 ± 0.002	0.29
9	0.17 ± 0.01	5.9
17	7.25 ± 0.72	> 10
18	3.39 ± 0.45	2.1
19	2.29 ± 0.21	6.2

Table 3.9-1 Biochemical and cellular activity of compound **1**,**9**, **17**, **18** and **19** measure in TR-FRET assay and in the PD induction cellular assay.

As illustrated in the graph in **figure 3.9-3**, by competing out compound **3** with compound **1** at 5 micromolar concentration, a 50% reduction of the bioorthogonal probe in the nuclei was observed. Consequently, compound **1** at that concentration occupied 50% of the target. The other compounds tested showed a lower target occupancy which correlates with their weaker cellular activity (**Table 3.9-1**). For example, compound **9** showed 50% target occupancy when dosed at 25 micromolar. While, compound **17**, a pyrazolopyrrolidinone derivative,[181] did not show occupancy up to 50 micromolar concentration, in agreement with its lack of cellular activity.
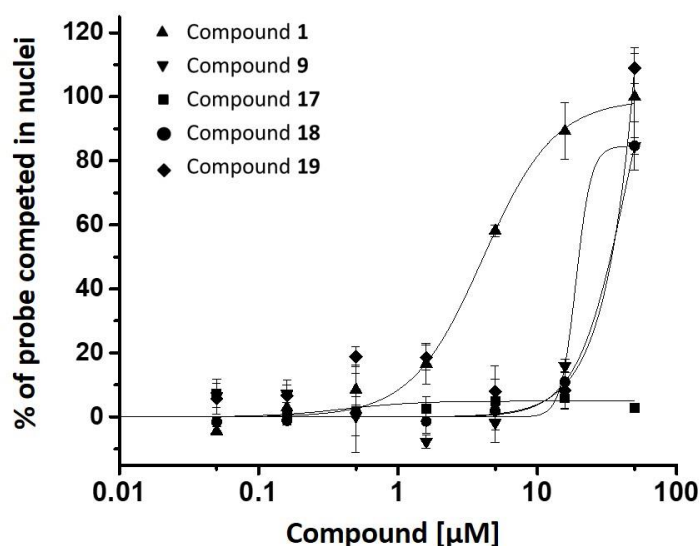
Figure 3.9-3 Target occupancy of un-tagged Mdm2-p53 PPI inhibitors. Compounds belonging to different chemical classes were used to compete the binding of compound **3** with Mdm2 in SJSA-1 cells. The cells were treated with 500 nM of compound **3** overnight followed by competition with increasing concentration of un-tagged compounds. The percentage of probe competed in the nuclei represented the target occupancy of the un-tagged compounds (Adapted from *D'Alessandro, P.L., et al. Angew. Chem. Int. Ed. Engl., 2016*).

In conclusion, the assay developed enabled quantification of target occupancy for compounds having different scaffolds and belonging to different chemical classes (e.g. LMW compounds and peptides). In principle, this assay could be applied for the identification of new chemical matter having the same mode of action as the bioorthogonal probe and binding into the same pocket.

3.10 Results and discussion

A toolbox of bioorthogonally reactive fluorescent reporters was built to enable the development of a "two step" approach for studying bioorthogonal probes in a cellular disease model.

After testing the reactivity of the fluorescent reporters and the bioorthogonal probe pairs in a cell-free *in vitro* assay, we investigated the intracellular behaviors of the fluorophores (e.g. permeability, distribution, intracellular aggregation). As a result, BODIPY and TAMRA based fluorophores were selected to enable the development of the EID-DA and SPAAC reactions with the bioorthogonal probes in fixed and live cells. All reactive pairs showed a dose-dependent intracellular increase in fluorescence upon bioorthogonal reaction. Consequently, a first method to assess

permeability of the bioorthogonal probes was established; we were able to detect cellular uptake for the Mdm2 ligand labeled with the TCO group with a LOD of 50 nanomolar.

Next, we ran a set of compound-target co-localization experiments using EID-DA and SPAAC bioorthogonal staining. By treating the cells with the bioorthogonal probes for a time sufficient to induce a PD effect (increased nuclear Mdm2 level) we observed translocation of our probes to the nuclei and co-localization of the target and the probes. Additionally, we confirmed that the observed PD effect was the result of the expected mode of action of our bioorthogonal probes by running the target engagement experiment in p53 mutant expressing cells, HT-29. In this cell line the mutant p53 is unable to bind DNA and therefore it is lacking transcriptional activity. As expected, the bioorthogonal probe did not induce the PD, confirming their mode of action.

Some reactive pairs clearly revealed a greater degree of co-localization and in particular, the TCO labeled chemical probe and the tetrazine BODIPY-FL dye showed a superior behavior in both fixed and live cell target engagement experiments. Therefore, this reactive pair was used for further biological studies.

By fluorescence single-cell analysis we demonstrated a good correlation between target protein and bioorthogonal probe levels in the nuclei. Incubating the cells with 500 nanomolar concentration of the bioorthogonal probe led to the maximal level of Mdm2 in the nuclei. Furthermore, at that concentration, all the bioorthogonal probes showed nuclear localization. Therefore, we assumed at that concentration of TCO labeled probe full target occupancy was reached. We showed that the probe bound to the target in the nucleus could be competed out with a set of un-labelled Mdm2-p53 PPI inhibitors and by measuring the reduction of fluorescent bioorthogonal staining we could assess target occupancy for the un-labelled inhibitors. Additionally, we reasoned that such an approach could be used for identifying new chemical matter binders for Mdm2.

Finally, we published this work in Angewandte Chemie in 2016 (P. L. D'Alessandro et al., "Bioorthogonal Probes for the Study of MDM2-p53 Inhibitors in Cells and Development of High-Content Screening Assays for Drug Discovery"; *Angew Chem Int Edit* 2016, 55, 16026-16030).[186]

3.11 Experimental section

3.11.1. Dynamic Light Scattering

See 2.9.4

3.11.2. Cell culture

SJSA-1 cells were cultured as described in 2.12.4. HT-29 cells were maintained in McCoy's 5A medium (ATCC) supplemented with 10% FCS heat inactivated (Bioconcept) and 1% Pen/Strep (Invitrogen). HT-29 cells were cultured following the procedure applied to SJSA-1 cells.

3.11.3. Bioorthogonal labelling of probes in fixed and live cells

SJSA-1 cells were plated in 384-well optical imaging, flat, clear-bottom, black microplates (Corning) at a density between 1000 and 3000 cells per well using an automated dispenser (Multidrop Combi, Thermo Scientific, Waltham, MA). Cells were incubated for 24 h at 37° C and 5% CO2 to allow them to attach. Probes were added manually to plates from a 10 mM stock in DMSO with a pre-dilution step in DMSO to keep DMSO concentration constant. Final DMSO concentration was 0.5%. Eight concentrations of probes (0.0158 to 15.8 uM) were tested incubating for either 1hour or 16 hours at 37C and 5% CO2. Following probe incubation, excess of compound was removed using a plate washer (Power Washer 384, Tecan, San Jose, CA). The biorthogonal reactions were performed either in fixed or live cells.

To fix cells 4% PFA (stock: 32%) diluted in H/H buffer adding 10 μL/ well for 15-20 minutes. Following a washing step with H/H buffer the cells are incubated with 10 μL of 1 μM dye. The dye is prepared from 10 mM stock solution either in H/H buffer if applied to fixed cells or in medium when applied directly to live cells. Live cells are incubated 2 h at 37 °C and 5% CO2 and fixed cells 2h at RT. Excess of dye is removed after incubation by washing with H/H buffer using Tecan Power Washer. Live cells are fixed, as described before, after performance of the biorthogonal reaction. To visualize the nuclei for later image analysis, nuclear staining is performed using Hoechst dye in a dilution of 1:10000 in H/H buffer. Cells are incubated for 10 minutes with 10 μL of the Hoechst solution followed by washing with H/H buffer using Tecan Power Washer. The cells are stored in H/H buffer containing 1 % Pen/Strep until imaging.

3.11.4. In cells competition assay

To perform the competition assay, the same protocol as described for intracellular labeling is used adding a step where a compound is allowed to compete the probe. To do that, following overnight incubation with the probe and washing, the competitor molecule is incubated in live cells for 1 hour at 37C and 5% CO2 at different doses (0.0158 to 15.8 uM). The labeling is then performed either in live or fixed cells as indicated above.

3.11.5. Image analysis and high content imaging

Images were acquired with an InCell2000 high throughput microscope (GE Healthcare) using a 20x objective. DAPI was excited at 350 nm and emission was sampled at 470 nm; Bodipy-FL-Tz and Bodipy-Fl-BCN was excited at 490 nm and emission was sampled at 525 nm, Bodipy-TMR-Tz was excited at 596 nm and emission was sampled at 614 nm. Alexa Fluor 647 was excited at 649 nm and emission was sampled at 666 nm. Image analysis was performed using Columbus software (Perkin Elmer). First, nuclei was detected based on Hoechst staining and cytoplasm was defined by Bodipy-FL or Bodipy-TMR staining. The intensity of the Bodipy-Fl or Bodipy-TMR signals were measured in the cytoplasm or nuclei region. The intensity of Alexa Fluor 647 was measured in the nuclei region. For the Mdm2 assay, an intensity threshold was set to calculate the number of cells overexpressing Mdm2. Data was exported as average of the well and for individual cells.

3.11.6. Data analysis for biology experiments

Dose response curves and statistical analysis were performed with OriginPro 9.1 software. Data were assessed for significance by two-Sample T-Test. Results were considered statistically significant for P values < 0.05.

3.11.7. Chemical material and Methods

General considerations

All chemicals were purchased from Sigma Aldrich, unless noted, and were used as received. All solvents were of reagent grade or higher and were used without further purification.

Instruments for chemical synthesis, characterization and reaction characterization

As reported in 2.12.10.1.

3.11.8. General procedure for bioorthogonal reaction characterization with LC-MS

A representative example of IED-DA:
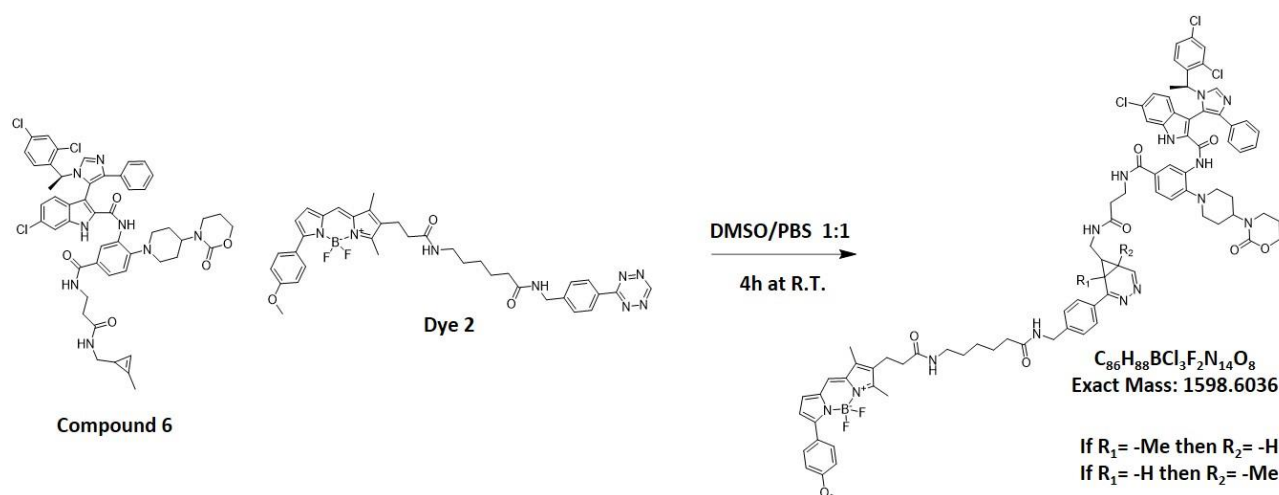
Dye 2 (60 μL, 0.600 μmol, 10mM solution in dry DMSO) and Compound **6** (15 μL, 0.150 μmol, 10mM solution in dry DMSO) were combined in 150 μL of DMSO and 150 μL of PBS at a final concentration of 0.42 mM for compound **6**. The reaction was analyzed with LC-MS after the addition of the last reagent and after 4 hours at room temperature shaking at R.T. Multiple peaks were identified with molecular mass consistent with the IED-Diels-Alder products (m/z 1597 [M-1]⁻).

A representative example of SPAAC:
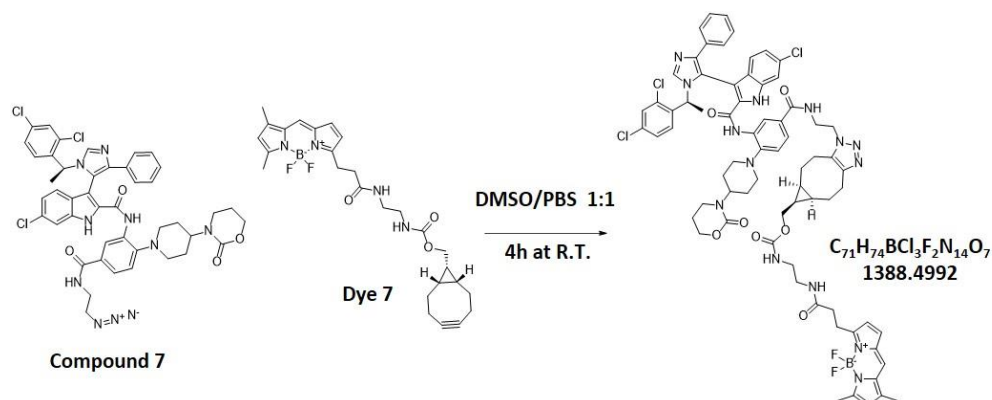
Dye 7 (60 μL, 0.600 μmol, 10mM solution in dry DMSO) and Compound **7** (15 μL, 0.150 μmol, 10mM solution in dry DMSO) were combined in 150 μL of DMSO and 150 μL of PBS at a final concentration of 0.42 mM for compound **7**. The reaction was analyzed with LC-MS after the addition of the last reagent and after 4 hours at room temperature shaking

ay R.T. A single peak with molecular mass consistent with the alkyne-azide cycloaddition product was identified (m/z 1389 [M+H]+ and m/z 1387 [M-1]-).

Reaction characterization between compound **3, 4, 5** and **6** and the tetrazine-fluorophores (**dyes 1-5**) were performed following the same procedure described for the reaction characterization between compound **6** and **dye 2**. Reaction characterization between compound 7 and alkyne fluorophores were performed using the same procedure described for the reaction characterization between compound **7** and **dye 7**.

Cmpd	Dye	Bioorth. Product Formula	Bioorth.Product Calcd. mass	Bioorth. Product Found mass	Bioorth.Product Retention time
3	1	$C_{76}H_{77}BCl_3F_2N_{13}O_7$	$[M+H]^+=1437.5$	1438.6	Multiple peaks 5.94 - 6.48min[a]
4	1	$C_{73}H_{71}BCl_3F_2N_{13}O_7$	$[M+H]^+=1396.4$	1396.5	Multiple peaks Main peak at 6.29min[a]
5	1	$C_{70}H_{66}BCl_3F_2N_{12}O_5$	$[M+H]^+=1308.4$	1309.5	Multiple peaks Main peak at 6.34min[a]
6	1	$C_{73}H_{71}BCl_3F2N_{13}O_6$	$[M+H]^+=1380.5$	1380.5	Multiple peaks Main peak at 6.13min[a]
3	2	$C_{89}H_{94}BCl_3F_2N_{14}O_9$	$[M+H]^+=1657.6$	1658.0	Multiple peaks 1.22-1.40min[b]
4	2	$C_{86}H_{88}BCl_3F_2N_{14}O_9$	$[M-1]^+=1613.6$	1613.0	Multiple peaks 1.25-1.50min[b]
5	2	$C_{83}H_{83}BCl_3F_2N_{13}O_7$	$[M+H]^+=1527.6$	1528.6	Multiple peaks Main peak at 6.63min[a]
3	3	$C_{74}H_{74}BCl_3F_2N_{12}O_6$	$[M+H]^+= 1381.4$	1381.4	Multiple peaks Main peak at 7.27min[a]
4	3	$C_{71}H_{68}BCl_3F_2N_{12}O_6$	$[M+H]^+= 1339.4$	1340.1	Multiple peaks Main peak at 9.44 min[a]
3	4	$C_{76}H_{79}BCl_3FN_{12}O_7$	$[M+H]^+=1407.5$	1407.5	Multiple peaks 7.59 – 8.12min[a]
4	4	$C_{73}H_{73}BCl_3FN_{12}O_7$	$[M+H]^+=1365.5$	1365.6	Multiple peaks 7.23 - 7.93min[a]
5	4	$C_{70}H_{68}BCl_3FN_{11}O_5$	$[M+H]^+=1280.5$	1280.6	Multiple peaks 7.24 - 8.24min[a]
6	4	$C_{73}H_{73}BCl_3FN_{12}O_6$	$[M+H]^+=1350.6$	1350.4	Multiple peaks Main peak at 7.80min[a]
4	5	$C_{87}H_{86}Cl_3N_{13}O_9Si$	$[M+H]^+= 1591.5$	1591.3	Small peak at 6.42 min[a] (reaction not completed)
7	6	$C_{82}H_{81}Cl_3N_{14}O_{10}$	$[M+H]^+=1527.5$	1527.6	Single peak at 5.52 min[a]
7	8	$C_{63}H_{53}Cl_3N_{10}O_7$	$[M+H]^+= 1167.3$	1167.2	Single peak at 5.80 min[a] (reaction not completed)

[a]   LC-MS 10 min run method
[b]   LC-MS 2 min run method

Fluorophores Synthesis and characterization

Dye 1: N-(4-(1,2,4,5-tetrazin-3-yl)benzyl)-3-(5,5-difluoro-7,9-dimethyl-5H-4λ^4,5λ^4-dipyrrolo[1,2-c:2',1'-f][1,3,2]diazaborinin-3-yl)propanamide
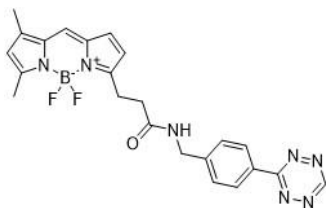
A mixture of Intermediate 13 (20 mg, 0.068 mmol), HATU (31.2 mg, 0.082 mmol), TEA (38.2 µl, 0.274 mmol) in DMF (0.5 mL) was stirred at R.T. for 20min in the dark. **Intermediate 14** (51.6 mg, 0.171 mmol) was added. The reaction mixture was stirred at R.T. for 3h. The reaction was diluted with DCM (100 mL). The organic solution was washed with NaHCO3 aq. sat sol. (60 mL X 2), brine (60 mL), dried with MgSO$_4$ and evaporated to dryness. The crude was purified via flash chromatography (silica column 12g, Ethyl acetate/ DCM mobile phase) to obtain Compound 8 (16 mg, 0.034 mmol, 50.2 % yield) as a red solid.

^{1}H NMR (400 MHz, Chloroform-d) δ 10.24 (s, 1H), 8.51 (d, J = 8.4 Hz, 2H), 7.36 (d, J = 8.4 Hz, 2H), 7.13 (s, 1H), 6.93 (d, J = 3.9 Hz, 1H), 6.35 (d, J = 4.0 Hz, 2H), 6.10 (s, 1H), 4.54 (d, J = 5.9 Hz, 2H), 3.35 (t, J = 7.3 Hz, 2H), 2.83 (t, J = 7.3 Hz, 2H), 2.56 (s, 3H), 2.26 (s, 3H).

LC-MS [M+Na]$^+$ m/z calcd. for [C$_{23}$H$_{22}$BF$_2$N$_7$NaO]$^+$= 484.2, found 484.2 at 1.05 min. (UV Detector: TIC). LC-MS [M-1]$^-$ m/z calcd. for [C$_{23}$H$_{21}$BF$_2$N7O]$^-$ 460.2, found 460.2 at 1.05 min. (UV Detector: TIC) (LC-MS method b).

Dye 2: N-(4-(1,2,4,5-tetrazin-3-yl)benzyl)-6-(3-(5,5-difluoro-7-(4-methoxyphenyl)-1,3-dimethyl-5H-4λ^4,5λ^4-dipyrrolo[1,2-c:2',1'-f][1,3,2]diazaborinin-2-yl)propanamido)hexanamide
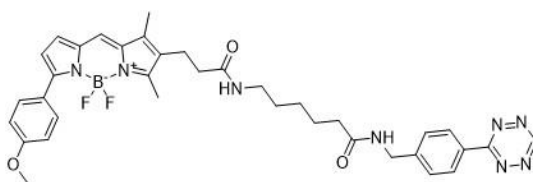
The title compound was prepared starting from **intermediate 14** following a literature described procedure.[66]

^{1}H NMR (400 MHz, Chloroform-d) δ 10.23 (s, 1H), 8.56 (d, J = 8.3 Hz, 2H), 7.86 (d, J = 8.9 Hz, 2H), 7.44 (d, J = 8.3 Hz, 2H), 7.11 (s, 1H), 6.99 − 6.92 (m, 3H), 6.54 (d, J = 4.1 Hz, 1H), 5.95 (t, J = 5.1 Hz, 1H), 5.52 (t, J = 5.5 Hz, 1H), 4.46 (d, J = 6.0 Hz, 2H), 3.85 (s, 3H), 3.23 (q, J = 6.5 Hz, 2H), 2.78 (t, J = 7.1 Hz, 2H), 2.55 (s, 3H), 2.31 (t, J = 7.1 Hz, 2H), 2.23 (s, 3H), 2.16 (t, J = 7.3 Hz, 2H), 1.68 − 1.60 (m, 2H), 1.45 (dq, J = 17.0, 10.1, 8.5 Hz, 2H), 1.30 − 1.21 (m, 2H).

LC-MS [M+Na]$^+$ m/z calcd. for [C36H39BF2N8NaO3]$^+$ 703.3, found 703.2 at 1.13 min. (UV Detector: TIC) and [M-1]$^-$ m/z calcd. for [C$_{36}$H$_{38}$BF$_2$N$_8$O$_3$]$^-$ 679.3, found 679.2 at 1.13 min. (UV Detector: TIC) (LC-MS method b).

Dye 3: 10-(3-(1,2,4,5-tetrazin-3-yl)phenyl)-5,5-difluoro-1,3,7,9-tetramethyl-4λ^4,5λ^4-dipyrrolo[1,2-c:2',1'-f][1,3,2]diazaborinine
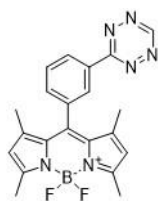
TFA (0.050 mL, 0.645 mmol) was added to a solution of **Intermediate 15** (240 mg, 1.289 mmol) and 2,4-dimethyl-1H-pyrrole (0.305 mL, 2.97 mmol) in DCM (Volume: 18 mL, Ratio: 1.000) at R.T. The reaction was stirred at R.T. for 1.5h. A solution of DDQ (351 mg, 1.547 mmol) in DCM (Volume: 18.00 mL, Ratio: 1.000) was added to the reaction mixture. After 30min DIPEA (4.50 mL, 25.8 mmol) was added followed by BF3.OEt2 (3.27 mL, 25.8 mmol). The reaction was stirred at R.T. for 7h. DCM was added to the reaction. The organic phase was washed with water and evaporated to dryness to afford the crude material. The crude was purified via prep. HPLC to afford the title compound , dye 3 (13 mg, 0.032 mmol, 2.5 % yield) as a red powder.

^{1}H NMR (400 MHz, DMSO-d6) δ 10.63 (d, J = 1.2 Hz, 1H), 8.67 (dd, J = 8.0, 1.6 Hz, 1H), 8.41 (q, J = 1.6 Hz, 1H), 7.89 (dd, J = 8.5, 7.0 Hz, 1H), 7.78 (dd, J = 7.8, 1.6 Hz, 1H), 6.22 (s, 2H), 1.42 (s, 6H).(The chemical shifts of 6H observed with HSCQ under the solvent peak).

^{13}C NMR (101 MHz, DMSO) δ 158.38, 128.05, 126.73, 130.27, 131.86, 121.19, 14.04, 0.86, 14.04

LC-MS [M+H]$^+$ m/z calcd. for [$C_{21}H_{20}BF_2N_6$]$^+$ 405.1, found 405.2 at 1.32 min. (UV Detector: TIC) and LC-MS [M+Na]$^+$ m/z calcd. for [$C_{21}H_{19}BF_2N_6Na$]$^+$ 427.1, found 427.4 at 1.32 min. (UV Detector: TIC) (LC-MS method b).

Dye 4: 5-((4-(1,2,4,5-tetrazin-3-yl)benzyl)oxy)-5-fluoro-1,3,7,9,10-pentamethyl-5H-4λ^4,5λ^4-dipyrrolo[1,2-*c*:2',1'-*f*][1,3,2]diazaborinine
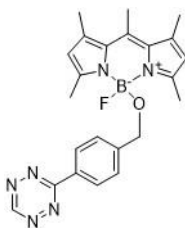
The title compound was prepared starting from **Intermediate 16** and **Intermediate 17** following a literature described procedure.[187]

^{1}H NMR (400 MHz, Chloroform-d) δ 10.20 (s, 1H), 8.51 (d, J = 8.4 Hz, 2H), 7.46 (d, J = 8.2 Hz, 2H), 6.06 (s, 2H), 4.16 (s, 2H), 2.64 (s, 3H), 2.55 (s, 6H), 2.45 (s, 6H).

LC-MS [M+Na]$^+$ m/z calcd. for [$C_{23}H_{24}BFN_6NaO$]$^+$ 453.2, found 453.3 at 1.32 min. (UV Detector: TIC) and LC-MS [M-1]$^-$ m/z calcd. for [$C_{23}H_{23}BFN_6O$]$^-$ 429.2, found 429.3 at 1.32 min. (UV Detector: TIC) (LC-MS method b).
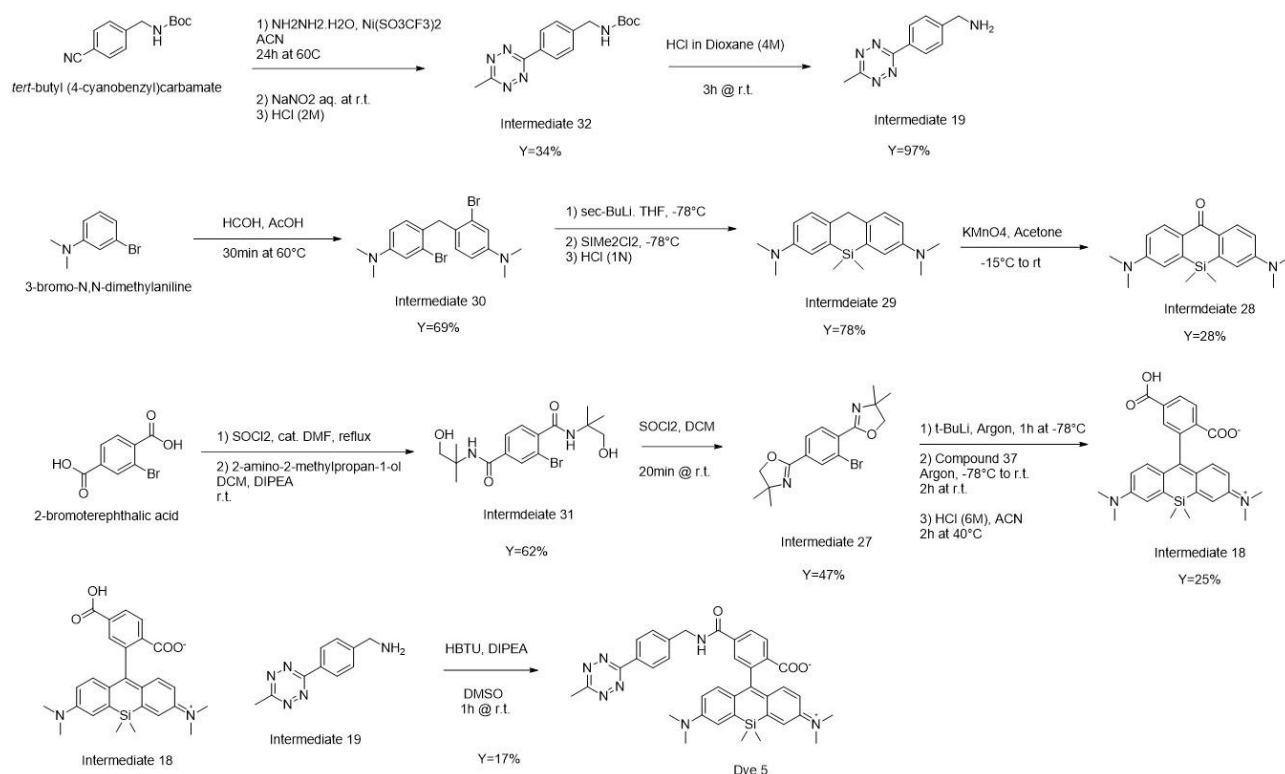
3.11-1 synthetic route for the preparation of dye 5

Dye 5: N-(10-(2-carboxy-5-((4-(6-methyl-1,2,4,5-tetrazin-3-yl)benzyl)carbamoyl)phenyl)-7-(dimethylamino)-5,5-dimethyldibenzo[b,e]silin-3(5H)-ylidene)-N-methylmethanaminium
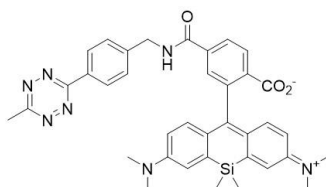
The title compound was synthesized starting from **Intermediate 18** and **Intermediate 19** following a similar procedure to one described in literature.[170] Amide coupling reagent TSTU was replaced with HBTU.

^{1}H NMR (400 MHz, Acetone-d6) δ 8.66 (s, 1H), 8.47 (dt, J = 7.8, 2.6 Hz, 2H), 8.25 – 8.14 (m, 1H), 8.02 (dd, J = 8.2, 4.0 Hz, 1H), 7.84 (s, 1H), 7.62 (dd, J = 7.2, 4.9 Hz, 2H), 7.12 (q, J = 3.3, 2.8 Hz, 2H), 6.77 (dt, J = 9.2, 2.7 Hz, 2H), 6.70 – 6.60 (m, 2H), 4.71 (d, J = 4.9 Hz, 2H), 3.02 (t, J = 2.8 Hz, 4H), 2.98 (s, 11H), 0.67 (t, J = 2.7 Hz, 3H), 0.55 (t, J = 2.7 Hz, 3H).

^{13}C NMR (101 MHz, Acetone) δ 13C NMR (101 MHz, Acetone) δ 128.93, 128.59, 128.03, 125.76, 123.60, 117.08, 114.15, 43.64, 39.89, 20.75.

LC-MS [M]$^+$ m/z calcd. for [C$_{37}$H$_{37}$N$_7$O$_3$Si]$^+$ 656.2, found 656.3 at 5.91 min. (UV Detector: TIC) and [M+H]$^+$ m/z calcd. for [C$_{37}$H$_{38}$N$_7$O$_3$Si]$^+$ 657.2, found 657.3 at 5.91 min. (UV Detector: TIC) (LC-MS method a).

Dye 6: ((1R,8S,9s)-bicyclo[6.1.0]non-4-yn-9-yl)methyl(2-(3',6'-bis(dimethylamino)-3-oxo-3H-spiro[isobenzofuran-1,9'-xanthene]-6-carboxamido)ethyl)carbamate
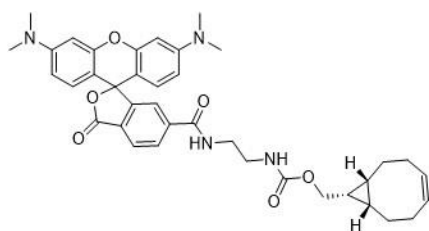
A solution of **Intermediate 20** (24.7 mg, 0.105 mmol) in dry DCM (Volume: 0.2 mL, Ratio: 1.000) was added drop wise to a solution of 6-TAMRA SE from Pharmten Chemical Co. (50 mg, 0.095 mmol) in dry DMF (Volume: 1 mL, Ratio: 5.00). DIPEA (0.033 mL, 0.190 mmol) was added and the reaction was stirred at R.T. overnight. The reaction mixture was purified via prep. HPLC. The fractions containing the desired product were combined. DCM (30 mL) and NaHCO3 aq. sat. solution (40 mL) were added. The organic phase was separated. The basic phase was acidified with HCl (4M) to pH=5. The aq. phase was extracted with DCM (30 mL X 2). The organic phases were combined, filtered via a separator phase cartridge and evaporated to dryness to obtain Compound 10 (45 mg, 0.068 mmol, 71.4 % yield) as a dark purple solid.

^{1}H NMR (600 MHz, DMSO-d6) δ 8.72 (t, J = 5.5 Hz, 1H), 8.14 (d, J = 8.1 Hz, 1H), 8.07 (d, J = 8.0 Hz, 1H), 7.63 (s, 1H), 7.19 (t, J = 5.7 Hz, 1H), 6.55 – 6.48 (m, 6H), 3.98 (d, J = 8.1 Hz, 2H), 3.25 (q, J = 5.8 Hz, 2H), 3.09 (q, J = 6.1 Hz, 2H), 2.95 (s, 12H), 2.19 (d, J = 13.0 Hz, 2H), 2.11 (d, J = 12.4 Hz, 4H), 1.48 (d, J = 9.8 Hz, 2H), 1.22 (dq, J = 17.1, 8.6, 8.0 Hz, 1H), 0.82 (t, J = 9.7 Hz, 2H).

^{13}C NMR (151 MHz, DMSO-d6) δ = 168.73, 165.25, 156.91, 153.28, 152.59, 152.40, 141.09, 129.67, 128.97, 125.11, 122.76, 109.51, 106.06, 99.44, 98.41, 85.18, 61.82, 29.02, 21.29, 19.99, 18.05. (4 carbon chemical shifts hidden under the solvent peak were observed using HBMC).

LC-MS [M+H]+ m/z calcd. for [C38H41N4O6]+ 649.3, found 649.4 at 0.89 min. (UV Detector: TIC) and [M-H+HCO2H]- m/z calcd. for [C$_{39}$H$_{41}$N$_4$O$_8$]- 693.3, found 693.4 at 1.13 min. (UV Detector: TIC) (LC-MS method b).

Dye 7: ((1R,8S,9s)-bicyclo[6.1.0]non-4-yn-9-yl)methyl(2-(3-(5,5-difluoro-7,9-dimethyl-5H-4λ^4,5λ^4-dipyrrolo[1,2-c:2',1'-f][1,3,2]diazaborinin-3-yl)propanamido)ethyl)carbamate
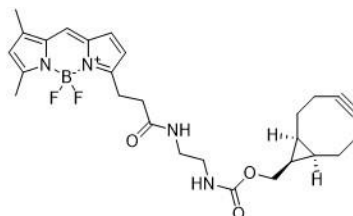
A solution of **Intermediate 13** (28 mg, 0.096 mmol), TEA (0.053 mL, 0.383 mmol) and HATU (72.9 mg, 0.192 mmol) in DMF (0.8 mL) was stirred at R.T. under N$_2$ for 10 min in a sealed vial. A solution of **Intermediate 20** (34.0 mg, 0.144 mmol) in DMF (0.2 mL) was added. The reaction was stirred at R.T. overnight. The reaction was poured in EA (100 mL) and washed with NaHCO3 aq. sat. sol. (80 mL x 3), brine (80 mL), dried with MgSO$_4$ and evaporated to dryness to obtain a residue. The crude material was purified via prep. HPLC (ACN/water mobile phase, TFA acid modifier). DCM (40 mL) and NaHCO3 aq. sat. sol. (40 mL) were added to the fraction containing the desired product. The organic phase was

separated. The aqueous phase was extracted with DCM (40 mL x 2). The organic phases were combined, dried with MgSO$_4$ and evaporated to dryness to obtain **Dye 7** (14.4 mg, 0.028 mmol, 28.8 % yield) as a red solid.

^{1}H NMR (600 MHz, Chloroform-d) δ 7.12 (s, 1H), 6.91 (d, J = 3.7 Hz, 1H), 6.31 (d, J = 3.9 Hz, 1H), 6.16 (s, 1H), 6.10 (s, 1H), 5.09 (s, 1H), 4.14 (d, J = 8.1 Hz, 2H), 3.37 – 3.32 (m, 2H), 3.29 (t, J = 7.4 Hz, 2H), 3.24 (d, J = 5.5 Hz, 2H), 2.68 (t, J = 7.4 Hz, 2H), 2.60 (s, 3H), 2.36 – 2.20 (m, 7H), 1.61 (d, J = 17.1 Hz, 2H), 1.35 (d, J = 8.4 Hz, 1H), 1.29 (dd, J = 13.0, 5.8 Hz, 2H), 0.99 – 0.88 (m, 2H).

^{13}C NMR (151 MHz, Chloroform-d) δ = 172.61, 160.63, 157.12, 156.86, 135.26, 133.31, 128.10, 123.88, 120.62, 117.45, 98.84, 62.86, 41.19, 39.85, 35.91, 29.06, 24.95, 21.45, 20.13, 17.77, 15.02, 14.20, 11.39.

LC-MS [M+H]$^+$ m/z calcd. for [C$_{27}$H$_{34}$BF$_2$N$_4$O$_3$]$^+$ 511.2.3, found 511.2 at 4.26 min. (UV Detector: TIC) and [M-1]$^-$ m/z calcd. for [C$_{27}$H$_{33}$BF$_2$N$_4$O$_3$]$^-$ 679.3, found 679.2 at 1.13 min. (UV Detector: TIC) (LC-MS method b).

Dye 8: 4,9-Dimethoxy-6,7-didehydro-1H-dibenzo[a,e]cyclopropa-[c]cycloocten-1-one
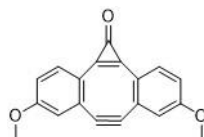
The tile compound was prepared starting from **Intermediate 21** following a literature described procedure.[172]

^{1}H NMR (400 MHz, Chloroform-d) δ 7.47 (d, J = 8.5 Hz, 2H), 6.63 (dd, J = 8.5, 2.6 Hz, 2H), 6.45 (d, J = 2.6 Hz, 2H), 3.81 (s, 6H).

^{13}C NMR (101 MHz, CDCl$_3$) δ 136.60, 113.47, 114.43, 55.28 (peaks visible in HSQC).

LC-MS [M+H]$^+$ m/z calcd. for [C$_{19}$H$_{13}$O$_3$]$^+$ 289.1, found 289.0 at 1.06 min. (UV Detector: TIC) (LC-MS method b).

Dye 9: Methyl 3-(5,5-difluoro-7,9-dimethyl-5H-4λ^4,5λ^4-dipyrrolo[1,2-c:2',1'-f][1,3,2]diazaborinin-3-yl)propanoate

The title compound was prepared starting from methyl 3-(1H-pyrrol-2-yl)propanoate [69917-80-2] (commercially available from Toronto Reasearch Chemicals) and 3,5-dimethyl-1H-pyrrole-2-carbaldehyde following a literature described procedure.[188]

^{1}H NMR (400 MHz, Chloroform-d) δ 7.11 (s, 1H), 6.91 (d, J = 3.9 Hz, 1H), 6.29 (d, J = 4.0 Hz, 1H), 6.14 (s, 1H), 3.72 (s, 3H), 3.32 (t, J = 7.6 Hz, 2H), 2.84 – 2.76 (m, 2H), 2.59 (s, 3H), 2.28 (s, 3H).

^{13}C NMR (101 MHz, CDCl3) δ = 172.96, 160.49, 157.07, 143.85, 135.24, 133.30, 128.03, 123.81, 120.45, 116.68, 51.73, 33.27, 23.98, 14.96, 11.31.

LC-MS [M+H]$^+$ m/z calcd. for [C$_{15}$H$_{18}$BF$_2$N$_2$O$_2$]$^+$ 307.1, found 307.1 at 1.13 min. (UV Detector: TIC) and [M-1]$^-$ m/z calcd. for [C$_{15}$H$_{16}$BF$_2$N$_2$O$_2$]$^-$ 305.1, found 305.1 at 1.13 min. (UV Detector: TIC) (LC-MS method b).

Compound 16: (S)-6-chloro-3-(1-(1-(2,4-dichlorophenyl)ethyl)-4-phenyl-1H-imidazol-5-yl)-N-(5-((2-(3-(5,5-difluoro-7,9-dimethyl-5H-4λ⁴,5λ⁴-dipyrrolo[1,2-c:2',1'-f][1,3,2]diazaborinin-3-yl)propanamido)ethyl)carbamoyl)-2-(4-(2-oxo-1,3-oxazinan-3-yl)piperidin-1-yl)phenyl)-1H-indole-2-carboxamide
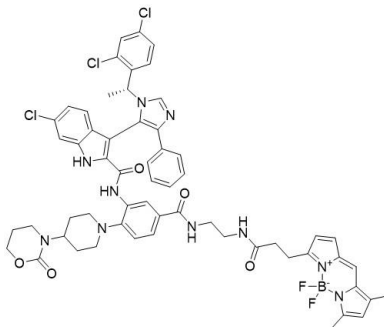
A mixture of **Intermediate 2** (30 mg, 0.035 mmol), **Intermediate 13** (15.39 mg, 0.053 mmol), HBTU (26.6 mg, 0.070 mmol) and DIPEA (0.012 mL, 0.070 mmol) in DMF (1 mL) were stirred at R.T. in the dark for 16h. The reaction was poured in DCM (50 mL). The organic phase was washed twice with NaHCO₃ aqueous saturated solution (40 mL), and twice with brine (40 mL), dried with MgSO₄ and evaporated to obtain the crude material. The crude was purified via flash chromatography (silica column 12g, MeOH and DCM as mobile phase). The fraction containing the desired product were combined and evaporated to dryness to obtain the Compound 14 (22 mg, 0.019 mmol, 54.4 % yield) as a red solid.

^{1}H NMR (600 MHz, DMSO-d6) δ = 12.37 (d, J=3.0, 1H), 8.80 (d, J=2.8, 1H), 8.72 (d, J=2.1, 1H), 8.48 - 8.41 (m, 2H), 8.14 - 8.08 (m, 1H), 7.67 (d, J=4.1, 1H), 7.54 (d, J=6.0, 1H), 7.46 (s, 2H), 7.40 (s, 1H), 7.34 (d, J=8.3, 1H), 7.18 - 7.12 (m, 3H), 7.11 - 7.07 (m, 1H), 7.07 - 7.03 (m, 2H), 6.78 (d, J=8.4, 1H), 6.63 (d, J=8.4, 1H), 6.35 (t, J=3.9, 1H), 6.33 - 6.27 (m, 2H), 5.57 - 5.52 (m, 1H), 4.03 (s, 1H), 3.95 (s, 1H), 3.84 (s, 1H), 3.35 - 3.29 (m, 2H), 3.27 (s, 2H), 3.10 (s, 2H), 2.96 - 2.84 (m, 2H), 2.71 (s, 2H), 2.52 - 2.43 (m, 5H), 2.37 - 2.27 (m, 2H), 2.24 (s, 3H), 1.79 - 1.69 (m, 1H), 1.69 - 1.59 (m, 1H), 1.59 - 1.52 (m, 1H), 1.52 - 1.46 (m, 4H), 1.30 - 1.22 (m, 2H).

^{13}C NMR (151 MHz, DMSO-d6) δ = 171.28, 165.92, 159.14, 158.70, 157.78 , 152.10, 145.25, 144.08, 141.28, 138.01, 137.76, 136.51, 134.44, 134.27, 132.99, 132.33, 131.87, 131.21, 130.66, 130.04, 129.05, 128.93, 128.20, 128.12 - 127.77 (m), 126.56, 125.99, 125.34, 124.76, 123.03, 121.41, 120.54, 120.33, 119.55, 118.27, 116.52, 111.71, 106.02, 65.50, 54.93, 53.02, 51.53, 50.41, 38.67, 38.31, 33.68, 28.46, 27.95, 23.93, 22.00, 19.55, 14.52, 11.00.

LC-MS [M+H]⁺ m/z calcd. for [C₅₈H₅₇BCl₃F₂N₁₀O₅]⁺ 1127.3, found 1127.3 at 1.28 min. (UV Detector: TIC) and [M-1]⁻ m/z calcd. for [C₅₈H₅₅BCl₃F₂N₁₀O₅]⁻ 1125.3, found 1125.3 at 1.28 min. (UV Detector: TIC) (LC-MS method b).

Intermediate 13: 3-(5,5-difluoro-7,9-dimethyl-5H-4λ4,5λ4-dipyrrolo[1,2-c:2',1'-f][1,3,2]diazaborinin-3-yl)propanoic acid
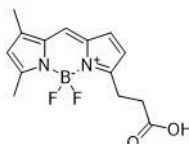
The title compound was prepared starting from **Dye 9** following a literature described procedure.[189]

^{1}H NMR (400 MHz, DMSO-d6) δ 12.32 (s, 1H), 7.72 (s, 1H), 7.10 (d, J = 4.0 Hz, 1H), 6.39 (d, J = 4.0 Hz, 1H), 6.33 (s, 1H), 3.09 (t, J = 7.7 Hz, 2H), 2.65 (t, J = 8.6, 6.9 Hz, 2H), 2.49 (s, 3H), 2.28 (s, 3H).

¹³C NMR (101 MHz, DMSO) δ = 173.91, 159.95, 157.47, 144.80, 135.05, 133.49, 129.31, 125.94, 120.88, 117.05, 32.84, 24.02, 15.00, 11.48.

LC-MS [M-1]⁻ m/z calcd. for [C$_{14}$H$_{15}$BF$_2$N$_2$O$_2$]⁻ 291.2, found 291.2 at 0.93 min. (UV Detector: TIC) (LC-MS method b).

Intermediate 14: (4-(1,2,4,5-tetrazin-3-yl)phenyl)methanamine
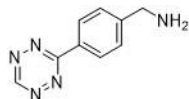
The title compound was prepared following a literature described procedure.[168]

¹H NMR (400 MHz, Deuterium Oxide) δ 10.32 (s, 1H), 8.46 (d, J = 8.4 Hz, 2H), 7.65 (d, J = 8.4 Hz, 2H), 4.25 (s, 2H).

LC-MS [M+H]⁺ m/z calcd. for [C$_9$H$_{10}$N$_5$]⁺ 188.09, found 188.0 at 0.35 min. (UV Detector: TIC) (LC-MS method b).

IIntermediate 15: 3-(1,2,4,5-tetrazin-3-yl)benzaldehyde
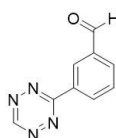
Dess-Martin periodinane (731 mg, 1.724 mmol) was added to a solution of **Intermediate 27** (295 mg, 1.568 mmol) in DCM (Volume: 15 mL). The solution was placed under N$_2$ and stirred at R.T. for 1 h. DCM was added to the reaction mixture. The mixture was washed with NaHCO3 aq. sat. sol., brine, dried with MgSO$_4$ and evaporated to dryness to obtain the crude as a pink solid. The crude material was purified via flash chromatography (silica column 24g, Ethyl acetate / cyclohexane mobile phase) to obtain the title Intermediate 15 (240 mg, 1.289 mmol, 82 % yield) as a bright purple solid.

¹H NMR (400 MHz, DMSO-*d$_6$*) δ 10.68 (d, *J* = 1.0 Hz, 1H), 10.21 (d, *J* = 1.1 Hz, 1H), 9.02 (q, *J* = 1.5 Hz, 1H), 8.81 (dd, *J* = 7.8, 1.6 Hz, 1H), 8.24 (dd, *J* = 7.7, 1.5 Hz, 1H), 7.93 (t, *J* = 7.7 Hz, 1H).

¹³C NMR (101 MHz, DMSO) δ 158.60, 26.64, 128.33, 132.78, 132.78, 130.05 (chemical shifts visible in HSQC).

Intermediate 16 5,5-difluoro-1,3,7,9,10-pentamethyl-5H-4λ4,5λ4-dipyrrolo[1,2-c:2',1'-f][1,3,2]diazaborinine
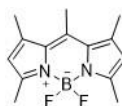
The title compound was prepared starting from 2,4-dimethyl-1H-pyrrole following a literature described procedure.[190]

¹H NMR (400 MHz, Chloroform-d) δ 6.09 (s, 2H), 2.62 (s, 3H), 2.56 (s, 6H), 2.46 (s, 6H).

LC-MS [M+H]⁺ m/z calcd. for [C$_{14}$H$_{18}$BF$_2$N$_2$]⁺ 262.15.07, found 263.2 at 1.21 min. (UV Detector: TIC) (LC-MS method b).

ntermediate 17: (4-(1,2,4,5-tetrazin-3-yl)phenyl)methanol
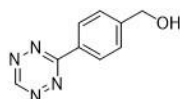
The title compound was prepared following a literature described procedure.[168]

^{1}H NMR (400 MHz, Chloroform-d) δ 10.24 (s, 1H), 8.66 (d, J = 8.4 Hz, 2H), 7.64 (d, J = 8.6 Hz, 2H), 4.88 (d, J = 5.7 Hz, 2H), 1.83 (t, J = 5.8 Hz, 1H).

LC-MS [M+H]$^+$ m/z calcd. for [C$_9$H$_9$N$_4$O]$^+$ 188.07, found 189.1 at 0.60 min. (UV Detector: TIC) (LC-MS method b).

Intermediate 18: 4-carboxy-2-(7-(dimethylamino)-3-(dimethyliminio)-5,5-dimethyl-3,5-dihydrodibenzo[*b,e*]silin-10-yl)benzoate
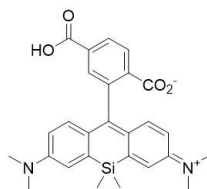
The title compound was synthesized starting from **Intermediate 27** and **Intermediate 28** following the literature described procedure.[170]

LC-MS [M+H]$^+$ m/z calcd. for [C$_{27}$H$_{29}$N$_2$O$_4$Si]$^+$ 473.2, found 473.1 at 1.17 min. (UV Detector: TIC) and [M-1]$^-$ m/z calcd. for [C$_{27}$H$_{27}$N$_2$O$_4$Si]$^-$ 471.2, found 471.2 at 1.17 min. (UV Detector: TIC) (LC-MS method b).

Intermediate 19: (4-(6-methyl-1,2,4,5-tetrazin-3-yl)phenyl)methanamine as HCl salt
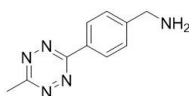
Intermediate 32 was added to HCl in dioxane (4M)(6 mL, 24.00 mmol) and stirred at R.T. for 3h. The reaction was evaporated to dryness to obtain a residue. The residue was dissolved in MeOH and re-evaporated to obtain the title compound as a bright pink solid (242 mg, 0.998 mmol, 97 % yield).

^{1}H NMR (400 MHz, Deuterium Oxide) δ 8.57 – 8.45 (m, 2H), 7.80 – 7.68 (m, 2H), 4.35 (s, 2H), 3.11 (s, 3H).

LC-MS [M+H]$^+$ m/z calcd. for [C$_{10}$H$_{12}$N$_5$]$^+$ 202.1, found 202.0 at 0.40 min. (UV Detector: TIC) (LC-MS method b).

Intermediate 20: ((1R,8S,9s)-bicyclo[6.1.0]non-4-yn-9-yl)methyl (2-aminoethyl)carbamate
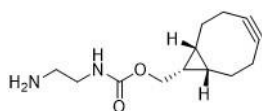
A solution of **Intermediate 22** (0.4 g, 1.269 mmol) in DCM (Volume: 8.6 mL, Ratio: 1.000) was added via a syringe pump (flow rate 1.5 mL/h) to a solution of ethane-1,2-diamine (0.848 mL, 12.69 mmol) in DCM (Volume: 17.20 mL, Ratio: 2) under N2. The reaction was diluted in DCM (150 mL). The organic phase was washed with water, dried with MgSO4 and evaporated to dryness on a high vacuum line to obtain Compound 25 (273 mg, 1.155 mmol, 91 % yield) as a white solid.

¹H NMR (400 MHz, Chloroform-d) δ 4.96 (s, 1H), 4.09 (d, J = 8.0 Hz, 2H), 3.16 (q, J = 5.8 Hz, 2H), 2.76 (t, J = 5.9 Hz, 2H), 2.29 – 2.10 (m, 6H), 1.52 (q, J = 13.3, 12.6 Hz, 2H), 1.38 – 1.11 (m, 1H), 0.93 – 0.83 (m, 2H).

¹³C NMR (101 MHz, CDCl3) δ = 98.84, 62.80, 43.63, 41.76, 29.07, 21.43, 20.12, 17.77.

Intermediate 21: (Z)-6,7-dibromo-4,9-dimethoxy-1*H*-dibenzo[*a,e*]cyclopropa[*c*][8]annulen-1-one
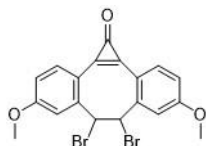
The title compound was prepared starting from **Intermediate 23** following a literature described procedure.[189]

¹H NMR (400 MHz, Chloroform-d) δ 8.07 (d, J = 8.5 Hz, 2H), 7.06 (dd, J = 8.5, 2.5 Hz, 2H), 6.97 (d, J = 2.6 Hz, 2H), 5.75 (s, 2H), 3.93 (s, 6H).

LC-MS [M+H]⁺ m/z calcd. for [C$_{19}$H$_{15}$Br$_2$O$_3$]$^+$ 450.9, found 450.9 at 1.02 min. (UV Detector: TIC) (LC-MS method b).

Intermediate 22: ((1R,8S,9s)-bicyclo[6.1.0]non-4-yn-9-yl)methyl (4-nitrophenyl) carbonate
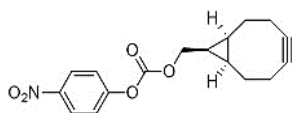
The title compound was prepared starting from ((1R,8S,9s)-bicyclo[6.1.0]non-4-yn-9-yl)methanol (BCN) [1263166-90-0] (commercially available from Synaffix) and 4-Nitrophenyl chloroformate following a literature described procedure.[191]

Intermediate 23: (Z)-4,9-dimethoxy-1*H*-dibenzo[*a,e*]cyclopropa[*c*][8]annulen-1-one
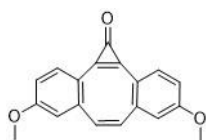
The title compound was prepared starting from **Intermediate 24** following a literature described procedure.[189]

¹H NMR (400 MHz, Chloroform-d) δ 7.44 (d, J = 8.4 Hz, 2H), 6.69 (dd, J = 8.4, 2.6 Hz, 2H), 6.60 (d, J = 2.6 Hz, 2H), 5.99 (s, 2H), 3.82 (s, 6H).

LC-MS [M+H]⁺ m/z calcd. for [C$_{19}$H$_{15}$O$_3$]$^+$ 291.1, found 291.0 at 1.02 min. (UV Detector: TIC) (LC-MS method b).

Intermediate 24: (Z)-3,3'-Dimethoxystilbene
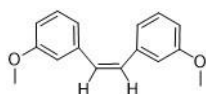
The title compound was prepared starting from **Intermediate 25** following a literature described procedure.[189]

¹H NMR (400 MHz, Chloroform-d) δ 7.15 (t, J = 7.9 Hz, 2H), 6.85 (dt, J = 7.6, 1.3 Hz, 2H), 6.81 (dd, J = 2.7, 1.5 Hz, 2H), 6.75 (ddd, J = 8.2, 2.7, 1.0 Hz, 2H), 6.58 (s, 2H), 3.67 (s, 6H).

LC-MS [M+H]$^+$ m/z calcd. for [C$_{16}$H$_{17}$O$_2$]$^+$ 241.1, found 241.0 at 1.26 min. (UV Detector: TIC) (LC-MS method b).

Intermdeiate 25: 1,2-bis(3-methoxyphenyl)ethyne
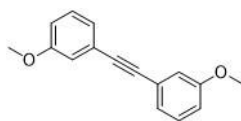
The title compound was prepared starting from commercially available 1-iodo-3-methoxybenzene and 1-ethynyl-3-methoxybenzene following a literature described procedure.[189]

LC-MS [M+H]$^+$ m/z calcd. for [C$_{16}$H$_{14}$O$_2$]$^+$ 239.1, found 239.1 at 1.29 min. (UV Detector: TIC) (LC-MS method b).

Intermediate 26: (3-(1,2,4,5-tetrazin-3-yl)phenyl)methanol
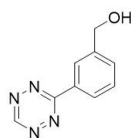
The title compound was prepared following a literature described procedure.[168]

^{1}H NMR (400 MHz, DMSO-d_6) δ 10.60 (d, J = 1.0 Hz, 1H), 8.50 (s, 1H), 8.43 – 8.35 (m, 1H), 7.64 (d, J = 6.3 Hz, 2H), 5.43 (t, J = 5.7 Hz, 1H), 4.66 (d, J = 5.6 Hz, 2H).

LC-MS [M+H]$^+$ m/z calcd. for [C$_9$H$_9$N$_4$O]$^+$ 188.01, found 189.1 at 0.60 min. (UV Detector: TIC) and [M-1]$^-$ m/z calcd. for [C$_9$H$_7$N$_4$O]$^-$ 187.1, found 187.9 at 0.60 min. (UV Detector: TIC) (LC-MS method b).

Intermediate 27: 2,2'-(2-bromo-1,4-phenylene)bis(4,4-dimethyl-4,5-dihydrooxazole)
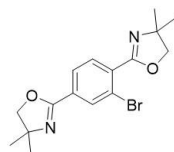
The title compound was synthesized starting from **Intermediate 31** following the literature described procedure.[170]

^{1}H NMR (400 MHz, DMSO-d_6) δ 8.07 (d, J = 1.6 Hz, 1H), 7.90 (dd, J = 8.1, 1.6 Hz, 1H), 7.75 (d, J = 8.1 Hz, 1H), 4.13 (d, J = 12.8 Hz, 4H), 1.30 (d, J = 7.5 Hz, 12H).

LC-MS [M+H]$^+$ m/z calcd. for [C$_{16}$H$_{20}$BrN$_2$O$_2$]$^+$ 351.0, found 350.1 at 1.12 min. (UV Detector: TIC) (LC-MS method b).

Intermediate 28: 3,7-bis(dimethylamino)-5,5-dimethyldibenzo[*b,e*]silin-10(5*H*)-one
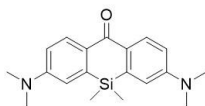
The title compound was synthesized starting from **Intermediate 29** following the literature described procedure.[170]

^{1}H NMR (400 MHz, Chloroform-d) δ 8.40 (d, J = 9.0 Hz, 2H), 6.84 (dd, J = 9.0, 2.8 Hz, 2H), 6.79 (d, J = 2.8 Hz, 2H), 3.10 (s, 12H), 0.47 (s, 6H).

LC-MS [M+H]$^+$ m/z calcd. for [C$_{19}$H$_{25}$N$_2$OSi]$^+$ 325.2, found 325.2 at 1.29 min. (UV Detector: TIC). (UV Detector: TIC) (LC-MS method b).

Intermediate 29 N^3,N^3,N^7,N^7,5,5-hexamethyl-5,10-dihydrodibenzo[*b,e*]siline-3,7-diamine
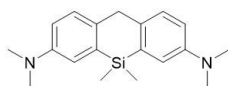
The title compound was synthesized starting from **Intermediate 30** following the literature described procedure.[170]

^{1}H NMR (400 MHz, Chloroform-d) δ 8.40 (d, J = 9.0 Hz, 2H), 6.84 (dd, J = 9.0, 2.8 Hz, 2H), 6.79 (d, J = 2.8 Hz, 2H), 3.10 (s, 12H), 0.47 (s, 6H).

LC-MS [M+H]$^+$ m/z calcd. for [C$_{19}$H$_{27}$N$_2$Si]$^+$ 311.2, found 311.4 at 1.36 min. (UV Detector: TIC). (UV Detector: TIC) (LC-MS method b).

Intermediate 30: 4,4'-methylenebis(3-bromo-*N*,*N*-dimethylaniline)
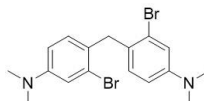
The title compound was synthesized starting from commercially available 3-bromo-N,N-dimethylaniline following the literature described procedure.[170]

^{1}H NMR (400 MHz, Chloroform-d) δ 6.97 (d, J = 2.7 Hz, 2H), 6.88 (d, J = 8.5 Hz, 2H), 6.62 (dd, J = 8.5, 2.7 Hz, 2H), 4.03 (s, 2H), 2.94 (s, 12H).

Intermediate 31: 2-bromo-*N*^{1},*N*^{4}-bis(1-hydroxy-2-methylpropan-2-yl)terephthalamide
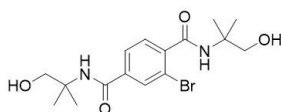
The title compound was synthesized starting from commercially available 2-bromoterephthalic acid and 2-amino-2-methylpropan-1-ol following the literature described procedure.[170]

LC-MS [M+H]$^+$ m/z calcd. for [C$_{16}$H$_{24}$BrN$_2$O$_4$]$^+$ 387.1, found 387.2 at 0.87 min. (UV Detector: TIC) and LC-MS [2M+H]$^+$ m/z calcd. for [C$_{32}$H$_{47}$Br$_2$N$_4$O$_8$]$^+$ 773.2, found 773.3 at 0.87 min. (UV Detector: TIC) (UV Detector: TIC) (LC-MS method b).

Intermediate 32: tert-butyl (4-(6-methyl-1,2,4,5-tetrazin-3-yl)benzyl)carbamate
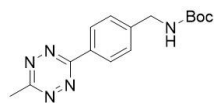
The title compound was prepared following a literature described procedure.[168]

^{1}H NMR (600 MHz, Chloroform-*d*) δ 8.64 – 8.50 (m, 2H), 7.53 (d, *J* = 8.1 Hz, 2H), 4.99 (s, 1H), 4.47 (d, *J* = 6.1 Hz, 2H), 3.13 (s, 3H), 1.51 (s, 9H).

^{13}C NMR (151 MHz, CDCl$_3$) δ 167.27, 163.94, 130.80, 128.24, 128.10, 44.40, 28.43, 21.21 (visible carbon signals).

Chapter 4. Bioorthogonal probe intracellular concentration determination

4.1 Probe permeability studies using the two step fluorescent imaging approach

Our "two step imaging" approach enabled the permeability assessment of bioorthogonal probes in our disease cellular model; we were able to detect LMW compounds in cells with a limit of detection of 50 nanomolar dose. A lower LOD was observed performing the bioorthogonal staining with EID-DA reactions, while a higher LOD using SPAAC reactions was observed (**Figure 4.1-1**). However, we should not conclude that EID-DA reactions enabled a more sensitive assessment of the compound permeability, because this would assume that the different bioorthogonal probes had the same permeability profile.
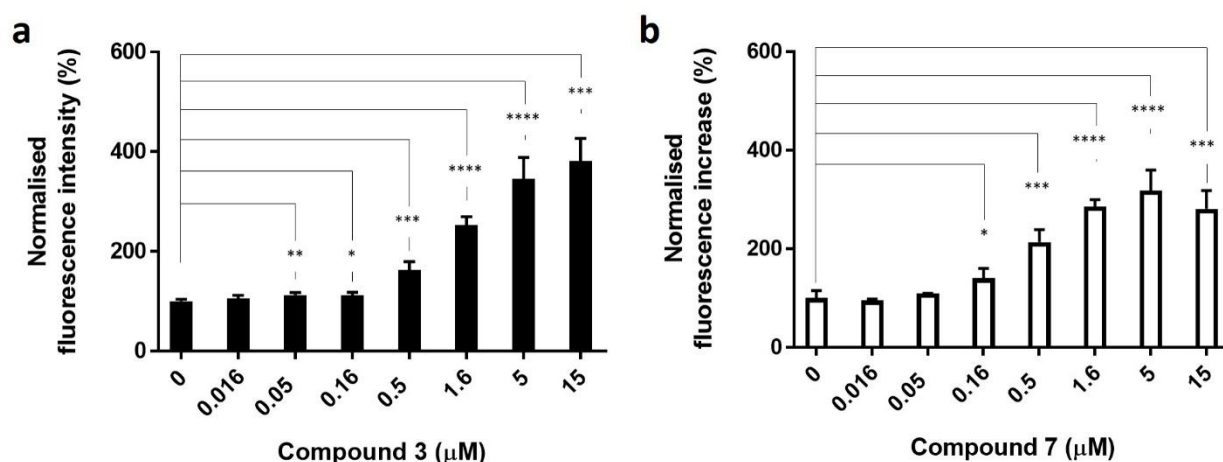
Figure 4.1-1 Assessment of compound permeability using the "two step"approach. SJSA-1 cells were treated with increasing concentration of the bioorthogonal probe (0.016 – 15 µ) for 2h at 37°C and 5% CO_2. After fixing the cells with PFA solution, **dye 1** (1µM) was incubated for 1h at R.T. Finally the cells imaging was performed. (**a**) Compound **3** was stained with **dye 1**. (**b**) Compound **7** was stained with **dye 7**. Compound uptake was detected with a LOD = 50 nM for compound **3** while a LOD = 160 nM was observed for compound **7**.

When we compared the uptake of compounds **3** and **7** using the permeability assay, we could detect internalization for the first bioorthogonal probe at 50 nanomolar (**Figure 4.1-1a**) while for second probe only at 160 nanomolar (**Figure 4.1-1b**). The two bioorthogonal probes, **3** and **7**, have very close cellular activities (**Table 2.7-1**, compound **3** EC_{50} = 43nM and compound **7** EC_{50} = 50nM). However, their biochemical potency and selectivity profile assessed by TR-FRET showed that compound **7** is more potent than compound **3** and also about 3 fold more selective against Mdm4 (**Table 2.6-1** on page 43, compound **3** hMdm2-p53 TR-FRET IC_{50}= 0.48 ± 0.03 nM and compound **7** hMdm2-p53 TR-FRET IC_{50}= 0.20 ±

0.02 nM). Therefore, the higher potency of compound **7** might counterbalance its lower permeability resulting in a cellular activity comparable to compound **3**.

To broaden the scope of our approach, we thought of extending our investigation to peptide molecules. This compound class offers some clear advantages over LMW compounds. For these molecules, a higher target affinity and a better selectivity over off targets are usually achievable. In addition, a favourable safety profile and a good tolerability have been observed for some of the peptides that have progressed to the clinic, which clearly raises the interest of pharmaceutical research toward this chemical class of molecules.[192]

Nevertheless, peptides often suffer from poor cellular permeability, so an assay enabling the investigation of peptide permeability would facilitate the design of bioorthogonal peptide probes for testing biological hypotheses.

Hence, we tested the permeability of peptides functionalized with the bioorthogonal group TCO (**10-12**) (**Figure 4.1-2** and **4.1-3**) and the azide (**14**) (**Figure 4.1-4**) in the "two step" permeability approach, staining the TCO peptides with **Dye 1** and the azide with **dye 7**.
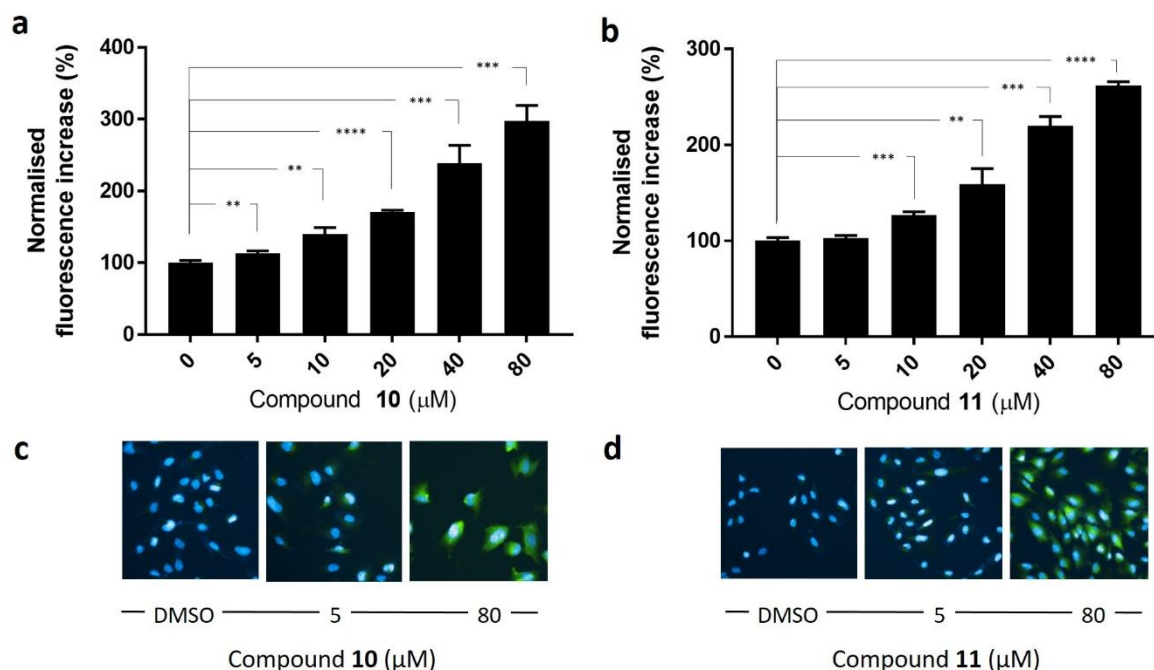
Figure 4.1-2 Peptides permeability assessment using the "two step" EID-DA approach. SJSA-1 cells were treated with the labelled peptides at five concentration ranging from 5 to 80 micromolar for 2h at 37°C and 5% CO_2. After fixing the cells with PFA solution, **dye 1** (1µM) was incubated for 1h at R.T. followed by Hoechst nuclear staining. Finally the cells imaging was performed. In (**a**) and (**b**) are the depicted the permeability assessment for compound **10** and **11**, respectively. Although, these peptides are derivative of the same parent compound **8,** a LOD of 5 µM was observed for **10** while **11** was detected only at 10 µM. Pictures in (**c**) and (**d**) are images of the cells treated with **10** and **11** at two concentrations, 5 and 80 µM or DMSO control, after performing the "two step" approach for permeability study.

While we could observe cellular permeability for **10** at 5 micromolar concentration, we could detect **11** only at 10 micromolar. These permeability data appeared to correlate well with the cellular activity profiles of the two peptides (**Figure 2.7-4b**, page 48). However, **10** and **11** did not show a significant nuclear induction of the PD marker in SJSA-1 cells at 5 and 10 micromolar, respectively. Therefore, we reasoned that **10** and **11** at their respective permeability LODs did not reach a sufficient target occupancy to trigger the pharmacodynamic effect.

On the contrary, peptide **12** and **14** appeared to be more cellular permeable (**Figure 4.1-3** and **4.1-4**). The TCO peptide (**12**) was detected at 500 nanomolar while the azide labelled peptide (**14**) showed permeability already at 50 nanomolar.

When comparing the cellular activity profile of **10** and **11** (**Figure 2.7-4b**, page 48) with the one of **12** (**Figure 2.7-4c** and **Table 2.7-2**, page 48), we could already expect a superior uptake of the latter, and this was clearly confirmed with the permeability assay.
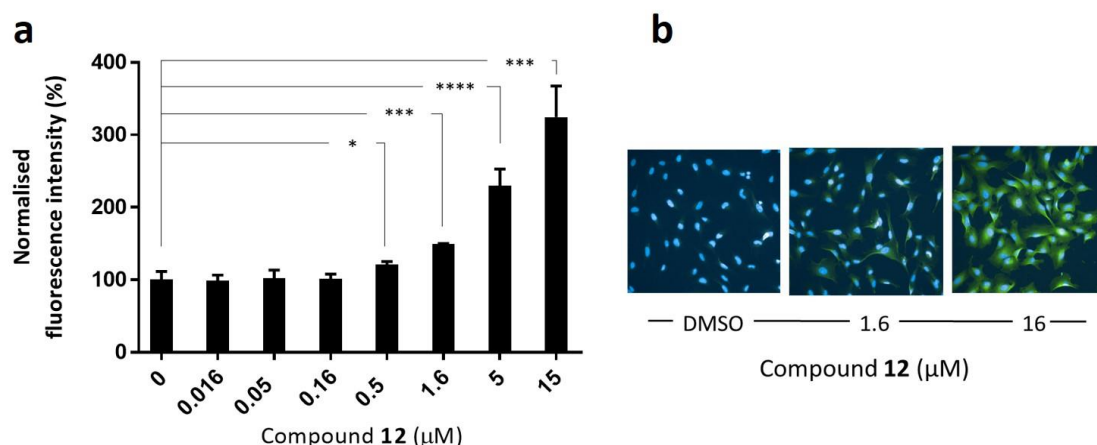
4.1-4 Peptide permeability assessment using the "two step" EID-DA approach. SJSA-1 cells were treated with compound **12** at seven concentration ranging from 0.016 to 80 micromolar for 2h at 37°C and 5% CO_2. After fixing the cells with PFA solution, **dye 1** (1 μM) was incubated for 1 h at R.T. followed by Hoechst nuclear staining. Finally the cells imaging was performed. (**a**) permeability graph for compound **12**. (**b**) images of the cells treated with **12** at two concentrations (1.6 and 16 μM) or DMSO control, after performing the "two step" approach for permeability study.
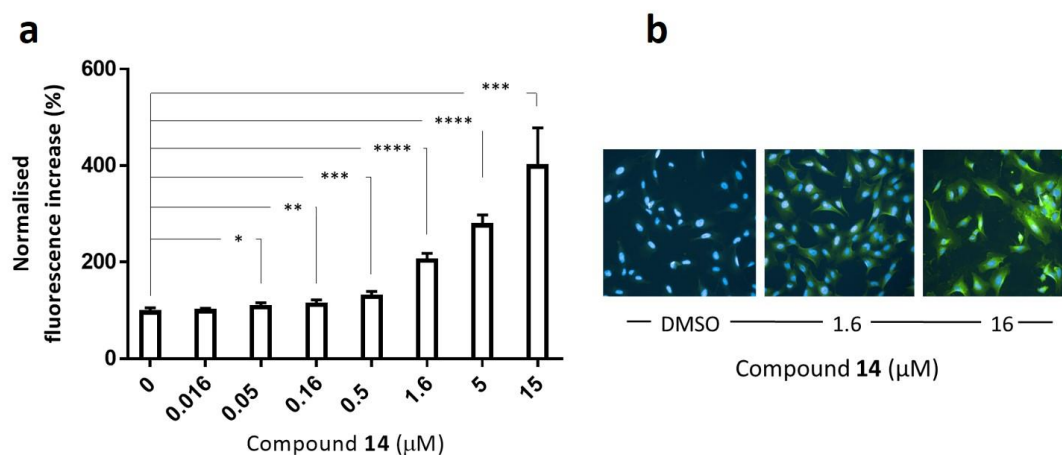
Figure 4.1-3 Peptide permeability assessment using the SPAAC reaction. SJSA-1 cells were treated with the azide labelled peptide, **14** at seven concentration ranging from 0.016 to 80 micromolar for 2 h at 37°C and 5% CO_2. After fixing the cells with PFA solution, **dye 6** (1 μM) was incubated for 1h at R.T. followed by Hoechst nuclear staining. Finally the cell imaging was performed. (**a**) permeability graph for compound **12**. (**b**) images of the cells treated with **12** at two concentrations (1.6 and 16 μM) or DMSO control, after performing the "two step" approach for permeability study.

In conclusion, the data generated with the "two step" permeability assay appeared to be well correlated with the compound cellular activities.

We reasoned that such an approach could be used for ranking compound permeability within a chemical series and to build structure-permeability relationships for compound optimization. However, this assay does not allow

determination of intracellular concentration and cellular uptake kinetics. Therefore, it would not allow more comprehensive investigations aiming to correlate compound cellular efficacy with permeability. The assessment of the compound intracellular concentration would be very important while investigating molecules for which cellular efficacy is not driven by their target occupancy. For instance, compounds with a catalytic mode of action (e.g. PROTACs) may exhibit high efficacy at extremely low intracellular concentrations which would require a more sensitive assay.[193]

Therefore, we tested if we could improve our assay sensitivity using a "three step" bioorthogonal approach.

4.2   A three step approach: an attempt for improving signal to background ratio

We reasoned that fluorescence background noise might be the limiting factor for assay sensitivity. Therefore, we tested if quenching the unreacted fluorophore inside the cells would decrease our LOD. This could be achieved with a "three step" approach (**Figure 4.2-1**), which is, to the best of our knowledge, unprecedented in the literature.

Figure 4.2-1 Schematic representation of the "three step" approach.

Step 1: cells are incubated with a molecule labelled with a bioorthogonal group. Step 2: cells are treated with a bioorthogonally reactive fluorophore, which reacts with the molecule of interest resulting in their staining. Step 3: A quencher molecule functionalized with a bioorthogonal group reactive with the fluorophore is applied to the cells. The quencher reacts with the free fluorophore leading to a decrease of the fluorescent background noise.

In the first step, the cells are treated with the bioorthogonal probe, which is then stained with the dye in the second step. In the last step, the cells are treated with a quencher functionalized with a bioorthogonal group enabling the irreversible "Click" reaction with the excess free fluorophore. We decided to test this approach using the SPAAC reaction because quenchers are available already functionalized with an azide group.

We reasoned that dark quenchers would be the best class of dyes for our purpose. This class of quencher dyes provides some clear advantages compared to more classical dyes used as quenchers such as TAMRA. First of all, being dark, they should not increase the overall fluorescent background noise, while using a dye with native fluorescence we will likely encounter this issue. Secondly, a good selection of available dark quenchers allows flexibility in the choice of the most suitable one based on the required fluorescent spectral profile for the specific application.

To apply this approach to the developed SPAAC reactions, we had to identify dark quenchers able to quench **dye 6** or **7**. The class named Black Hole Quenchers (BHQ) meet this criterion.

We investigated the quenching of **Dye 7** using the commercially available BHQ-1 azide (**Figure 4.2-2**). This Black Hole Quencher with an absorption maximum of 534 nm should perfectly be able to quench the fluorescent signal of **dye 7**. First, we confirmed that BHQ-1 azide underwent through SPAAC with **dye 7** by reacting the two molecules
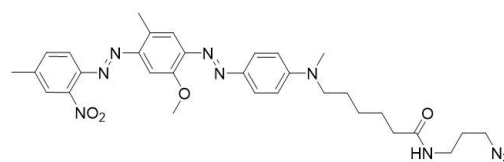
Figure 4.2-2 BHQ-1 azide

in PBS and analyzing the reaction with LC-MS. Subsequently, we investigated if there was an effective quenching of **dye 7** using BHQ-1 azide. Hence, to a PBS solution containing **dye 7** BHQ-1 azide or DMSO in equimolar concentration was added and the reaction was placed in a fluorescence spectrophotometer for a one hour reading (**Figure 4.2-3A**). In parallel, to test if the quenching was due to the "Click" cycloaddition and not to intermolecular interaction between the dyes in solution, we prepared a solution of PBS containing **dye 9** (**Figure 3.3-8**) and to this we added BHQ-1 azide and we read the fluorescence signal over one hour (**Figure 4.2-3B**). **Dye 9** is lacking the bioorthogonal group for reacting with the azide, therefore we should not observed quenching due to the conjugation of the dyes.
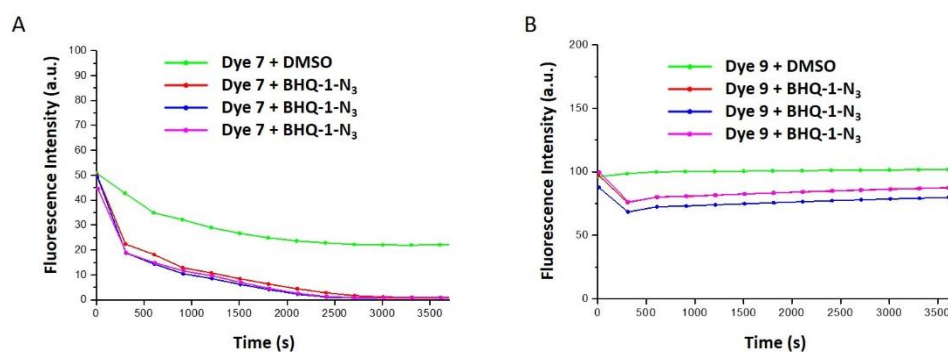
Figure 4.2-3 Testing the bioorthogonal cycloaddition between **dye 7** and BHQ-1 azide induced fluorophore quenching. (A) To a solution of **dye 7** in PBS (3µM) was added BHQ-1 azide in equimolar concentration or DMSO. (**B**) To a solution of **dye 9** in PBS (3µM) was added BHQ-1 azide in equimolar concentration or DMSO. The reactions were placed in a fluorescence spectrophotometer and reading was performed every 5 min for 1 hour. (Ex wavelength = 490nm and Em wavelength = 510 nm).

BHQ-1 azide appeared to efficiently quench the fluorescent signal of **dye 7** (100 % signal reduction), despite a decrease in fluorescent signal over time also being observed in the sample containing **dye 7** and DMSO control (50% signal reduction) (**Figure 4.2-3A**). This intensity decrease might suggest a dye precipitation under the experimental conditions. On the contrary, only about 20% signal reduction was observed in the samples containing **dye 9** and the BHQ-1 azide, while for the sample containing **dye 9** and the DMSO control a stable fluorescent signal was observed overtime (**Figure 4.2-3B**). These data appeared to confirm that the bioorthogonal reaction brings the dyes to the right distance for observing a FRET effect.

Next, we decided to investigate if we could observe a quenching effect in a cellular system. Therefore, SJSA-1 cell were treated with **dye-7** at 1 micromolar concentration for 2 hours. After fixing the cells, BHQ-1 azide was applied in doses ranging from 16 nanomolar to 15 micromolar. The quenching reaction was run for 2h before fluorescence imaging was performed (**Figure 4.2-4**).
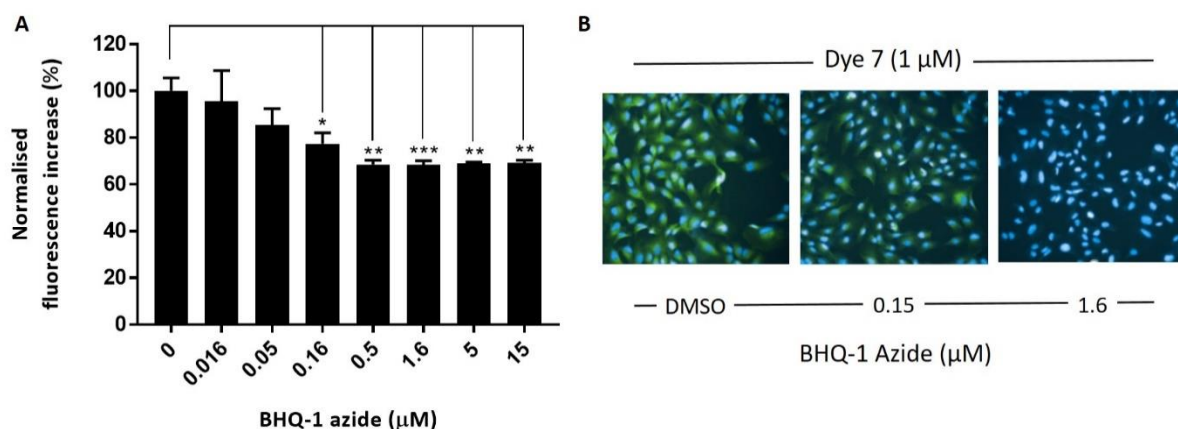
Figure 4.2-4 Intracellular quenching of dye 7 with BHQ-1 azide. SJSA-1 cells were treated with **dye 7** for 2h at 37°C and 5% CO_2. Next cells were fixed with PFA and after washing, increasing concentrations of BHQ-1 azide were applied (ranging from 16 nM to 15 μM). (**A**) A dose-dependent fluorescence decrease was observed starting plateauing at 500 nM. (**B**) Cell imaging showed clearly a decrease in fluorescence. BODIPY fluorescence (green) and nuclear staining with Hoechst dye (blue).

We observed a dose-dependent fluorescence quenching which reached a plateau at 0.5 micromolar of BHQ-1 azide treatment. However, with 30 percent of maximal fluorescence reduction this effect was clearly not as strong as expected. We then engaged in testing the "three step" approach. Thus, SJSA-1 cells were incubated with compound **7** at five concentrations ranging from 0 to 20 micromolar for 1 hour at 37 °C and 5% CO_2. After fixing the cells, we stained compound **7** with **dye 7** using the previously established fixed cells protocol. Next, we applied BHQ-1 azide at 10 micromolar concentration to the cells, and we let the quenching reaction proceed for 2 hours before imaging.
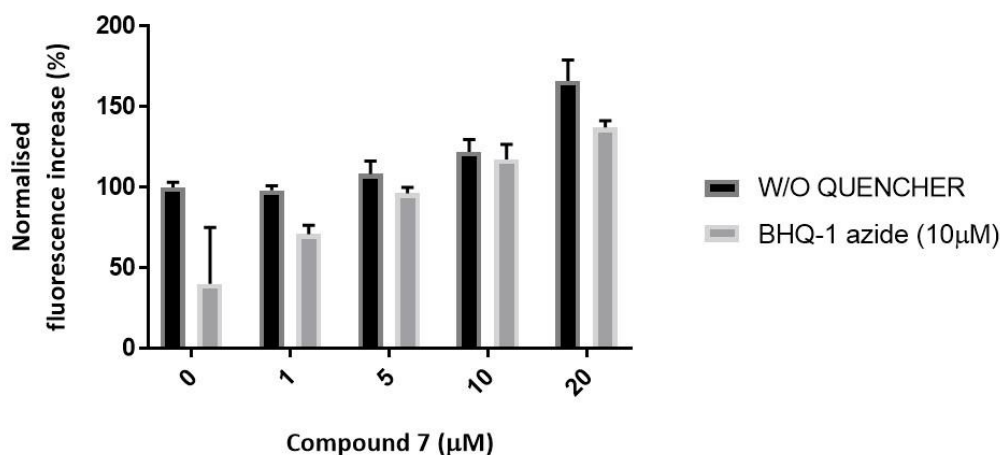
Figure 4.2-5 validation of the "three step" approach using the bioorthogonal probe (**7**), **dye 7** and BHQ-1 azide on SJSA-1 cell. SJSA-1 cells were treated with (**7**) at five concentrations ranging from 1 to 20 μM. The bioorthogonal probe staining were performed using the fixed cell protocol applying dye 7 at 1 μM concentration. Finally, the quencher, BHQ-1 azide was applied to the cells (10 μM). The imaging was performed after nuclear staining with Hoechst dye.

As depicted in **figure 4.2-5**, a dose-dependent increase in fluorescence was observed, and also the quencher appeared to reduce the fluorescence background, although, the error bar was large at the zero compound **7** concentration point. Nevertheless, we decided to further investigate if this approach could have enabled a permeability assessment of the

bioorthogonal probe with a lower LOD, so we repeated the experiment treating the cells with eight concentration of (**7**) (**Figure 4.2-6**).
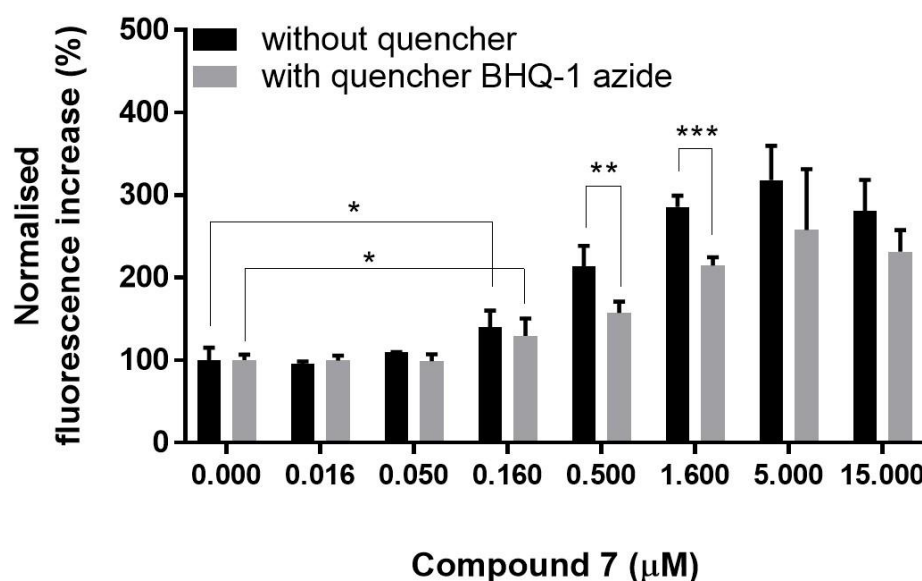
Figure 4.2-6 Testing the effect of quencher, BHQ-1 azide, on the cellular permeability assessment for the bioorthogonal probe (**7**). SJSA-1 cells were treated with (**7**) at eight concentrations ranging from 0 to 15 µM. The bioorthogonal probe staining was performed using the fixed cell protocol applying **dye 7** at 1 µM concentration. Finally, the quencher, BHQ-1 azide was applied to the cells (10 µM). The imaging was performed after nuclear staining with Hoechst dye.

With disappointment, we observed that a significant quenching effect was only noteworthy at concentration of bioorthogonal probe **7** equal to or higher than 500 nanomolar. Furthermore, the cellular uptake LOD for (**7**) did not change**.** Finally, we noticed that at higher compound concentrations, the variability of the quenching effect was increasing. Further experiments, not here reported here, were run aiming at improving this approach (e.g. use of **dye 6** and BHQ-2 azide, assessing the best concentration ratio of dye to quencher etc.), however all of them showed high variability and consequently poor reproducibility; therefore this approach was abandoned.

4.3　Mdm2-p53 PPI inhibitor chemical probes intracellular concentration using BLI

Having already tested two approaches to measure cellular up-take of compounds using fluorescence imaging (the "two step" and the "three step" bioorthogonal approaches) we concluded that a more sensitive quantification of cellular up-take was difficult to achieve due to fluorescence background noise.

To overcome this issue we devised a bioluminescence assay based on a bioorthogonal chemistry approach. Bioluminescence imaging (BLI) offers as advantage over fluorescence imaging in that it is almost free of background noise.

For that reason, BLI is more sensitive than fluorescent imaging. The main principle behind this technology is that D-Luciferin, a substrate of firefly luciferase, can be oxidized by this enzyme to oxiluciferin (**Figure 4.3-1**). This molecule is in an excited energy state and emits yellow-green light when falling back to its ground state. The number of photons

released by oxiluciferin is consequently equal to the number of molecules of D-Luciferin undergoing the oxidation reaction. Finally, the number of photons released can be detected by optical systems (e.g. plate reader, charge-coupled device cameras).
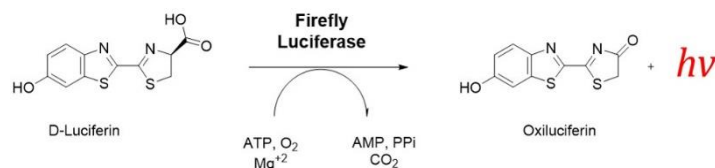
Figure 4.3-1 Bioluminescence imaging principle. D-luciferin is catalytically oxidized by Firefly luciferase to oxiluciferin releasing light.

Mc Elroy investigated the D-Luciferin scaffold binding mode onto the firefly luciferase enzyme and built SAR around this interesting molecule by screening several D-luciferin analogues.[194,195] These pioneering studies opened up new avenues leading to a broad application of this chemotype in BLI. The developed SAR highlighted the importance of electron-donating substituent at the 6'-position of the D-luciferin scaffold; this substitution is required for light emission. For instance, 6'-hydroxy-D-luciferin alkylated or acylated analogues did not produce light, although it also binds to Firefly Luciferase.[194] In a similar way, the acylation of the 6'-amino-D-luciferin resulted in analogues with insignificant bioluminescence emission.[195]

To date, caged-Luciferin BLI approaches have been applied to intracellular concentration and cellular uptake studies (e.g. studies applied to metabolites, peptides, small molecules)[70,196-198] and enzymatic activity investigations (e.g. caspase protease activity)[199]. These approaches have been developed using three different strategies, all of them leading to release or formation of free luciferin (**Figure 4.3-2**).
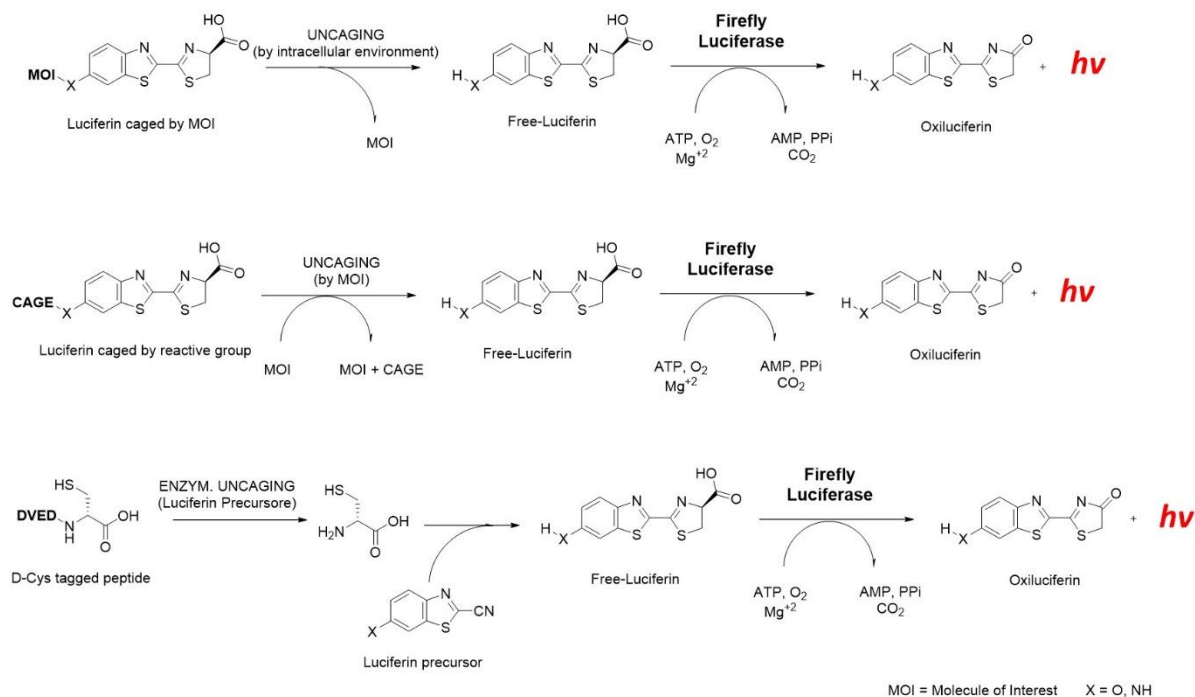
Figure 4.3-2 The three main strategies applied to caged Luciferin BLI approaches

The first strategy involves caging a Luciferin by its conjugation to the molecule of interest. The conjugate is not recognized by the enzyme, which is consequently unable to catalyze the oxidation reaction. Upon uptake of the conjugate by Firefly Luciferase expressing cells, endogenous molecules (e.g. glutathione, GSH) or the intracellular environment (e.g. intracellular pH) trigger the Luciferin de-caging leading to the bioluminescence signal.[197,198] The second strategy is based on the ability of a molecule to trigger Luciferin de-caging. This is usually achieved by redox cleavage of the caging[200] or, as recently reported by our group at EPFL, by bioorthogonal reactions such as Staudinger ligation[201]. The final strategy is based on the intracellular formation of D-Luciferin by conjugating a protease substrate with a Luciferin precursor able to be released inside the cell, which forms D-Luciferin upon reaction with a second Luciferin precursor.[199]

4.3.1. Investigation of the bioorthogonal de-caging *in vitro*

In order to develop the cellular up-take assays, we decided to investigate two published bioorthogonal de-protection reactions. We reasoned that these reactions could be used for de-protecting a masked reporter such as a caged luciferin leading to a detectable signal; similar to the second strategy reported above.

The first reaction we planned to investigate was the EID-DA between a TCO containing a carbamate at the allylic position ((*E*)-Cyclooct-2-enolyl carbamate) and a tetrazine which leads to carbamate elimination after cyclization (**Figure 4.3-3**).[202] This reaction was reported for the first time in 2013 by Robillard et al.[202] In their publication, the authors proposed the reaction mechanism (**Figure 4.3-3**) and they studied the reaction kinetics and proved the reaction principle using LC-MS and NMR techniques. Finally, they successfully applied this "Click" elimination approach to the de-protection of a Doxorubicin TCO* conjugated prodrug in a proof of concept cellular study.[202]
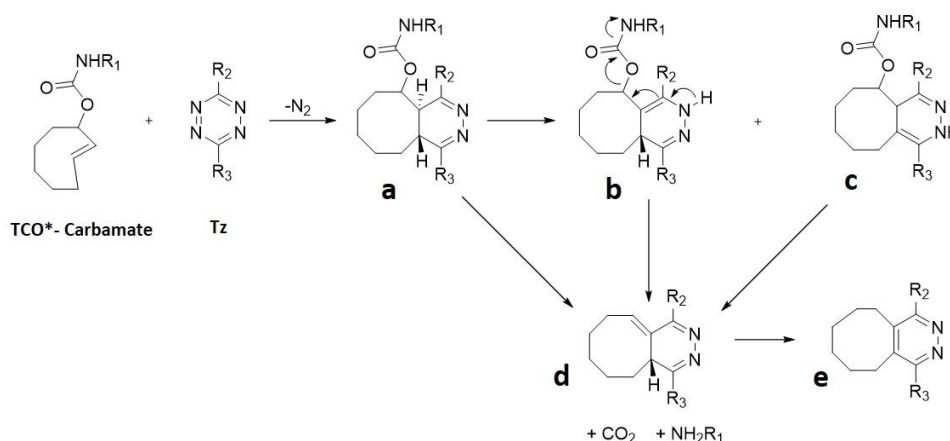
Figure 4.3-3 Mechanism of reaction for EID-DA between a TCO functionalized at the allylic position with a carbamate (TCO*-Carbamate) and a Tetrazine (Tz) proposed by Robillard. The cyclization leads to the formation of a bicyclic intermediate (**a**) which quickly isomerizes to the I,4 tautomer (**b**). This tautomer undergoes 1,4-elimination releasing CO_2 and an amine to afford (**d**). Subsequently (**d**) undergoes isomerization to (**e**). The authors did not exclude the possibility that (**d**) could be formed by decarboxylation of (**a**) or (**c**). Herein, we indicate for simplicity the (*E*)-cyclooct-2-en-1-ol as TCO* (adapted from *R. M. Versteegen et al., Angew. Chemie. Int. Ed. 2013, 52, 14112 - 14116*).

We reasoned that this interesting N-monosubstituted carbamate ester masking group could enable the caging of an amino-luciferin. Hence, we decide to prepare two caged amino-luciferins functionalized with the (*E*)-cyclooct-2-en-1-ol, compound **20** and **21** (**Figure 4.3-4**).

Compound 20   Compound 21
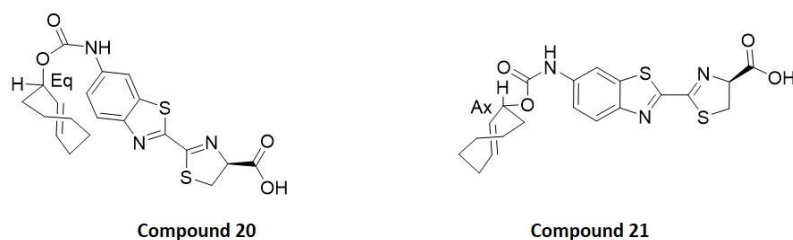
Figure 4.3-4 Structure of Compound **20** and **21**.

This approach would require the labelling of our probes or peptides with a tetrazine moiety. Before engaging in the tetrazine probe labelling, we decided to investigate first the reaction between the caged luciferins and some simple tetrazines.

The synthesis of compounds **20** and **21** was achieved using a five step synthetic route starting from (Z)-cyclooctene and yielded the desired molecules as racemic mixtures (**Figure 4.3-5**). The chemistry involved the allylic bromination of the starting material using NBS followed by hydrolysis of the allyl bromide to afford the (Z)-cyclooct-2-en-1-ol. The cis-cyclooctene was subjected to photo-irradiation in flow and the mixture of trans-diastereoisomers was trapped by pumping the solution through a AgNO$_3$ column as described by Royzen.[202,203]
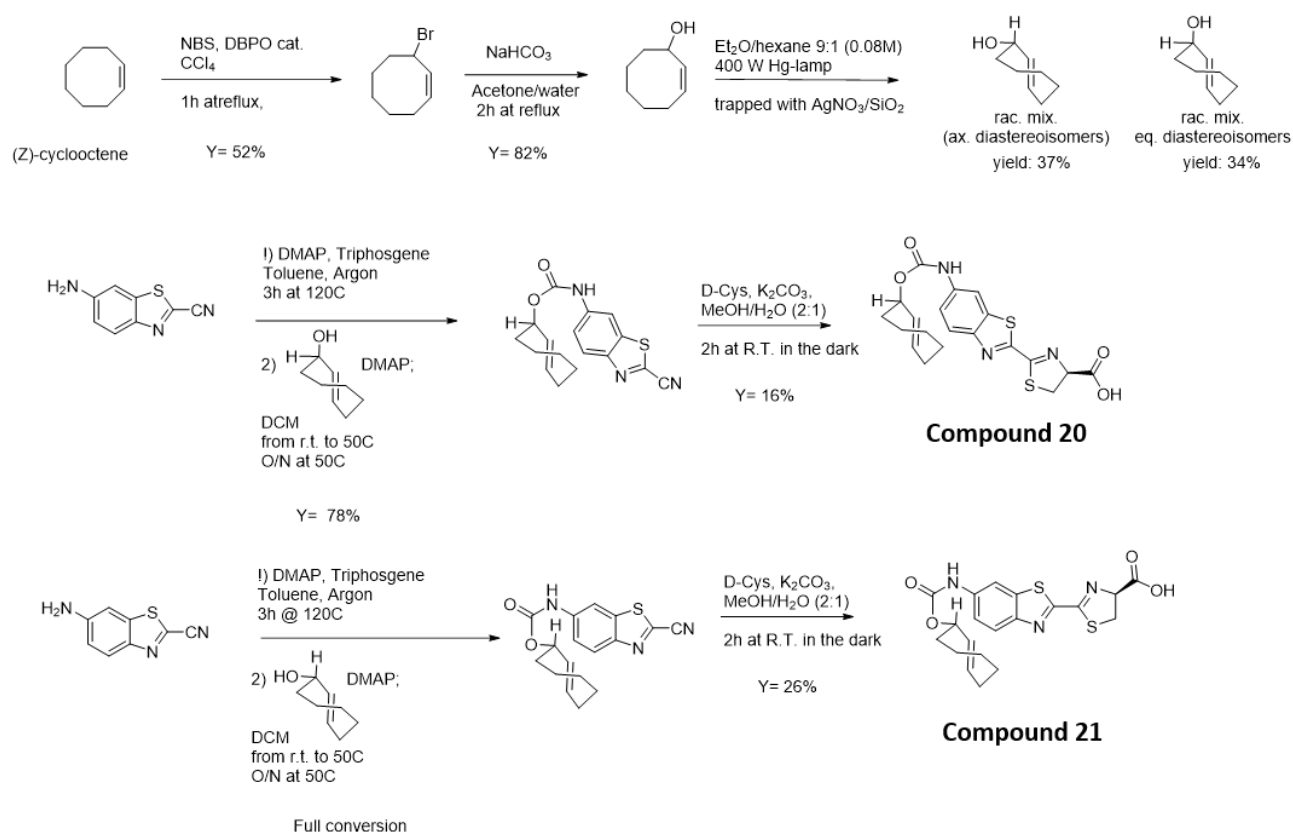
Figure 4.3-5 Synthetic routes for the synthesis of compounds **20** and **21**.

The racemic mixtures of equatorial and axial diastereoisomers were separated and then engaged in the carbamate formation with 6-aminobenzo[d]thiazole-2-carbonitrile to obtain the cyano derivatives. Finally, these compounds were reacted with D-Cysteine to obtain the final compounds, **20** and **21**.

Planning to develop this technology to investigate not only LMW molecules but also peptides, we opted to test the reaction between compounds **20** and **21** with a previously reported tetrazine protected amino acid, compound **22** (**Figure 4.3-6**).[204] This would allow us to easily introduce the tetrazine functionality into the peptides using conventional peptide chemistry. This amino acid was synthesized in a three step linear synthesis starting from thiocarbonyldihydrazide (**Figure 4.3-6**).
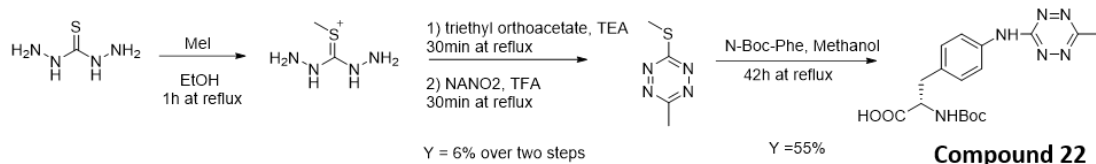
Figure 4.3-6 Synthesis of compound **22**.

Despite the two initial synthetic steps being quite low yielding, there was no need to further optimize the chemistry due to the low cost and consequently easy availability of the starting material.

Next, we tested the reaction between the caged luciferins, compound **20** and **21**, with compound **22** in PBS, analyzing the results over time with LC-MS. The reaction should proceed with the formation of the EID-DA cycloadducts (**Figure 4.3-7A,** one of the possible DA cycloadduct, product (**c**)) which should undergo through 1,4-elimination to release the un-caged amino-luciferin (**Figure 4.3-7A** as (**a**)) and the aromatic fused bycicle pyridazines (**Figure 4.3-7A,** (**b**) one of the possible DA cycloaddition products). The reaction analyses run just after the addition of the last reagent, after 2 hours
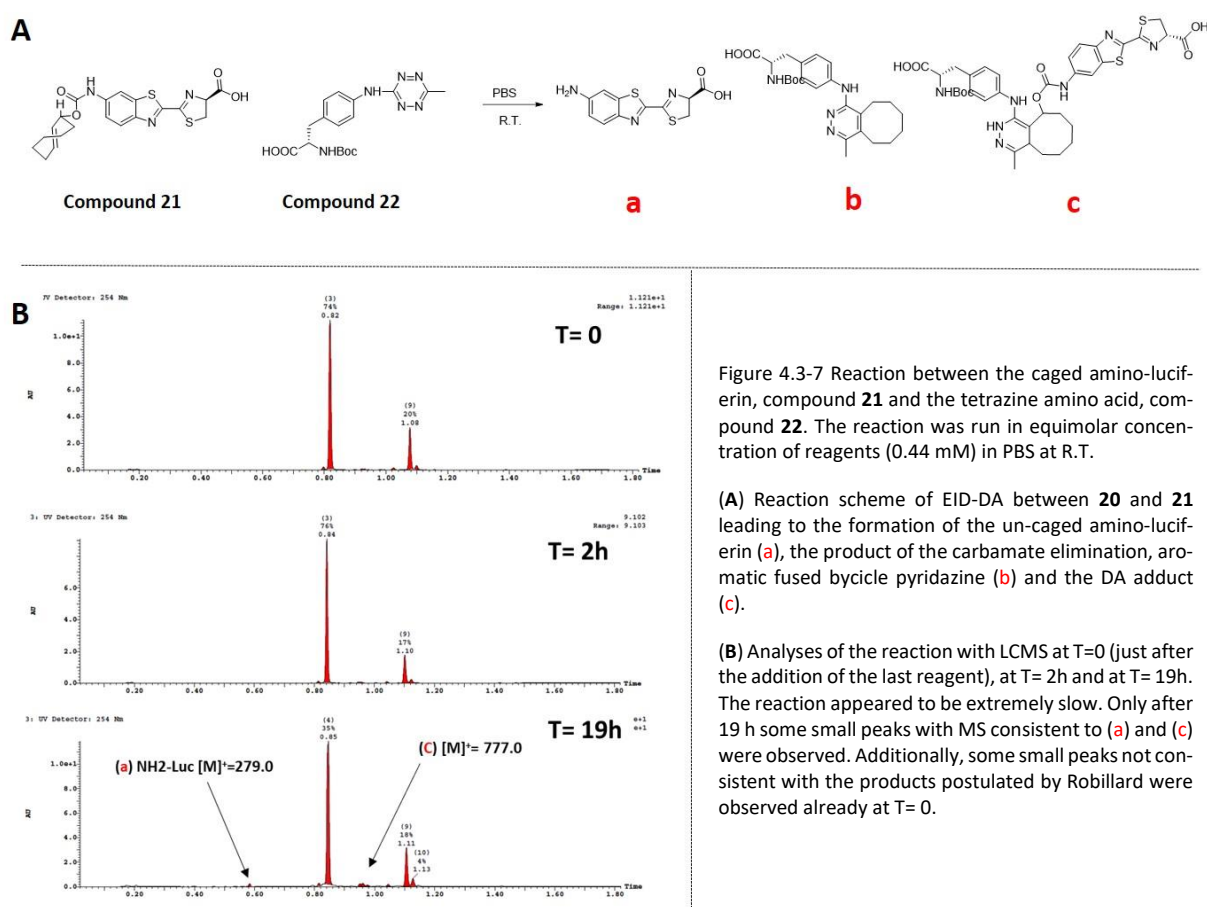
Figure 4.3-7 Reaction between the caged amino-luciferin, compound **21** and the tetrazine amino acid, compound **22**. The reaction was run in equimolar concentration of reagents (0.44 mM) in PBS at R.T.

(**A**) Reaction scheme of EID-DA between **20** and **21** leading to the formation of the un-caged amino-luciferin (a), the product of the carbamate elimination, aromatic fused bycicle pyridazine (b) and the DA adduct (c).

(**B**) Analyses of the reaction with LCMS at T=0 (just after the addition of the last reagent), at T= 2h and at T= 19h. The reaction appeared to be extremely slow. Only after 19 h some small peaks with MS consistent to (a) and (c) were observed. Additionally, some small peaks not consistent with the products postulated by Robillard were observed already at T= 0.

and after 19 hours showed that, the reaction was extremely slow (**Figure 4.3-7B**). Only small peaks with MS and retention time consistent with the amino-luciferin and the DA cycloadduct were detected after 19 hours.

Disappointed by these results, we decided to investigate if the reaction between compound **21** and a more reactive tetrazine, the 3,6-di(pyridin-2-yl)-1,2,4,5-tetrazine, compound **23** (**Figure 4.3-8A**),[205] would enable a more efficient and fast un-caging.

Hence, we reacted compound **21** and **23** in PBS following the reaction progression with LC-MS (**Figure 4.3-8B**). The analysis of the reaction after the addition of the last reagent showed already a small peak consistent by MS and retention time with the un-caged amino-luciferin, also several peaks with MS consistent with the DA cycloaddition adducts were observed (**Figure 4.3-8B**). However, analyzing the reaction after 2h, we did not observed a great improvement in terms of further conversion and reduction of reaction intermediates. Furthermore, the reactions between compound **20** and the tetrazine derivatives (**22**) and (**23**) gave very similar outcomes.

These results were quite discouraging and while we were considering further investigation of the reaction kinetics, we decided instead to investigate a second bioorthogonal reaction. This was a recently published bioorthogonal de-protection based on a 1,3-dipolar click cycloaddition between TCO and an aromatic azide moiety. This cycloaddition reaction has been previously used for prodrug de-protection by Matikonda et al.[120]
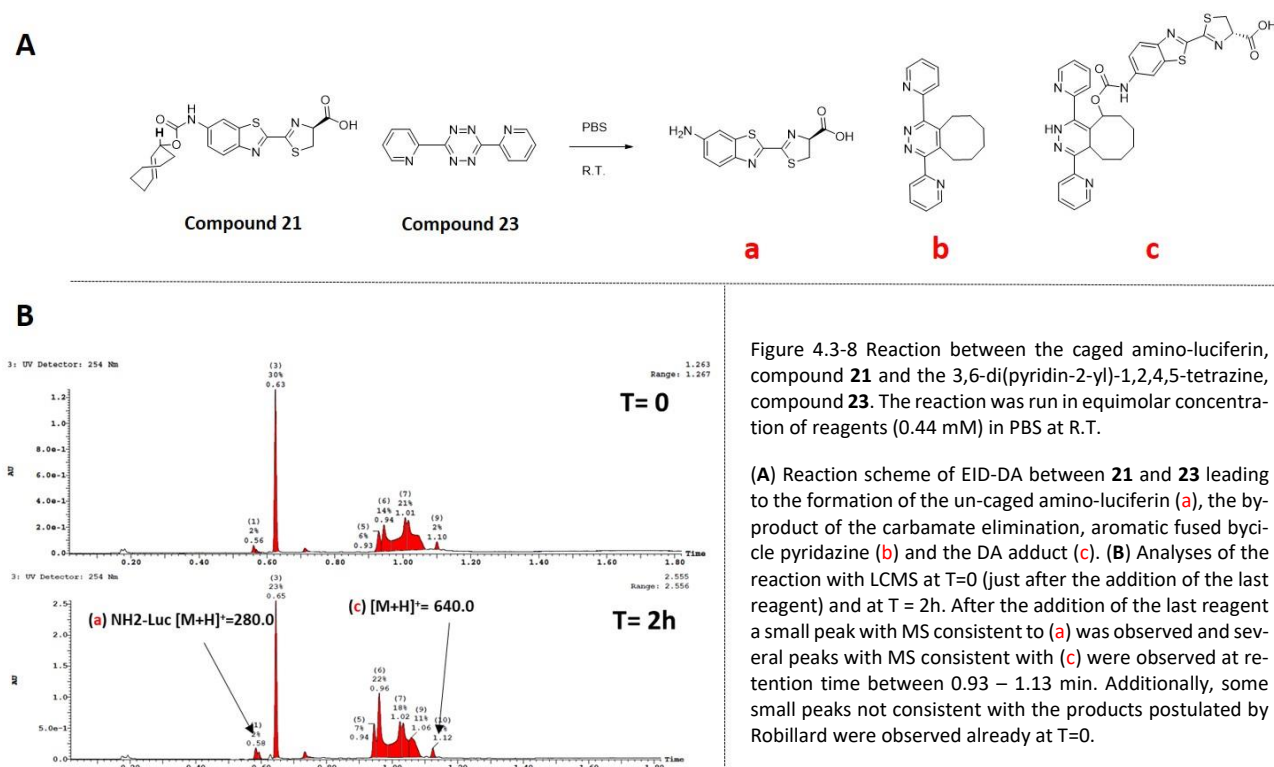
Figure 4.3-8 Reaction between the caged amino-luciferin, compound **21** and the 3,6-di(pyridin-2-yl)-1,2,4,5-tetrazine, compound **23**. The reaction was run in equimolar concentration of reagents (0.44 mM) in PBS at R.T.

(**A**) Reaction scheme of EID-DA between **21** and **23** leading to the formation of the un-caged amino-luciferin (a), the by-product of the carbamate elimination, aromatic fused byci-cle pyridazine (b) and the DA adduct (c). (**B**) Analyses of the reaction with LCMS at T=0 (just after the addition of the last reagent) and at T = 2h. After the addition of the last reagent a small peak with MS consistent to (a) was observed and sev-eral peaks with MS consistent with (c) were observed at re-tention time between 0.93 − 1.13 min. Additionally, some small peaks not consistent with the products postulated by Robillard were observed already at T=0.

The reaction mechanism of this cycloaddition was first studied by Shea in 1992.[206] He reported that the reaction between TCO and picryl azide (2,4,6-trinitrophenylazide) in organic solvent resulted in the formation of three products arising from the decomposition of an unstable intermediate triazoline (**Figure 4.3-9**).
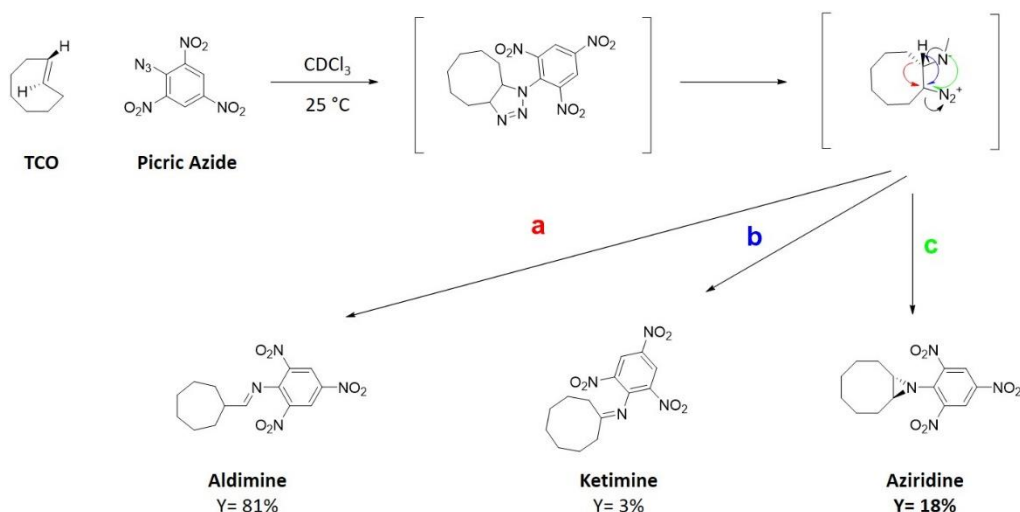
Figure 4.3-9 Mechanism of triazoline degradation upon diatomic nitrogen release suggested by Shea
(adapted from *Shea, K.J. et al. Journal of the American Chemical Society **114**, 4846-4855 (1992)*).

Matikonda applied this reaction to the de-protection of a *p*-azidobenzyloxycarbonyl linker quenched coumarin in PBS and subsequently for the de-protection of a Doxorubicin prodrug in cells.

Consequently, we hypothesized that this de-protection reaction would enable a combination of the "two step" fluorescent imaging approach for functional pharmacology studies with the intracellular quantification of the chemical probe labelled with the bioorthogonal group TCO. Therefore, the use of a common bioorthogonal moiety as a labelling of our chemical probes would have provided an appealing complementarity of the two technologies allowing a stronger process for the validation of bioorthogonal probes in cellular disease model.

As reported by Matikonda applying Shea findings, the 1,3-dipolar cycloaddition of trans-cyclooctenes and aromatic azides yields a triazoline intermediate unstable under aqueous conditions. The intermediate undergoes through a rearrangement in which diatomic nitrogen, a cycloheptane aldehyde and an electron-deficient self-eliminating linker (paraminobenzyloxycarbonyl, PABC) are formed (**Figure 4.3-10**).
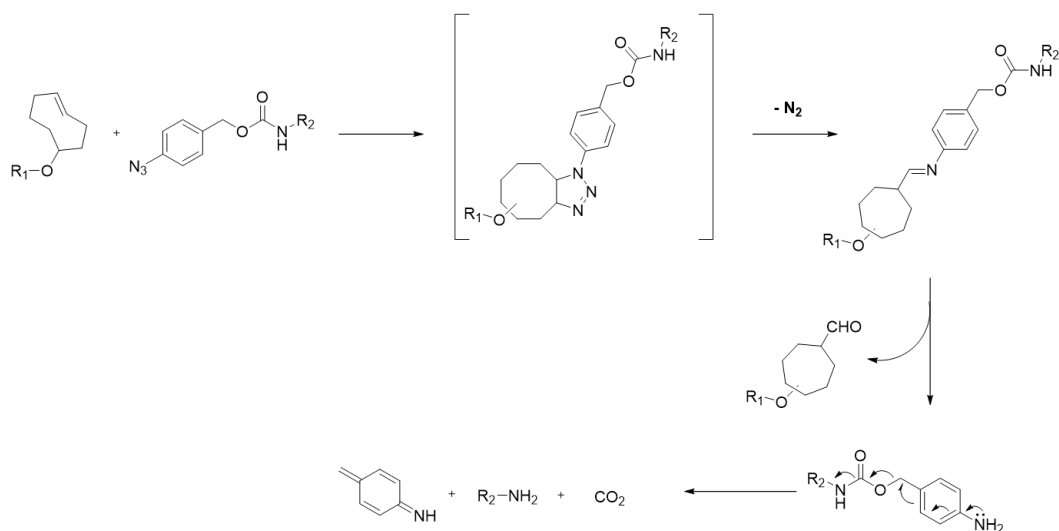
Figure 4.3-10 De-protection of the 4-benzyloxycarbonyl azide group triggered with TCO. (Figure adapted *from Chemical Science **6**, 1212-1218 (2015)*)

Aiming at investigating this de-protection reaction, we synthesized a 6'-amino-D-luciferin N-protected with the 4-azidobenzyloxycarbonyl group, compound **24**. This compound was synthesized in four synthetic steps starting from the commercially available 6-aminobenzo[d]thiazole-2-carbonitrile and (4-aminophenyl)methanol with an overall yield of 20% (**Figure 4.3-11**).
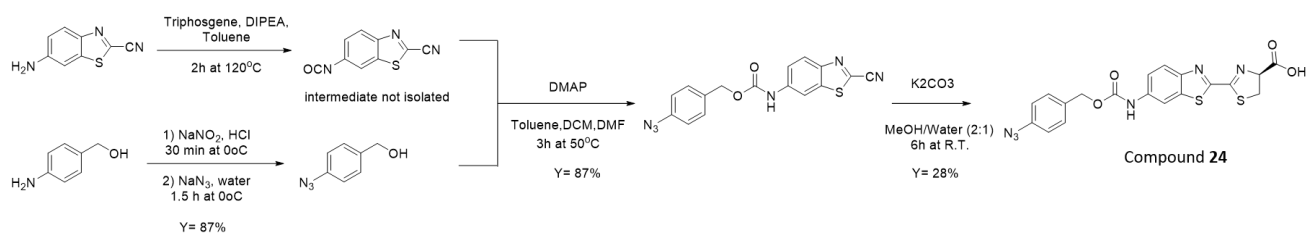
Figure 4.3-11 Synthetic route for the preparation of the caged luciferin, compound **24**.

Next, we tested the reaction between the newly synthesized caged luciferin (**24**) and (*E*)-cyclooct-4-en-1-ol (TCO) in PBS at R.T. analyzing the reactions with LC-MS immediately after the addition of the last reagent (TCO) and after 24h (**Figure 4.3-12A**).
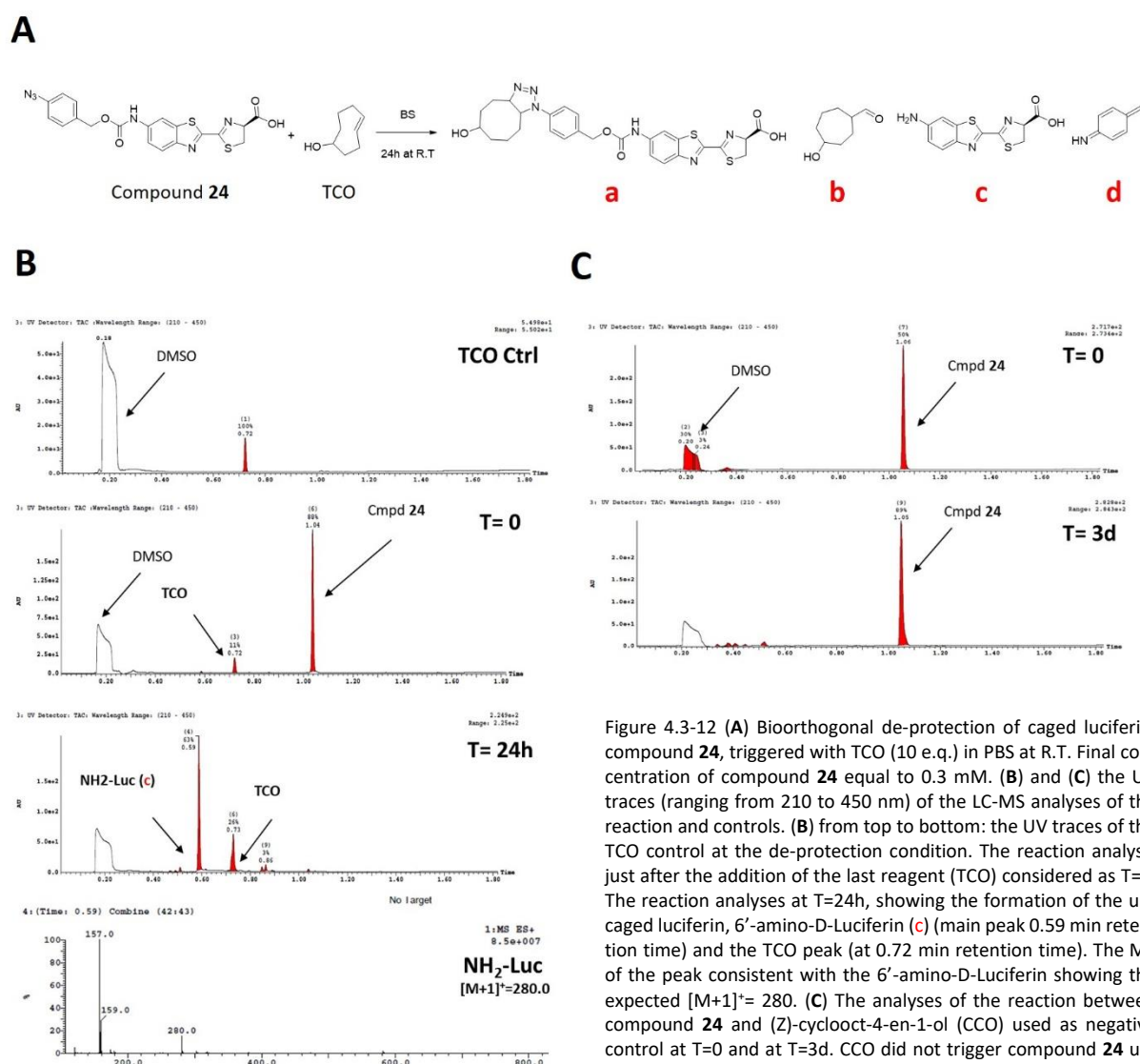
Figure 4.3-12 (**A**) Bioorthogonal de-protection of caged luciferin, compound **24**, triggered with TCO (10 e.q.) in PBS at R.T. Final concentration of compound **24** equal to 0.3 mM. (**B**) and (**C**) the UV traces (ranging from 210 to 450 nm) of the LC-MS analyses of the reaction and controls. (**B**) from top to bottom: the UV traces of the TCO control at the de-protection condition. The reaction analysis just after the addition of the last reagent (TCO) considered as T=0. The reaction analyses at T=24h, showing the formation of the uncaged luciferin, 6'-amino-D-Luciferin (c) (main peak 0.59 min retention time) and the TCO peak (at 0.72 min retention time). The MS of the peak consistent with the 6'-amino-D-Luciferin showing the expected [M+1]+= 280. (**C**) The analyses of the reaction between compound **24** and (Z)-cyclooct-4-en-1-ol (CCO) used as negative control at T=0 and at T=3d. CCO did not trigger compound **24** uncaging even after 3 days.

After 24h, a clear de-protection of the caged luciferin with formation of the expected 6-amino-D-Luciferin was observed (compound (c) in **Figure 4.3-12A**). No cyclo-addition adduct was observed (compound (a) in **Figure 4.3-12A**). Finally, the UV trace of the analysis showed also some small peaks with MS not consistent with the expected reaction products. We reasoned that these traces might arise from reactions of the highly reactive electrophilic products formed ((b) and (d) in **Figure 4.3-12A**).

Finally, to confirm that compound **24** was de-protected chemo-selectively by TCO, we ran the reaction between (**24**) and (Z)-cyclooct-4-en-1-ol (Cis-Cyclooctene, CCO) as a negative control using the same reaction conditions and analyzing the reaction with LC-MS. No de-caging reaction was observed even analyzing the reaction after 3 days (**Figure 4.3-12c**) which confirmed that only the *trans* isomer reacts with the azide moiety triggering the de-caging. Additionally, the luciferin reporter (**24**) appeared to be stable in PBS at R.T. for a reasonable amount of time.

Next, we investigated the bioorthogonal de-protection reaction in a biochemical setting. Hence, compound **24** was diluted in Tris-buffer before addition of TCO at either equimolar concentration or in a 10 fold excess. The reactions were run at R.T. up to 48 hours sampling 3 microliters of reaction mixture at different time points. The reaction samples were added to a Firefly Luciferase cocktail and the emitted luminescence was read using a plate reader. The obtained data were compared to a 6-amino-D-Luciferin (compound **25**) standard curve (**Figure 4.3-13A**) in order to extrapolate the amount of amino-Luciferin produced by the reaction (**Figure 4.3-13B**).
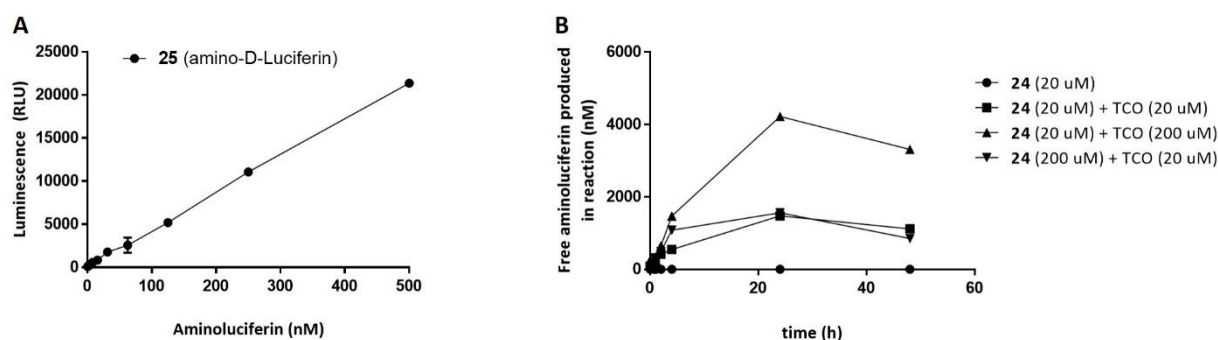
Figure 4.3-13 (**A**) standard curve of luminescence signal (Relative Luminescence Unit, RLU) generated using increasing concentration of (**25**) (amino-D-Luciferin) in Tris-Buffer. (**B**) Amino-Luciferin produced over time by reacting (**24**) with TCO equimolar (20 μM) or in 10 fold excess (200 μM) in Tris-Buffer.

The initial results of the biochemical experiment were encouraging; TCO enabled the de-caging of **24**, producing the expected luminescence signal over time (**Figure 4.3-13B**). However, we reasoned that the assay required further optimization to improve sensitivity; at the lowest concentrations (less than 100 nanomolar), we did not observe a linear correlation between (**25**) concentration and Luminescence signal (as depicted in the standard curve graph, **Figure 4.3-14A**). After optimizing the assay (e.g. use of Quantilum® recombinant Luciferase instead of Firefly Luciferase, modifying the enzyme concentration and addition of bovine serum albumin (BSA) and Tween-20 (detergent) to the Tris-Buffer), we re-ran our assay validation by reacting increasing concentrations of (**24**) with a fixed concentration of TCO (or CCO as a negative control) and reading luminescence at 24 hours (**Figure 4.3-14**). As depicted in **figure 4.3-14A** and **4.3-14C**, the assay optimization allowed a more sensitive detection of the aminoluciferin (reduction of standard curve LOD from 100 nanomolar to 100 picomolar) which consequently enabled a more sensitive assessment of the de-caging reaction. For instance, the profile of the de-caging reaction after assay optimization displayed the expected plateauing effect

(signal saturation) not observed before (**Figure 4.3-14D** and **4.3-14B** respectively). As depicted in Figure 4.3-14D, TCO at 20 micromolar concentration when reacted with an equal concentration of (**24**) for 24h released 700 nanomolar of free aminoluciferin. Finally, CCO did not induced de-caging of **24**.
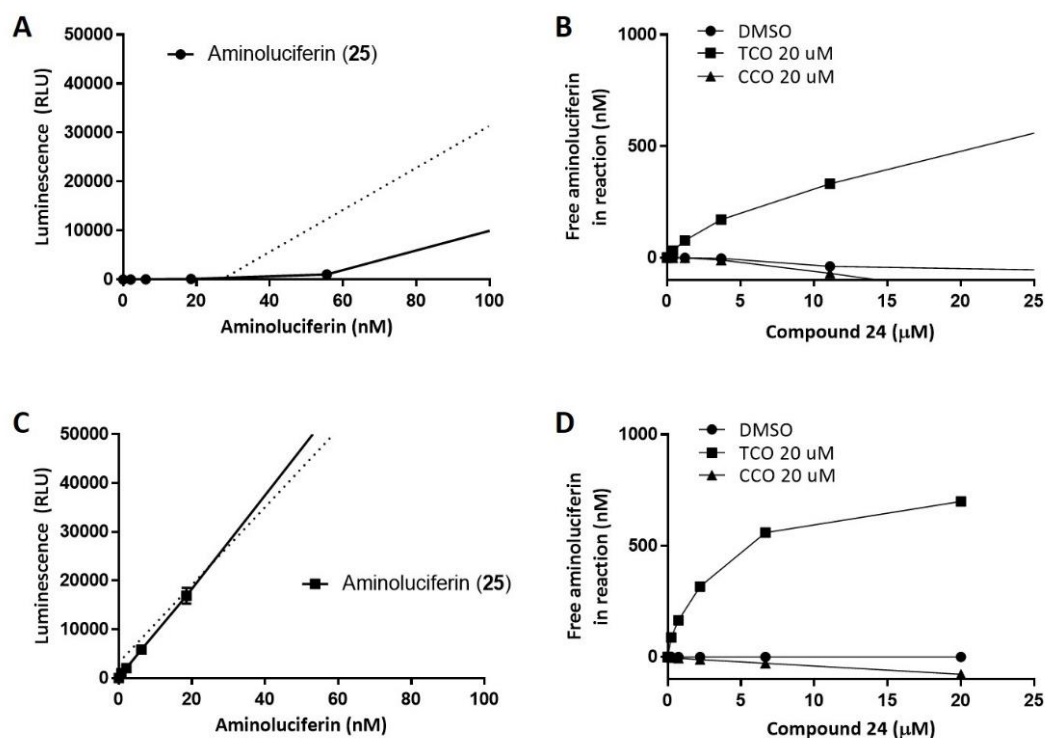
Figure 4.3-14 Comparison of Luciferin assay for measuring de-caging of compound **24** triggered by TCO in Tri-Buffer before (**A** and **B**) and after (**C** and **D**) optimization of conditions. A lower LOD was observed for the standard curve after assay optimization (**A** and **C** respectively). The de-caging reaction showed the expecting plateauing when reaching saturation (**D**) while this effect was not observed before optimization (**B**). As expected CCO did not trigger de-caging of **24**.

4.3.2. Testing the de-caging of luciferin analogues with the Mdm2-p53 bioorthogonal probe

Aiming at finding a caged luciferin reporter enabling fast reaction kinetics, a small library of azidobenzyloxycarbonyl amino-luciferin carbamate was synthesized (compounds **26**-**30**, **Figure 4.3-15**). The azido phenyl moiety was functionalized by introducing halogens *meta* to the azide group (**26**-**28**), replacing the phenyl ring with a pyridine to afford a 3-azido-pyridinyl group (**29**) and finally moving the azide group from the *para* to *ortho* position (**30**).

While working on the development of this approach, Li and colleagues published a new method for detecting hydrogen sulfide (H$_2$S) in vivo using a BLI approach.[207] Their method was based on the use of azido caged luciferin reporters undergoing de-caging by the reduction of the azide group to an amine induced by hydrogen sulfide. Furthermore, they compared three caged azido-luciferins, including compound **24**, reporting the 6-azido-D-Luciferin as the most sensitive and selective BLI reporter for H$_2$S detection. For this reason, we decided to synthesize and evaluate this analogue (**31**) (**Figure 4.3-15**) in our approach.
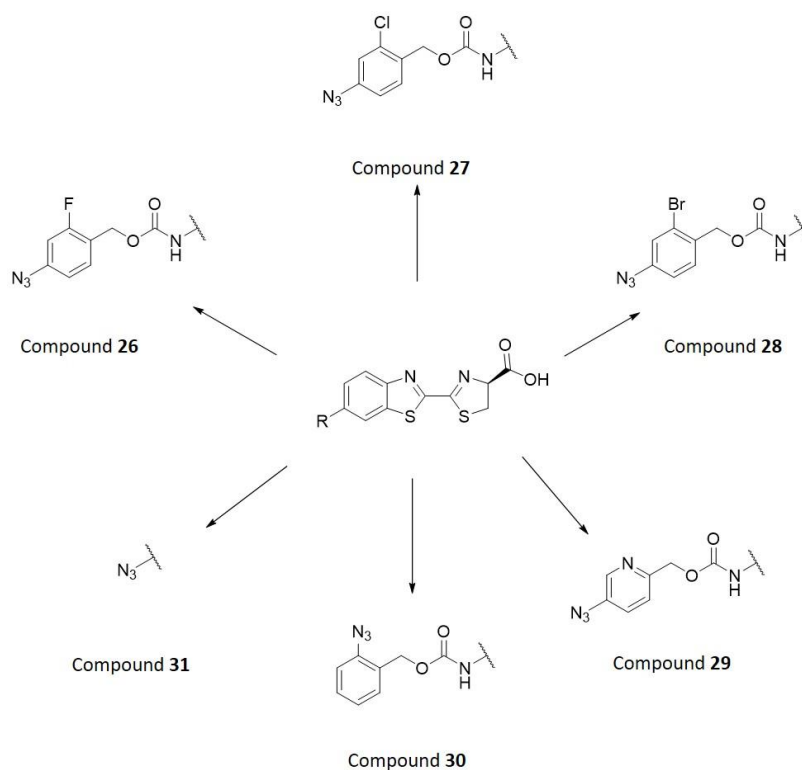
Figure 4.3-15 Caged Luciferin analogues

Initially, we tested if our Mdm2-p53 PPI inhibitor bioorthogonal probe labelled with TCO, compound **3**, would enable the de-caging of the caged luciferins synthesized, **24** and **26**-**31** to determine which bioluminescence reporter was the most efficient (**Figure 4.3-16**).

The caged luciferin analogues at 1 micromolar and 10 micromolar concentrations were reacted with TCO labelled bioorthogonal probe (**3**) (**Figure 4.3-16**) at 10 micromolar concentration. The reactions were ran up to 48 hours and at different time points reaction samples were added to the luciferase assay buffer just before reading.

As depicted in **Figure 4.3-16**, all the reactions produced free aminoluciferin, however some caged luciferin such as **24**, **26 27** and **30** appeared to be more efficiently un-caged by (**3**) at the two concentrations tested. Nevertheless, when looking at the at the 24 hours reaction profile (**Figure 4.3-17**), it appeared that while most of the de-caging reactions achieved the same signal at saturation, some plateaued at lower concentrations of the caged luciferin (e.g. reactions between **3** and **24** or **30**). Compound **24** was slightly more efficiently un-caged at both 1 and 10 micromolar compared to **30**, so we decided to progress compound **24** in the next experiments.

Figure 4.3-16 De-caging of luciferin analogues **24** and **26**-**31** triggered with Mdm2-p53 PPI inhibitor bioorthogonal probe (**3**). The caged lucif-erin analogues at 1 and 10 μM concentration were reacted with (**3**) (10 μM) for 48h. Depicted in the picture analysis of the different reaction after 24 and 48h. At 24 and 48h, 3 microliters of reaction was sampled and added to the luciferase cocktail and placed in a plate reader for luminescence detection. Free aminoluciferin production was extrapolated using a standard curve.

Figure 4.3-17 Dose-response of the De-caging of luciferin analogues **24** and **26**-**31** triggered with Mdm2-p53 PPI inhibitor bioorthogonal probe (**3**) (10 μM) or DMSO control at 24h. At 24h, one tenth of the all reaction volume was added to the luciferase cocktail and placed in a plate reading for luminescence detection. Free aminoluciferin production was extrapolated using standard curve. Most of the reaction reached similar signal saturation. DMSO did not elicit a luminescence signal under any conditions.

4.3.3. Investigation of the bioorthogonal de-caging in cells lysate

Having established that the bioorthogonal probe (**3**) triggered the de-protection of the caged luciferin (**24**), we investigated if the bioorthogonal de-caging would work efficiently in a more complex system. Thus, SJSA-1 cells were
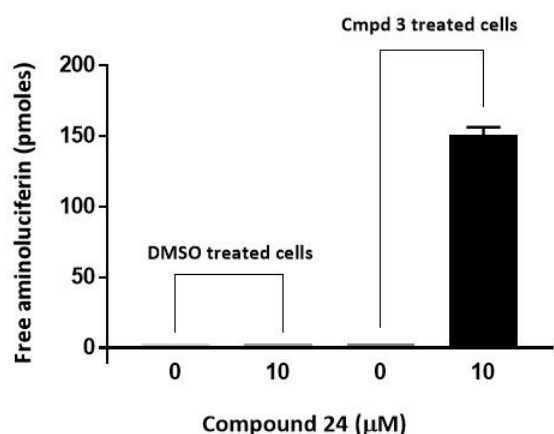
Figure 4.3-18 Performing bioorthogonal de-caging in cell lysate obtained from cells pre-treated with compound 3 or DMSO control for 24h at 37°C and 5% CO_2. Biorthogonal reaction was performed with compound **24** or DMSO control for 24h.

incubated with (**3**) at 10 micromolar concentration or DMSO control for 24 hours at 37°C and 5% CO_2. Next, cells were lysed and compound **24** at 10 micromolar concentration or DMSO control was added. The reaction was run for 24h and then reaction samples were diluted in the Luciferase buffer before luminescence reading. While the controls did not elicit a significant luminescence signal, the samples co-treated with the caged luciferin (**24**) and the bioorthogonal probe (**3**) displayed de-caging corresponding to 150 picomoles of free aminoluciferin (**Figure 4.3-18**). Theoretically, if all the compound would have been taken up by the cells, lysate treated with 100 nmols of the bioorthogonal probe (**3**) (10 mL media containing 10 micromolar compound and 5 million cells) would have elicited 1.2 nmols of free luciferin. Therefore, 1.2 percent of the bioorthogonal probe was taken up by the cells.

4.3.4. Optimization of the assay for the assessment of the cellular up-take of bioorthogonal probes

After proving that we were able to assess bioorthogonal probe cellular up-take using the de-caging reaction using lysate of cells pre-treated with the bioorthogonal probe, we engaged in a further optimization of the assay sensitivity. We reasoned that the bioorthogonal de-caging was the limiting factor for achieving even higher sensitivity. Therefore, we decided to test if this could be improved by extrapolating the amount of compound take up by cells upon treatment not

from the aminoluciferin standard curves but from the standard curve of the reaction between **3** and **24** in cell lysate, where **3** was added only after cell lysis.

Thus, we treated SJSA-1 cells with compound **3** at five concentrations ranging from 0.25 micromolar to 10 micromolar for 24h at 37°C and 5% CO_2. Next, we lysed the cells and we added to the cell lysates compound **24** at 10 micromolar concentration and we let the de-caging reaction run up to 48 hours. In parallel, we built the reaction standard curves in SJSA-1 cell lysates (un-treated cells) by adding compound **3** at five concentrations, also ranging from 0.25 micromolar to 10 micromolar, followed by addition of the caged luciferin, compound **24** and 48h incubation. Additionally, we included compound **1** in the experiment as a negative control (**Figure 4.3-19**).
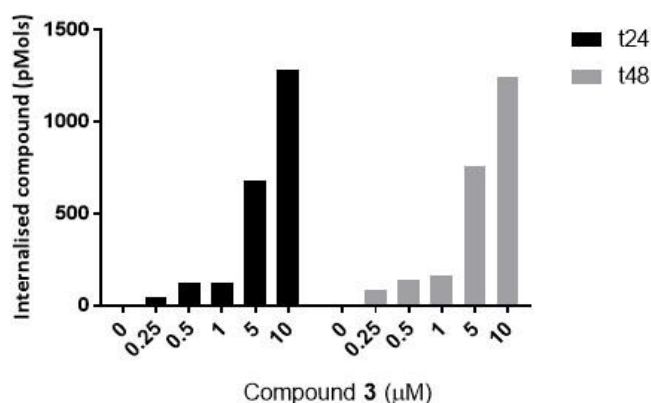
Figure 4.3-19 BLI measurments of amount of compound **3** internalized in SJSA-1 cells after 24 h incubation. Cells were treated with DMSO or compounds 3 at five concentraction ranging from 0.25 μM to 10 μM for 24h at 37 °C and 5% CO_2. Next cells were lysated and compound **24** (10 μM) was added to samples of the lysate. The reaction was run for 48h at R.T. before reading.   The values of the de-caged internalized compounds were extrapolated from standad curve of the reaction run in cells not pre-treated with the labeled compound.

As shown in the graph, no great differences were observed running the reaction for 24 or 48 hours; meaning that the reaction was already close to completion at 24 hours. We could observe a dose-dependent cellular uptake of compound **3**, which was not directly proportional to the dose. Using the previous assay protocol we measured an uptake of (**3**) equal to 150 picomoles while treating the cells with 10 micromolar of compound. Whereas, using the later developed protocol we obtained a value about 9 fold higher, 1280 picomoles. Therefore, the percentage of compound internalized was equal to 1.28. Finally, the negative control, compound **1** did not trigger the luciferin un-caging and no luminescence signal was detected.

Finally, we decided to investigate the up-take of the Mdm2-p53 PPI inhibitor peptides labeled with the TCO group using this new protocol. Thus, SJSA-1 cells were treated with compounds **10-13** (dosed at 1 and 10 micromolar concentrations) or DMSO control for 24 hours followed by cell lysis. Compound **24** at 10 micromolar was added to the lysates and the de-caging reaction was run up to 48 hours. As negative controls, the two un-labeled parent peptides **8** and **9** were included.

As depicted in **Figure 4.3-20**, we were able to measure cellular uptake for the TCO tagged peptides while no luminescence signal was observed for their parent compounds which are unable to trigger the luciferin de-caging. Additionally, a dose-dependent internalization for **10**-**13** was observed.
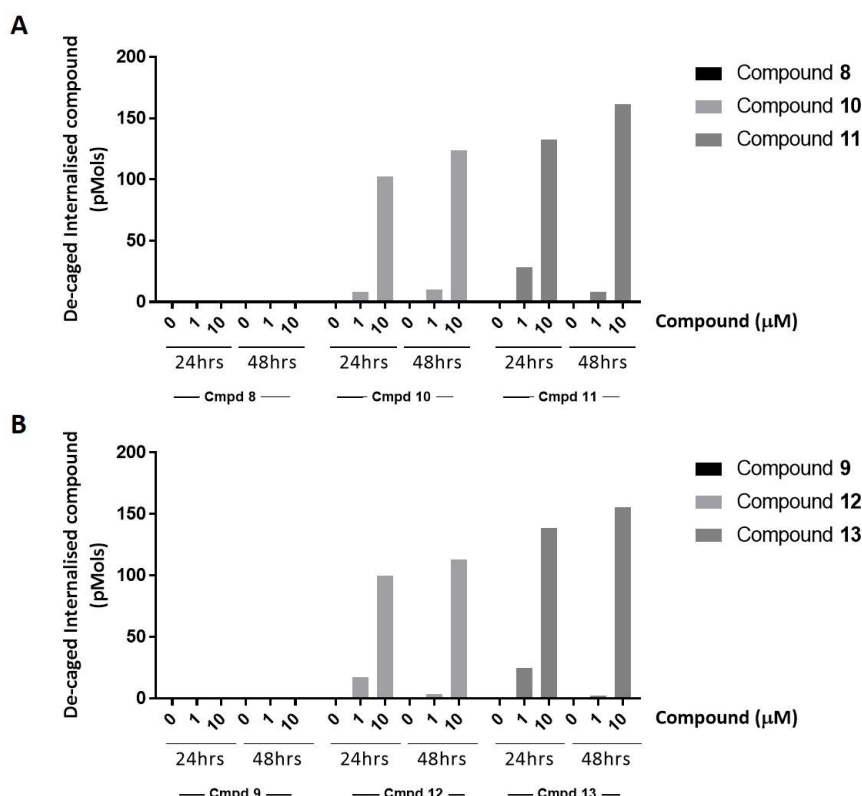
Figure 4.3-20 BLI measurments of amount of compound **10-11 (a)** and **12- 13 (b)** internalized in SJSA-1 cells after 24 h incubation. Cells were treated with DMSO or tagged compounds at 1 and 10 μM concentration for 24h at 37 °C and 5% CO_2. Next cells were lysated. Compound 24 (10 μM) was added to samples of the lysates and the reactions were run for 48h at R.T. before reading. The values of the de-caged internalized compounds were extrapolated from the standard curve of the reaction run in cells not pre-treated with the labeled compound. As additional controls, the un-labeled compounds 8 and 9 were added.

We did not observe a great difference between the uptake of the TCO functionalized analogues of **8** and **9**, contrary to what we expected by their respective cell activities (**Figure 2.7-4**, page 48) and by the data generated with the "two step" imaging approach (**Figure 4.1-2** and **4.1-3**). All the peptides displayed a very low uptake; less than 0.3 percent of the dosed peptide was detected in the cells (**Table 4.3-1**). When we compared the percentages of peptide uptake to that for LMW compound **3**, we observed that the latter showed a value about three fold higher. This observation is in agreement with its superior cellular activity.

We formulated two hypotheses to rationalize the observed discrepancies between the peptide cellular uptake values measured using the BLI assay and their cellular activities.

The first hypothesis relies on differences in the internalization and excretion kinetics of the compounds. For instance, a compound with a fast cellular uptake might be able to reach its target in sufficient concentration for triggering the biological effect and subsequently be excreted by the cell. On the contrary, compounds with slower uptake might not be able to reach their target promptly at sufficient concentration for triggering the biological effect before being excreted or processed by the cell (e.g. metabolized or compartmentalized). If the internalization and excretion kinetics are the reason for the observed discrepancy, we may have expected a similar discrepancy between cellular activities and the uptake measured with "two step" fluorescence assay. However, for the BLI assay we treated the cells for 24

hours before lysis while the fluorescence imaging experiment was run after 2 hours compound incubation. Therefore, further investigation using comparable incubation times might shed more light on these interesting findings.

Table 4.3-1

Cmpd	Dose (µM)	Dose in cell media (nmoles)	Concentration measured (nM)	Calculated amount of compound in all lysate (nmoles)	% Uptake
3	0.25	2.5	52	0.048	**1.90**
	0.5	5	173	0.123	**2.46**
	1	10	160	0.124	**1.24**
	5	50	933	0.679	**1.36**
	10	100	1733	1.284	**1.28**
10	1	10	12	0.008	**0.08**
	10	100	188	0.102	**0.10**
11	1	10	47	0.028	**0.28**
	10	100	197	0.133	**0.13**
12	1	10	27	0.017	**0.17**
	10	100	167	0.100	**0.10**
13	1	10	42	0.025	**0.25**
	10	100	229	0.139	**0.14**

The second hypothesis is based on the fact that the de-caging reaction is not run on live or intact cells but on lysates. Therefore, some compound may be lost during lysate sample preparation (e.g. remaining in the supernatant) or the assessment of the lysate protein content (by bicinchoninic acid kit, BCA kit)[208] used for preparing the lysate solution for the de-caging reaction is not sensitive enough.

In the light of these results, we decided to investigate the peptide permeability using an additional BLI assay, the "Split Luciferin" assay which was under development in our group at EPFL.

4.3.5. Split Luciferin BLI assay for real time peptide uptake studies

The Split luciferin assay is based on the bioorthogonal reaction between 2-cyano-6-hydroxy-benzothiazole (CBT) and D-Cysteine (D-Cys) forming D-Luciferin (**Figure 4.3-21**). This reaction has been previously used as a biocompatible cyclization reaction in cellular systems for nanoparticle assembly,[209] for building an assay for monitoring multiple analytes in cells,[210] for testing enzymatic activity[211] and so on.

Both reactant pairs, CBT and D-Cys, can be masked and de-protected inside the cells to engage in the cyclization reaction leading to the formation of the D-Luciferin reporter.

In the "Split Luciferin" assay for studying peptide internalization the D-Cysteine is masked by conjugation to the peptide of interest via a disulfide bond. When the D-Cysteine labeled peptide penetrates the cell, the D-Cys is released by disulfide bond cleavage in the reducing environment of the cytosol where glutathione is present in high concentration (1-10 mM)[212]. The D-Cys is then free to react with CBT, previously incubated with cells transfected with firefly luciferase,

forming the D-Luciferin BLI reporter *in situ*. By reading the bioluminescence signal the uptake of the peptide can be measured in real time (**Figure 4.3-21b**).

The D-Cys can be inserted into the peptide via disulfide conjugation chemistry on a cysteine residue already present on the peptide of interest or if the peptide does not contain a free cysteine by introducing a linker moiety containing a reactive thiol group (e.g. a mercaptopropionate linker) on the N-terminus or C-terminus of the peptide.
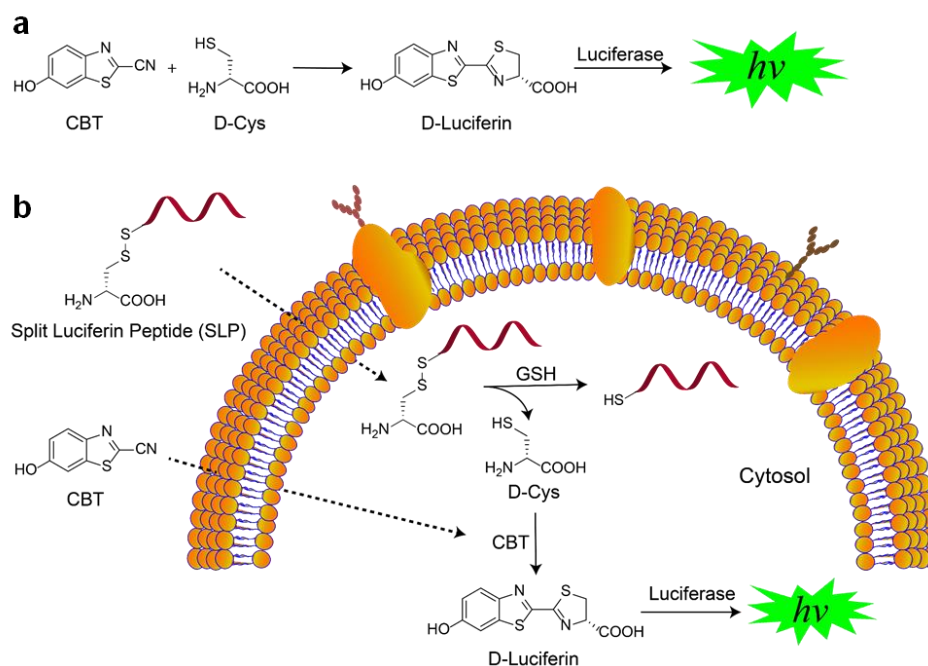
Figure 4.3-21 The "Split Luciferin" assay for real-time imaging and quantification of peptide uptake. (**a**) Cycloaddition reaction between CBT and D-Cys forming D-Luciferin. (**b**) schematic representation of the cellular assay (H. Karatas et al. "Real-time imaging and quantification of peptide uptake in vitro and in vivo", unpublished paper)

The use of this approach was beyond the original scope of our project, which was focused on wild-type cell lines and bioorthogonal molecule labeling to enable EID-DA and SPAAC reactions. However, we reasoned that comparing our approach with the "Split Luciferin" might provide important insights on the relative advantages and disadvantages of the different approaches.

Thus, we modified peptides **8** and **9** by introducing a D-Cys through a mercaptopropionate linker on their N-termini to obtain **32** and **33** respectively (**Figure 4.3-22**). Furthermore, we selected an additional Mdm2-p53 PPI inhibitor linear peptide **34**, which we labeled on the N-terminus to obtain **35**. The peptides were tested in the PD marker cellular induction assay (**Figure 4.3-23**).

The D-Cysteine labeling appeared to be detrimental for the compound cellular activity. The labeling of the peptide was introduced in a position where modification should be tolerated, although we did not generate biochemical data to further understand if this drop in activity was due to a decreased binding affinity.

Compound 32

Compound 33

Compound 34
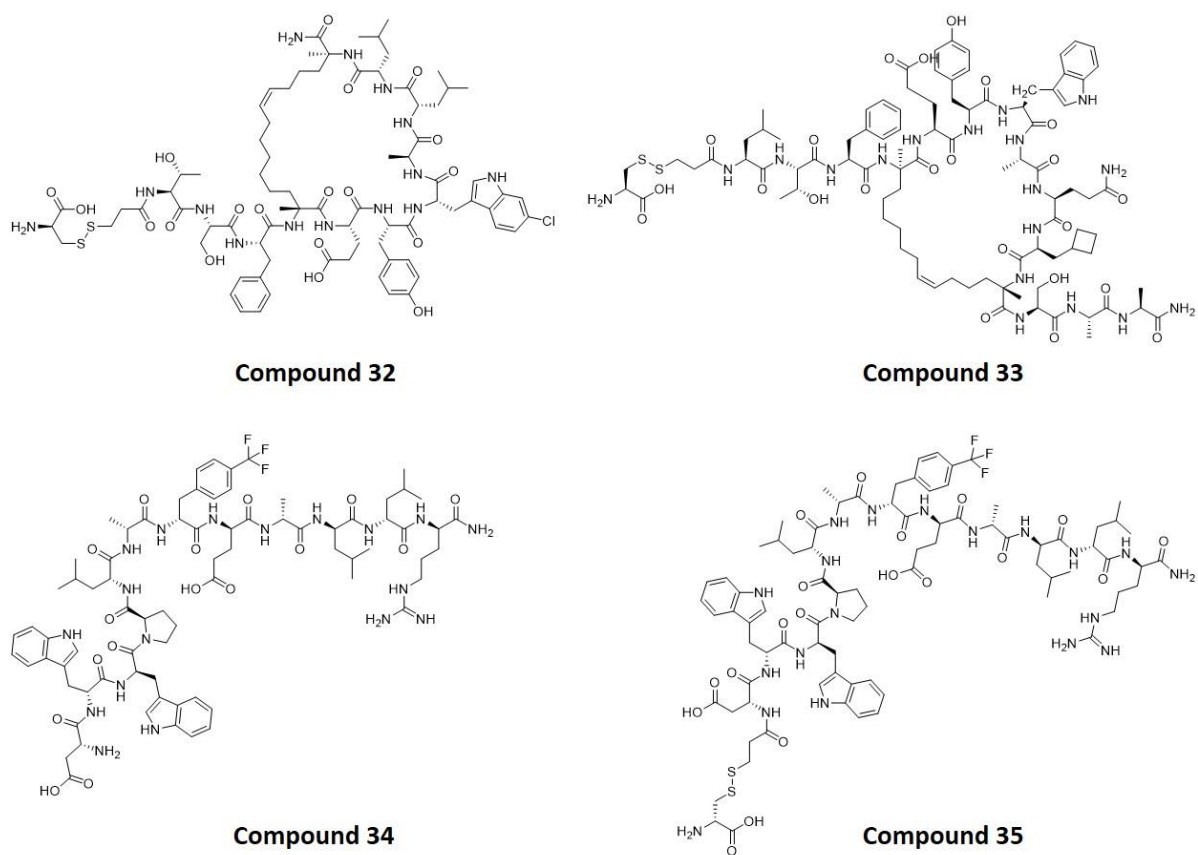
Compound 35

Figure 4.3-22 Structure of compounds **32-35**
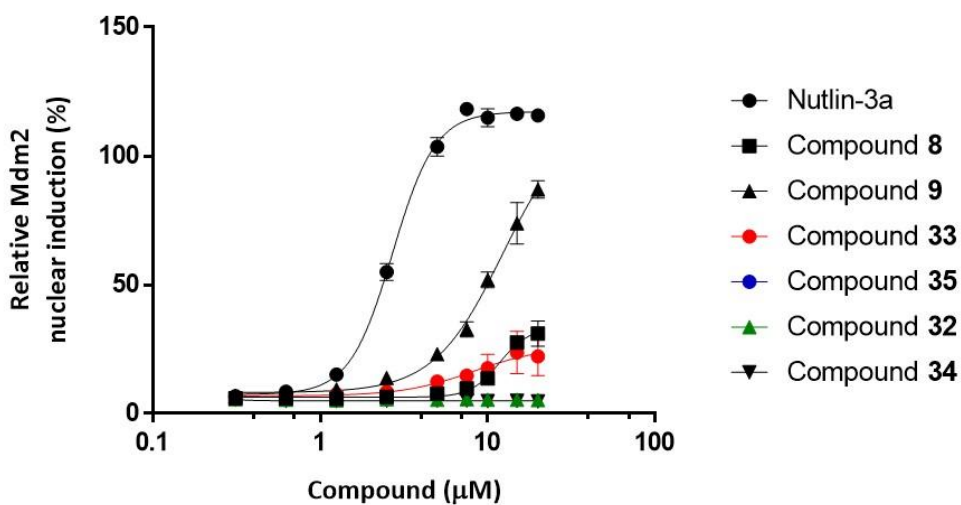
Figure 4.3-23 Cellular activity of **32-35** tested in the Mdm2 nuclear induction immunostaining assay. Activity of the compound was measure as percentage of Mdm2 nuclear induction triggered by Nutlin-3a at 10 micromolar concentration.

Next, the D-Cys labeled peptides were tested in the "Split Luciferin" assay by colleagues in the Goun group at EPFL (**Figure 4.3-24**) (data not yet published). The compounds were incubated at 20 micromolar concentration in SJSA-1-Luc cells pretreated with CBT at 50 micromolar concentration. The internalization of the compounds was monitored over time by bioluminescence reading.
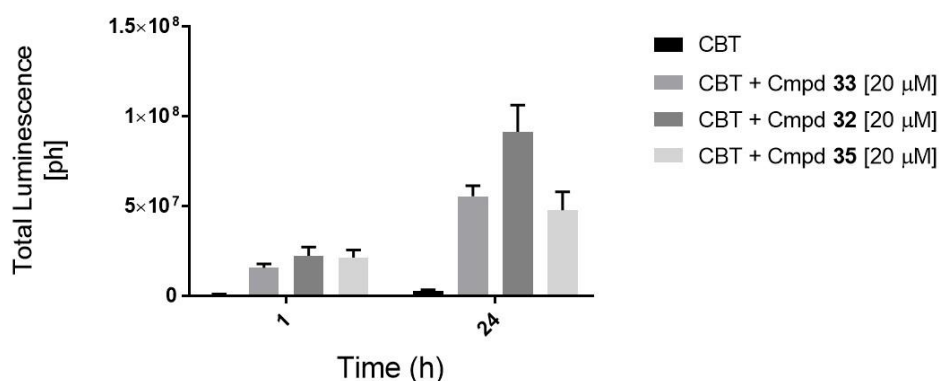
Figure 4.3-24 cellular uptake of compound **32**, **33** and **35** in SJSA-1-Luc cells measure with the "Split Luciferin" assay. Cells were pre-incubated with CBT (50µM) for 30 minutes followed by addition of the D-Cys labeled peptides at (20 µM). The total uptake was calculated from the area under the corresponding kinetic curves (AUC) at 1h and 24h post incubation.

The kinetic data of the internalization of compound **32**-**33** and **35** showed an initial fast internalization which gradually decreased (data not shown). The area under the corresponding kinetic curves of each compound showed a time dependent internalization plateauing after 24 hours. The uptake of **32** appeared to be superior to the one of **33** (ca. two fold) in discrepancy with data generated with the cellular activity assay and the data generated with their TCO labelled analogues in the "two step" fluorescence imaging assay. The results show the complexity of working with these systems. Both BLI approaches were able to show peptidic uptake in cells, although clear correlation to cellular PD read-out was not achieved.

4.4   Results

We investigated fluorescent and bioluminescence imaging approaches to measure the cellular uptake of our bioorthogonal probes.

The "two step" fluorescence imaging approach enabled us to assess uptake for the LMW compounds with a limit of detection of 50 nanomolar concentration for the bioorthogonal probe labelled with TCO. This approach was also applied to investigate the uptake of the Mdm2-p53 PPI stapled peptide inhibitors for which we observed the expected correlation between the measured uptake and their cellular activity profiles. For example, one of the most cellularly active peptide analogues was detected with an LOD of 50 nanomolar while for the peptides showing the weakest activities a LOD of 5 micromolar was observed. Besides, we also tested a "three step" approach with the purpose of

decreasing the observed LODs by reducing the fluorescent background noise. However, this approach did not show the expected sensitivity improvement.

We reasoned that the measurement of the compound intracellular concentration might enable more meaningful correlation between cellular activity and permeability while studying molecules for which cellular efficacy is not driven by their target occupancy.

Therefore, aiming at measuring compound intracellular concentrations, we decided to explore bioluminescence imaging approaches based on the de-caging of masked luciferin reporters via EID-DA and 1,3-dipolar cycloaddition. While the cell-free *in vitro* evaluation of the first investigated reaction (EID-DA) did not provide the reaction profile we were looking for, the 1,3-dipolar cycloaddition did. For that reason, this reaction was investigated further. After testing a set of caged luciferins to improve the reaction kinetics and optimizing assay conditions, we were able to measure the intracellular concentration of our bioorthogonal probes, although the obtained measurement values for the peptides poorly correlate with their cellular activities.

We hypothesized that assessing the compound uptake kinetics might have shed some light on the observed discrepancy between peptide uptakes and their cellular activities. For that reason, we prepared some Mdm2 peptidic ligands labelled with a D-Cysteine and we investigated their up-take kinetics in a "Split Luciferin" assay developed by our group in EPFL. This approach provided sensitive real-time assessment of the peptide internalization, but once more, no correlation with cellular activity was achieved.

In conclusion, the investigated BLI approaches gave quantitative and sensitive measurements of the cellular uptake for the different compounds. However, the "two step" fluorescence approach provided more meaningful uptake data that correlate well with the cellular PD effects.

Finally, we reasoned that the "two step" uptake assay might be used to build structure permeability relationships aiming at improving compound cellular uptake within LMW and peptidic chemical series.

4.5 Experimental session

4.5.1. Bioluminescence assays

Biochemical experiment

TCO at 20 or 200 uM in Tris buffer (TrisHCl 100 mM pH7.4) was supplemented by caged luciferin (20 or 200 uM) to start the reaction. Reaction was left at 20°C in the dark under mild agitation (300 rpm) up to 48h. Reaction products were assessed at different time points by sampling 3 uL and subsequent analysis using a luciferase bioluminescence assay described below.

Aminoluciferin standard curve was performed at each time point. Aminoluciferin (Compound **25**, MW:318.4 g/mol; 1 mM stock solution dissolved in 10% DMSO/ 90 % 0.1M Tris-HCl pH7.4) was serial diluted in Tris-HCl (5 uM starting concentration, 7 points dilution, factor 3).

3 uL of either aminoluciferin standard curve or test sample was added to 27 uL luciferase assay buffer (Tris-HCl pH7.4 supplemented with ATP 1 mM; MgCl2 2 mM; DTT 1 mM; 40 ug/mL Firefly luciferase) in a 384 well plate. Luminescence data was generated using a Tecan M1000 reader (luminescence module; 1 sec integration time).

Aminoluciferin concentrations were extrapolated from standard curves using blank subtracted luminescence data in Excel. Transformed data were transferred to GraphPad Prism for generation of graphs.

Biochemical experiment (compound 24 + TCO or CCO)

Caged luciferin was serial diluted in Tris buffer (TrisHCl 100 mM pH7.4) and reaction was started at T= 0 by addition of 20 uM TCO or CCO. Reaction was left at 20°C in the dark under mild agitation (300 rpm). Reaction products were assessed at different time points by sampling 3 uL and subsequent analysis using a luciferase bioluminescence assay described below.

Aminoluciferin standard curve was performed at each time point. Aminoluciferin (Compound **25,** MW:318.4 g/mol; 1 mM stock solution dissolved in 10%DMSO/90% 0.1M Tris-HCl pH7.4) was serial diluted in Tris-HCl (5 uM starting concentration, 7 points dilution, factor 3).

3 uL of either aminoluciferin standard curve or test sample was added to 27 uL luciferase assay buffer (non optimised vs optimised buffer) in a 384 well plate. Non optimised buffer contained Tris-HCl pH7.4 supplemented with ATP 1 mM; MgCl2 2 mM; DTT 1 mM; 40 ug/mL Firefly luciferase; while optimised buffer contained Tris-HCl pH7.4 supplemented with ATP 1 mM; MgCl2 2 mM; DTT 1 mM; BSA 0.02%; Tween 0.02%; 20 ug/mL QuantiLum recombinant luciferase). Luminescence data was generated using a Tecan M1000 reader (luminescence module; 1 sec integration time).

Aminoluciferin concentrations were extrapolated from standard curves using blank subtracted luminescence data in Excel. Transformed data were transferred to GraphPad Prism for generation of graphs.

Biochemical experiment for testing caged luciferin analogues

Caged luciferins were serial diluted in Tris buffer (TrisHCl 100 mM pH7.4) and reaction were started at t=0 by addition of Compound **3** at 10 uM. Reactions were left at 20°C in the dark under mild agitation (300 rpm). Reaction products were assessed at different time points by sampling 3 uL and subsequent analysis using a luciferase bioluminescence assay described below.

Aminoluciferin standard curve was performed at each time point. Aminoluciferin (Compound **25,** MW:318.4 g/mol; 1 mM stock solution dissolved in 10%DMSO/90% 0.1M Tris-HCl pH7.4) was cascade-diluted in Tris-HCl (5 uM starting concentration, 7 points dilution, factor 3).

3 uL of either aminoluciferin standard curve or test sample was added to 27 uL luciferase assay buffer (Tris-HCl pH7.4 supplemented with ATP 1 mM; MgCl2 2 mM; DTT 1 mM; BSA 0.02%; Tween 0.02%; 20 ug/mL QuantiLum recombinant luciferase) in a 384 well plate. Luminescence data was generated using a Tecan M1000 reader (luminescence module; 1 sec integration time).

Aminoluciferin concentrations were extrapolated from standard curves using blank subtracted luminescence data in Excel. Transformed data were transferred to GraphPad Prism for generation of graphs.

Bioluminescence assay in cell lysate

SJSA-1 cells were cultivated in RPMI 1640 (Amimed 1-41F01-I), 10% FCS (Amimed 2-01F36-I), 1x Glutamine (Amimed 5-100K50-H) at 37°C and 5% CO2. Cells (px+4) were seeded at a 5x10^6 cells/mL density and kept overnight before treatment. Cells were treated with DMSO or Compound **3** at 10 uM for 24 hrs. Cells lysis was performed using standard protocol in 400 uL lysis buffer containing Tris-HCl pH7.5 150 mM, NaCl 150 mM, NaF 10 mM, EDTA 1mM, EGTA 1 mM, Triton 1x, protease and phosphatase inhibitors cocktails. Protein concentrations in samples were determined using BCA protein determination kit, and samples were frozen before use in uncaging reactions.

Cell lysates were diluted in lysis buffer to obtain a 2 ug/uL concentration and supplemented with 10 uM caged luciferin (or DMSO for controls). Reaction was left at 20°C in the dark under mild agitation (300 rpm). Reaction products were assessed at different time points by sampling 3 uL and subsequent analysis using a luciferase bioluminescence assay described below.

Aminoluciferin standard curve was performed at each time points. Aminoluciferin (Compound **25**, MW:318.4 g/mol; 1 mM stock solution dissolved in 10%DMSO/90% 0.1M Tris-HCl pH7.4) was serial diluted in Tris-HCl (5 uM starting concentration, 7 points dilution, factor 3).

3 uL of either aminoluciferin standard curve or test sample was added to 27 uL luciferase assay buffer (Tris-HCl pH7.4 supplemented with ATP 1 mM; MgCl2 2 mM; DTT 1 mM; BSA 0.02%; Tween 0.02%; 20 ug/mL QuantiLum recombinant luciferase) in a 384 well plate. Luminescence data was generated using a Tecan M1000 reader (luminescence module; 1 sec integration time).

Blank subtracted data were used to extrapolate compound concentration and amount of moles using standard curves in Excel. Transformed data were transferred to GraphPad Prism for generation of graphs.

Bioluminescence assay in cell lysate for measuring compounds permeability

SJSA-1 cells were cultivated in RPMI 1640 (Amimed 1-41F01-I), 10% FCS (Amimed 2-01F36-I), 1x Glutamine (Amimed 5-100K50-H) at 37°C and 5% CO2. Cells (px+5) were seeded at a 5x10^6 cells/mL density and kept overnight before treatment. Cells were treated with DMSO or compounds at 1 or 10 uM for 4 hrs. Cells lysis was performed using standard protocol in 400 uL of lysis buffer containing Tris-HCl pH7.5 150 mM, NaCl 150 mM, NaF 10 mM, EDTA 1mM, EGTA 1 mM, Triton 1x, protease and phosphatase inhibitors cocktails. Protein concentrations in samples were determined using BCA protein determination kit, and samples were frozen before use in uncaging reactions.

Cell lysates were diluted in lysis buffer to obtain a 1 ug/uL concentration and supplemented with 1 uM caged luciferin to start the reactions. Reactions were left at 20°C in the dark under mild agitation (300 rpm). Reaction products were assessed at different time points by sampling 3 uL and subsequent analysis using a luciferase bioluminescence assay described below.

A reaction standard curve was performed for each test compound by treating SJSA-1 cell lysate (at 1 ug/uL obtained from DMSO treated cells) with the test compound of interest at 1 uM. Cell lysate supplemented with 1 uM of test

compound was serial diluted in SJSA-1 lysate. Standard curve reactions were initiated at t0 by addition of 1 uM of caged luciferin (MWE162). The time of start of reaction was the same for test samples and standard curves.

3 uL of either compound standard curve or test sample was added to 27 uL luciferase assay buffer (Tris-HCl pH7.4 supplemented with ATP 1 mM; MgCl2 2 mM; DTT 1 mM; BSA 0.02%; Tween 0.02%; 20 ug/mL QuantiLum recombinant luciferase) in a 384 well plate. Luminescence data was generated using a Tecan M1000 reader (luminescence module; 1 sec integration time).

Blank subtracted data were used to extrapolate compound concentration using standard curves in Excel. Number of moles detected was then worked out and transformed data were transferred to GraphPad Prism for generation of graphs.

4.5.2. Chemical material and Methods

General considerations

All chemicals were purchased from Sigma Aldrich, unless noted, and were used as received. All solvents were of reagent grade or higher and were used without further purification. The instruments for chemical synthesis, characterization and LC-MS reaction characterization were reported in 2.12.10.1 with the exceptions of the PhotoFlow equipment and the Gas Chromatography.

Photo flow equipment:

 Water 600 HPLC pump with a maximum flow rate of 45 mL/min. A 400 W Hg medium pressure lamp, and a FEP coil (ca 30 mL total volume) wrapped around a quarz photo reactor. The lamp was used without any filter and was water cooled. The reaction liquid was pumped through the coil followed by a Biotage Snap cartridge, filled with 120 g of AgNO3 loaded silica. From there the reaction solution was collected in an Erlenmeyer flask, from where it was fed back to the pump.

Compounds synthesis

Compound 20: (*S*)-2-(6-(((((*E*)-cyclooct-2-en-1-yl)oxy)carbonyl)amino)benzo[d]thiazol-2-yl)-4,5-dihydrothiazole-4-carboxylic acid
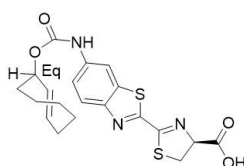
A mixture of **Intermediate 33** (132 mg, 0.403 mmol), D-Cystein [921-01-7] (53.7 mg, 0.443 mmol) and K_2CO_3 (61.3 mg, 0.443 mmol) in MeOH (3.8 mL, Ratio: 2) and Water (1.9 mL) was stirred at R.T. for 2h. The reaction was diluted with EA (70 mL) and HCl (0.5M) (40 mL) was added. The organic phase was separated The aqueous phase was extracted with EA (50 mL x 2). The organic phases were combined and evaporated to dryness. The crude material was purified via flash chromatography ((silica column 12g, MeOH/DCM mobile phase, 0.25% Acetic acid) obtain **compound 20** (30 mg, 0.065 mmol, 16 % yield) as a yellow solid.

^{1}H NMR (600 MHz, Chloroform-d) δ 8.36 (s, 1H), 8.05 (d, J = 8.9 Hz, 1H), 7.28 (s, 1H), 6.88 (s, 1H), 5.85 (t, J = 11.7 Hz, 1H), 5.60 (dd, J = 16.2, 9.6 Hz, 1H), 5.44 (t, J = 9.7 Hz, 1H), 5.25 – 5.18 (m, 1H), 3.81 (d, J = 9.5 Hz, 2H), 2.47 (d, J = 9.7 Hz,

1H), 2.34 – 2.27 (m, 1H), 2.01 (d, J = 8.6 Hz, 2H), 1.95 – 1.81 (m, 2H), 1.60 (q, J = 12.0 Hz, 2H), 1.46 (d, J = 16.2 Hz, 1H), 0.97 – 0.80 (m, 2H).

^{13}C NMR (151 MHz, CDCl3) δ 175.58, 167.77, 158.50, 149.21, 137.68, 137.53, 133.84, 131.17, 130.33, 124.95, 118.73, 110.33, 79.74, 77.87, 40.92, 35.61, 35.52, 34.88, 28.99, 27.44.

LC-MS [M+H]$^+$ m/z calcd. for [$C_{20}H_{22}N_3O_4S_2$]$^+$ 432.1, found 432.2 at 1.08 min. (UV Detector: TIC) and [M-1]$^-$ m/z calcd. for [$C_{20}H_{20}N_3O_4S_2$]$^-$ 430.1, found 430.2 at 1.08 min. (LC-MS method b).

Compound 21: (S)-2-(6-(((((E)-cyclooct-2-en-1-yl)oxy)carbonyl)amino)benzo[d]thiazol-2-yl)-4,5-dihydrothiazole-4-carboxylic acid
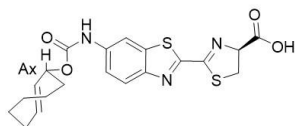
A mixture of **Intermediate 34** (120 mg, 0.367 mmol), D-Cystein [921-01-7] (48.8 mg, 0.403 mmol) and K_2CO_3 (55.7 mg, 0.403 mmol) in MeOH (3.5 mL) and Water (1.7 mL) was stirred at R.T. for 2h. The reaction was poured in EA (70 mL) and HCl (0.5M) (40 mL) was added. The organic phase was separated. The aqueous phase was extracted with EA (50 mL x 2) and the organic phases were combined and evaporated to obtain the crude material. The crude product was purified via flash chromatography (silica column 12g, MeOH/DCM mobile phase, 0.25% Acetic acid) to obtain after evaporation the desired product, **compound 21** (42 mg, 0.097 mmol, 26.6 % yield) as a yellow solid.

^{1}H NMR (600 MHz, Chloroform-d) δ 8.35 (s, 1H), 8.04 (d, J = 8.7 Hz, 1H), 7.30 – 7.27 (m, 1H), 6.89 (s, 1H), 5.84 (t, J = 13.6 Hz, 1H), 5.59 (dd, J = 16.3, 9.6 Hz, 1H), 5.44 (t, J = 9.7 Hz, 1H), 5.21 (dd, J = 15.0, 8.6 Hz, 1H), 3.80 (d, J = 9.7 Hz, 2H), 2.46 (d, J = 10.7 Hz, 1H), 2.33 – 2.24 (m, 1H), 2.00 (d, J = 11.1 Hz, 2H), 1.89 (q, J = 17.4, 15.6 Hz, 2H), 1.59 (q, J = 12.5 Hz, 1H), 1.45 (q, J = 13.5 Hz, 1H), 0.98 – 0.77 (m, 2H).

^{13}C NMR (151 MHz, CDCl3) δ 171.96, 167.76, 158.45, 149.17, 137.63, 137.51, 133.81, 133.81, 131.14, 124.91, 118.71, 110.27, 79.70, 77.85, 40.89, 35.58, 35.48, 34.84, 28.96, 27.41.

LC-MS [M+H]$^+$ m/z calcd. for [$C_{20}H_{22}N_3O_4S_2$]$^+$ 432.1, found 432.1 at 4.47 min. (UV Detector: TIC) (LC-MS method a).

Compound 22: (S)-2-((tert-butoxycarbonyl)amino)-3-(4-((6-methyl-1,2,4,5-tetrazin-3-yl)amino)phenyl)propanoic acid
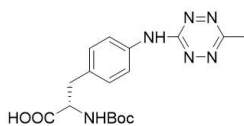
(S)-3-(4-aminophenyl)-2-((tert-butoxycarbonyl)amino)propanoic acid (610 mg, 2.177 mmol) and **Intermediate 35** (258 mg, 1.815 mmol) were dissolved in MeOH (6 mL) to give a red solution. The reaction was refluxed at 110 °C for 18h. The reaction was monitored by TLC. The reaction did not go to completion, therefore 3-(4-aminophenyl)-2-((tert-butoxycarbonyl)amino)propanoic acid (1.526 g, 5.44 mmol) was added and the reaction was refluxed at 110 °C for additional 24h. the solution was adsorbed on silica gel. The crude material was purified via flash chromatography (silica column 12 g, dichlormethane/methanol mobile phase, 0.25% AcOH) to obtain the desired product, compound **22** (375 mg, 1.0 mmol, 55% of yield) as a red-orange solid.

^{1}H NMR (400 MHz, DMSO-d6) δ 10.59 (s, 1H), 7.63 – 7.56 (m, 2H), 7.26 – 7.19 (m, 2H), 4.06 (td, J = 9.4, 8.9, 4.6 Hz, 1H), 2.97 (dd, J = 13.8, 4.8 Hz, 1H), 2.83 – 2.77 (m, 1H), 2.75 (s, 3H), 1.31 (s, 9H); Consistent with the literature reported data.[204]

LC-MS [M+H]$^+$ m/z calcd. for [C$_{17}$H$_{23}$N$_6$O$_4$]$^+$ 375.2, found 375.3 at 0.82 min. (UV Detector: TIC) and [M-1]$^-$ m/z calcd. for [C$_{17}$H$_{23}$N$_6$O$_4$]$^-$ 373.2, found 373.3 at 0.82 min. (UV Detector: TIC) (LC-MS method b).

Compound 23: 3,6-di(pyridin-2-yl)-1,2,4,5-tetrazine
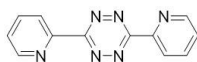
The title compound [1671-87-0] was purchased from Sigma Aldrich.

Compound 24: (S)-2-(6-(((((4-azidobenzyl)oxy)carbonyl)amino)benzo[d]thiazol-2-yl)-4,5-dihydrothiazole-4-carboxylic acid
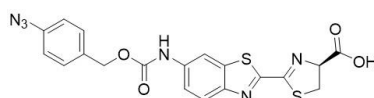
A mixture of **Intermediate 36** (40 mg, 0.114 mmol), D-Cystein (15.22 mg, 0.126 mmol) and K$_2$CO$_3$ (17.36 mg, 0.126 mmol) in MeOH (1.5 mL) and Water (0.750 mL) was stirred at R.T. for 6h in the dark. The reaction was diluted with EA (70 mL) and HCl (0.5M) (40 mL) was added. The organic phase was separated. The aqueous phase was extracted with EA (50 mL x 2). The organic phase were combined and evaporated to obtain the crude product which was purified via flash chromatography (silica column 12g, MeOH/DCM mobile phase containing 0.25% acetic acid) to obtain after evapo ration the desired product, compound **24** (15 mg, 0.032 mmol, 28.3 % yield) as a white powder

^{1}H-NMR (600 MHz, DMSO-d6) δ 13.20 (s, 1H), 10.26 (s, 1H), 8.39 (s, 1H), 8.08 (d, J = 8.9 Hz, 1H), 7.58 (dd, J = 9.0, 1.8 Hz, 1H), 7.51 (d, J = 8.3 Hz, 2H), 7.17 (d, J = 8.3 Hz, 2H), 5.47 - 5.40 (m, 1H), 5.19 (s, 2H), 3.79 (t, J = 10.5 Hz, 1H), 3.70 (dd, J = 11.1, 8.3 Hz, 1H).

^{13}C-NMR (151 MHz, DMSO) δ 171.60, 164.85, 159.07, 153.79, 148.61, 139.74, 139.11, 136.98, 133.71, 130.63, 124.79, 119.65, 119.30, 110.45, 78.57, 66.01, 35.19.

LC-MS [M+H]$^+$ m/z calcd. for [C$_{19}$H$_{15}$N$_6$O$_4$S$_2$]$^+$ 455.1, found 455.1 at 1.06 min. (UV Detector: TIC) and [M-1]$^-$ m/z calcd. for [C$_{19}$H$_{13}$N$_6$O$_4$S$_2$]$^-$ 453.1, found 453.1 at 1.06 min. (UV Detector: TIC) (LC-MS method b).

Compound 25: (S)-2-(6-aminobenzo[d]thiazol-2-yl)-4,5-dihydrothiazole-4-carboxylic acid
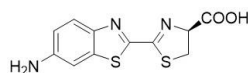
The title compound was prepared following a literature described procedure.[213]

6-aminobenzo[d]thiazole-2-carbonitrile [7724-12-1] (175 mg, 1.0 mmol) and D-Cysteine (128 mg) were suspended in a MeOH (4.0 mL) and Water (2.0 mL) in a 10 mL round bottom flask. Potassium carbonate (146 mg, 1.060 mmol) was added and the reaction mixture was stirred at R.T. under N$_2$ for 1h. The MeOH was removed under vacuum. The obtained residue was purified via prep. HPLC (ACN/water mobile phase, TFA acid modifier). The fractions containing the desired product were combined and lyophilized to obtain the desire product, compound **25** (88 mg, 0.315 mmol, 31.5 % yield).

^{1}H-NMR (400 MHz, Methanol-d4) δ 7.95 (dd, J = 8.8, 0.6 Hz, 1H), 7.49 (d, J = 2.2 Hz, 1H), 7.17 (dd, J = 8.8, 2.3 Hz, 1H), 5.41 (dd, J = 9.5, 8.7 Hz, 1H), 3.78 (dd, J = 9.1, 3.8 Hz, 2H).

LC-MS [M+H]$^+$ m/z calcd. for [$C_{11}H_{10}N_3O_2S_2$]$^+$ 280.0, found 280.1 at 0.58 min. (UV Detector: TIC) (LC-MS method b).

Compound 26: (S)-2-(6-((((4-azido-2-fluorobenzyl)oxy)carbonyl)amino)benzo[d]thiazol-2-yl)-4,5-dihydrothiazole-4-carboxylic acid
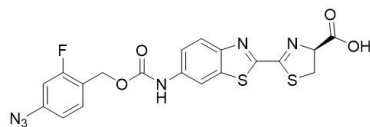
A solution of D-Cystein (99 mg, 0.814 mmol) and K_2CO_3 (56.3 mg, 0.407 mmol) in Water (3 mL) and MeOH (3 mL) was added drop-wise to a suspension of **Intermediate 37** (150 mg, 0.407 mmol) in MeOH (5 mL) and DCM (2 mL) at R.T. under Argon. The reaction was stirred at R.T. for 3h in the dark. Acetic acid (400μL) was added to the reaction mixture, which was subsequently evaporated to dryness to afford the crude material as a pale yellow solid. The crude was purified via flash chromatography (silica column 40g, MeOH/DCM mobile phase, AcOH modifier). The fractions containing the desired product were combined and evaporated to dryness to obtain a solid. The solid was triturated with Toluene (5 mL) to obtain the desired product, compound 26 (97 mg, 0.201 mmol, 49.4 % yield) as a pale yellow powder.

^{1}H NMR (400 MHz, DMSO-d6) δ 13.16 (s, 1H), 10.23 (s, 1H), 8.36 (d, J = 1.7 Hz, 1H), 8.05 (d, J = 8.9 Hz, 1H), 7.62 - 7.52 (m, 2H), 7.10 (dd, J = 10.9, 2.1 Hz, 1H), 7.03 (dd, J = 8.2, 2.1 Hz, 1H), 5.41 (dd, J = 9.7, 8.4 Hz, 1H), 5.20 (s, 2H), 3.82 - 3.71 (m, 1H), 3.67 (dd, J = 11.2, 8.3 Hz, 1H).

^{13}C NMR (101 MHz, DMSO-d6) δ 171.55, 164.85, 162.81, 160.35, 159.10, 153.56, 148.65, 142.25, 138.99, 136.96, 133.14, 124.76, 120.30 (d, J = 15.3 Hz), 115.76, 110.50, 107.31 (d, J = 25.2 Hz), 78.56, 60.31, 35.17.

LC-MS [M+H]$^+$ m/z calcd. for [$C_{19}H_{14}FN_6O_4S_2$]$^+$ 473.0 found 473.0 at 1.08 min. (UV Detector: TIC) and [M-1]$^-$ m/z calcd. for [$C_{19}H_{12}FN_6O_4S_2$]$^-$ 471.0, found 471.1 at 1.08 min. (UV Detector: TIC) (LC-MS method b).

Compound 27: (S)-2-(6-((((4-azido-2-chlorobenzyl)oxy)carbonyl)amino)benzo[d]thiazol-2-yl)-4,5-dihydrothiazole-4-carboxylic acid
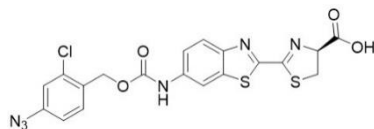

A mixture of D-Cystein (44.1 mg, 0.364 mmol) and K_2CO_3 (25.1 mg, 0.182 mmol) in MeOH (0.8 mL) and Water (0.8 mL) was added to a suspension of **Intermediate 38** (70 mg, 0.182 mmol) in MeOH (1.2 mL) and DCM (1.2 mL) at R.T under Argon. The reaction was stirred at R.T. under Argon in the dark for 1.5 h. Next the reaction was concentrated under reduced pressure to obtain an oil to which AcOH (0.8 mL) and Water (5 mL) were added. The mixture was lyophilized O/N to obtain the crude material. The crude was purified via flash chromatography (silica column 12g, MeOH/DCM mobile phase, AcOH modifier) to obtain after solvent evaporation a solid which was re-dissolved in desired product, compound **27** (71 mg, 0.142 mmol, 78 % yield) as a yellow/orange powder in Toluene (10 mL). The solution was

evaporated under reduced pressure and placed on the HV for 2h to afford the desired product, compound **27** (71 mg, 0.142 mmol, 78 % yield) as a white/yellow powder.

^{1}H NMR (400 MHz, DMSO-d6) δ 13.14 (s, 1H), 10.28 (s, 1H), 8.37 (d, J = 1.9 Hz, 1H), 8.06 (d, J = 8.9 Hz, 1H), 7.61 (d, J = 8.3 Hz, 1H), 7.57 (dd, J = 9.0, 2.1 Hz, 1H), 7.30 (d, J = 2.3 Hz, 1H), 7.18 (dd, J = 8.3, 2.3 Hz, 1H), 5.41 (dd, J = 9.7, 8.4 Hz, 1H), 5.24 (s, 2H), 3.80 - 3.73 (m, 1H), 3.67 (dd, J = 11.3, 8.3 Hz, 1H).

^{13}C NMR (101 MHz, DMSO) δ 171.56, 164.84, 159.14, 153.56, 148.67, 141.64, 138.99, 136.97, 134.62, 132.63, 130.74, 124.78, 120.42, 119.33, 118.68, 110.54, 78.58, 63.61, 35.18.

LC-MS [M+H]$^{+}$ m/z calcd. for [C$_{19}$H$_{14}$ClN$_6$O$_4$S$_2$]$^{+}$ 489.0 found 489.0 at 1.11 min. (UV Detector: TIC) and [M-1]$^{-}$ m/z calcd. for [C$_{19}$H$_{12}$ClN$_6$O$_4$S$_2$]$^{-}$ 487.0, found 487.1 at 1.11 min. (UV Detector: TIC) (LC-MS method b).

Compound 28: (S)-2-(6-((((4-azido-2-bromobenzyl)oxy)carbonyl)amino)benzo[d]thiazol-2-yl)-4,5-dihydrothiazole-4-carboxylic acid
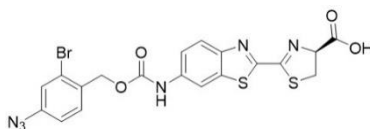
A solution of D-Cystein (82 mg, 0.680 mmol) and K2CO3 (47.0 mg, 0.340 mmol) in Water (3.00 mL) and MeOH (3.0 mL) was added drop-wise to a suspension of **Intermediate 39** (146 mg, 0.340 mmol) in MeOH (5 mL) and DCM (2.0 mL) at R.T. under Argon. The reaction was stirred for 2h in the dark and then acetic acid (400μL) was added; the formation of a white precipitate was observed. The solid was filtered and washed with c-Hexane, MeOH and water before purifying via prep. HPLC (ACN/water mobile phase, TFA acid modifier) to obtain after lyophilization the desired product, compound **28** (95 mg, 0.175 mmol, 51.3 % yield) as a pale yellow solid.

LC-MS [M]+=533 and [M+2]+=535 at 1.1min, UV purity 100%.

^{1}H NMR (400 MHz, DMSO-d6) δ 13.18 (d, J = 15.6 Hz, 1H), 10.29 (s, 1H), 8.37 (d, J = 1.9 Hz, 1H), 8.06 (d, J = 8.9 Hz, 1H), 7.63 - 7.54 (m, 2H), 7.44 (d, J = 2.3 Hz, 1H), 7.22 (dd, J = 8.3, 2.3 Hz, 1H), 5.41 (dd, J = 9.7, 8.3 Hz, 1H), 5.22 (s, 2H), 3.77 (dd, J = 11.2, 9.9 Hz, 1H), 3.67 (dd, J = 11.3, 8.3 Hz, 1H).

^{13}C NMR (101 MHz, DMSO) δ 171.56, 164.85, 153.53, 148.66, 141.58, 138.99, 136.96, 132.46, 132.37, 124.78, 124.51, 123.47, 119.33, 119.18, 110.54, 78.56, 65.78, 53.69, 35.17.

LC-MS [M+H]$^{+}$ m/z calcd. for [C$_{19}$H$_{14}$BrN$_6$O$_4$S$_2$]$^{+}$ 533.0 found 533.0 at 1.14 min. (UV Detector: TIC) and [M-1]$^{-}$ m/z calcd. for [C$_{19}$H$_{12}$BrN$_6$O$_4$S$_2$]$^{-}$ 531.0, found 531.0 at 1.14 min. (UV Detector: TIC) (LC-MS method b).

Compound 29: (S)-2-(6-((((5-azidopyridin-2-yl)methoxy)carbonyl)amino)benzo[d]thiazol-2-yl)-4,5-dihydrothiazole-4-carboxylic acid
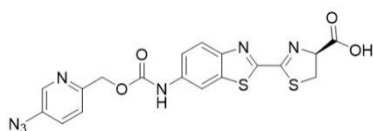
A solution of D-Cystein (103 mg, 0.854 mmol) and K_2CO_3 (59.0 mg, 0.427 mmol) in MeOH (2.9 mL) and Water (2.2 mL) was added drop-wise a suspension of **Intermediate 40** (150 mg, 0.427 mmol) in MeOH (3 mL) at R.T. under Argon. The reaction was stirred at R.T. under argon for 2h in the dark. Acetic acid (400µl) was added to the reaction mixture and the resulting solution was concentrated under reduced pressure to obtain the crude material. The crude was purified via flash chromatography (silica column 40g, MeOH/DCM mobile phase, 0.25% acetic acid modifier) to obtain after evaporation the desired product, compound **29** (74 mg, 0.161 mmol, 37.7 % yield) as a pale yellow solid.

LC-MS $[M+1]^+$=456 and $[M-1]^-$=454 at 0.86 min, UV purity 98%.

^{1}H NMR (400 MHz, DMSO-d6) δ 13.14 (s, 1H), 10.32 (s, 1H), 8.37 (t, J = 2.7 Hz, 2H), 8.07 (d, J = 8.9 Hz, 1H), 7.67 (dd, J = 8.4, 2.7 Hz, 1H), 7.58 (dd, J = 9.0, 2.1 Hz, 1H), 7.53 (d, J = 8.4 Hz, 1H), 5.41 (dd, J = 9.7, 8.3 Hz, 1H), 5.24 (s, 2H), 3.80 - 3.63 (m, 2H).

^{13}C NMR (101 MHz, DMSO) δ 171.56, 164.85, 159.12, 153.63, 152.76, 148.66, 141.00, 139.03, 136.97, 136.54, 127.74, 124.78, 123.35, 119.35, 110.55, 78.56, 66.67, 35.17.

LC-MS $[M+H]^+$ m/z calcd. for $[C_{18}H_{14}N_7O_4S_2]^+$ 456.0 found 456.0 at 0.86 min. (UV Detector: TIC) and $[M-1]^-$ m/z calcd. for $[C_{18}H_{12}N_7O_4S_2]^-$ 454.0, found 454.0 at 0.86 min. (UV Detector: TIC) (LC-MS method b).

Compound 30 (S)-2-(6-((((2-azidobenzyl)oxy)carbonyl)amino)benzo[d]thiazol-2-yl)-4,5-dihydrothiazole-4-carboxylic acid
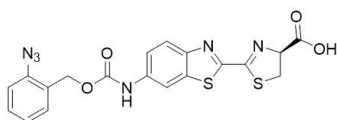
A mixture of **Intermediate 41** (103 mg, 0.294 mmol), D-Cystein (39.2 mg, 0.323 mmol) and K_2CO_3 (44.7 mg, 0.323 mmol) in MeOH (7.5 mL),Water (3.2 mL) and DCM (2 mL) was stirred 5h at R.T. in the dark. AcOH (200µl) was added. The reaction was evaporated to obtain an oil. Water and MeOH (10 mL) were added. The mixture was lyophilized to obtain a pale yellow solid. The crude material was purifed via Flash Chromatography (silica column 12g, MeOH/DCM mobile phase, 0.25% AcOH acid modifier) to obtain after solvent evaporation the desired product, compound **30** (74 mg, 0.160 mmol, 54.3 % yield) as a pale yellow powder.

^{1}H NMR (400 MHz, DMSO-d6) δ 13.10 (s, 1H), 10.23 (s, 1H), 8.36 (s, 1H), 8.05 (d, J = 8.9 Hz, 1H), 7.56 (d, J = 9.0 Hz, 1H), 7.53 - 7.42 (m, 2H), 7.36 (d, J = 8.0 Hz, 1H), 7.22 (t, J = 7.5 Hz, 1H), 5.41 (t, J = 9.0 Hz, 1H), 5.13 (s, 2H), 3.76 (t, J = 10.3 Hz, 1H), 3.67 (dd, J = 10.5, 8.4 Hz, 1H).

^{13}C NMR (101 MHz, DMSO) δ 171.58, 164.88, 159.09, 153.70, 148.65, 139.10, 138.52, 137.00, 130.98, 130.62, 127.49, 125.53, 124.82, 119.34, 119.27, 110.49, 78.59, 62.30, 35.19.

LC-MS $[M+H]^+$ m/z calcd. for $[C_{19}H_{15}N_6O_4S_2]^+$ 455.0 found 455.1 at 1.02 min. (UV Detector: TIC) and $[M-1]^-$ m/z calcd. for $[C_{19}H_{13}N_6O_4S_2]^-$ 453.0, found 453.2 at 1.02 min. (UV Detector: TIC) (LC-MS method b).

Compound 31: (S)-2-(6-azidobenzo[d]thiazol-2-yl)-4,5-dihydrothiazole-4-carboxylic acid

The tithe compound was prepared following a literature procedure.[207]
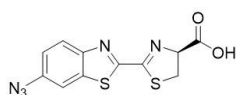
A mixture of **Intermediate 42** (100 mg, 0.497 mmol) and D-Cystein (120 mg, 0.994 mmol) in MeOH (2 mL), Water (2.0 mL) and DCM (2.0 mL) was stirred at R.T. under Argon in the dark for 2h. AcOH (200 µl) and HCl (4M) (0.5 mL) were added to the reaction mixture. The mixture was filtered and the filter cake was washed with DCM and EA. The obtained solid was placed under HV O/N to afford the desired product, compound **30** (110 mg, 0.353 mmol, 71.0 % yield) as a pale yellow powder. The analyses are consistent with the desired product and the literature data.

^{1}H NMR (400 MHz, DMSO-d6) δ 13.21 (s, 1H), 8.16 (d, J = 8.8 Hz, 1H), 8.06 (d, J = 2.2 Hz, 1H), 7.32 (dd, J = 8.8, 2.3 Hz, 1H), 5.43 (dd, J = 9.7, 8.4 Hz, 1H), 3.83 - 3.73 (m, 1H), 3.69 (dd, J = 11.3, 8.3 Hz, 1H).

LC-MS [M+H]$^+$ m/z calcd. for [C$_{11}$H$_8$N$_5$O$_2$S$_2$]$^+$ 306.0 found 306.0 at 0.88 min. (UV Detector: TIC) and [M-1]$^-$ m/z calcd. for [C$_{11}$H$_6$N$_5$O$_2$S$_2$]$^-$ 304.0, found 304.0 at 0.88 min. (UV Detector: TIC) (LC-MS method b).

Compound 32
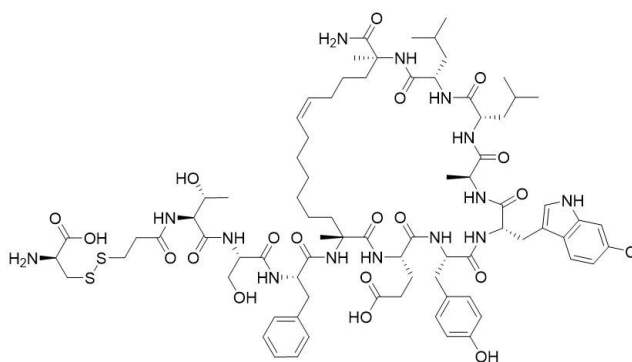
A solution of **Intermediate 9** (22 mg, 0.014 mmol) and DIPEA (22.04 µl, 0.126 mmol) in DMF (2 mL) was added to a solution of SPDP (7.3 mg, 0.023 mmol) in ACN (4 mL) at room temperature. After 3 h, the reaction was recharged with a solution of SPDP (2.1 mg, 6.72 µmol) in ACN (0.07 mL) and stirred for 2 h. A solution of BOC-D-Cys (0.2 M in ACN) (155 µl, 0.031 mmol) was added, and the reaction was allowed to proceed for 10 min at room temperature before being evaporated to dryness. Next, 95% TFA (500 µl, 6.17 mmol) was added to the crude material, and the deprotected compound was stirred for 10 min before purification through prep. HPLC. The purified compound was lyophilized to obtain **Compound 32** (6.2 mg, 3.61 µmol, 26% yiled) as a white solid.

LC-MS [M+H]$^+$ m/z calc. for [C$_{79}$H$_{114}$ClN$_{14}$O$_{19}$S$_2$] 1661.7, found 1661.7, found at 5.77 min. (UV Detector: TIC) (LC-MS method 3).

Compound 33
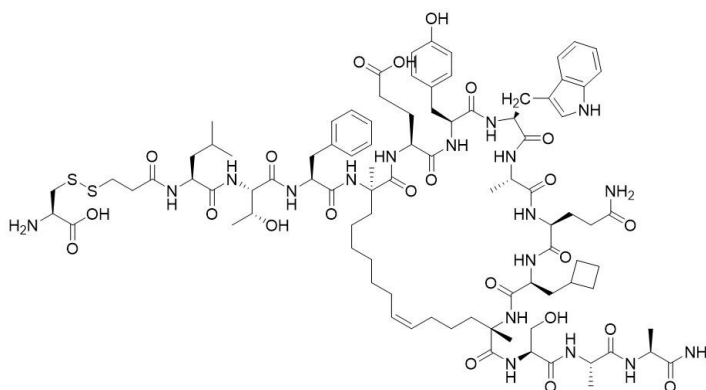
3-(pyridin-2-yldisulfaneyl)propanoic acid [68617-64-1] (Fluorochem) (5.12 mg, 0.016 mmol) was dissolved in DMA (100 µL) and TPTU (43mg, 0.015 mmol) and DIEA (13µl, 0.073 mmol) were added. The reaction was stirred at R.T> for 10 min. The reaction was added to a solution of Intermediate 10 (20.03 mg, 10.36 µmol) in DMA (1 mL) and the resulting solution was stirred at R.T. 10 min. Boc-D-Cys-OH (10% in NMP) (2.293 mg, 10.36 µmol) was added and the reaction was run 2 min at R.T. 95% TFA was added to the mixture and after 10 min. The reaction was directly injected in the prep. HPLC for purification. The fractions containing the desired product were lyophilize to obtain compound 33 (8.14mg, 3.94 µmol, 38% of yield) as a white solid.

LC-MS [M+H]$^+$ m/z calc. for [C$_{91}$H$_{133}$N$_{18}$O$_{23}$S$_2$] 1910.0, found 1910.0 at 5.75 min (UV Detector: TIC) (LC-MS method c).

Compound 34
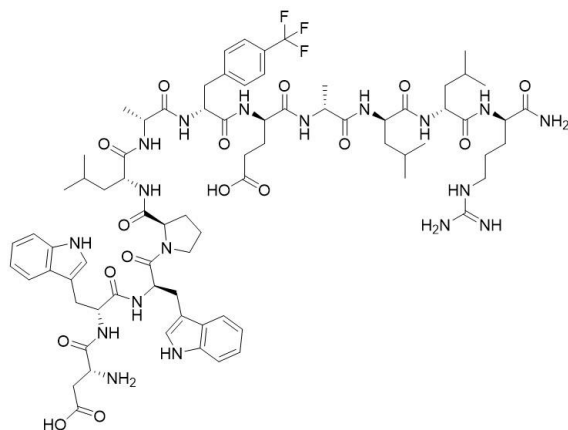
The linear peptide was Aurigene Discovery Ltd. India.

Compound 35:
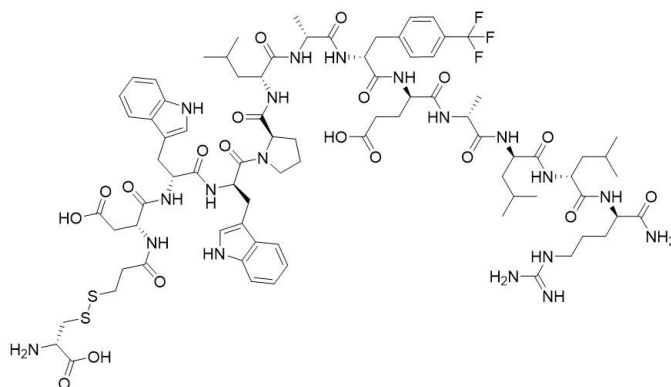
A solution of **Compound 34** (20 mg, 0.011 mmol) in DMF (3 mL) was added dropwise to a solution of SPDP (4.83 mg, 0.015 mmol) and DIPEA (14.46 µl, 0.083 mmol) in ACN (3 mL). The reaction was stirred at room temperature for 3 h. BOC-D-Cys (0.181 M in ACN) (91 µl, 0.017 mmol) was added to the stirring reaction mixture, which turned yellow. The reaction mixture was stirred at room temperature for 1 h and then evaporated to dryness. Next, 95% TFA (500 µL, 6.17 mmol) was added, and the reaction was stirred for 1 min at room temperature before purification through prep. HPLC

to obtain after lyophilization of the fractions containing the desired product, compound **35** (8.1 mg, 4.26 µmol, 39% yield) as a white solid.

LC-MS [M+H]$^+$ m/z calc. for [C$_{82}$H$_{115}$F$_3$N$_{19}$O$_{19}$S$_2$] 1790.8005, found 1790.8075 at 5.77min (UV Detector: TIC) (LC-MS method c).

Intermediate 33: (*E*)-cyclooct-2-en-1-yl (2-cyanobenzo[d]thiazol-6-yl)carbamate
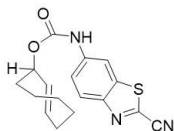
A sealed vial containing dry toluene (5.5 mL) was charged with 6-aminobenzo[d]thiazole-2-carbonitrile (90 mg, 0.514 mmol), triphosgene (168 mg, 0.565 mmol) and DMAP (126 mg, 1.027 mmol). The reaction was placed under Argon and then heated at 120°C for 3 hours. The reaction was allowed to reach R.T. A solution of **Intermediate 44** (162 mg, 1.284 mmol) in dry DMF (2 mL) was added and the reaction was stirred for 2h at 50°C. The reaction was evaporate to obtain an oil which was re-dissolved in 50% MeOH/DCM (5 mL). The solution was adsorbed on silica. The crude was purified via flash chromatography (silica column 12g, ethyl acetate /cyclohexane mobile phase) to obtain **Intermediate 33** (132 mg, 0.403 mmol, 78 % yield) as a yellow solid.

^{1}H NMR (600 MHz, Chloroform-*d*) δ 8.44 (s, 1H), 8.09 (d, *J* = 8.9 Hz, 1H), 7.32 (dd, *J* = 9.0, 2.2 Hz, 1H), 6.88 (s, 1H), 5.84 (ddd, *J* = 15.6, 11.1, 3.9 Hz, 1H), 5.57 (ddd, *J* = 25.7, 16.3, 9.4 Hz, 1H), 5.21 (td, *J* = 10.0, 5.6 Hz, 1H), 2.29 (dt, *J* = 12.3, 5.4 Hz, 1H), 2.05 − 1.82 (m, 3H), 1.65 − 1.34 (m, 4H), 0.88 (dddd, *J* = 33.2, 20.4, 13.7, 6.5 Hz, 2H).

LC-MS [M+H]$^+$ m/z calcd. for [C$_{17}$H$_{18}$N$_3$O$_2$S]$^+$ 328.1, found 328.2 at 1.26 min. (UV Detector: TIC) and [M-1]$^-$ m/z calcd. for [C$_{17}$H$_{16}$N$_3$O$_2$S]$^-$ 326.1, found 326.2 at 1.26 min. (UV Detector: TIC) (LC-MS method b).

Intermediate 34: (*E*)-cyclooct-2-en-1-yl (2-cyanobenzo[d]thiazol-6-yl)carbamate
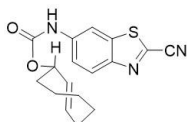
A sealed vial containing dry toluene (3.3 mL) was charged with 6-aminobenzo[d]thiazole-2-carbonitrile (55 mg, 0.314 mmol), triphosgene (93 mg, 0.314 mmol) and DMAP (77 mg, 0.628 mmol). The reaction was placed under Argon and then heated at 120°C for 3 hours. The reaction was allowed to reach R.T. A solution of **Intermediate 45** (100 mg, 0.792 mmol) in dry DCM (6 mL) was added to the reaction. The reaction was heated at 50°C O/N. The reaction was evaporate to obtain an oil which was subsequently re-dissolved in 50% MeOH/DCM (5 mL). The solution was adsorbed on silica. The crude was purified via flash chromatography (silica column 12g, ethyl acetate /cyclohexane mobile) to obtain **Intermediate 34** (110 mg, 0.33 mmol., 97% UV purity, full conversion).

LC-MS [M+H]$^+$ m/z calcd. for [C$_{17}$H$_{18}$N$_3$O$_2$S]$^+$ 328.1, found 328.1 at 5.43 min. (UV Detector: TIC) and [M-1]$^-$ m/z calcd. for [C$_{17}$H$_{16}$N$_3$O$_2$S]$^-$ 326.1, found 326.1 at 5.43 min. (UV Detector: TIC) (LC-MS method a).

Intermediate 44 (racemic mixture equatorial alcohol) and **Intermediate 45** (racemic mixture axial alcohol) E)-cyclooct-2-en-1-ol:

A solution of **Intermediate 46** (5 g, 39.6 mmol), methyl benzoate (4.99 mL, 39.6 mmol) and Dodecane (0.93g, 39.6 mmol) (internal standard) in a mixture of diethyl ether (450 mL) and hexane (50 mL) was pumped through the Photo Flow reactor system with a maximum flow rate of 45 mL/min and irradiated with a 400 W Hg medium pressure lamp for 10.5h. The reaction was monitored with GC calculating the disappearance of the starting material using the internal standard as reference. The system was flushed with 900 mL Et$_2$O/hexane 9:1 (45 mL/min). The column was dried with nitrogen for 1.5 h, then unpacked and slurred for 5 min with 33% aq. NH3 solution (600 mL) and DCM (600 mL). After filtration, the aq. phase was washed with another 300 mL DCM, then the combined organic phases were washed with water (300 mL), dried over sodium sulfate, filtered and concentrated at reduce pressure (400 mbar) and 30°C to yield a yellow oil. The crude material was purified via flash (120 g silica gel column, EtOAc/heptane mobile phase) to afford **Intermediate 44** and (1.78 g, 13.40 mmol, 33% of yield) ((diastereoisomers mixture, equatorial alcohol) as a colorless oil and **Intermediate 45** (1.93 g, 14.53 mmol, 37% yiled) (diastereoisomers mixture, axial alcohol) as a colorless oil.

Intermediate 44 (E)-cyclooct-2-en-1-ol (racemic mixture equatorial alcohol)

^{1}H NMR (400 MHz, Chloroform-*d*) δ 5.96 (dddd, *J* = 16.3, 11.2, 3.8, 1.2 Hz, 1H), 5.58 (dd, *J* = 16.5, 2.4 Hz, 1H), 4.61 (dt, *J* = 3.5, 1.7 Hz, 1H), 2.49 (dtd, *J* = 10.9, 3.8, 1.8 Hz, 1H), 2.11 – 1.91 (m, 3H), 1.85 (dddt, *J* = 14.9, 11.2, 5.4, 1.8 Hz, 1H), 1.73 – 1.41 (m, 4H), 1.19 – 1.05 (m, 1H), 0.83 – 0.71 (m, 1H). (consistent with literature data).

Intermediate 45 (E)-cyclooct-2-en-1-ol (racemic mixture axial alcohol)

^{1}H NMR (400 MHz, Chloroform-*d*) δ 5.66 (ddd, *J* = 16.2, 10.7, 3.7 Hz, 1H), 5.54 (dd, *J* = 16.2, 9.1 Hz, 1H), 4.26 (td, *J* = 9.5, 5.6 Hz, 1H), 2.40 (dddd, *J* = 8.6, 5.4, 4.5, 1.5 Hz, 1H), 2.21 – 2.11 (m, 1H), 2.02 – 1.72 (m, 5H), 1.56 – 1.36 (m, 2H), 0.91 – 0.83 (m, 2H).

Intermediate 46: (*Z*)-cyclooct-2-en-1-ol

A solution of **Intermediate 47** (25.5 g, 135 mmol) in acetone (200 mL) and NaHCO3 (28.3 g, 337 mmol) dissolved in water (100 mL) was refluxed for 2 h. The solid was filtrated off and the solution was concentrated. Diethyl ether was added to extract the product. The ethereal phase was separated, dried with MgSO$_4$ and concentrated. The crude product was vacuum distilled to afford **Intermediate 46** (13.9 g, 110 mmol, 82 % yield).

^{1}H NMR (400 MHz, Chloroform-*d*) δ 5.69 – 5.39 (m, 2H), 4.64 (dt, *J* = 10.4, 5.5 Hz, 1H), 2.31 – 2.01 (m, 2H), 1.90 (ddt, *J* = 11.8, 5.2, 2.7 Hz, 1H), 1.73 – 1.29 (m, 8H).

^{13}C NMR (101 MHz, CDCl3) δ 134.88, 128.54, 69.42, 38.71, 29.19, 26.37, 25.89, 23.67.

Intermediate 47: (Z)-3-bromocyclooct-1-ene

Dibenzoyl peroxide (200 mg, 0.826 mmol) was added to a solution of (Z)-cyclooctene (50 mL, 385 mmol) and NBS (6.8g, 385 mmol) in CCl$_4$ (250 mL) and the reaction was heated under reflux for 1h. The mixture was cooled to 0°C and filtered. The filtrated organic solution was washed with H$_2$O, 5% NaHCO$_3$ and concentrate under vacuum to obtain an oil residue. The crude material was purified via fractional distillation under reduced pressure (4mbar) at 82°C to obtain the desired product **Intermediate 47** (25.536 g, 135 mmol, 35 % yield) as a yellow oil.

^{1}H NMR (400 MHz, Chloroform-d) δ 5.78 (ddd, J = 10.1, 8.3, 1.4 Hz, 1H), 5.59 (dddd, J = 10.5, 8.9, 7.5, 1.3 Hz, 1H), 5.00 – 4.88 (m, 1H), 2.32 – 2.05 (m, 3H), 1.99 (ddt, J = 13.4, 12.2, 5.1 Hz, 1H), 1.75 – 1.44 (m, 4H), 1.35 (dtdd, J = 24.7, 12.5, 6.5, 3.2 Hz, 2H).

^{13}C NMR (101 MHz, CDCl3) δ 132.49, 129.09, 48.26, 40.26, 28.53, 25.57 (chemical shift reported from HSQC).

Intermediate 35: 3-methyl-6-(methylthio)-1,2,4,5-tetrazine
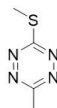
A mixture of MeI (7.78 mL, 124 mmol) in Ethanol (50 mL) was added drop-wise to a mixture of Thiocarbohydrazide (12 g, 113 mmol) in Ethanol (350 mL) at reflux. The solution was allowed to reflux for 1 h and then filtered hot using a C type filter crucible. The filtrate was allowed to cool to room temperature and the product was precipitated out of solution in a fridge. The solution was decanted away and the product was dried in vacuo to obtain **Intermediate 48** (17.5 g, 146 mmol, 129 % yield) which was used in the next synthetic step without any purification.

Intermediate 48 (6 g, 49.9 mmol) was dissolved in Ethanol (150 mL). Triethyl orthoacetate (10.12 mL, 54.9 mmol) was added forming a yellow solution. TEA (6.96 mL, 49.9 mmol) was added, turning the solution a light pink. The solution was refluxed for 30 min. NaNO$_2$ (3.44 g, 49.9 mmol) followed by TFA (3.85 mL, 49.9 mmol) were added and heating was continued for an additional 30 min turning the solution a deep red. The reaction was allowed to reach R.T. and hexane (150 mL) was added under a stream of air for purging developed gases. The solution was cooled to room temperature and water (300 mL) was added. The mixture was extracted with ether (300 mL x 2) and the resulting organic phase was dried with MgSO$_4$ and evaporated to obtain a residue. The crude was purified via flash chromatography (silica column 24g, hexane/diethyl ether mobile phase) to afford the desired product, **Intermediate 35** (414 mg, 2.91 mmol, 6 % yield over two steps) as a red oil.

^{1}H NMR (400 MHz, Chloroform-d) δ 2.97 (s, 3H), 2.72 (s, 3H).

^{13}C NMR (101 MHz, CDCl3) δ 21.33, 13.94 (chemical shift reported from HSQC).

Intermediate 36: 4-azidobenzyl (2-cyanobenzo[d]thiazol-6-yl)carbamate
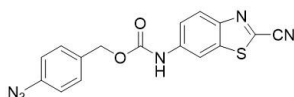
To a mixture of 6-aminobenzo[d]thiazole-2-carbonitrile (140 mg, 0.8 mmol) and DIPEA (0.559 mL, 3.20 mmol) in anhydrous Toluene (8 mL) at 0°C under argon was added dropwise a solution of triphosgene (285 mg, 0.960 mmol) in Toluene (2 mL) over 2h in a sealed vial. After the addition, the reaction was heated at 120°C for 2h. The reaction was allowed to reach room temperature and DCM (5 mL) was added. The mixture was stirred for 20min. DMAP (48.9 mg, 0.400 mmol), **Intermediate 49** (119 mg, 0.800 mmol) and DMF (2 mL) were added and the resulting solution was heated at 50°C for 3h. The reaction was concentrated in vacuum to obtain a residue. EA (100 mL) was added and the organic solution was washed with NaHCO$_3$ aqueous saturated solution (70 mL x 3) and brine (70 mL), dried with MgSO$_4$ and evaporated to dryness to obtain a crude. The crude was purified via flash chromatography (silica column 40g, MeOH/DCM mobile phase) to obtain **Intermediate 36** (244 mg, 0.696 mmol, 87 % yield) as a pale yellow solid.

LC-MS [M+H]$^+$ m/z calcd. for [C$_{16}$H$_{11}$N$_6$O$_2$S]$^+$ 350.0, found 351.1 at 1.25 min. (UV Detector: TIC) and [M-1]$^-$ m/z calcd. for [C$_{16}$H$_9$N$_6$O$_2$S]$^-$ 349.0, found 349.1 at 5.43 min. (UV Detector: TIC) (LC-MS method b).

Intermediate 49: (4-azidophenyl)methanol
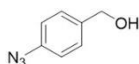
4-aminobenzyl alcohol (597 mg, 4.85 mmol) was dissolved in Hydrochloric Acid (4M) (Volume: 6 mL), the yellow-brown solution was cooled to 0°C with an ice bath then a solution of NaNO$_2$ (360 mg, 5.22 mmol) in water (10 mL) was added dropwise. After 0.5 h, NaN$_3$ (1.37 g, 21.07 mmol) was added slowly in portion at 0°C. A brown solid has precipitated. After 1.5 h, the reaction was poured into an ice-water slurry (150 mL). The quenched solution was adjusted to pH=8 by adding NaHCO$_3$. The mixture was extracted with EA (2 x 150 mL). The organic phases were washed with water (3x70 mL), dried over MgSO$_4$ and evaporated avoiding heating the water bath. The brown residue was suspended in hexane (ca. 20 mL) and vigorously stirred for 20min. The mixture was placed at 4 °C overnight to form a precipitate. The solid was filtered and washed with cold Hexane to afford desired product (515 mg, 3.42 mmol, 70% yield) as light brown needles.

^{1}H NMR (400 MHz, Chloroform-*d*) δ 7.43 – 7.32 (m, 2H), 7.09 – 6.92 (m, 2H), 4.68 (s, 2H).

^{13}C NMR (101 MHz, CDCl$_3$) δ 127.87, 77.16, 118.47, 64.15 (by HSQC)

IR spectra was recorded showing peak at 2114 cm-1.

Intermediate 37 4-azido-2-fluorobenzyl (2-cyanobenzo[d]thiazol-6-yl)carbamate
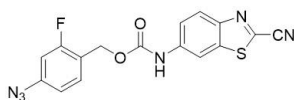
To a solution of (4-azido-2-fluorophenyl)methanol from FCH Group Co. (150 mg, 0.897 mmol) and TEA (0.500 mL, 3.59 mmol) in DCM (8 mL) at 0°C under Argon was added a solution of **Intermediate 50** (181 mg, 0.897 mmol) in DMF (4 mL). The reaction was stirred at 0°C under argon for 1h. After, it was allowed to reach R.T. and was stirred at R.T. for 14h. The reaction mixture was poured in DCM (80 mL) to obtain a solution. The solution was washed with NaHCO$_3$ saturated aqueous solution (80 mL x 2), brine (80 mL x 2), dried with MgSO$_4$ and evaporated to dryness to obtain the crude material as a solid. The crude was purified via flash chromatography (silica column 24g, EA/Hexane mobile phase) to afford after

solvent evaporation a solid which was dissolved 10% EA/DCM. The solution was filtered through a plug of silica and evaporated to obtain the desired material **Intermediate 37** (250 mg, 0.679 mmol, 76 % yield).

^{1}H NMR (400 MHz, DMSO-d6) δ 10.36 (s, 1H), 8.51 (d, J = 2.0 Hz, 1H), 8.15 (d, J = 9.0 Hz, 1H), 7.65 (dd, J = 9.0, 2.1 Hz, 1H), 7.57 (t, J = 8.2 Hz, 1H), 7.10 (dd, J = 10.9, 2.2 Hz, 1H), 7.03 (dd, J = 8.2, 2.2 Hz, 1H), 5.21 (s, 2H).

^{13}C NMR (101 MHz, DMSO) δ 153.56, 147.73, 142.44, 140.26, 137.40, 133.20, 125.35, 120.49, 115.81, 114.08, 110.37, 107.49, 107.24, 60.48.

LC-MS [M+H]$^+$ m/z calcd. for [$C_{16}H_9FN_6O_2S$]$^+$ 369.0, found 369.0 at 1.24 min. (UV Detector: TIC) and [M-1]$^-$ m/z calcd. for [$C_{16}H_7FN_6O_2S$]$^-$ 367.0, found 367.1 at 1.24 min. (UV Detector: TIC) (LC-MS method a).

Intermediate 50: 6-isocyanatobenzo[d]thiazole-2-carbonitrile
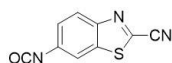
To a suspension of 6-aminobenzo[d]thiazole-2-carbonitrile (304 mg, 1.735 mmol) in Dioxane (11 mL) at R.T under Argon was added a solution of triphosgene (618 mg, 2.082 mmol) in Toluene (6.5 mL) drop-wise. The reaction was stirred for 1h at R.T. and then heated at reflux for 16h. The reaction went in solution. The reaction mixture was evaporated to dryness. Toluene (5 mL) was added to the solid and the suspension was evaporated to afford **Intermediate 50** (349 mg, 1.735 mmol, 100 % yield) as a white solid. A small amount of the solid was added to a solution of MeOH and TEA and the resulting solution was analyzed via LC-MS. The analysis showed the formation of the methyl (2-cyanobenzo[d]thiazol-6-yl)carbamate which confirmed the formation of the isocyanate desired product. The compound was used in the next synthetic step without any purification.

Intermediate 38 4-azido-2-chlorobenzyl (2-cyanobenzo[d]thiazol-6-yl)carbamate
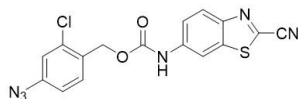
A solution of **Intermediate 50** (113 mg, 0.562 mmol) in DMF (1.5 mL Ratio: 1.000) was added drop-wise to a solution of **Intermediate 51** (166.5 mg, 0.907 mmol) and TEA (0.314 mL, 2.247 mmol) in DCM (3.5 mL) at 0°C under argon. The reaction was allowed to reach R.T. and was stirred for 18h. DCM (100 mL) and NaHCO₃ saturated aqueous solution (100 mL) were added. The organic phase was separated. The aq. phase was extracted with DCM (100 mL x 2) and the organic phases were combined, washed with brine (150 mL x 2), dried with MgSO₄ and evaporated to dryness to obtain a residue. The residue was purified via flash chromatgraphy (silica column 12g, Hexane/Ethyl acetate mobile phase) to obtain a solid which was triturated for 2h in MeOH to afford **Intermediate 38** (70 mg, 0.176 mmol, 31.4 % yield) as a pale yellow solid.

LC-MS [M+1]$^+$= 385 and [M-1]$^-$= 383 at 1.29 min. UV purity 97%.

^{1}H NMR (400 MHz, DMSO-d6) δ 10.41 (s, 1H), 8.52 (d, J = 2.0 Hz, 1H), 8.16 (d, J = 9.0 Hz, 1H), 7.67 (dd, J = 9.0, 2.1 Hz, 1H), 7.62 (d, J = 8.3 Hz, 1H), 7.30 (d, J = 2.3 Hz, 1H), 7.18 (dd, J = 8.3, 2.3 Hz, 1H), 5.25 (s, 2H).

<superscript>13</superscript>C NMR (101 MHz, DMSO) δ 153.50, 147.71, 141.68, 140.22, 137.37, 134.64, 132.66, 130.63, 125.32, 120.42, 118.67, 110.35, 63.74, 40.68

LC-MS [M+H]$^+$ m/z calcd. for [C$_{16}$H$_9$ClN$_6$O$_2$S]$^+$ 385.0, found 385.1 at 1.29 min. (UV Detector: TIC) and [M-1]$^-$ m/z calcd. for [C$_{16}$H$_7$ClN$_6$O$_2$S]$^-$ 383.0, found 383.2 at 1.29 min. (UV Detector: TIC) (LC-MS method a).

Intermediate 51: (4-azido-2-chlorophenyl)methanol
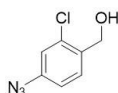
A suspension of (4-amino-2-chlorophenyl)methanol (0.452 g, 2.87 mmol) in HCl (4M) (5 mL, 20.00 mmol) was cooled at 0°C. A solution of NaNO$_2$ (0.218 g, 3.15 mmol) in Water (8.0 mL) was added. After 1h, NaN$_3$ (0.746 g, 11.47 mmol) was added portion wise. The reaction was allowed stirred at 0°C for 1.5h. THF (6 mL) was added and the reaction was stirred at 0°C for another 1h. The reaction was quenched pouring the reaction in ice water. The pH was adjusted to 8 by adding NaHCO$_3$ and NaOH (4M). The aq. solution was extracted with EA (100 mL x 3), dried with MgSO$_4$ and evaporated to dryness to obtain the desired product **Intermediate 51** (520 mg, 2.83 mmol, 99 % yield) as a yellow/brown solid.

^{1}H NMR (400 MHz, DMSO-d6) δ 7.53 (d, J = 8.3 Hz, 1H), 7.19 - 7.08 (m, 2H), 5.39 (s, 1H), 4.51 (s, 2H).

IR analysis showed a peak at 2112 cm^{-1} consistent with the azide.

Intermediate 39 4-azido-2-bromobenzyl (2-cyanobenzo[d]thiazol-6-yl)carbamate
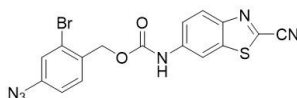
To a solution of **Intermediate 52** (228 mg, 1.002 mmol) and TEA (0.466 mL, 3.34 mmol) in DCM (7.5 mL) at 0°C under Argon was added a solution of **Intermediate 50** (168 mg, 0.835 mmol) in DMF (3 mL). The reaction was stirred at 0°C under argon for 1h in the dark and then it was allowed to reach R.T. and stirred for 14h. The reaction was poured in DCM (80 mL). The obtained solution was washed with NaHCO$_3$ aqueous saturated solution (80 mL x 2), brine (80 mL x 2), dried with MgSO$_4$ and evaporated to dryness to obtain the crude material as a solid. The crude was purified via Flash Chromatography (silica column, 40g, EA/DCM mobile phase) to obtain a solid after evaporation. The solid was dissolved 10% EA/DCM and the solution was filtered through a plug of silica to afford **Intermediate 39** (153 mg, 0.339 mmol, 40.6 % yield) as a white solid.

^{1}H NMR (400 MHz, DMSO-d6) δ 10.42 (s, 1H), 8.52 (d, J = 2.0 Hz, 1H), 8.16 (d, J = 9.0 Hz, 1H), 7.68 (dd, J = 9.0, 2.1 Hz, 1H), 7.60 (d, J = 8.3 Hz, 1H), 7.44 (d, J = 2.3 Hz, 1H), 7.21 (dd, J = 8.3, 2.3 Hz, 1H), 5.22 (s, 2H).

^{13}C NMR (101 MHz, DMSO) δ 153.51, 147.74, 141.65, 140.26, 137.41, 135.07, 132.53, 132.30, 125.36, 124.57, 123.50, 120.50, 119.20, 114.08, 110.39, 65.93.

LC-MS [M+H]$^+$ m/z calcd. for [C$_{16}$H$_{10}$BrN$_6$O$_2$S]$^+$ 429.0, found 429.0 at 1.32 min. (UV Detector: TIC) and [M-1]$^-$ m/z calcd. for [C$_{16}$H$_8$BrN$_6$O$_2$S]$^-$ 427.0, found 427.0 at 1.32 min. (UV Detector: TIC) (LC-MS method a).

Intermediate 52: (4-azido-2-bromophenyl)methanol

A mixture of **Intermediate 53** (514 mg, 2.54 mmol) in HCl (4M) (4.45 mL, 17.81 mmol) and THF (5.6 mL) was cooled at 0°C. A solution of $NaNO_2$ (193 mg, 2.80 mmol) in Water (5 mL) was added. The reaction was stirred at 0°C open flask for 1h. A solution of sodium azide (662 mg, 10.18 mmol) in Water (4 mL) was added drop-wise. The reaction was allowed stirred at 0°C for 30 min and at R.T. for 2h. The reaction was quenched pouring the reaction in ice water. The pH was adjusted to 8 by adding $NaHCO_3$ aqueous saturated solution. The solution was extracted with DCM (3x 80 mL) and after combining the organic solution a washed with Brine (150 mL) was performed. The organic solution was dried with $MgSO_4$ and evaporated to dryness to obtain **Intermediate 52** (575 mg, 2.52 mmol, 99 % yield) as a yellow solid.

^{1}H NMR (400 MHz, DMSO-d6) δ 7.52 (d, J = 8.3 Hz, 1H), 7.31 (d, J = 2.3 Hz, 1H), 7.16 (dd, J = 8.3, 2.3 Hz, 1H), 5.43 (t, J = 5.5 Hz, 1H), 4.47 (d, J = 5.0 Hz, 2H).

^{13}C NMR (101 MHz, DMSO) δ 139.68, 138.30, 129.74, 122.78, 122.13, 118.85, 62.64.

Intermediate 53: (4-amino-2-bromophenyl)methanol
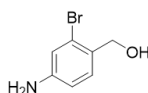
$NiCl_2$ (0.048 g, 0.2 mmol) was added to a solution of **Intermediate 54** (0.638 g, 2.75 mmol) in Acetonitrile (8.4 mL) and Water (0.8 mL). The reaction was stirred 5min at R.T. and $NaBH_4$ (0.416 g, 11.00 mmol) was added portion wise. Evolution of gas and a black precipitate formation were observed. The reaction was stirred at R.T. for 5min. The reaction was poured in DCM (70 mL) and water (50 mL) was added. The organic phase was separated and the aq. phase was extracted with DCM (60 mL x 2). The organic phases were combined, dried with $MgSO_4$ and evaporated to obtain **Intermediate 53** (514 mg, 2.54 mmol, 93 % yield) as a white solid.

^{1}H NMR (400 MHz, DMSO-d6) δ 7.10 (d, J = 8.2 Hz, 1H), 6.75 (d, J = 2.2 Hz, 1H), 6.52 (dd, J = 8.2, 2.2 Hz, 1H), 5.22 (s, 2H), 4.95 (t, J = 5.6 Hz, 1H), 4.33 (d, J = 5.6 Hz, 2H).

LC-MS [M+H]$^+$ m/z calcd. for $[C_7H_9BrNO]^+$ 201.1, found 202.0 at 0.54 min. (UV Detector: TIC) (LC-MS method a).

Intermediate 54: (2-bromo-4-nitrophenyl)methanol
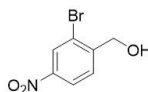
Borane-methyl sulfide complex in THF (12 mL, 24.00 mmol) was added to a solution of 2-bromo-4-nitrobenzoic acid [16426-64-5] from Combi-Blocks Inc. (2 g, 8.13 mmol) and TEA (1.2 mL, 8.61 mmol) in THF (60 mL) at 0°C. The reaction was allowed to reach R.T. and then heated at 70°C O/N. The reaction was cooled to reach R.T. and water (30 mL) was added followed by HCl (2M) to reach pH=1. The reaction was heated at reflux for 30min. and then cooled to R.T. DCM (200 mL) was added. The organic phase was separated. The aq. phase was extracted with DCM (150 mL x 2). The organic phases were combined, washed with brine (300 mL), dried with $MgSO_4$, evaporated and placed under HV for 2 days to obtain **Intermediate 54** (1.81 g, 7.49 mmol, 92 % yield).

^{1}H NMR (400 MHz, Chloroform-d) δ 8.40 (d, J = 2.2 Hz, 1H), 8.21 (dd, J = 8.5, 2.2 Hz, 1H), 7.76 (d, J = 8.5 Hz, 1H), 4.83 (s, 2H).

Intermediate 40 (5-azidopyridin-2-yl)methyl (2-cyanobenzo[d]thiazol-6-yl)carbamate
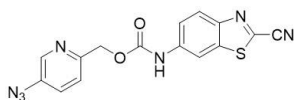
To a solution of **Intermediate 55** (130 mg, 0.866 mmol) and TEA (0.483 mL, 3.46 mmol) in DCM (7 mL) at 0°C under Argon was added a solution of **Intermediate 50** (174 mg, 0.866 mmol) in DMF (2.8 mL). The reaction was stirred at 0°C for 10min. and then at R.T. in the dark for 2h. The reaction was poured in DCM (50 mL) and NaHCO$_3$ saturated aqueous solution (40 mL) was added. The organic phase was separated. The aq. phase was extracted with DCM (30 mL x 2). The organic phases were combined, washed with brine (70 mL x 2), dried with MgSO$_4$ and evaporated to dryness to obtain the crude as pale yellow solid. The crude was purified via flash chromatography (silica column 24g, MeOH/DCM mobile phase) to obtain **Intermediate 40** (223 mg, 0.590 mmol, 68.2 % yield) as a pale yellow solid.

^{1}H NMR (400 MHz, DMSO-d6) δ 10.45 (s, 1H), 8.51 (d, J = 2.0 Hz, 1H), 8.37 (d, J = 2.6 Hz, 1H), 8.17 (d, J = 9.0 Hz, 1H), 7.67 (ddd, J = 8.3, 4.8, 2.4 Hz, 2H), 7.53 (d, J = 8.4 Hz, 1H), 5.25 (s, 2H).

^{13}C NMR (101 MHz, DMSO) δ 153.61, 152.69, 147.74, 141.04, 140.31, 137.41, 136.60, 135.06, 127.77, 125.37, 123.41, 120.52, 114.08, 110.40, 66.79.

LC-MS [M+H]$^+$ m/z calcd. for [C$_{15}$H$_{10}$N$_7$O$_2$S]$^+$ 352.0, found 352.1 at 1.03 min. (UV Detector: TIC) and [M-1]$^-$ m/z calcd. for [C$_{15}$H$_8$N$_7$O$_2$S]$^-$ 350.0, found 350.0 at 1.03 min. (UV Detector: TIC) (LC-MS method a).

Intermediate 55: (5-azidopyridin-2-yl)methanol
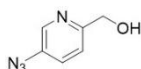
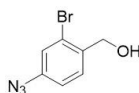A solution of **Intermediate 56** (230 mg, 1.853 mmol) in HCl (4M) (5 mL, 20.00 mmol) was cooled at 0°C. A solution of NaNO$_2$ (153 mg, 2.223 mmol) in Water (2 mL) was added drop-wise. The reaction was stirred for 1h at 0°C open flask. A solution of NaN$_3$ (482 mg, 7.41 mmol) in Water (3 mL) was added drop-wise and the reaction was stirred at 0°C for 30min. The reaction was allowed to reach R.T. and was stirred for 1h. The mixture was poured in ice water. NaHCO$_3$ aqueous saturated solution was added to reach pH=8. The aq. sol. was extracted with DCM (70 mL x 3). The organic phase were combined, washed with brine (100 mL), dried with MgSO$_4$ and evaporated to obtain **Intermediate 55** (223 mg, 1.381 mmol, 74.6 % yield).

^{1}H NMR (400 MHz, DMSO-d6) δ 8.26 (d, J = 2.6 Hz, 1H), 7.61 (dd, J = 8.4, 2.7 Hz, 1H), 7.48 (d, J = 8.4 Hz, 1H), 5.43 (t, J = 5.6 Hz, 1H), 4.53 (d, J = 5.1 Hz, 2H).

^{13}C NMR (101 MHz, DMSO) δ 159.06, 140.21, 135.22, 127.46, 121.56, 64.29.

LC-MS [M+H]$^+$ m/z calcd. for [C$_6$H$_7$N$_4$O]$^+$ 151.0, found 151.1 at 0.50 min. (UV Detector: TIC) (UV Detector: TIC) (LC-MS method a).

Intermediate 56: (5-aminopyridin-2-yl)methanol
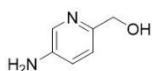
To a 100 mL two necked round bottom flask was added methyl 5-aminopicolinate [67515-76-8] from Synnovator Inc. (0.650 g, 4.27 mmol) in THF (14.2 mL). The mixture was placed under Argon and cooled in an ice bath. Lithium aluminum hydride in THF (2M) (6.41 mL, 12.82 mmol) was added drop-wise and the mixture was stirred at 0°C under Argon for 1h, then the reaction was allowed to reach R.T. and was stirred for 2h. Next, the reaction was cooled at 0°C and a NH$_4$Cl saturated aqueous solution (15 mL) was added. Water (50 mL) and EA (150 mL) were added. The mixture was poured in a solution of Rochelle salt (50 mL) and stirred for 20min. The organic phase was separated and the aq. phase was extracted with EA (3 x 100 mL). Next, the organic phase were combined, dried with MgSO$_4$ and evaporated to obtain the desired product as brown oil. The crude material was purified via flash chromatography (silica column 24g, MeOH/DCM mobile phase) to obtain after purification **Intermediate 56** (0.232 g, 1.869 mmol, 43.7 % yield).

^{1}H NMR (400 MHz, DMSO-d6) δ 7.82 (d, J = 2.6 Hz, 1H), 7.07 (d, J = 8.3 Hz, 1H), 6.90 (dd, J = 8.3, 2.7 Hz, 1H), 5.12 (s, 2H), 4.99 (s, 1H), 4.35 (s, 2H).

Intermediate 41 2-azidobenzyl (2-cyanobenzo[d]thiazol-6-yl)carbamate
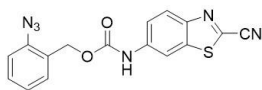
To a mixture of 6-aminobenzo[d]thiazole-2-carbonitrile (132 mg, 0.753 mmol) and DIPEA (0.526 mL, 3.01 mmol) in anhydrous Toluene (8 mL) at 0°C under argon in a sealed vial was added dropwise a solution of triphosgene (268 mg, 0.904 mmol) in Toluene (2 mL). The reaction mixture was heated at 120°C for 2h and then allowed to reach room temperature. DCM (5 mL) was added to the reaction mixture and the solution was stirred for 10min. DMAP (46.0 mg, 0.377 mmol), (2-azidophenyl)methanol from Enamine (169 mg, 1.130 mmol) and DMF (2 mL) were added to the reaction and the resultant solution was heated at 70°C for 3h. The reaction mixture was concentrated in vacuum to obtain a residue. EA (100 mL) was added. The organic solution was washed with NaHCO$_3$ saturated aqueous solution (70 mL x 3) and brine (70 mL), dried with MgSO$_4$ and evaporated to dryness to obtain the crude material. The crude was purified via flash chromatography (silica column 24g, MeOH/DCM mobile phase) to obtain after solvent evaporation under reduced pressure the desired product INTERMEDIATE 41 (104 mg, 0.297 mmol, 39.4 % yield) as a pale yellow solid.

LC-MS [M+1]+=351 at 1.21 min.

^{1}H NMR (400 MHz, DMSO-d6) δ 10.35 (s, 1H), 8.51 (d, J = 2.0 Hz, 1H), 8.15 (d, J = 9.0 Hz, 1H), 7.66 (dd, J = 9.1, 2.1 Hz, 1H), 7.53 - 7.42 (m, 2H), 7.37 (d, J = 7.2 Hz, 1H), 7.22 (td, J = 7.5, 1.0 Hz, 1H), 5.14 (s, 2H).

LC-MS [M+H]$^+$ m/z calcd. for [C$_{16}$H$_{11}$N$_6$O$_2$S]$^+$ 351.0, found 351.1 at 1.21 min. (UV Detector: TIC) and [M-1]$^-$ m/z calcd. for [C$_{16}$H$_9$N$_6$O$_2$S]$^-$ 349.0, found 349.1 at 1.21 min. (UV Detector: TIC) (LC-MS method a).

Intermediate 42: 6-azidobenzo[d]thiazole-2-carbonitrile

The title compound was prepared following a literature procedure.[207]
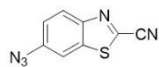
To a mixture of 6-aminobenzo[d]thiazole-2-carbonitrile (0.3 g, 1.712 mmol) and HCl (4M) (25.7 mL, 103 mmol) in ice bath was added solution of $NaNO_2$ (0.236 g, 3.42 mmol) in Water (6 mL) via a syringe pump (12 mL/h). The reaction was stirred in the ice bath for 1h. A solution of NaN_3 (0.445 g, 6.85 mmol) in Water (11.0 mL) was added drop-wise. The reaction was allowed to reach R.T. and was stirred for 3h. A solid precipitated.The solid was filtered and washed with water (20 mL x 2) before drying under high vacuum O/N to obtain **Intermediate 42** (312 mg, 1.551 mmol, 91 % yield) as a pale yellow solid. The analysis is consistent with the reported literature data.

^{1}H NMR (400 MHz, Chloroform-d) δ 8.18 (d, J = 8.9 Hz, 1H), 7.59 (d, J = 2.1 Hz, 1H), 7.31 (dd, J = 8.9, 2.2 Hz, 1H).

LC-MS [M+H]$^+$ m/z calcd. for $[C_8H_4N_5S]^+$ 202.0, found 202.1 at 1.0 min. (UV Detector: TIC) (LC-MS method a).

Chapter 5. Conclusion

5.1 Achieved results

Well-validated chemical probes play a key role in the drug discovery process. These compounds enable testing of biological hypotheses, investigation of target tractability and translatability to the clinical phase. Their validation in disease cellular models is a key step before engaging these molecules in pharmacological studies in more complex model systems such as tissues or animals.

Bioorthogonal probes offer some advantages compared to the classical chemical probes. Not only can these molecules trigger a functional response similar to a classical chemical probe, but they can also be engaged in reactions with chemical reporters to provide further information about selected disease cellular models.

Herein, we selected the Mdm2-p53 interaction inhibition as a biological model for bioorthogonal probe design and their validation in osteosarcoma cells. We chose a published inhibitor chemical series to build our bioorthogonal probes. The compounds were functionalized on an exit vector pointing toward the solvent with strained alkenes and azide to enable EID-DA and SPAAC reaction in cells respectively. Their biochemical and cellular activities were confirmed along with an excellent selectivity profile against Mdm4.

Next, we built a set of assays based on a "two step" fluorescence imaging approach which enables the investigation of the permeability of the bioorthogonal probes, their target engagement and occupancy. These assays were developed using a toolbox of reactive fluorophores enabling the bioorthogonal staining of the compounds in situ.
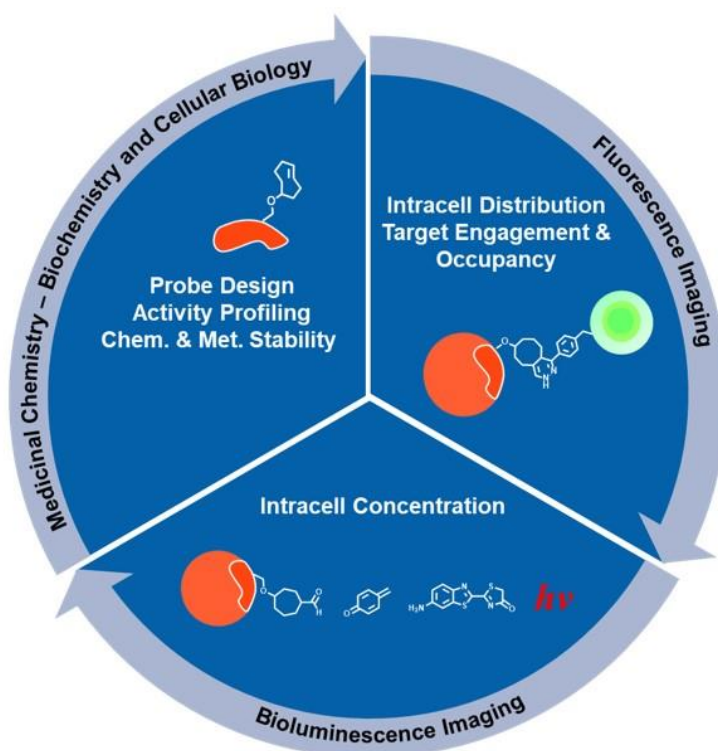
Finally, we explored two BLI approaches to accurately measure the intracellular concentration of the bioorthogonal probes either by in situ de-caging of a masked luciferin reporter (via 1,3-dipolarcycloaddition) or by releasing a label (D-Cys) resulting in intracellular synthesis of the luciferin reporter.

From the probe designs evaluated, we identified the TCO group as a privileged label for our bioorthogonal probes enabling investigation of the compound uptake, its target engagement and occupancy and also to measure its absolute intracellular concentration. Thus, a single bioorthogonally reactive tool provides us the flexibility to run multiple studies using fluorescent and bioluminescent reporters to both validate our probe and also gain an extensive understanding of our cellular disease model.

5.2   Future development

The design and validation of our bioorthogonal probes was applied to a biological model which was already extensively studied and understood. However, this approach could be applied also to design and validate bioorthogonal probes for generating biological hypotheses on less investigated targets and pathways.

The bioorthogonal label (e.g. TCO) on the probe could be used not only to enable the use of fluorescence and bioluminescence imaging techniques but also as a handle for approaches supported by MS technology. For example, one could envisage chemoproteomics or pull-down experiments (e.g. by reacting the strained alkene with tetrazine functionalized beads or tetrazine-biotin conjugates). This may help to improve our understanding of the selectivity of the probe against unexpected targets or shed some light on the interaction of the probe with transient protein complexes that are difficult to study using other approaches.

Curriculum Vitae Pier Luca D'Alessandro

PROFESSIONAL EXPERIENCE

- **Investigator II, New Modalities Group, Global Discovery Chemistry, Novartis Institutes for BioMedical Research, Basel , CH (Jan 2013 – present)**

Research Scientist working on new technologies with potential application in Drug Discovery.

Responsibilities:

Chemistry project team head for an exploratory investigation project in the field of Targeted Protein Degradation.
Evaluation, validation and development of new technologies with potential applications in drug discovery.

- **Scientist I, Innovation, Technologies Group, Global Discovery Chemistry, Novartis Institutes for BioMedical Research, Basel , CH (Jan 2013 – 2016)**

Research Scientist working on new technologies with potential application in Drug Discovery.

Responsibilities:

Directly responsible for an "*in vivo*" chemistry project.
Evaluation, validation and development of new technologies with potential applications in drug discovery.
Evaluation and development of new Bioorthogonal Reactions.

- **Scientist I, Musculo-Skeletal Disorders, Global Discovery Chemistry, Novartis Institutes for BioMedical Research, Basel , CH (Nov 2008 – Dec 2012)**

Medicinal Chemist working on Hit to Candidate Program for Muskolo-Skeletal Disorders (e.g.Smurf-1 inhibitors).

Responsibilities:

Directly responsible for the lead optimization of a Chemical Series which I personally designed and developed.
Interpretation of *in vivo/in vitro* biological data to establish structure-activity relationship and follow-up activities.
Liaising with members of different department (e.g. CADD, DMPK) and other project team members.
Presenting, on regular basis, results and plans at the project team and chemistry team meeting.
Supervision of other associates research scientist (temporary contract employees and students).
Continuous training by attending conference and courses.
Organization of internal chemistry poster symposium.

- **Scientist, Medicinal Chemistry 3, Psychiatry CEDD, GlaxoSmithKline, Harlow, UK (Mar 2007-Oct 2008)**

Medicinal Chemist working on lead to candidate programs for the treatment of psychiatric disorders (e.g. mGLUR5 antagonist program, mGLUR2 positive modulator program).

Responsibilities:

Design of CNS drug-like molecules.
Interpretation of *in vivo/in vitro* biological data to establish structure-activity relationship and follow-up activities.
Liaising with members of different department and other project team members.
Presenting, on regular basis, results and plans at the project team meeting, department meeting and conference.
Students Supervision.

- **Associate Scientist, 7TM System based Research Department of High Throughput Chemistry, GlaxoSmithKline, Harlow, UK (Oct 2005 - Mar 2007)**

Medicinal Chemist working on hit to lead programs for the treatment of psychiatric disorders (e.g. mGLUR2 positive modulator program).

Responsibilities:

Directly responsible for the hit to lead chemistry of a Chemical Series
Design of CNS drug-like molecules.
Interpretation of *in vivo/in vitro* biological data to establish structure-activity relationship and follow-up activities.
Presenting, on regular basis, results and plans at the project team meeting.

- **Associate Scientist, SACT, Department of High Throughput Chemistry, GlaxoSmithKline, Harlow, UK (Dec 2004 - Oct 2005)**

Medicinal chemist working on array synthesis for hit identification.

Responsibilities:

Design and synthesis of libraries in solid and liquid phase synthesis for hit identification.

- **Internship within the Pharmaceutical Biotechnology Laboratory of Advance Biotechnology Centre, Genoa (Jun 2002 – Jul 2004)**

Synthesis of benzo-α-pyrone and benzo-γ-pyrone derivatives with anti HCV activity.

Synthesis of cMyc inhibitor peptides.

News design, pictures selection and pagination Responsible at "Il Secolo XIX", Genoa (Jun 1996 – Jul 1999)

EDUCATION

Master of Science, Chemistry and Pharmaceutical Technology with major in Science and Drug Development (July 2004).

Dipartimento di Scienze Farmaceutiche della Facoltà di Farmacia dell'Università di Genova, IT.

Thesis entitled**: "Synthesis of benzo-α-pyrone and benzo-γ-pyrone derivatives with anti HCV activity".**

SKILLS

Chemistry Skills

- Good synthetic skills (liquid and solid phase chemistry)
- Combinatorial and Parallel Synthesis
- Purification techniques (Flash Chromatography, prep. HPLC, MDAP, prep. TLC, catching and release cartridge, solid supported scavengers)
- Analytical techniques (LCMS, MS, NMR, IR, TLC)

IT Skills

- Microsoft (Words, Excel and PowerPoint),
- Scientific softwares (Discovery Explorer, INCA, ISISnet, Spotfire, Adamantis, Moga, Adept, Radical, Crossfire, Scifinder, Molecular Operating Environment, Focus, etc…)

Language

- Italian (mother tongue),
- Fluent English

PUBLICATIONS, PATENTS AND POSTER

- Karatas, H., **D'Alessandro, P.L**., Tamara M., Yevtodiyenko, A., Vorherr, T., Hollingworth, G., Goun, E., " Real-time imaging and quantification of peptide uptake in vitro and in vivo" , submitted paper.

- Scarabelli S., Tan K. T., Griss R., Hovius R., **D'Alessandro P. L.**, Vorherr T., Johnsson K., *ACS Sens.* 2017, 2, 1191-1197.

- **D'Alessandro P.L**, Buschmann N., Kaufmann M., Furet P., Baysang F., Brunner R., Marzinzik A., Vorherr T., Stachyra T. M., Ottl J., Lizos D. E., Cobos-Correa A., *Angew Chem Int Ed Engl* 2016, 55, 16026-16030.

- Arista L.; Beerli R; Cotesta S.; **D'Alessandro PL**; Lattmann R.; Pulz R.; Troxler T.J. "Carboxamide derivatives as Smurf-1 inhibitors and their preparation"; World Intellectual Property Publication (WO/2015/173659 A2)

- Arista L; Cotesta S; **D'Alessandro PL**; D'Souza AM; Lattmann R; Lizos D; Pulz RA; Rooney L; Smith, N; Taylor J; Troxler T J.; "Carboxamide derivatives as Smurf-1 inhibitors and their preparation"; World Intellectual Property Publication (WO 2015/173656 A2)

- Pilla M., Andreoli M., Tessari M., Delle-Fratte S, Roth A., Butler S., Brown F., Shah P., Bettini E., Cavallini P., Benedetti R., Minick D., Smith P., Tehan B., **D'Alessandro P**., Lorthioir O., Ball C., Garzya V., Goodacre C and Watson S. "The identification of novel orally active mGluR5 antagonist GSK2210875", *Bioorg. Med. Chem. Lett.* **2010**; 20 (24); 7521-7524.

- **D'Alessandro P.L**, Corti C, Roth A, Ugolini A, Sava A, Montanari D, Bianchi F, Garland SL, Powney B, Koppe EL, Rocheville M, Osborne G, Perez P, de la Fuente J, De Los Frailes M, Smith PW, Branch C, Nash D, Watson S.P. "The identification of structurally novel, selective, orally bioavailable positive modulators of mGluR2", *Bioorg. Med. Chem. Lett.* **2010**; 20 (2); 759-62.

- **D'Alessandro P**, Lorthioir O. E., Watson S.P., "Use of thiazoloimidazoles, thiazolotetrazoles and thiazolotriazoles as mGLUR5 antagonist", World Intellectual Property Publication (WO/2009/087220, 16.07.**2009**).

- **D'Alessandro P.L**., Lorthioir O. E., Watson S.P., "Thiazolotriazoles and thiazoloimidazoles as antagonist of the mGLUR5 receptor", World Intellectual Property Publication (WO/2009/087218, 16.07.**2009**).

- Rimlandc J., Dunneb A., Suchete S. Hunjanb, Sasseb R., Uingse I., Montanaric D., Caivanob M., Shahb P., David Standingb, David Grayb, David Brownb, William Cairnsb, Ryan Trumpd, Smith P.W., Berthelemea N., **D'Alessandro P.**, Gulb S, Vimalb M., Smith D.N. and Stephen P. Watsona "The Identification a Novel, Selective, Non-Steroidal, Functional Glucocorticoid Receptor Antagonist*", Bioorg. Med. Chem. Lett.* **2010**, 20 (7); 2340-2343.

- **D'Alessandro P**, et all; "New orally bioavailable metabotropic glutamate subtype 2 receptor positive modulators" poster presented at the GSK Worldwide Medicinal Chemistry Symposium, Verona (Italy), April **2007**.

AWARDS

- Novartis Institute for Biomedical Research Catalyst Award received in 2011
- Novartis Institute for Biomedical Research Spot Awards received in 2009, 2010 and 2013
- GlaxoSmithKline Exceptional Science Award received in June 2007

References:

1. Bunnage, M.E., Chekler, E.L.P. & Jones, L.H. Target validation using chemical probes. *Nature Chemical Biology* **9**, 195-199 (2013).
2. Arrowsmith, C.H. et al. The promise and peril of chemical probes (vol 11, pg 536, 2015). *Nature Chemical Biology* **11**, 887-887 (2015).
3. Swinney, D.C. & Anthony, J. How were new medicines discovered? *Nature Reviews Drug Discovery* **10**, 507-519 (2011).
4. Cunha, A. Genomic technologies-from tools to therapies. *Genome Medicine* **9**(2017).
5. Penrod, N.M., Cowper-Sal-lari, R. & Moore, J.H. Systems genetics for drug target discovery. *Trends in Pharmacological Sciences* **32**, 623-630 (2011).
6. Moffat, J.G., Vincent, F., Lee, J.A., Eder, J. & Prunotto, M. Opportunities and challenges in phenotypic drug discovery: an industry perspective. *Nature Reviews Drug Discovery* **16**, 531-543 (2017).
7. Sams-Dodd, F. Target-based drug discovery: is something wrong? *Drug Discovery Today* **10**, 139-147 (2005).
8. Garbaccio, R.M. & Parmee, E.R. The Impact of Chemical Probes in Drug Discovery: A Pharmaceutical Industry Perspective. *Cell Chemical Biology* **23**, 10-17 (2016).
9. Frye, S.V. The art of the chemical probe. *Nat Chem Biol* **6**, 159-161 (2010).
10. Lee, D.H. & Goldberg, A.L. Proteasome inhibitors cause induction of heat shock proteins and trehalose, which together confer thermotolerance in Saccharomyces cerevisiae. *Molecular and Cellular Biology* **18**, 30-38 (1998).
11. Grobler, J.A. et al. Diketo acid inhibitor mechanism and HIV-1 integrase: Implications for metal binding in the active site of phosphotransferase enzymes. *Proceedings of the National Academy of Sciences of the United States of America* **99**, 6661-6666 (2002).
12. Collins, J.L. et al. Identification of a nonsteroidal liver X receptor agonist through parallel array synthesis of tertiary amines. *Journal of Medicinal Chemistry* **45**, 1963-1966 (2002).
13. Fischer, E.S., Bohm, K. & Thoma, N.H. Structure of the DDB1-CRBN E3 ubiquitin ligase in complex with thalidomide: insights into CRL4 inhibition by small molecules. *Febs Journal* **281**, 248-249 (2014).
14. Ito, T. et al. Identification of a Primary Target of Thalidomide Teratogenicity. *Science* **327**, 1345-1350 (2010).
15. Sehgal, S.N., Baker, H. & Vezina, C. Rapamycin (Ay-22,989), a New Antifungal Antibiotic .2. Fermentation, Isolation and Characterization. *Journal of Antibiotics* **28**, 727-732 (1975).
16. Filippakopoulos, P. et al. Selective inhibition of BET bromodomains. *Nature* **468**, 1067-1073 (2010).
17. Dale, T. et al. A selective chemical probe for exploring the role of CDK8 and CDK19 in human disease. *Nature Chemical Biology* **11**, 973-980 (2015).
18. Edwards, S.R. & Wandless, T.J. The rapamycin-binding domain of the protein kinase mammalian target of rapamycin is a destabilizing domain. *Journal of Biological Chemistry* **282**, 13395-13401 (2007).
19. Seto, B. Rapamycin and mTOR: a serendipitous discovery and implications for breast cancer. *Clin Transl Med* **1**, 29 (2012).
20. Soliman, G.A. The Role of Mechanistic Target of Rapamycin (mTOR) Complexes Signaling in the Immune Responses. *Nutrients* **5**, 2231-2257 (2013).
21. ANTITUMOR AGENT. (ed. Mitsubishi Tanabe Pharma, C.) (2009).
22. Allen, B.L. & Taatjes, D.J. The Mediator complex: a central integrator of transcription. *Nature Reviews Molecular Cell Biology* **16**, 155-166 (2015).
23. Mallinger, A. et al. Discovery of Potent, Orally Bioavailable, Small-Molecule Inhibitors of WNT Signaling from a Cell-Based Pathway Screen. *Journal of Medicinal Chemistry* **58**, 1717-1735 (2015).
24. Clarke, P. et al. Discovery of preclinical development candidate inhibitors of the mediator complex-associated kinases CDK8 and CDK19 and evaluation of their therapeutic potential. *Cancer Research* **76**(2016).
25. Workman, P. & Collins, I. Probing the Probes: Fitness Factors For Small Molecule Tools. *Chemistry & Biology* **17**, 561-577 (2010).
26. Blagg, J. & Workman, P. Choose and Use Your Chemical Probe Wisely to Explore Cancer Biology. *Cancer Cell* **32**, 9-25 (2017).
27. Blagg, J. & Workman, P. Chemical biology approaches to target validation in cancer. *Current Opinion in Pharmacology* **17**, 87-100 (2014).
28. Workman, P. & Collins, I. Probing the probes: fitness factors for small molecule tools. *Chem Biol* **17**, 561-77 (2010).
29. Tamaoki, T. et al. Staurosporine, a potent inhibitor of phospholipid/Ca++dependent protein kinase. *Biochem Biophys Res Commun* **135**, 397-402 (1986).
30. Karaman, M.W. et al. A quantitative analysis of kinase inhibitor selectivity. *Nat Biotechnol* **26**, 127-32 (2008).
31. Weiss, W.A., Taylor, S.S. & Shokat, K.M. Recognizing and exploiting differences between RNAi and small-molecule inhibitors. *Nature Chemical Biology* **3**, 739-744 (2007).
32. Moore, J.D. The impact of CRISPR-Cas9 on target identification and validation. *Drug Discov Today* **20**, 450-7 (2015).
33. Ong, S.E. et al. Identifying the proteins to which small-molecule probes and drugs bind in cells. *Proceedings of the National Academy of Sciences of the United States of America* **106**, 4617-4622 (2009).
34. Mackinnon, A.L. & Taunton, J. Target Identification by Diazirine Photo-Cross-linking and Click Chemistry. *Curr Protoc Chem Biol* **1**, 55-73 (2009).
35. Barglow, K.T. & Cravatt, B.F. Activity-based protein profiling for the functional annotation of enzymes. *Nature Methods* **4**, 822-827 (2007).

36. Salisbury, C.M. & Cravatt, B.F. Activity-based probes for proteomic profiling of histone deacetylase complexes. *Proc Natl Acad Sci U S A* **104**, 1171-6 (2007).
37. Finley, A. & Copeland, R.A. Small molecule control of chromatin remodeling. *Chem Biol* **21**, 1196-210 (2014).
38. Marks, P. et al. Histone deacetylases and cancer: causes and therapies. *Nat Rev Cancer* **1**, 194-202 (2001).
39. Smith, E. & Collins, I. Photoaffinity labeling in target- and binding-site identification. *Future Med Chem* **7**, 159-83 (2015).
40. Rostovtsev, V.V., Green, L.G., Fokin, V.V. & Sharpless, K.B. A stepwise Huisgen cycloaddition process: Copper(I)-catalyzed regioselective "ligation" of azides and terminal alkynes. *Angewandte Chemie-International Edition* **41**, 2596-+ (2002).
41. Jones, L.H. et al. In-cell click labelling of small molecules to determine subcellular localisation. *J Chem Biol* **4**, 49-53 (2011).
42. Blair, J.A. et al. Structure-guided development of affinity probes for tyrosine kinases using chemical genetics. *Nat Chem Biol* **3**, 229-38 (2007).
43. Oprea, T.I. et al. A crowdsourcing evaluation of the NIH chemical probes. *Nat Chem Biol* **5**, 441-7 (2009).
44. Yang, N.J. & Hinner, M.J. Getting Across the Cell Membrane: An Overview for Small Molecules, Peptides, and Proteins. in *Site-Specific Protein Labeling: Methods and Protocols* (eds. Gautier, A. & Hinner, M.J.) 29-53 (Springer New York, New York, NY, 2015).
45. Jin, X.N. et al. Comparison of MDCK-MDR1 and Caco-2 cell based permeability assays for anti-malarial drug screening and drug investigations. *Journal of Pharmacological and Toxicological Methods* **70**, 188-194 (2014).
46. Burlina, F., Sagan, S., Bolbach, G. & Chassaing, G. A direct approach to quantification of the cellular uptake of cell-penetrating peptides using MALDI-TOF mass spectrometry. *Nature Protocols* **1**, 200-205 (2006).
47. Guillaume-Gentil, O. et al. Single-Cell Mass Spectrometry of Metabolites Extracted from Live Cells by Fluidic Force Microscopy. *Analytical Chemistry* **89**, 5017-5023 (2017).
48. Rubakhin, S.S., Romanova, E.V., Nemes, P. & Sweedler, J.V. Profiling metabolites and peptides in single cells. *Nature Methods* **8**, S20-S29 (2011).
49. Fischer, R., Waizenegger, T., Kohler, K. & Brock, R. A quantitative validation of fluorophore-labelled cell-permeable peptide conjugates: fluorophore and cargo dependence of import. *Biochimica Et Biophysica Acta-Biomembranes* **1564**, 365-374 (2002).
50. Jones, S.W. et al. Characterisation of cell-penetrating peptide-mediated peptide delivery. *British Journal of Pharmacology* **145**, 1093-1102 (2005).
51. Kondo, E. et al. Tumour lineage-homing cell-penetrating peptides as anticancer molecular delivery systems. *Nature Communications* **3**(2012).
52. Li, Q. et al. Subcellular drug distribution: mechanisms and roles in drug efficacy, toxicity, resistance, and targeted delivery. *Drug Metab Rev* **50**, 430-447 (2018).
53. Zheng, N., Tsai, H.N., Zhang, X., Shedden, K. & Rosania, G.R. The subcellular distribution of small molecules: a meta-analysis. *Mol Pharm* **8**, 1611-8 (2011).
54. Zheng, N., Tsai, H.N., Zhang, X. & Rosania, G.R. The subcellular distribution of small molecules: from pharmacokinetics to synthetic biology. *Mol Pharm* **8**, 1619-28 (2011).
55. Ochocki, J.D., Mullen, D.G., Wattenberg, E.V. & Distefano, M.D. Evaluation of a cell penetrating prenylated peptide lacking an intrinsic fluorophore via in situ click reaction. *Bioorganic & Medicinal Chemistry Letters* **21**, 4998-5001 (2011).
56. Simon, G.M., Niphakis, M.J. & Cravatt, B.F. Determining target engagement in living systems. *Nature Chemical Biology* **9**, 200-205 (2013).
57. Bigott-Hennkens, H.M., Dannoon, S., Lewis, M.R. & Jurisson, S.S. In vitro receptor binding assays: general methods and considerations. *Q J Nucl Med Mol Imaging* **52**, 245-53 (2008).
58. Day, R.N. & Davidson, M.W. Fluorescent proteins for FRET microscopy: Monitoring protein interactions in living cells. *Bioessays* **34**, 341-350 (2012).
59. Robers, M.B. et al. Target engagement and drug residence time can be observed in living cells with BRET. *Nat Commun* **6**, 10091 (2015).
60. Tsukiji, S. & Hamachi, I. Ligand-directed tosyl chemistry for in situ native protein labeling and engineering in living systems: from basic properties to applications. *Current Opinion in Chemical Biology* **21**, 136-143 (2014).
61. Karen, J., Sioberg, C., Shalaly, N.D. & Molina, D.M. Physiologically relevant target engagement using the cellular thermal shift assay (CETSA). *Cancer Research* **77**(2017).
62. Tan, B.X. et al. Assessing the Efficacy of Mdm2/Mdm4-Inhibiting Stapled Peptides Using Cellular Thermal Shift Assays. *Scientific Reports* **5**(2015).
63. Schurmann, M., Janning, P., Ziegler, S. & Waldmann, H. Small-Molecule Target Engagement in Cells. *Cell Chemical Biology* **23**, 435-441 (2016).
64. Isherwood, B. et al. Live Cell in Vitro and in Vivo Imaging Applications: Accelerating Drug Discovery. *Pharmaceutics* **3**, 141-170 (2011).
65. Peng, T. & Hang, H.C. Site-Specific Bioorthogonal Labeling for Fluorescence Imaging of Intracellular Proteins in Living Cells. *Journal of the American Chemical Society* **138**, 14423-14433 (2016).
66. Devaraj, N.K., Hilderbrand, S., Upadhyay, R., Mazitschek, R. & Weissleder, R. Bioorthogonal turn-on probes for imaging small molecules inside living cells. *Angew Chem Int Ed Engl* **49**, 2869-72 (2010).
67. Reiner, T., Earley, S., Turetsky, A. & Weissleder, R. Bioorthogonal small-molecule ligands for PARP1 imaging in living cells. *Chembiochem* **11**, 2374-7 (2010).
68. Yang, K.S., Budin, G., Reiner, T., Vinegoni, C. & Weissleder, R. Bioorthogonal Imaging of Aurora Kinase A in Live Cells. *Angewandte Chemie International Edition* **51**, 6598-6603 (2012).
69. Budin, G., Yang, K.S., Reiner, T. & Weissleder, R. Bioorthogonal probes for polo-like kinase 1 imaging and quantification. *Angew Chem Int Ed Engl* **50**, 9378-81 (2011).
70. Henkin, A.H. et al. Real-time noninvasive imaging of fatty acid uptake in vivo. *ACS Chem Biol* **7**, 1884-91 (2012).

71. Meyer, J.P. et al. F-Based Pretargeted PET Imaging Based on Bioorthogonal Diels-Alder Click Chemistry. *Bioconjug Chem* (2015).

72. Rossin, R. & Robillard, M.S. Pretargeted imaging using bioorthogonal chemistry in mice. *Curr Opin Chem Biol* **21**, 161-9 (2014).

73. Godinat, A. et al. A biocompatible "split luciferin" reaction and its application for non-invasive bioluminescent imaging of protease activity in living animals. *Curr Protoc Chem Biol* **6**, 169-89 (2014).

74. Chung, H.J. et al. Bioorthogonal nanosensors for magnetic and optical detection of infectious pathogens. *Abstracts of Papers of the American Chemical Society* **243**(2012).

75. Chung, H.J. et al. Ubiquitous Detection of Gram-Positive Bacteria with Bioorthogonal Magnetofluorescent Nanoparticles. *Acs Nano* **5**, 8834-8841 (2011).

76. Devaraj, N.K., Haun, J.B. & Weissleder, R. Application of bioorthogonal tetrazine chemistry to nanoparticle based cell detection. *Abstracts of Papers of the American Chemical Society* **240**(2010).

77. Godinat, A. et al. A biocompatible in vivo ligation reaction and its application for noninvasive bioluminescent imaging of protease activity in living mice. *ACS Chem Biol* **8**, 987-99 (2013).

78. Cohen, A.S., Dubikovskaya, E.A., Rush, J.S. & Bertozzi, C.R. Real-time bioluminescence imaging of glycans on live cells. *J Am Chem Soc* **132**, 8563-5 (2010).

79. Nodwell, M.B. & Sieber, S.A. ABPP methodology: introduction and overview. *Top Curr Chem* **324**, 1-41 (2012).

80. Cravatt, B.F., Wright, A.T. & Kozarich, J.W. Activity-based protein profiling: from enzyme chemistry to proteomic chemistry. *Annu Rev Biochem* **77**, 383-414 (2008).

81. Simon, G.M., Niphakis, M.J. & Cravatt, B.F. Determining target engagement in living systems. *Nat Chem Biol* **9**, 200-5 (2013).

82. Morgan, P. et al. Can the flow of medicines be improved? Fundamental pharmacokinetic and pharmacological principles toward improving Phase II survival. *Drug Discovery Today* **17**, 419-424 (2012).

83. Chene, P. Inhibiting the p53-MDM2 interaction: an important target for cancer therapy. *Nat Rev Cancer* **3**, 102-9 (2003).

84. Barak, Y., Juven, T., Haffner, R. & Oren, M. Mdm2 Expression Is Induced by Wild Type-P53 Activity. *Embo Journal* **12**, 461-468 (1993).

85. Zhao, Y., Aguilar, A., Bernard, D. & Wang, S. Small-molecule inhibitors of the MDM2-p53 protein-protein interaction (MDM2 Inhibitors) in clinical trials for cancer treatment. *J Med Chem* **58**, 1038-52 (2015).

86. Roth, J., Dobbelstein, M., Freedman, D.A., Shenk, T. & Levine, A.J. Nucleo-cytoplasmic shuttling of the hdm2 oncoprotein regulates the levels of the p53 protein via a pathway used by the human immunodeficiency virus rev protein. *Embo Journal* **17**, 554-564 (1998).

87. Shieh, S.Y., Ikeda, M., Taya, Y. & Prives, C. DNA damage-induced phosphorylation of p53 alleviates inhibition by MDM2. *Cell* **91**, 325-334 (1997).

88. Hannoun, Z., Greenhough, S., Jaffray, E., Hay, R.T. & Hay, D.C. Post-translational modification by SUMO. *Toxicology* **278**, 288-293 (2010).

89. Hu, W., Feng, Z. & Levine, A.J. The Regulation of Multiple p53 Stress Responses is Mediated through MDM2. *Genes Cancer* **3**, 199-208 (2012).

90. Shvarts, A. et al. MDMX: a novel p53-binding protein with some functional properties of MDM2. *The EMBO Journal* **15**, 5349-5357 (1996).

91. Nomura, K. et al. Structural analysis of MDM2 RING separates degradation from regulation of p53 transcription activity. *Nat Struct Mol Biol* **24**, 578-587 (2017).

92. Li, Q. & Lozano, G. Molecular pathways: targeting Mdm2 and Mdm4 in cancer therapy. *Clin Cancer Res* **19**, 34-41 (2013).

93. Linares, L.K., Hengstermann, A., Ciechanover, A., Muller, S. & Scheffner, M. HdmX stimulates Hdm2-mediated ubiquitination and degradation of p53. *Proceedings of the National Academy of Sciences of the United States of America* **100**, 12009-12014 (2003).

94. Levine, A.J. & Oren, M. The first 30 years of p53: growing ever more complex. *Nature Reviews Cancer* **9**, 749-758 (2009).

95. Gao, J.J. et al. Integrative Analysis of Complex Cancer Genomics and Clinical Profiles Using the cBioPortal. *Science Signaling* **6**(2013).

96. Donehower, L.A. et al. Mice deficient for p53 are developmentally normal but susceptible to spontaneous tumours. *Nature* **356**, 215-21 (1992).

97. Kemp, C.J., Donehower, L.A., Bradley, A. & Balmain, A. Reduction of p53 gene dosage does not increase initiation or promotion but enhances malignant progression of chemically induced skin tumors. *Cell* **74**, 813-22 (1993).

98. Caelles, C., Helmberg, A. & Karin, M. P53-Dependent Apoptosis in the Absence of Transcriptional Activation of P53-Target Genes. *Nature* **370**, 220-223 (1994).

99. Rotter, V. P53, a Transformation-Related Cellular-Encoded Protein, Can Be Used as a Biochemical Marker for the Detection of Primary Mouse-Tumor Cells. *Proceedings of the National Academy of Sciences of the United States of America-Biological Sciences* **80**, 2613-2617 (1983).

100. Wolf, D. & Rotter, V. Major Deletions in the Gene Encoding the P53 Tumor-Antigen Cause Lack of P53 Expression in Hl-60 Cells. *Proceedings of the National Academy of Sciences of the United States of America* **82**, 790-794 (1985).

101. Eliyahu, D. et al. Meth A fibrosarcoma cells express two transforming mutant p53 species. *Oncogene* **3**, 313-21 (1988).

102. Halevy, O., Rodel, J., Peled, A. & Oren, M. Frequent p53 mutations in chemically induced murine fibrosarcoma. *Oncogene* **6**, 1593-600 (1991).

103. Baker, S.J. et al. Chromosome-17 Deletions and P53 Gene-Mutations in Colorectal Carcinomas. *Science* **244**, 217-221 (1989).

104. Malkin, D. & Friend, S.H. Germ Line P53 Mutations in a Familial Syndrome of Breast-Cancer, Sarcomas, and Other Neoplasms (Science, Vol 250, Pg 1233, 1990). *Science* **259**, 878-878 (1993).

105. Donehower, L.A. et al. Mice Deficient for P53 Are Developmentally Normal but Susceptible to Spontaneous Tumors. *Nature* **356**, 215-221 (1992).
106. Momand, J., Zambetti, G.P., Olson, D.C., George, D. & Levine, A.J. The Mdm-2 Oncogene Product Forms a Complex with the P53 Protein and Inhibits P53-Mediated Transactivation. *Cell* **69**, 1237-1245 (1992).
107. Kussie, P.H. et al. Structure of the MDM2 oncoprotein bound to the p53 tumor suppressor transactivation domain. *Science* **274**, 948-53 (1996).
108. Lane, D.P. Exploiting the p53 pathway for cancer diagnosis and therapy. *Br J Cancer* **80 Suppl 1**, 1-5 (1999).
109. Lain, S., Xirodimas, D. & Lane, D.P. Accumulating active p53 in the nucleus by inhibition of nuclear export: a novel strategy to promote the p53 tumor suppressor function. *Exp Cell Res* **253**, 315-24 (1999).
110. Oliner, J.D. et al. Oncoprotein Mdm2 Conceals the Activation Domain of Tumor Suppressor-P53. *Nature* **362**, 857-860 (1993).
111. Bottger, V. et al. Identification of novel mdm2 binding peptides by phage display. *Oncogene* **13**, 2141-2147 (1996).
112. Garcia-Echeverria, C., Chene, P., Blommers, M.J.J. & Furet, P. Discovery of potent antagonists of the interaction between human double minute 2 and tumor suppressor p53. *Journal of Medicinal Chemistry* **43**, 3205-3208 (2000).
113. Ran, X. & Gestwicki, J.E. Inhibitors of protein-protein interactions (PPIs): an analysis of scaffold choices and buried surface area. *Current Opinion in Chemical Biology* **44**, 75-86 (2018).
114. Vassilev, L.T. et al. In vivo activation of the p53 pathway by small-molecule antagonists of MDM2. *Science* **303**, 844-848 (2004).
115. Burgess, A. et al. Clinical Overview of MDM2/X-Targeted Therapies. *Frontiers in Oncology* **6**(2016).
116. Furet, P. et al. The central valine concept provides an entry in a new class of non peptide inhibitors of the p53-MDM2 interaction. *Bioorg Med Chem Lett* **22**, 3498-502 (2012).
117. Furet, P., Kallen, J., LORBER, J. & Masuya, K. 3 - imidazolyl- indoles for the treatment of proliferative diseases. (2012).
118. Patterson, D.M., Nazarova, L.A. & Prescher, J.A. Finding the right (bioorthogonal) chemistry. *ACS Chem Biol* **9**, 592-605 (2014).
119. Versteegen, R.M., Rossin, R., ten Hoeve, W., Janssen, H.M. & Robillard, M.S. Click to release: instantaneous doxorubicin elimination upon tetrazine ligation. *Angew Chem Int Ed Engl* **52**, 14112-6 (2013).
120. Matikonda, S.S. et al. Bioorthogonal prodrug activation driven by a strain-promoted 1,3-dipolar cycloaddition. *Chemical Science* **6**, 1212-1218 (2015).
121. Lebraud, H., Wright, D.J., Johnson, C.N. & Heightman, T.D. Protein Degradation by In-Cell Self-Assembly of Proteolysis Targeting Chimeras. *ACS Cent Sci* **2**, 927-934 (2016).
122. Blackman, M.L., Royzen, M. & Fox, J.M. Tetrazine ligation: fast bioconjugation based on inverse-electron-demand Diels-Alder reactivity. *J Am Chem Soc* **130**, 13518-9 (2008).
123. Ramil, C.P. & Lin, Q. Bioorthogonal chemistry: strategies and recent developments. *Chem Commun (Camb)* **49**, 11007-22 (2013).
124. Agard, N.J., Prescher, J.A. & Bertozzi, C.R. A strain-promoted [3 + 2] azide-alkyne cycloaddition for covalent modification of biomolecules in living systems. *J Am Chem Soc* **126**, 15046-7 (2004).
125. Sletten, E.M. & Bertozzi, C.R. A hydrophilic azacyclooctyne for Cu-free click chemistry. *Org Lett* **10**, 3097-9 (2008).
126. Codelli, J.A., Baskin, J.M., Agard, N.J. & Bertozzi, C.R. Second-generation difluorinated cyclooctynes for copper-free click chemistry. *J Am Chem Soc* **130**, 11486-93 (2008).
127. Baskin, J.M. et al. Copper-free click chemistry for dynamic in vivo imaging. *Proc Natl Acad Sci U S A* **104**, 16793-7 (2007).
128. Ning, X., Guo, J., Wolfert, M.A. & Boons, G.J. Visualizing metabolically labeled glycoconjugates of living cells by copper-free and fast huisgen cycloadditions. *Angew Chem Int Ed Engl* **47**, 2253-5 (2008).
129. Furet, P., Kallen, J., Lorber, J. & Masuya, K. 3-IMIDAZOLYL-INDOLES FOR THE TREATMENT OF PROLIFERATION DISEASES. *WO2012/176123* (2012).
130. Sisko, J., Mellinger, M., Sheldrake, P.W. & Baine, N.H. Efficient method for the synthesis of substituted TosMIC precursors. *Tetrahedron Letters* **37**, 8113-8116 (1996).
131. Vanleusen, A.M., Wildeman, J. & Oldenziel, O.H. Base-Induced Cycloaddition of Sulfonylmethyl Isocyanides to C,N Double-Bonds - Synthesis of 1,5-Disubstituted and 1,4,5-Trisubstituted Imidazoles from Aldimines and Imidoyl Chlorides. *Journal of Organic Chemistry* **42**, 1153-1159 (1977).
132. Sisko, J. et al. An investigation of imidazole and oxazole syntheses using aryl-substituted TosMIC reagents. *Journal of Organic Chemistry* **65**, 1516-1524 (2000).
133. Chang, Y.S. et al. Stapled alpha-helical peptide drug development: A potent dual inhibitor of MDM2 and MDMX for p53-dependent cancer therapy. *Proceedings of the National Academy of Sciences of the United States of America* **110**, E3445-E3454 (2013).
134. Brown, C.J. et al. Stapled peptides with improved potency and specificity that activate p53. *ACS Chem Biol* **8**, 506-12 (2013).
135. Berghausen, J. et al. Substituted isoquinolinones and quinazolinones. (Google Patents, 2011).
136. Corzo, J. Time, the forgotten dimension of ligand binding teaching. *Biochem Mol Biol Educ* **34**, 413-6 (2006).
137. Copeland, R.A., Pompliano, D.L. & Meek, T.D. Drug-target residence time and its implications for lead optimization (vol 5, pg 730, 2006). *Nature Reviews Drug Discovery* **6**, 249-249 (2007).
138. Arkin, M.R., Tang, Y.Y. & Wells, J.A. Small-Molecule Inhibitors of Protein-Protein Interactions: Progressing toward the Reality. *Chemistry & Biology* **21**, 1102-1114 (2014).
139. Wang, J. & Matayoshi, E. Solubility at the Molecular Level: Development of a Critical Aggregation Concentration (CAC) Assay for Estimating Compound Monomer Solubility. *Pharmaceutical Research* **29**, 1745-1754 (2012).
140. Wang, B., Fang, L.M., Zhao, H., Xiang, T. & Wang, D.C. MDM2 inhibitor Nutlin-3a suppresses proliferation and promotes apoptosis in osteosarcoma cells. *Acta Biochimica Et Biophysica Sinica* **44**, 685-691 (2012).

141. Roberts, W.M., Douglass, E.C., Peiper, S.C., Houghton, P.J. & Look, A.T. Amplification of the Gli Gene in Childhood Sarcomas. *Cancer Research* **49**, 5407-5413 (1989).

142. Oliner, J.D., Kinzler, K.W., Meltzer, P.S., George, D.L. & Vogelstein, B. Amplification of a Gene Encoding a P53-Associated Protein in Human Sarcomas. *Nature* **358**, 80-83 (1992).

143. Wender, P.A. et al. The design, synthesis, and evaluation of molecules that enable or enhance cellular uptake: Peptoid molecular transporters. *Proceedings of the National Academy of Sciences of the United States of America* **97**, 13003-13008 (2000).

144. Mohamadi, F. et al. Macromodel - an Integrated Software System for Modeling Organic and Bioorganic Molecules Using Molecular Mechanics. *Journal of Computational Chemistry* **11**, 440-467 (1990).

145. Spate, A.K. et al. Rapid labeling of metabolically engineered cell-surface glycoconjugates with a carbamate-linked cyclopropene reporter. *Bioconjug Chem* **25**, 147-54 (2014).

146. Yang, J., Liang, Y., Seckute, J., Houk, K.N. & Devaraj, N.K. Synthesis and Reactivity Comparisons of 1-Methyl-3-Substituted Cyclopropene Mini-tags for Tetrazine Bioorthogonal Reactions. *Chemistry-a European Journal* **20**, 3365-3375 (2014).

147. Liu, D.S. et al. Diels-Alder Cycloaddition for Fluorophore Targeting to Specific Proteins inside Living Cells. *Journal of the American Chemical Society* **134**, 792-795 (2012).

148. Yang, J., Seckute, J., Cole, C.M. & Devaraj, N.K. Live-Cell Imaging of Cyclopropene Tags with Fluorogenic Tetrazine Cycloadditions. *Angewandte Chemie-International Edition* **51**, 7476-7479 (2012).

149. Griffin, B.A., Adams, S.R., Jones, J. & Tsien, R.Y. Fluorescent labeling of recombinant proteins in living cells with FlAsH. *Methods Enzymol* **327**, 565-78 (2000).

150. Laughlin, S.T. et al. Metabolic labeling of glycans with azido sugars for visualization and glycoproteomics. *Methods Enzymol* **415**, 230-50 (2006).

151. Neef, A.B. & Schultz, C. Selective fluorescence labeling of lipids in living cells. *Angew Chem Int Ed Engl* **48**, 1498-500 (2009).

152. Chakraborty, A., Wang, D.Y., Ebright, Y.W. & Ebright, R.H. Azide-Specific Labeling of Biomolecules by Staudinger-Bertozzi Ligation: Phosphine Derivatives of Fluorescent Probes Suitable for Single-Molecule Fluorescence Spectroscopy. *Methods in Enzymology, Vol 472: Single Molecule Tools, Pt A: Fluorescence Based Approaches* **472**, 19-30 (2010).

153. Luo, Z., Tikekar, R.V. & Nitin, N. Click Chemistry Approach for Imaging Intracellular and Intratissue Distribution of Curcumin and Its Nanoscale Carrier. *Bioconjugate Chemistry* **25**, 32-42 (2014).

154. Besanceney-Webler, C. et al. Increasing the Efficacy of Bioorthogonal Click Reactions for Bioconjugation: A Comparative Study. *Angewandte Chemie International Edition* **50**, 8051-8056 (2011).

155. Gaetke, L.M. & Chow, C.K. Copper toxicity, oxidative stress, and antioxidant nutrients. *Toxicology* **189**, 147-163 (2003).

156. Stadtman, E.R. & Oliver, C.N. Metal-catalyzed oxidation of proteins. Physiological consequences. *J Biol Chem* **266**, 2005-8 (1991).

157. Liu, Y., Sun, G., David, A. & Sayre, L.M. Model studies on the metal-catalyzed protein oxidation: structure of a possible His-Lys cross-link. *Chem Res Toxicol* **17**, 110-8 (2004).

158. Nagaraj, R.H., Sell, D.R., Prabhakaram, M., Ortwerth, B.J. & Monnier, V.M. High correlation between pentosidine protein crosslinks and pigmentation implicates ascorbate oxidation in human lens senescence and cataractogenesis. *Proceedings of the National Academy of Sciences* **88**, 10257-10261 (1991).

159. Besanceney-Webler, C. et al. Increasing the Efficacy of Bioorthogonal Click Reactions for Bioconjugation: A Comparative Study. *Angewandte Chemie-International Edition* **50**, 8051-8056 (2011).

160. Baskin, J.M. et al. Copper-free click chemistry for dynamic in vivo imaging. *Proceedings of the National Academy of Sciences* **104**, 16793-16797 (2007).

161. Agard, N.J., Prescher, J.A. & Bertozzi, C.R. A strain-promoted [3+2] azide-alkyne cycloaddition for covalent modification of biomolecules in living systems. *Journal of the American Chemical Society* **126**, 15046-15047 (2004).

162. Cunningham, C.W. et al. Uptake, Distribution and Diffusivity of Reactive Fluorophores in Cells: Implications toward Target Identification. *Molecular Pharmaceutics* **7**, 1301-1310 (2010).

163. Bittel, A.M. et al. Varied Length Stokes Shift BODIPY-Based Fluorophores for Multicolor Microscopy. *Scientific Reports* **8**(2018).

164. Devaraj, N.K., Hilderbrand, S., Upadhyay, R., Mazitschek, R. & Weissleder, R. Bioorthogonal Turn-On Probes for Imaging Small Molecules inside Living Cells. *Angewandte Chemie-International Edition* **49**, 2869-2872 (2010).

165. Boger, D.L. Diels-Alder reactions of heterocyclic aza dienes. Scope and applications. *Chemical Reviews* **86**, 781-793 (1986).

166. Carlson, J.C.T., Meimetis, L.G., Hilderbrand, S.A. & Weissleder, R. BODIPY-Tetrazine Derivatives as Superbright Bioorthogonal Turn-on Probes. *Angewandte Chemie-International Edition* **52**, 6917-6920 (2013).

167. Yang, K.S., Budin, G., Reiner, T., Vinegoni, C. & Weissleder, R. Bioorthogonal Imaging of Aurora Kinase A in Live Cells. *Angewandte Chemie-International Edition* **51**, 6598-6603 (2012).

168. Yang, J., Karver, M.R., Li, W.L., Sahu, S. & Devaraj, N.K. Metal-Catalyzed One-Pot Synthesis of Tetrazines Directly from Aliphatic Nitriles and Hydrazine. *Angewandte Chemie-International Edition* **51**, 5222-5225 (2012).

169. Courtis, A.M. et al. Monoalkoxy BODIPYs-A Fluorophore Class for Bioimaging. *Bioconjugate Chemistry* **25**, 1043-1051 (2014).

170. Lukinavicius, G. et al. A near-infrared fluorophore for live-cell super-resolution microscopy of cellular proteins. *Nature Chemistry* **5**, 132-139 (2013).

171. Sivakumar, K. et al. A Fluorogenic 1,3-Dipolar Cycloaddition Reaction of 3-Azidocoumarins and Acetylenes. *Organic Letters* **6**, 4603-4606 (2004).

172. Friscourt, F., Fahrni, C.J. & Boons, G.J. A Fluorogenic Probe for the Catalyst-Free Detection of Azide-Tagged Molecules. *Journal of the American Chemical Society* **134**, 18809-18815 (2012).

173. Dommerholt, J. et al. Readily Accessible Bicyclononynes for Bioorthogonal Labeling and Three-Dimensional Imaging of Living Cells. *Angewandte Chemie-International Edition* **49**, 9422-9425 (2010).
174. Loudet, A. & Burgess, K. BODIPY dyes and their derivatives: Syntheses and spectroscopic properties. *Chemical Reviews* **107**, 4891-4932 (2007).
175. Terasaki, M., Loew, L., Lippincott-Schwartz, J. & Zaal, K. Fluorescent staining of subcellular organelles: ER, Golgi complex, and mitochondria. *Curr Protoc Cell Biol* **Chapter 4**, Unit 4.4 (2001).
176. Cox, G. *Fundamentals of Fluorescence Imaging*, (Jenny Stanford Publishing, 2019).
177. Beatty, K.E., Szychowski, J., Fisk, J.D. & Tirrell, D.A. A BODIPY-Cyclooctyne for Protein Imaging in Live Cells. *ChemBioChem* **12**, 2137-2139 (2011).
178. Cheng, Z. et al. Near-Infrared Fluorescent Deoxyglucose Analogue for Tumor Optical Imaging in Cell Culture and Living Mice. *Bioconjugate Chemistry* **17**, 662-669 (2006).
179. Tovar, C. et al. Small-molecule MDM2 antagonists reveal aberrant p53 signaling in cancer: Implications for therapy. *Proceedings of the National Academy of Sciences of the United States of America* **103**, 1888-1893 (2006).
180. Furet, P. et al. Discovery of a novel class of highly potent inhibitors of the p53-MDM2 interaction by structure-based design starting from a conformational argument. *Bioorganic & Medicinal Chemistry Letters* **26**, 4837-4841 (2016).
181. Furet, P. et al. Pyrazolopyrrolidine compounds. *WO2013/80141* (2013).
182. Holzer, P. et al. Discovery of a Dihydroisoquinolinone Derivative (NVP-CGM097): A Highly Potent and Selective MDM2 Inhibitor Undergoing Phase 1 Clinical Trials in p53wt Tumors. *J Med Chem* **58**, 6348-58 (2015).
183. Berghausen, J. et al. SUBSTITUTED ISOQUINOLINONES AND QUINAZOLINONES. *WO2011/76786* (2011).
184. Gessier, F. et al. Discovery of dihydroisoquinolinone derivatives as novel inhibitors of the p53-MDM2 interaction with a distinct binding mode. *Bioorg Med Chem Lett* **25**, 3621-5 (2015).
185. Guerlavais, V. et al. PEPTIDOMIMETIC MACROCYCLES. *WO2013/123266* (2013).
186. Stachyra-Valat, T. et al. NVP-HDM201: Biochemical and biophysical profile of a novel highly potent and selective PPI inhibitor of p53-Mdm2. *Cancer Research* **76**(2016).
187. Courtis, A.M. et al. Monoalkoxy BODIPYs--a fluorophore class for bioimaging. *Bioconjug Chem* **25**, 1043-51 (2014).
188. Gießler, K., Griesser, H., Göhringer, D., Sabirov, T. & Richert, C. Synthesis of 3'-BODIPY-Labeled Active Esters of Nucleotides and a Chemical Primer Extension Assay on Beads. *European journal of organic chemistry* **2010**, 3611-3620 (2010).
189. Giessler, K., Griesser, H., Gohringer, D., Sabirov, T. & Richert, C. Synthesis of 3 '-BODIPY-Labeled Active Esters of Nucleotides and a Chemical Primer Extension Assay on Beads. *European Journal of Organic Chemistry*, 3611-3620 (2010).
190. Guo, B.C. et al. Synthesis and spectral properties of new boron dipyrromethene dyes. *Dyes and Pigments* **73**, 206-210 (2007).
191. Schieber, C. et al. Conjugation of Transferrin to Azide-Modified CdSe/ZnS Core-Shell Quantum Dots using Cyclooctyne Click Chemistry. *Angewandte Chemie-International Edition* **51**, 10523-10527 (2012).
192. Fosgerau, K. & Hoffmann, T. Peptide therapeutics: current status and future directions. *Drug Discovery Today* **20**, 122-128 (2015).
193. Gadd, M.S. et al. Structural basis of PROTAC cooperative recognition for selective protein degradation. *Nature Chemical Biology* **13**, 514 (2017).
194. Denburg, J.L., Lee, R.T. & McElroy, W.D. Substrate-binding properties of firefly luciferase: I. Luciferin-binding site. *Archives of Biochemistry and Biophysics* **134**, 381-394 (1969).
195. White, E.H., Worther, H., Seliger, H.H. & Mcelroy, W.D. Amino Analogs of Firefly Luciferin and Biological Activity Thereof. *Journal of the American Chemical Society* **88**, 2015-& (1966).
196. Wender, P.A. et al. Real-time analysis of uptake and bioactivatable cleavage of luciferin-transporter conjugates in transgenic reporter mice. *Proceedings of the National Academy of Sciences* **104**, 10340-10345 (2007).
197. Jones, L.R. et al. Releasable Luciferin–Transporter Conjugates: Tools for the Real-Time Analysis of Cellular Uptake and Release. *Journal of the American Chemical Society* **128**, 6526-6527 (2006).
198. Eiríksdóttir, E., Mäger, I., Lehto, T., El Andaloussi, S. & Langel, Ü. Cellular Internalization Kinetics of (Luciferin-)Cell-Penetrating Peptide Conjugates. *Bioconjugate Chemistry* **21**, 1662-1672 (2010).
199. Godinat, A. et al. A Biocompatible "Split Luciferin" Reaction and Its Application for Non-Invasive Bioluminescent Imaging of Protease Activity in Living Animals. *Current Protocols in Chemical Biology* **6**, 169-189 (2014).
200. Van de Bittner, G.C., Dubikovskaya, E.A., Bertozzi, C.R. & Chang, C.J. In vivo imaging of hydrogen peroxide production in a murine tumor model with a chemoselective bioluminescent reporter. *Proceedings of the National Academy of Sciences* **107**, 21316-21321 (2010).
201. Maric, T. et al. Bioluminescent-based imaging and quantification of glucose uptake in vivo. *Nat Methods* (2019).
202. Versteegen, R.M., Rossin, R., Ten Hoeve, W., Janssen, H.M. & Robillard, M.S. Click to release: Instantaneous doxorubicin elimination upon tetrazine ligation. *Angewandte Chemie - International Edition* **52**, 14112 - 14116 (2013).
203. Royzen, M., Yap, G.P.A. & Fox, J.M. A photochemical synthesis of functionalized trans-cyclooctenes driven by metal complexation. *Journal of the American Chemical Society* **130**, 3760-+ (2008).
204. Seitchik, J.L. et al. Genetically Encoded Tetrazine Amino Acid Directs Rapid Site-Specific in Vivo Bioorthogonal Ligation with trans-Cyclooctenes. *Journal of the American Chemical Society* **134**, 2898-2901 (2012).
205. Blackman, M.L., Royzen, M. & Fox, J.M. Tetrazine Ligation: Fast Bioconjugation Based on Inverse-Electron-Demand Diels–Alder Reactivity. *Journal of the American Chemical Society* **130**, 13518-13519 (2008).
206. Shea, K.J. & Kim, J.S. Influence of strain on chemical reactivity. Relative reactivity of torsionally strained double bonds in 1,3-dipolar cycloadditions. *Journal of the American Chemical Society* **114**, 4846-4855 (1992).
207. Ke, B. et al. Bioluminescence Probe for Detecting Hydrogen Sulfide in Vivo. *Anal Chem* **88**, 592-5 (2016).
208. Smith, P.K. et al. Measurement of protein using bicinchoninic acid. *Analytical Biochemistry* **150**, 76-85 (1985).

209. Liang, G.L., Ren, H.J. & Rao, J.H. A biocompatible condensation reaction for controlled assembly of nanostructures in living cells (vol 2, pg 54, 2009). *Nature Chemistry* **2**, 239-239 (2010).
210. Van de Bittner, G.C., Bertozzi, C.R. & Chang, C.J. Strategy for Dual-Analyte Luciferin Imaging: In Vivo Bioluminescence Detection of Hydrogen Peroxide and Caspase Activity in a Murine Model of Acute Inflammation. *Journal of the American Chemical Society* **135**, 1783-1795 (2013).
211. Godinat, A. et al. A Biocompatible in Vivo Ligation Reaction and Its Application for Noninvasive Bioluminescent Imaging of Protease Activity in Living Mice. *Acs Chemical Biology* **8**, 987-999 (2013).
212. Forman, H.J., Zhang, H. & Rinna, A. Glutathione: Overview of its protective roles, measurement, and biosynthesis. *Molecular Aspects of Medicine* **30**, 1-12 (2009).
213. McCutcheon, D.C., Paley, M.A., Steinhardt, R.C. & Prescher, J.A. Expedient Synthesis of Electronically Modified Luciferins for Bioluminescence Imaging. *Journal of the American Chemical Society* **134**, 7604-7607 (2012).